Investigating the role of TRPC3 in the biogenesis of extracellular vesicles

Elise Hannah Padbury

March 2022

This thesis is submitted in partial fulfilment of the requirements of the award of

Doctor of Philosophy at

Oxford Brookes University

Department of Biological and Medical Sciences

Author's Declaration

I, Elise Hannah Padbury, declare that this thesis titled 'Investigating the role of TRPC3 in the biogenesis of extracellular vesicles' and submitted for assessment is an original work of my own. Any works of other authors used within this thesis, or the work presented in it are properly acknowledged. A list of the references employed is included.

Acknowledgements

Wow, what a journey. Not one I'd like to repeat again in a hurry, but certainly one I am grateful for. I am grateful for the experiences that I have both relished and at times endured, the knowledge I have gained, the people I have met, and most of all, the journey of self-discovery that has made me the person I am today. I am forever grateful to the people who have afforded me this opportunity. To my supervisor Dave Carter, for poaching me at undergraduate and seeing potential in me that I didn't. Your support both practically and emotionally has guided me through this experience, and I wouldn't be the scientist that I am today without you. To my co-supervisor Esther Becker, who has seen me through this experience from my very first interview at the DTP. Your scientific insight has been invaluable to this project, and your impression upon me as a female role model in science will always stay with me. Thank you to the BBSRC and the Oxford Interdisciplinary Bioscience DTP, through which my funding is provided, and without which this work would not have been possible. And to Oxford Brookes, a place I first stepped foot in 7 years ago and couldn't bring myself to leave, for providing a fun and nourishing environment to work in.

"I'm not the smartest fellow in the world, but I can sure pick smart colleagues". This quote could not be truer. Thank you to all members, both past and present, of the Carter-Pink and Becker labs for their bright ideas, support and encouragement over the past four and a half years. Thank you in particular to Lizzie, Manu, Shamma, Genevieve and Jamie for the many celebratory pints after work, and consoling cups of tea when nothing seemed to work. I have learnt so much from you all. A special thank you also to Stefan, whose generosity and incredible microscope skills made this project possible. Thank you too to the many housemates who have passed through Mark Road, in particular Grace and Matt, who have made Oxford a home away from home.

But most of all, thank you to my amazing family, friends and boyfriend for supporting me through this experience. Will, thank you for not running a mile when I was fashionably late to all of our first dates because I'd spent too long in the lab; life is better with you by my side. To Ashley, Elle, Ella, Hannah, Liv and Emily, thank you for the many pep talks and cocktails which have kept me going (although sometimes with a hangover). Mum, Nan and Grandad, no words will ever be enough to express my love and gratitude to you. You are my biggest cheerleaders. Your love and endless encouragement are what made this possible. Mum – *I am because of you.* For every hug, every "you can do it", and every sacrifice you made for me to be here. Who'd have thought we'd make it here? You did, and this PhD is for us. We did it!!

Abstract

Cells within multicellular organisms transcribe, package and release nano-sized spheres called extracellular vesicles (EVs) that carry an array of biomolecules that can be transferred between cells. EV-mediated communication contributes to a wide range of physiological and pathological processes including cancer progression, yet the molecular mechanisms underlying their formation and release remain incompletely characterised. Elevated intracellular calcium (Ca^{2+}) induces EV release in a variety of cell types - with preliminary data to suggest the Ca^{2+} permeable transient receptor potential (TRP) channel TRPC3 may facilitate Ca^{2+}-mediated EV biogenesis. TRPC3 contributes to the progression of ovarian cancer (OC) *in vitro* and *in vivo*, but its role in EV biogenesis and how this influences the pathogenesis of OC is unknown. This thesis therefore aimed to investigate the role of TRPC3 and TRPC3-mediated EV communication in ovarian cells, and how TRPC3 activation, Ca^{2+} influx and upstream GPCR stimulation influence EV biogenesis and cargo. Initial experiments detected TRPC3 expression across a panel of ovarian cell lines, with SKOV3 chosen as the principal line of study. Activating TRPC3 amplified Ca^{2+} signalling in SKOV3 cells, and significantly increased cell growth and migration, whilst cell invasion was unchanged. In contrast, inhibiting TRPC3 attenuated histamine-induced Ca^{2+} signalling, indicating that TRPC3 is activated downstream of histamine GPCRs. To enable specific detection and analysis of SKOV3-EVs, EVs were extracted in serum-free media which yielded a purer population of EVs that present typical markers and morphology. TRPC3 activation induced the release of EVs that promoted recipient SKOV3 cell growth, but bore no effect on SKOV3 motility or invasiveness. Preliminary results also indicated that TRPC3 and its upstream regulator mGluR1 are incorporated into SKOV3-EVs. Using live single-cell imaging, histamine, Ca^{2+}, and TRPC3 activation were shown to stimulate the release of EVs with distinct characteristics and fusion dynamics, including localised, synchronised EV release. Proteomic profiling of these treatment-induced EVs revealed previously unappreciated roles for CD81, NDPKs and Ca^{2+}-dependent interactions with the syndecan-syntenin-ALIX axis in EV biogenesis. Proteomic analysis also evidenced the endosomal origin and enriched metastatic potential of TRPC3 activator-induced EVs, as well as presenting novel characterisation of the effect of DMSO on EV proteomes. Overall, these results present strong evidence that TRPC3 mediates EV biogenesis in ovarian cells, and through altering EV characteristics and proteomic cargo, contributes to the development of OC. This thesis provides a novel contribution to our understanding of the molecular mechanisms and dynamics which underly EV biogenesis, with potential therapeutic applications in cancer.

Table of contents

List of figures

Chapter 1

Chapter 2

Chapter 3

Chapter 4

Chapter 6

Chapter 7

Supplementary figures

List of tables

Abbreviations

3’ UTR	3’ untranslated region
ADAM	Disintegrin and metalloproteinase
AKT	Protein kinase B
ALIX	ALG-2 interacting protein X
APC	Allophycocyanin
ATP/ADP	Adenosine triphosphate/ Adenosine diphosphate
BM	Basement membrane
BMSCs	Bone marrow-derived cells
BRCA1/2	Breast cancer gene 1/2
BRIP1	BRCA1-interacting protein 1
BSA	Bovine serum albumin
CA125	Cancer antigen 125
Ca^{2+}	Calcium
CAFs	Cancer-associated fibroblasts
CAM	Calmodulin
CD9/63/81	Cluster of differentiation 9/63/81
CE	Cornified envelope
CFSE	Carboxyfluorescein succinimidyl ester
DAG	Diacylglycerol
DAPI	4',6-diamidin-2-fenilindolo
DMSO	Dimethyl sulfoxide
DTT	Dithiothreitol
ECL	Enhanced chemiluminescent
ECM	Extracellular matrix
EDTA	Ethylenediamine tetra acetic acid
EGF(R)	Epidermal growth factor (receptor)
EGFP	Enhanced green fluorescent protein
EMT	Epithelial to mesenchymal transition
EOC	Epithelial ovarian cancer
ER	Endoplasmic reticulum
ERK	Extracellular signal-regulated kinases
ESCRT	Endosomal sorting complex responsible for transport

EV	Extracellular vesicle
FBS	Foetal bovine serum
FDR	False discovery rate
FHS	Follicle-stimulating hormone
FITC	Fluorescein isothiocyanate
FPS	Frames per second
GFP	Green fluorescent protein
GO	Gene ontology
GPCR	G protein-coupled receptors
GTP	Guanosine-5'-triphosphate
H^+	Hydrogen
H1/H2HR	Histamine H1/H2 receptor
HGSC	High-grade serous carcinoma
hIPSCs	Human induced pluripotent stem cells
HPMCs	Human peritoneal mesothelial cells
HRS	Hepatocyte growth factor-regulated tyrosine kinase substrate
HSP	Heat shock protein
Ig	Immunoglobulin
ILV	Intraluminal vesicle
IP_3	Inositol 1,4,5-trisphosphate
LFQ	Label-free quantification
LncRNA	Long non-coding RNA
MAPK	Mitogen activated protein kinase
MET	Mesenchymal to epithelial transition
Mg^{2+}	Magnesium
mGluR1	Metabotropic glutamate receptor subtype 1
MHC-I/II	Major histocompatibility complex I/II
miRNA	MicroRNA
MMP	Matrix metalloproteinase
mRNA	Messenger RNA
MSCs	Mesenchymal stem cells
MTT	3-(4,5-Dimethylthiazol-2-yl)-2,5-diphenyltetrazolium bromide
MV	Microvesicle
MVB	Multivesicular body

Na^+	Sodium
NCM	Non-conditioned media
NDPKs	Nucleoside-diphosphate kinases
NFAT	Nuclear factor of activated T-cells
nSMase	Neutral sphingomyelinase
NTA	Nanoparticle tracking analysis
OC	Ovarian Cancer
PBS	Phosphate-buffered saline
PCA	Principal component analysis
PDCD4/6	Programmed cell death 4/6
PFA	Paraformaldehyde
PI	Propidium iodide
PIP2	Phosphatidylinositol 4,5-biphosphate
PLC	Phospholipase C
PLP	Proteolipid protein
PM	Plasma membrane
RAB	Ras-associated binding protein
RAD51C/D	RAD51 recombinase homolog C/D
RIPA	Radioimmunoprecipitation assay buffer
ROCE	Receptor-operated Ca^{2+} entry
RPM	Revolutions per minute
RPMI	Roswell park memorial institute medium
rRNA	Ribosomal RNA
RT	Room temperature
RTK	Receptor tyrosine kinase
S1P	Sphingosine 1-phosphate
SD	Standard deviation
SDS	Sodium dodecyl sulfate
SEC	Size exclusion chromatography
SEM	Standard error of the mean
SFM	Serum free media
SNAP23	Synaptosomal-associated protein 23
SNARE	Soluble N-ethylmaleimide-sensitive factor attachment protein receptors
snoRNA	Small nucleolar RNA

SOCE	Store-operated Ca^{2+} entry
TAMs	Tumour-associated macrophages
TEM	Transmission electron microscopy
TEMs	Tetraspanin-enriched microdomains
TGF-β	Transforming growth factor β
TIRF	Total internal reflection fluorescence microscopy
TME	tumour microenvironment
TNFα	Tumour necrosis factor α
tRNA	Transfer RNA
TRP	Transient receptor potential
TSG101	Tumour susceptibility gene 101
Tspan	Tetraspanin
UC	Ultracentrifugation
uPA	Urokinase-type plasminogen activator
VEGF	Vascular endothelial growth factor
VPS4	Vacuolar protein associated sorting 4

Units of measurement

µg	Microgram
µl	Microlitre
µM	Micromolar
µm	Micrometre
Hz	Hertz
ml	Millilitre
ng	Nanogram
nm	Nanometre
v/v	volume per volume
w/v	weight per volume

Chapter 1

Introduction

1. Introduction

1.1. EXTRACELLULAR VESICLES

1.1.1. INTERCELLULAR COMMUNICATION IN HEALTH AND DISEASE

Cell-to-cell communication is a central determinant of all biological processes, and is essential for the maintenance of proper cellular function and tissue homeostasis. Impaired cellular communication can therefore lead to cell damage and subsequent pathological processes of disease, or conversely, diseases can hijack cellular communication mechanisms to propagate pathogenesis[1]. A pertinent example of this is in cancer metastasis, a process driven mainly by intercellular interactions within the local and distant tumour microenvironment (TME)[2, 3]. Classically, cells communicate via direct cell-cell interactions and the secretion of soluble factors such as cytokines, chemokines and growth factors[4-6]. In addition to these canonical secreted factors, extracellular vesicles (EVs) are emerging as fundamental cell-cell communicators in both normal physiological systems and disease. Because of the multifaceted roles of EVs in human physiology, understanding the factors which underly their formation and how these pathways can be manipulated, and the ensuing effects on their cargo and disease mechanisms holds significant therapeutic potential.

1.1.2. A BRIEF HISTORY OF EXTRACELLULAR VESICLES

Extracellular vesicles (EVs) are a heterogenous group of small membrane-bound structures that are released by essentially all cell types into the extracellular environment[1]. The first description of functional, cell-derived vesicles was by Peter Wolf in 1967[7], who identified small platelet-derived structures with pro-coagulant activity in human blood, and initially termed them “platelet-dust”. The term “extracellular vesicles” was coined in 1971 by Aaronson *et al*.[8], who was the first to suggest that extracellular membrane-bound structures derived from several subcellular compartments. Further distinctions were made between “vesicles of the multivesicular body” and “microvesicles” in foetal bovine serum (FBS) by Dalton in 1975[9], which were later validated by descriptions of two distinct populations of EVs; one of 500-1000nm, and one with an average size of 40nm[10]. The release of multivesicular body (MVB)-derived EVs upon fusion with the plasma membrane (PM) was initially described as a mechanism for reticulocytes to rid themselves of the transferrin receptor in order to become mature red blood cells, therefore leading to the belief that EVs function primarily as a means of cellular waste disposal[11, 12]. However, later work demonstrated that EVs carry surface antigens capable of inducing an immune response in recipient cells, thus indicating their potential as intercellular

communicators[13]. It's now well-established that EVs contain an array of functional biomolecules that can be transferred between cells, and are regarded as major contributors to diverse biological functions; from neuronal communication[14] to cancer progression[15].

1.1.3. BIOGENESIS AND CLASSIFICATION

As suggested in these seminal studies, EVs can arise from multiple biogenesis pathways. They are broadly classified into three main subpopulations based upon their mechanism of biogenesis and size: microvesicles (MVs) and apoptotic bodies are shed by budding of the external PM from alive and dying cells respectively, and can range in size between 100–1000nm, and smaller 40-150nm exosomes which are a product of the endocytic pathway, and released upon MVB-PM fusion (Figure 1.1)[16]. Additional subtypes of overlapping EV-like nanoparticles have been defined more recently, including oncosomes, exomeres and nucleosomes. The defining features of each subtype are detailed in Table 1.1, and here the biogenesis of the three main populations will be further discussed.

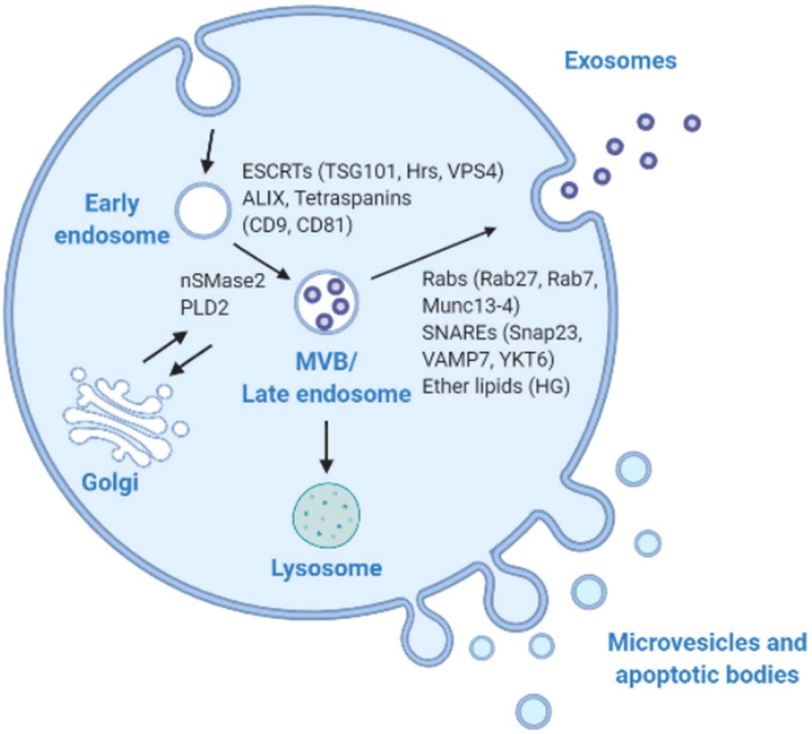

Figure 1.1 Biogenesis of exosomes, microvesicles and apoptotic bodies

Microvesicles and apoptotic bodies are shed by budding of the external PM from alive and dying cells, respectively. Exosomes are a product of the endocytic pathway, whereby maturing early endosomes internalise intraluminal vesicles containing an array of biomolecules, ultimately forming MVBs. MVBs then follow one of two pathways: their canonical fate of fusing with the lysosome for degradation of their constituents, or fusion with the PM to release their contents as exosomes. The molecules involved at each stage are detailed.

Table 1.1 Overview of classification of EVs and EV-like nanoparticles

Type	Size	Biogenesis	Reference
Exosome	**40-150nm**	**Multivesicular body**	**17**
Microvesicle/ectosome	**100-1000nm**	**Membrane shedding**	**17**
Apoptotic body	**50-5000nm**	**Apoptosis**	**18**
Oncosome	1-10µm	Membrane shedding of cancer cells	19, 20
Exomere	35-50nm	Unknown	21, 22
Migrasome	50-100nm	Cell migration	23
Nucleosome	13-57nm	Amphisome (active) Cell death (passive)	24, 25
Ribonucleoprotein particle	~41nm	Unknown, non-exosomal	24, 26

Microvesicles

Microvesicles (MVs), also referred to as ectosomes, are typically large EVs ranging in size between 100-1000nm[17]. Whilst they are released by distinct mechanisms to exosomes and cover a larger size range, they overlap in terms of both size and cargo - notably marker proteins – therefore distinctions between the two populations are limited[17]. MVs are released from both transformed and non-transformed cell types, whereas oncosomes represent a larger population of 1-10µm MVs secreted exclusively by cancer cells[20]. MVs arise through direct outward budding and fission of the PM following cellular activation in response to stimuli such as serine proteases, thrombin, calcium (Ca^{2+}) ionophores, ADP, inflammatory cytokines, growth factors and shear forces[27-31]. Cellular activation and a subsequent increase in intracellular Ca^{2+} drives rearrangements in the asymmetry of membrane phospholipids through Ca^{2+}-dependent lipid translocases including flippases and floppases, scramblases and calpain[32, 33]. These Ca^{2+}-dependent enzymatic machineries reposition phosphatidylserine and phosphatidylethanolamine from the inner-facing leaflet of the PM to the cell surface, resulting in physical bending of the PM and destabilization of PM-cytoskeleton anchorage. Calpain concurrently cleaves several cytoskeletal components including actin, ankyrin, protein 4.1 and spectrin[34, 35], further disrupting attachment to the PM and ultimately causing these localised regions to bud outwards as MVs[27]. Other lipid components such as cholesterol, which is abundantly expressed in MVs, can also contribute to MV biogenesis and is necessary for MV release in activated neutrophils[36]. In addition to lipids, endosomal machinery responsible for exosome formation likewise contributes to MV release. This includes several small GTPases, including members of the ARF (ARF6[37], ARF1[38]), Rab[39] and Rho (Rac1[40], RhoA[41]) families which

contribute to MV shedding by regulating actin dynamics, as well components of the endosomal sorting complex required for transport (ESCRT), TSG101 and ARRDC1, which induce localized changes in membrane curvature in a process similar to viral budding[42]. Exosomes and MVs likewise share mechanisms of cargo sorting, as cargoes are localised to MVBs and sites of MV budding through their affinity for lipid rafts[43, 44]. In addition, proteins ARF6 and Rab22, both implicated in exosome biogenesis, selectively recruit and traffic proteins into MVs[37, 39]. MVs are also enriched for cytosolic and PM associated proteins such as tetraspanins, as they are non-specifically "pinched" off into MVs upon budding from the PM[45, 46]. The non-specific incorporation of membrane-bound proteins, together with shared cargo loading pathways, explains the significant overlap in cargo between exosomes and MVs.

Apoptotic bodies

Apoptotic bodies are large vesicles, ranging in size between 50-5000nm, released by blebbing of the PM during programmed cell death[18]. Membrane blebbing and the subsequent formation of apoptotic bodies is a mechanism for apoptotic cell removal, by fragmenting larger dying cells into smaller particles which can then be engulfed by phagocytes[18]. There is also emerging evidence to suggest smaller "ApoEVs" (<1µm) may act as a means of intercellular communication, particularly in regulating immune cell functions[47]. These bodies are formed by increased actomyosin contraction initiated in the apoptotic cascade, resultantly increasing hydrostatic pressure and destabilising PM-cytoskeleton anchorage, causing the membrane to bleb outwards[48]. In multiple cell types, caspase 3-mediated cleavage of RHO-associated protein kinase 1 (ROCK1) promotes actomyosin contractility by enhancing the phosphorylation of myosin light chain[49, 50]. In contrast to MVs and exosomes, apoptotic bodies are not intentionally "loaded" with cargo, and conversely sequester a random sampling of cytoplasmic, nuclear and organelle fragments that are trapped in the forming membrane bleb[51, 52]. Therefore, whilst apoptotic bodies may likewise contain membrane-bound tetraspanins, they can be differentiated from other vesicle populations by higher expression levels of organelle-associated proteins, such as histones (nucleus), cytochrome C (mitochondria), GM130 (Golgi) and GRP78 (endoplasmic reticulum)[51].

Exosomes

Exosome biogenesis is arguably the best characterised pathway for EV release. Exosomes are often referred to as "small EVs", with a diameter between 40-150nm, and derive from the endocytic pathway as intraluminal vesicles (ILVs) in MVBs released upon MVB fusion with the

PM[17, 53]. The endosomal system dynamically facilitates the internalisation of extracellular ligands and their recycling to the PM, and/or their degradation by fusing with the lysosome[53, 54]. Early endosomes form at invaginations of the PM, and as they mature, they segregate cargo at the delimiting membrane of the endosome as the membrane buds inwards and is "pinched" off, generating ILVs[53]. Mature endosomes containing an accumulation of ILVs, referred to as MVBs, then follow one of two pathways: their canonical fate of fusing with the lysosome for degradation of their constituents, or fusion with the PM to release their contents as exosomes. The factors which determine the fate of a specific MVB are poorly understood, although it is thought that MVBs within the same cell have distinct molecular compositions that target them for either degradation or secretion. For example, Möbius *et al.*[55] demonstrated that cholesterol-rich MVBs are directed to the PM for exosome secretion, whereas another morphologically identical, but cholesterol-poor, population were sent to the lysosome for degradation. Conversely, lysobisphosphatidic acid is absent in exosomes but clearly present in MVBs containing epidermal growth factor (EGF) indicated for lysosomal targeting[56]. How cells regulate the balance between degradative and secretory MVBs is unknown, although cells appear to adjust their exosome secretion according to their needs[57].

The biogenesis of exosomes is thought to arise by one of two essential processes; one involving specific proteins associated with ESCRT machinery and the other being ESCRT-independent[58]. Of the ESCRT-independent pathways, exosome biogenesis can be mediated by neutral sphingomyelinase (nSMase) through the generation of ceramide[59]. Ceramides give rise to rigid lipid raft domains which impose a spontaneous negative curvature on the MVB membrane, resulting in ILV formation[60]. Alternatively, ceramide is metabolized to sphingosine 1-phosphate (S1P) which subsequently activates G protein-coupled S1P receptors, that are essential for cargo sorting into exosomal ILVs[61]. These observations are consistent with the exosomal enrichment of cholesterol, sphingolipids and ceramides, and associated proteins such as flotillins and caveolins[62]. In addition, tetraspanins and canonical EV markers CD63, CD81 and CD9, have been shown to regulate ESCRT-independent endosomal sorting by clustering on the membrane surface to form tetraspanin-enriched microdomains that will bud into the MVB[63-65]. Tetraspanins are also required for cargo targeting to ILVs[66].

ESCRT-dependent biogenesis is considered the primary pathway of exosome formation and is responsible for the sorting of protein cargo into MVBs[17]. The ESCRT machinery is composed of four main protein complexes, ESCRT-0, -I, -II and -III, which operate in a stepwise manner together with accessory proteins such as tumour susceptibility gene 101 (TSG101), AlG-2

interacting protein X (ALIX) and vacuolar protein associated sorting 4 (VPS4), to generate MVBs[67]. The ESCRT-0 complex contains hepatocyte growth factor-regulated tyrosine kinase substrate (HRS), that recognises mono-ubiquitylated cargo proteins and clusters them at the delimiting membrane of the endosome[68]. HRS also recruits the ESCRT-I complex through TSG101, which together with ESCRT-II, forms a super complex that acts to deform the membrane into buds containing the sequestered cargo[69, 70]. Subsequently, ESCRT-I recruits ESCRT-III, either via ESCRT-II or ALIX, which drives membrane scission into ILVs[71, 72]. ALIX can also function independently of the canonical ESCRT pathway by forming a complex with syndecan and syntenin, which catalyses membrane budding in the formation of ILVs[73]. Finally, the ATPase VPS4 is recruited to the MVB membrane to dissociate and recycle the ESCRT machinery[74].

MVBs are transported to the PM to release their constituents as exosomes through interactions with the actin and microtubule cytoskeleton, mediated by a variety of proteins including cortactin and several members of the Rab GTPase family[75, 76]. Rab GTPases regulate many steps of membrane trafficking, including vesicle budding, transport to and fusion with the PM. For example, independent studies suggest that both Rab35 and Rab27a are required for the docking/tethering of MVBs to the PM[77, 78]. At the PM, Rab and other Ras GTPases interact with soluble N-ethylmaleimide-sensitive factor attachment protein receptors (SNAREs) to facilitate MVB-PM fusion[79, 80]. SNARE complexes mediate general vesicle fusion with both the PM and organelle membranes, and are formed of three or four SNARE proteins which can be divided into two groups: *vesicle* or v-SNAREs, incorporated into the vesicle membrane, and *target* or t-SNAREs, associated with the target membrane[80, 81]. In MVB-PM fusion, v-SNAREs on the ILV surface associate with t-SNAREs on the inner leaflet of the PM. T-SNAREs such as syntaxin 5, SNAP23 and syntaxin 4 have recognised roles in MVB-PM fusion, as well as v-SNAREs Ytk6 and VAMP7[79, 82-84].

As evident, the mechanisms of EV biogenesis and secretion are highly heterogenous. This heterogeneity is reflected in their cargo, and translates to issues in defining specific EV markers to identify a homogenous population of EVs for analysis. As discussed, there is also significant overlap in size between EV subpopulations, therefore current isolation techniques which are based on size, density, and molecular composition, are unable to differentiate between each subtype. In this study, EVs were isolated by size exclusion chromatography (SEC) which isolates small EVs, between approximately 80-200nm[85], that will be defined as “EVs” throughout this thesis except in cases where the exact mechanism of biogenesis is experimentally determined.

1.1.4. CARGO AND FUNCTIONS

EVs carry a range of functional biomolecules including proteins, lipids and nucleic acids (both DNA and a variety of RNA species) that are intentionally targeted for EV secretion[86]. EVs and their accompanying cargo can be taken up by both neighbouring and distant cells where they elicit significant pleiotropic effects on cell behaviour, and are hence regarded as potent intercellular communicators. Assaying EV cargo can provide valuable insights into their biological function, the physiological state of their parental cell and biogenesis mechanisms.

Lipids

EVs are encased in a lipid-rich bilayer which consists of sphingolipids, cholesterol, phosphoglycerides, ceramides and derivatives thereof[87]. These lipid components confer structural rigidity to the EV which enables them to withstand physical pressures in the extracellular environment, and reach their target cell intact[87]. The distribution of EV membrane lipids, namely phosphatidylserine, is also thought to facilitate EV uptake by recipient cells[88]. EVs are enriched for bioactive lipids compared to their parental cells, suggestive of their involvement in EV biogenesis[87]. Indeed, lipids play an essential role in cargo sorting by forming lipid raft domains that constitute a platform for loading into ILVs[44]. In addition, a study exploring the role of ceramide in EV biogenesis demonstrated that ceramide is required for loading proteolipid protein (PLP) into EVs in an oligodendrocyte cell line, as well EGFP-CD63 from EGFP-CD63-transfected PC-3 cells[62]. Ceramide, as well as phosphatidic acid, also have demonstrated roles in ILV formation and EV biogenesis[62, 89].

RNA

The discovery that EV cargo contained functional mRNA and miRNAs that could be internalised and translated by target cells contributed to an explosion in the study of EVs and their cargo[90, 91]. Since, a variety of RNA species have been identified within EVs in numerous publications and cell types, including long non-coding RNAs (lncRNAs), ribosomal RNAs (rRNAs), transfer RNAs (tRNAs) and small nucleolar RNAs (snoRNAs)[92, 93]. The horizontal transfer of EV-RNA can modify the target gene expression, signal, and overall biological function of recipient cells, with demonstrable effects on cell survival and proliferation[94], differentiation[95], tumorigenesis[96], immune response[97] and transfer of chemotherapy resistance[98]. EV-RNA expression is also altered under physiological and pathological conditions, and could therefore provide a novel source of disease biomarkers[99]. In addition, certain RNAs are enriched in EVs relative to their parental cell, indicating that RNAs are selectively sorted into EVs for intercellular transfer[90, 93,

[100]. The mechanisms of RNA cargo loading are as of yet unresolved, although it would appear that RNAs in EVs share specific sequence motifs and are enriched in 3'UTR fragments that may target them to EVs[101, 102].

Proteins

EVs derived from different cellular origins sequester a common set of proteins which are likely involved in their formation, including chaperones (Hsp70, Hsp90), cytoskeletal proteins (actin, tubulin), tetraspanins (CD81, CD63, CD9), several components of the ESCRT complex (TSG101, Alix) and proteins involved in vesicle transport and fusion (Rab7, Rab2, Annexins)[103]. The commonality of these proteins suggests they are conserved mediators of EV biogenesis and are used as "marker" proteins for their isolation, detection and characterisation, although they do not necessarily represent a specific subtype of EVs[104, 105]. EV-proteins can be embedded in or attached to the EV lipid bilayer, likely due to their affinity for lipid rafts[44], as well as contained within the EV lumen[106]. Protein modifications such as ubiquitylation and farnesylation are also thought to target proteins for EV secretion[107, 108]. Transmembrane proteins which include tetraspanins, antigen presenting molecules (MHC class I and II), adhesion molecules and glycoproteins can facilitate EV cargo delivery through membrane fusion and internalization, as well as binding surface receptors on recipient cells and initiating signalling cascades in a manner reminiscent of direct cell-cell communication[109, 110]. The expression of EV membrane proteins is also thought to direct specific cell targeting[111]. Alternatively, EVs can deliver intact surface receptor proteins to recipient cells, which are incorporated into the target cell membrane and confer receptivity to new stimulatory or inhibitory signals[112]. The intercellular transfer of EV-proteins which also include transcription factors, growth factors and chemokines can modulate a wide range of physiological and pathological processes, including transduction of viral and bacterial infections, immune response, neurodegenerative diseases and tumour metastasis[113-117].

1.1.5. EV UPTAKE AND CARGO DELIVERY

EVs can elicit their biological function on recipient cells through several different modes of action; including aforementioned receptor-ligand interactions at the PM and transfer of membrane constituents, or by being internalised within the recipient cell for direct delivery of their cargo to the cytoplasm[118, 119]. Three main mechanisms for EV uptake have been proposed; firstly, EVs can fuse directly with the PM through a similar process to viral membrane fusion, and deliver their cargo directly to the cytoplasm[120, 121]. Secondly, EVs may be transferred via cell-

contact dependent mechanisms through synapses or nanotube structures[122, 123] – most prevalent for the uptake of apoptotic bodies[124]. And lastly, believed to be the primary mechanism of EV uptake, EVs can be endocytosed by recipient cells through a variety of endocytic pathways, which include clathrin-mediated, caveolin-dependent and receptor-mediated endocytosis, micropinocytosis, and phagocytosis[125]. Upon internalisation through these different pathways, EVs follow the endocytic pathway and fuse with late endosomes, which in most cases are targeted to the lysosome for degradation[121, 126]. Importantly, this degradative pathway could offer metabolites to recipient cells[127]. To avoid degradation and access cytoplasmic and nuclear targets, EVs must escape digestion by back fusion with the limiting membrane of the endosome[128]. Endosomal escape has been suggested as a key limiting factor for effective cargo delivery, with an estimated 10-30% of internalised EVs bypassing degradation to fulfil their signalling function[129-131]. The endoplasmic reticulum (ER) may also provide a route for lysosomal escape, as EVs sorted into endosomal trafficking circuits are targeted to scan the ER, a nucleation site for translation, as a possible site of cargo release[132]. Nuclear cargos may also be trafficked from the endosome into the nucleoplasm via nuclear envelope invaginations[133]. Other possible routes that permit lysosomal escape include cargo release from "leaky" EVs or ruptured endosomal/lysosomal compartments, as well as redirection of EVs back to the PM from early endosomes via recycling endosomes[126, 134-136]. It is also possible for EV membrane cargo to trigger signalling cascades from within the endosomal compartment, either by binding endosomal receptors such as toll-like receptors[97] or through sustained activation of pH-sensitive ligands in the acidic endosomal environment, as reported for EV-mediated latent transforming growth factor β-1 (TGFβ-1) signalling in primary mesenchymal stem cells[137].

1.2. THE ROLE OF CALCIUM IN EV BIOGENESIS

1.2.1. CALCIUM IN EXOSOME BIOGENESIS AND RELEASE

Ca^{2+}-induced exocytosis initiates many forms of intercellular communication, as exemplified in synaptic transmission, neuroendocrine signalling and the immune response[138-141]. In these physiological processes, Ca^{2+} acts on a cascade of conserved molecular targets including members from the Rab, Sec1/Munc18 (SM), Ca^{2+}-dependent activator protein for secretion (CAPS)/Munc13, and SNARE protein families that function in the tethering, priming, and fusion of secretory vesicles with the PM[142]. With a number of these proteins likewise implicated in MVB trafficking and MVB-PM fusion (described in Section 1.1.3), it was therefore hypothesised that intracellular Ca^{2+} signalling may similarly induce exosome release. Indeed, Savina *et al.*[143]

demonstrated that the treatment of human erythroleukemia K562 cells with Monensin – a Na^+/H^+ exchanger that increases intracellular Ca^{2+} – or the Ca^{2+} ionophore A23187, increased exosome secretion. In line with this data, the Ca^{2+} ionophore ionomycin was shown to enhance CD63+, CD9+, and ALIX+ exosome release by approximately fivefold in breast carcinoma cells[144], as well as facilitate exosomal release of PLP from oligodendrocytes[145]. A similar effect of Ca^{2+} is also apparent *in vivo*, as treatment with dimethyl amiloride, an inhibitor of H^+/Na^+ and Na^+/Ca^{2+} exchangers, inhibited exosome release from tumour cells in three different mouse tumour models[146].

Although the molecular mechanisms that facilitate Ca^{2+}-induced exosome release are not fully understood, intracellular Ca^{2+} may regulate exosome release at several stages of the biogenesis pathway. Firstly, as mentioned, several critical components of the MVB transport/fusion machinery are Ca^{2+}-dependent. Of these proteins, Rab11 has been shown to facilitate MVB-PM fusion only in the presence of Ca^{2+}, and together with the Rab binding protein Munc13-4, generate MVBs competent for exosome release in a Ca^{2+}-dependent trafficking pathway[144, 147]. Synaptotagmins which activate SNARE fusion complexes upon Ca^{2+}-binding[148] have likewise been implicated in exosome release, with the knockdown of synaptotagmin-7 shown to reduce exosome secretion in invasive head and neck squamous cell carcinoma cells[149]. Alternatively, Ca^{2+} stimulation could upregulate the ESCRT pathway, thereby increasing MVB biogenesis. Through a Ca^{2+}-dependent interaction, apoptosis-linked gene 2 (ALG-2) induces a conformational change in ALIX that enables its association with ESCRT machinery[150], which in turn assembles ESCRT-III and Vps4 complexes that mediate endosomal membrane budding and abscission of MVBs[151, 152]. An ALIX-mediated pathway involving syndecan-4 and syntenin-1 also facilitates MVB sorting and formation[73], which is proposed to upregulate EV release following high frequency acoustic cell stimulation through a Ca^{2+}-dependent mechanism[153]. This same study noted that in addition to ALIX and syntenin-1; TSG101, CD63, flotillin-1 and Rab27a were likewise upregulated in EVs following acoustic stimulation and a subsequent rise in intracellular Ca^{2+}, suggestive of their role in Ca^{2+}-induced EV biogenesis.

1.2.2. CALCIUM IN MV BIOGENESIS

In addition to ESCRT and MVB transport/fusion machinery, an increase in intracellular Ca^{2+} can likewise activate Ca^{2+}-sensitive proteins involved in MV biogenesis. As discussed in Section 1.1.3, Ca^{2+} drives rearrangements in the asymmetry of membrane phospholipids through Ca^{2+}-dependent lipid translocases, which together with the concurrent Ca^{2+} activation of proteolytic calpain and gelsolin, a ubiquitous actin binding protein that can remodel the actin cytoskeleton,

promotes cytoskeleton detachment and ultimately induces membrane blebbing[32-34, 154]. Furthermore, Annexin-2, a protein involved in Ca^{2+}-induced exocytosis, has been shown to promote MV release[155]. Increases in intracellular Ca^{2+} induce MV release through these mechanisms in a range of cell types, including erythrocytes, platelets, glioblastoma tumour spheroids and malignant MCF-7 breast cancer cells[156-158]. Interestingly, malignant cells have a significantly higher basal production of MVs compared to non-malignant cells, driven by a higher resting concentration of free cytosolic Ca^{2+} and subsequent activation of a Ca^{2+}-calpain dependent pathway[159]. In a follow-up study, resting vesiculation in malignant cells was found to occur via mobilization of Ca^{2+} from the ER rather than Ca^{2+} entry through channels at the PM, with store-operated calcium entry (SOCE) serving as a failsafe mechanism to drive vesiculation in the event of ER store depletion[156]. More recently, the Ca^{2+} channel TRPC5 of the canonical transient receptor potential channel (TRPC) family has been shown to be required for EV release from chemoresistant breast cancer cells, suggesting Ca^{2+} entry through transmembrane Ca^{2+} channels may also drive EV biogenesis in malignant cells[112]. Although, whether TRPC5-mediated Ca^{2+} entry acts on the endosomal pathway to induce exosome biogenesis, or on the PM to derive MVs, remains undefined.

1.2.3. CALCIUM, EVS AND CANCER

In the context of malignancy, aberrant Ca^{2+} signalling is a key driver of disease progression[160]. The overexpression and/or overactivity of Ca^{2+} channels and transporters is a characterizing feature of cancer, acting to increase intracellular Ca^{2+} in tumour cells by enhancing extracellular Ca^{2+} entry at the cell membrane or facilitating release from internal stores[160, 161]. Disrupted Ca^{2+} homeostasis subsequently deregulates Ca^{2+}-sensitive downstream effectors that, in turn, promotes pathophysiological cancer hallmarks such as enhanced survival, proliferation and invasion[162]. As discussed, increases in intracellular Ca^{2+} also act to induce EV release in a number of cancer cell types[143-145]. Notably, tumour cells produce and secrete significantly more EVs than normal proliferating cells, and the concentration of circulating EVs in the plasma of cancer patients is frequently elevated, correlating with disease progression[163-165]. With EVs emerging as fundamental cell-cell communicators in the tumour microenvironment (TME) (detailed in Section 1.4), there is evidence to suggest that EVs may act as Ca^{2+}-driven downstream effectors in cancer progression. To this effect, EVs released by cancer cells with disrupted Ca^{2+} signalling show enhanced metastatic capacity. For example, Ca^{2+} stimulation of a highly aggressive breast cancer cell line induced a ~10-fold increase in proteolytic matrix metalloproteinase (MMP) EV release, which enhanced the degradation of the extracellular matrix (ECM) and thus the ability

of cancer cells to invade into neighbouring tissues and vasculature[144, 166]. Similarly, removal of free extracellular Ca^{2+} stimulated the release of EVs by ovarian cancer (OC) cells that induced biophysical and functional changes in OC-derived fibroblasts, and elicited a pronounced effect on recipient cell adhesion and migration[167]. The EV-mediated transfer of Ca^{2+} channels, such as the aforementioned TRPC5, can also upregulate Ca^{2+} signalling in recipient cells, and subsequently promote chemoresistance in a chemosensitive cell population[112]. From these many examples, the interconnected relationship between Ca^{2+} homeostasis, EVs and tumorigenesis is stark, and poses as a potential node of therapeutic intervention in cancer treatment. Unravelling the pathway(s) and channels involved in Ca^{2+}-induced EV biogenesis may therefore lead to significant clinical applications.

1.3. CANCER AND METASTASIS

All human cancers share six essential biological capabilities that collectively dictate malignant growth, characterised by Hanahan and Weinberg as "the hallmarks of cancer". These are: (1) self-sufficiency in growth signals; (2) insensitivity to growth-inhibitory signals; (3) evasion of programmed cell death; (4) limitless replicative potential; (5) sustained angiogenesis; and (6) tissue invasion and metastasis[168]. Continued research over the past two decades has since recognised reprogramming of energy metabolism and evading immune destruction as additional cancer hallmarks, as well as a critical role for intercellular communication within the TME in facilitating metastasis[169]. Typically, metastasis is the final hallmark acquired by a primary tumour and leads to the establishment of secondary tumour sites[168]; which constitutes the primary cause of death for >90% of patients with cancer[170]. Yet despite being the key cause of mortality and failure of cancer therapy, the dynamics of metastasis and contributing molecular pathways remain poorly understood.

1.3.1. THE METASTATIC CASCADE

The process of metastasis is characterised by a series of interconnected steps that enable cancer cells to leave their primary site, circulate in the bloodstream and colonize at distant sites[171, 172]. The metastatic cascade originates in the primary tumour where the shortage of oxygen and nutrients stimulates the formation of new blood vessels that serve the growing mass and facilitate metastasis, known as tumour angiogenesis[173, 174]. The onset of angiogenesis, termed the 'angiogenic switch', is initiated by a shift in the balance of pro- and anti-angiogenic factors, favouring pro-angiogenic gene expression and thus inappropriate angiogenesis[174]. Tumour-associated vessels are often incompletely formed with abnormal architecture, characterised by

increased fenestration and 'leakiness' which serves as an outlet for the cancer cells to enter the systemic circulation[175, 176].

In order to dissociate from the primary tumour and enter the circulation, cancer cells must acquire a more motile phenotype, detach from the cytoskeleton of adjacent cells and basement membrane (BM) and advance their invasive capabilities[177]. The acquisition of these traits is mediated by a transdifferentation process known as epithelial-mesenchymal transition (EMT), whereby cancerous epithelial cells undergo molecular and biochemical alterations to gain a mesenchymal phenotype[178, 179]. Through the process of EMT, adhesion molecules within the primary tumour including cadherins and integrins, and their cytosolic binding partners on the cytoskeleton, α-, β- and γ-catenins, are downregulated, diminishing intercellular adhesiveness and hence aiding initial dissemination[178, 180]. As a result, tight junctions, adherens junctions and desmosomes which maintain epithelial apical-basal polarity are lost, and together with the downregulation of cytokeratin's and subsequent reorganisation of the cytoskeleton, cancer cells are able to travel more effectively[178, 179]. Simultaneously with the loss of epithelial markers, EMT upregulates the expression of mesenchymal markers such as vimentin, fibronectin and neural cadherin (N-cadherin) which causes cells to adopt a more mesenchymal phenotype; showing elongated morphology with front-end/back-end polarity, a higher turnover of adhesion assembly/disassembly, and increased contractility of the actin cytoskeleton to ultimately enhance cell motility[181, 182]. The release of proteolytic MMPs is also upregulated at mesenchymal protrusions such as invadopodia, which degrade the underlying ECM and permit cell invasion into the BM[183, 184].

In cancer cell invasion, motile cells initially adhere to the BM and ECM via interactions with integrin adhesion receptors, mediated by a variety of ECM components such as collagen, laminin and fibronectin[171]. Reciprocal communication between tumour cells, the ECM and adjacent non-transformed cells contributes to creating a microenvironment conducive to metastatic cancer cell behaviour, such as increased proliferation, migration and invasive capacity[171, 185]. Tumour cells, as well as cells within the local TME, secrete an array of proteolytic enzymes including MMPs, cathepsins and urokinase-type plasminogen activator (uPA) that aid tumour cell invasion by degrading the BM and surrounding ECM[186-188]. Tumour cells can also navigate through collagenous matrices by physically deforming their shape, even in the absence of protease activity[189]. Once tumour cells have invaded through the epithelial BM and surrounding ECM, they will continue to migrate towards tumour-associated vasculature where they will adhere to and traverse the endothelial BM in the same manner[171]. This process is aided by the defective

and highly permeable architecture of tumour-associated blood vessels. Upon bypassing the BM, tumour cells then adhere to the vascular endothelial cells which retract, and enable cells to pass between them and enter the systemic circulation – termed 'intravasation'[171, 190]. Whilst it's generally accepted that distant metastases occur predominantly through the haematogenous route described, many cancer types metastasize to local lymph nodes through the lymphatic system by bypassing the comparatively weak intercellular junctions between endothelial cells of the lymphatics. This can occur early in tumour progression, and is a poor prognostic marker of widespread dissemination[191, 192].

When circulating tumour cells reach the capillary bed of their target organ, they will attach to the vessel endothelium through a similar mechanism to that of leukocyte recruitment at inflammatory sites[193]. Initially, tumour cells loosely associate with selectins expressed on endothelial cells, and are pushed along the vascular endothelium by the flow of blood in a rolling movement[194]. This early tethering and rolling of tumour cells along the endothelium is transient and reversible, however upon reaching the target site, this interaction is stabilised to form a firm adhesive connection by the upregulation of integrins and immunoglobulin (Ig) superfamily members[194]. Once this connection is established, tumour cells migrate out of the blood vessel and extravasate to the target organ. There are a number of proposed methods by which tumour cells penetrate the endothelium and migrate out of the blood vessel wall, known as diapedesis or transendothelial migration[195]. Firstly, *in vivo* imaging of tumour cells in the portal vein of mice showed that upon tumour cell adhesion and integrin recognition, endothelial cells retract as in intravasation, allowing tumour cells to pass through and migrate to the underlying BM[171, 196]. Alternatively, tumour cells can disrupt interendothelial adherens junctions by stimulating the phosphorylation of vascular endothelial (VE)-cadherin – a prerequisite for adherens junction disassembly – as well as activating Rac1, which stimulates an increase in reactive oxygen species in endothelial cells[197-199]. Once tumour cells have migrated through the vascular endothelium, they degrade and invade through the underlying BM and into the local tissue by the same mechanisms as invasion at the site of the primary tumour[171]. Upon successful extravasation to the secondary tissue, tumour cells can remain dormant until activation at a future time point or begin to proliferate to form secondary tumours[200]. Secondary tumour cells lose their invasive capacity and acquire self-renewal competence through the process of mesenchymal to epithelial transition (MET), reverting back to an epithelial cell phenotype that allows them to reattach to the tissue matrix and become highly proliferative, colonizing at the new site[201-203].

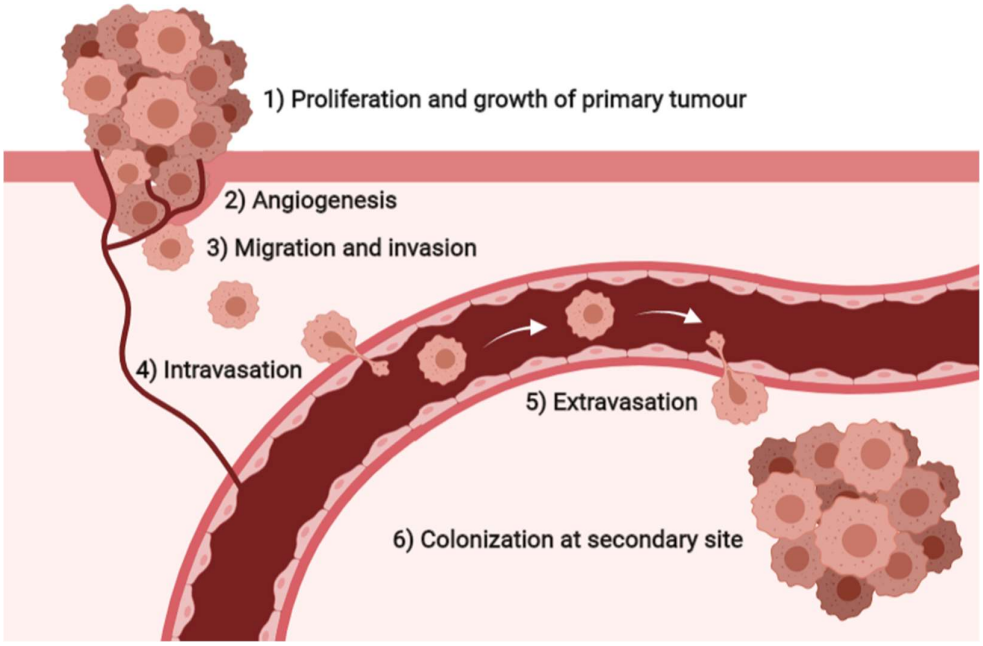

Figure 1.2 Illustrated overview of the metastatic cascade

Development of the primary tumour triggers altered gene expression profiles which drive the expansive proliferation and growth of the primary tumour (1), which in turn stimulates the formation of new blood vessels serving the primary tumour in (2) angiogenesis. Cancer cells become more motile and leave the primary tumour site, invading through the basement membrane and migrating through the extracellular matrix (3). Invaded cells intravasate into the vasculature (4) and circulate in the bloodstream before adhering to the vascular endothelium at secondary sites and extravasating into the local tissue (5). Proliferation at the secondary site instigates colonization in the metastatic organ (6).

1.3.2. THE ROLE OF EVS IN THE METASTATIC CASCADE

As evident throughout the metastatic cascade, the process of metastasis relies on an intricate communication network between cancer cells and cells within the local and distant TME. EVs are emerging as fundamental cell-cell communicators within this network, with roles identified in every stage of the metastatic cascade from promoting cell proliferation in primary tumours, to the migration, invasion and extravasation which permit their secondary metastasis[204, 205]. Here, the contribution of EVs in the metastatic cascade are summarised.

Tumour growth and malignant transformation

Tumour-derived EVs can promote tumour growth by upregulating proliferative signalling and increasing resistance to growth suppressors and apoptosis in recipient cells[206]. Active cancer cells typically sustain proliferation through activation of the phosphatidylinositol 3-kinase/protein kinase B (PI3K/AKT) and mitogen-activated protein kinase/extracellular signal-

regulated kinase (MAPK/ERK) pathways[169]. By transfer of these biomolecules, or oncogenic proteins which activate these signalling pathways, EVs have shown to stimulate proliferation in bladder, prostate, gastric and non-small cell lung cancer cells[207-211]. EV-mediated transfer of receptors with oncogenic activity such as epidermal growth factor receptor (EGFR) can likewise activate downstream signalling pathways which sustain proliferation, as demonstrated in both glioma and melanoma cells[33, 212]. Some studies suggest that tumour-derived EVs can also promote down-regulation of tumour suppressors by transfer of oncogenic H-ras and N-ras transcripts or Rab proteins[213], as well as miR-21 which acts as post-transcriptional inhibitor of the tumour suppressor programmed cell death 4 (PDCD4) in renal cell and ovarian serous carcinoma[214, 215]. Moreover, EVs derived from several distinct cancer cell lines are enriched with inhibitors of apoptosis proteins such as survivin, XIAP and cIAP1/2, and are thought to convey an anti-apoptotic phenotype to recipient cells[216, 217].

EMT

Metastatic cells with a mesenchymal-like phenotype are capable of maintaining their own EMT process or inducing EMT in recipient cells through the release of highly oncogenic EVs[218]. Following EMT, metastatic cells release EVs enriched for mesenchymal markers such as vimentin, MMP-1, MMP-19 and MMP-14, and are depleted of epithelial markers E-cadherin and EpCAM[219]. Functional studies demonstrate that treating non-metastatic/normal cells with EVs derived from tumour cells undergoing EMT can induce the EMT phenotype in recipient cells[220]. Likewise, several studies report that EVs released from metastatic cell lines can induce mesenchymal features in epithelial cancer cells through delivery of EGFR, LMP-1, miRNA-105 and miRNA-200[221-224].

Migration and Invasion

Tumour cells remodel the surrounding TME in order to detach from the primary tumour and invade through neighbouring tissues and vasculature. This is in part driven by EV-mediated cross-talk between tumour cells and a variety of cell types in the TME[225-227]. For example, OC-derived EVs containing CD44 can be internalised by human peritoneal mesothelium cells (HPMCs) where they upregulate the secretion of MMP-9 and downregulate E-cadherin, thus promoting ECM degradation and reducing cell-cell adhesions to aid OC invasion[228]. Various classes of proteolytic enzymes have likewise been identified within tumour-derived EVs, including several members of the MMP family[149, 219], a disintegrin and metalloproteinase members ADAM-10 and ADAMTS1[219, 229], and extracellular matrix metalloproteinase inducer

(EMMPRIN)[230, 231]. These EVs can drive ECM degradation as demonstrated in OC, whereby ascites-derived EVs containing MMP-2, MMP-9 and uPA induced OC cell invasion through an artificial Matrigel® layer[232]. EV-mediated interactions within the TME can also enhance cancer cell motility: EVs secreted by hypoxic OC cells activate tumour-associated macrophages (TAMs) which in turn promote OC migration in a feedback loop[233]. In breast cancer, cancer-associated fibroblasts (CAFs) release EVs that increase tumour cell protrusions and the rate of migration through activation of Wnt-signaling pathways[234]. Notably, EV secretion correlates with invadopodia synthesis in head and neck squamous cell carcinoma cells, signifying an essential role for EVs in cancer cell motility[149]. In line with these findings, Sung *et al.*[235, 236] demonstrated that EVs mediate the direction and speed of migrating cancer cells *in vivo*, stabilize leading-edge protrusions and leave a 'chemotactic' trail for migrating cells to follow.

Intravasation, circulation and extravasation

In order to successfully metastasise to secondary tissues, tumour cells must traverse the endothelial BM of blood vessels, evade the immune response whilst travelling through the blood stream, and exit at their target site – detailed in Section 1.3.1. Two independent studies investigating the role of breast cancer EVs in intravasation demonstrated that through EV-mediated transfer of miRNA-105 and miRNA-181c, EVs degraded tight junctions connecting the endothelial layer, thus increasing vascular permeability and permitting brain and lung metastasis[237, 238]. In the circulation, tumour-derived EVs can modulate the immune response by increasing immune suppressor cell populations, reducing antigen presentation, and inhibiting T-cell and natural killer (NK) cell proliferation[239]. The latter was demonstrable in prostate[240], leukaemia[241] and colorectal[242] cancer cell lines, as well as the sera of cancer patients[243], as tumour-derived EVs inhibited the anti-tumour T-cell response by inhibiting T-cell proliferation and promoting apoptosis. So that tumour cells can reach their target organ, they recruit platelets in the bloodstream to shield them from physical pressures and aid their adhesion to the endothelium via E-, L- or P- selectin expression[244]. A study by Heijnen *et al.* showed that platelet-derived EVs contained P-selectin, amongst other adhesion molecules, and can therefore aid tumour cell extravasation to the secondary tissue[245].

1.4. OVARIAN CANCER

1.4.1. EPIDEMIOLOGY

Ovarian cancer (OC) is the seventh most commonly diagnosed cancer among women worldwide and the deadliest gynaecologic malignancy[246, 247]; with a 10-year survival rate of only 35%

compared to 51% for cervical cancer and 73% for uterine[248]. The case-to-fatality ratio for OC is also much higher than more common cancers such as breast (24%), colorectal (47%) and prostate (22%)[248]. The high mortality rate associated with OC is attributable to late symptom onset and a lack of early-stage biomarkers for preventable screening[249], with 75% of cases presenting at stage III or IV when metastasis to the peritoneal cavity or upper abdominal organs is already established[250]. Only 15-20% of OC cases are diagnosed at a localized stage (stage I); when the 5-year survival rate is still high (93%)[248, 251].

1.4.2. CLASSIFICATION

OC is a highly heterogenous disease and can originate from three potential cell types: epithelial cells that cover the surface of the ovary, germ cells derived from the endoderm that proliferate and differentiate into oocytes, and stromal cells of the primitive sex cords (granulosa, sertoli and theca cells) or ovary tissue[252]. Of these cell types, germ cell tumours are the rarest, accounting for only 5% of malignant disease, followed in incidence by sex cord stromal tumours which constitute 7% of cases, and epithelial OCs (EOCs) which account for up to 90% of all malignant OC diagnoses[252, 253]. Depending on the histology of the epithelial cells, EOC can be further divided into five main subtypes: high-grade and low-grade serous, endometroid, clear cell and mucinous[252, 254]. Each subtype differs in their morphological, molecular and genetic characteristics, and are classified by their aggressiveness into type I and type II tumours[255]. Typically, type I tumours which include endometrioid, clear cell, mucinous and low-grade serous carcinomas are low-grade, genetically stable and slow-growing, and thus associated with an elevated survival time of 82 months compared to 30 months for type II tumours[256]. Conversely, type II tumours include more aggressive subtypes such as high-grade endometroid, serous and undifferentiated carcinomas, which are typically high-grade, genetically unstable, poorly differentiated and show a high propensity to metastasize[250]. Type II tumours represent ~75% of all OC cases, and are often diagnosed at an advanced stage with poor prognosis[250].

1.4.3. TREATMENT

The first line of treatment for OC consists of maximal cytoreductive, or 'debulking' surgery, whereby as much of the cancerous tissue as possible is removed from the ovaries and peritoneal cavity. This is most effective for low-grade, localised OC, and may result in complete remission without the need for adjuvant chemotherapy[257]. In cases where metastasis to the reproductive organs (uterus, fallopian tubes), sigmoid colon and omentum lining of the bowel and abdominal cavity is already established in advanced disease (stage III/IV), surgery may involve complete resection of these anatomical structures[257]. Patients with inoperable lesions or residual tumour

nodules following surgery are treated with a regime of intravenous or intraperitoneal chemotherapy, consisting of platinum (cisplatin, oxaliplatin, carboplatin) and taxane (paclitaxel, docetaxel)-based drugs[257, 258].

Cisplatin, or its less toxic derivative carboplatin, are the most commonly employed first-line chemotherapy regimens[259, 260]. These platinum-derived drugs exert anticancer effects by binding to and distorting DNA conformation, subsequently inhibiting replication and transcription. This activates a DNA damage response, thereby triggering multiple repair pathways that induce cell-cycle arrest and apoptosis[261, 262]. Despite a consistent rate of initial responses, almost 45% of OC cases ultimately relapse, gaining a chemoresistant phenotype that results in therapeutic failure[262]. OC cells can activate multiple molecular mechanisms to confer cisplatin resistance. These include mechanisms of pre-target resistance, whereby OC cells deregulate the expression of transmembrane transporters to reduce uptake and increase efflux of cisplatin; on-target resistance to impair recognition of DNA adducts and/or increase tolerance to unrepaired DNA lesions; and defects in apoptosis signalling pathways elicited by cisplatin-mediated DNA damage or compensating molecular circuitries (post-target and off-target resistance)[262]. In an attempt to overcome chemoresistance, cisplatin treatment is often combined with taxane-based drugs, or recently approved anti-angiogenics, poly(ADP-ribose) polymerase (PARP) inhibitors, growth factor or folate receptor inhibitors, as well as several novel immunotherapeutic approaches[257]. Yet despite these recent therapeutic advances, metastatic OC is still largely an incurable disease, with successive chemotherapeutic regimens considered life-extending, rather than curative.

1.4.4. OC METASTASIS

OC is unique in its method of metastasis, differing markedly from the classical haematogenous route detailed in 1.3.1 used by most cancers. The process of metastasis appears to be less complex for OC, as dissociated OC cells are able to passively migrate through the peritoneal fluid where they invade into the mesothelial cell layers that line all organs within the peritoneal cavity[263]. Interestingly, OC dissemination follows the "seed and soil" hypothesis proposed by Paget in 1889, whereby cancer cells preferentially metastasise to specific organs/tissues that support their survival and outgrowth, now referred to as the "pre-metastatic niche"[264, 265]. In the case of OC, the mesothelium acts as the "soil", with metastasis into the deeper layers of the peritoneum or outside of the abdominal cavity rare, even following an infusion of malignant OC cells into the systemic circulation[266]. Although the favourable characteristics of the mesothelium and the factors that confer them are poorly understood, EVs released by OC cells or the TME have shown to prime the pre-metastatic niche to promote OC colonization and metastasis[264].

Despite favouring a different route of metastasis, the cellular mechanisms required to dissociate from the primary tumour and invade into the secondary tissue (detailed in Section 1.3.1) remain largely the same in OC. For example, OC cells must undergo EMT in order to detach from the BM and adjacent cells at the primary site, resist stress and apoptosis, and acquire a more invasive phenotype[267]. The loss of E-cadherin - an epithelial adhesion glycoprotein - in EMT appears to be critical for OC dissemination and invasion, as E-cadherin expression is lower in highly invasive, dissociated OC cells floating in ascites and at metastatic sites compared to the primary tumour[268]. Moreover, the absence of E-cadherin expression in OC predicts poor patient survival[269]. Simultaneously with the loss of E-cadherin, EMT upregulates the expression of N- and P-cadherins and α2β1 and α3β1 integrins that subsequently activate MMP-1 and -9 to cleave the remaining E-cadherin ectodomain, causing OC cells to shed from the epithelial layer into the peritoneal fluid as single cells or clusters[250, 270]. Dissociated OC cells are then transported by the physiological movement of the peritoneal fluid through the peritoneal cavity, where they preferentially attach to the mesothelial cells covering the BM of the peritoneum and omentum. Adhesion is mediated by the up-regulation of several integrins, including α5β1 which binds to the ECM component fibronectin[271], and αvβ3 which binds vitronectin[272], as well as the surface receptor CD44[273] and cancer antigen 125 (CA125)[274]. The upregulation of MMP-2 by OC cells aids α5β1- and αvβ3-integrin adhesion by cleaving fibronectin and vitronectin into smaller fragments, enabling stronger adhesions to be formed[275]. Once attached to the mesothelium, OC cells undergo MET and stimulate the formation of new blood and lymphatic vessels to sustain their growth, ultimately colonizing at the secondary site[250, 276]. Alternatively, clusters of OC cells can accumulate within the peritoneal lymphatic vessels as they are transported through the peritoneal cavity, leading to lymphatic dissemination[277]. Indeed, metastasis to the pelvic and/or para-aortic lymph nodes is seen in more than 60% of OC cases, and lymph node metastasis is therefore used for identification of stage III and IV OC[278-280].

Whilst passive metastasis to the peritoneal cavity and lymphatic dissemination appear to be the predominant routes of OC metastasis, there is evidence to suggest that OC can also disseminate through the vasculature. A study by Pradeep *et al.* demonstrated that SKOV3 OC cells were able to spread between a host-mouse, directly injected with SKOV3 cells, to a naïve guest-mouse through a surgically united circulation, by first colonizing the omentum and subsequently metastasising to the peritoneum and abdominal organs[281]. The molecular mechanisms that contribute to OC metastasis, regardless of dissemination route, are poorly understood, and require further investigation. Independent studies propose EV-mediated communication within

the TME (detailed in Section 1.3.2), and the deregulation of cation channels to be significant contributing factors to OC metastasis.

1.5. TRANSIENT RECEPTOR POTENTIAL CHANNELS

1.5.1. PHYLOGENY AND FUNCTIONS

The transient receptor potential (TRP) superfamily constitutes one of the largest and most diverse ion channel families, displaying a broad range of activation mechanisms and cation selectivities[282, 283]. TRP channels are differentially expressed across almost all cell types, and are present in all cellular membranes with the exception of the nuclear envelope and mitochondria[283]. At the plasma membrane where TRP channels are predominantly located, they are essential mediators of Ca^{2+}, magnesium (Mg^{2+}) and trace metal ion influx, and therefore contribute to a range of physiological processes including sensory functions (taste, nociception, thermosensation), homeostatic functions (Ca^{2+}/Mg^{2+} reabsorption, osmoregulation), and other motile functions such as muscle contraction and vasomotor control[282, 283]. The function of TRP channels is determined by their associations with accessory proteins, and by formation of signalling complexes with various signalling proteins[283].

All TRP channels contain six transmembrane domains with a pore-forming re-entrant loop between domains 5 and 6, and are flanked by intracellular N- and C-termini[284, 285]. The TRP family is subdivided into seven subfamilies, which can be broadly categorized into group 1 and 2 TRPs by their sequence and topological differences (Figure 1.3)[282]. Group 1 TRPs include TRPC (canonical), TRPV (vanilloid), TRPM (melastatin), TRPCA (ankyrin) and TRPN (NOMPC-like), and group 2 consists of TRPP (polycystin) and TRPML (mucolipin). Both group 1 and 2 TRP channels are highly conserved in invertebrates and vertebrates, bar TRPC2 which is a pseudogene in humans, and TRPN which is not present in mammals[282]. The canonical TRP family (TRPC 1-7) is most closely related to *Drosophila* TRP, the first described TRP channel[286].

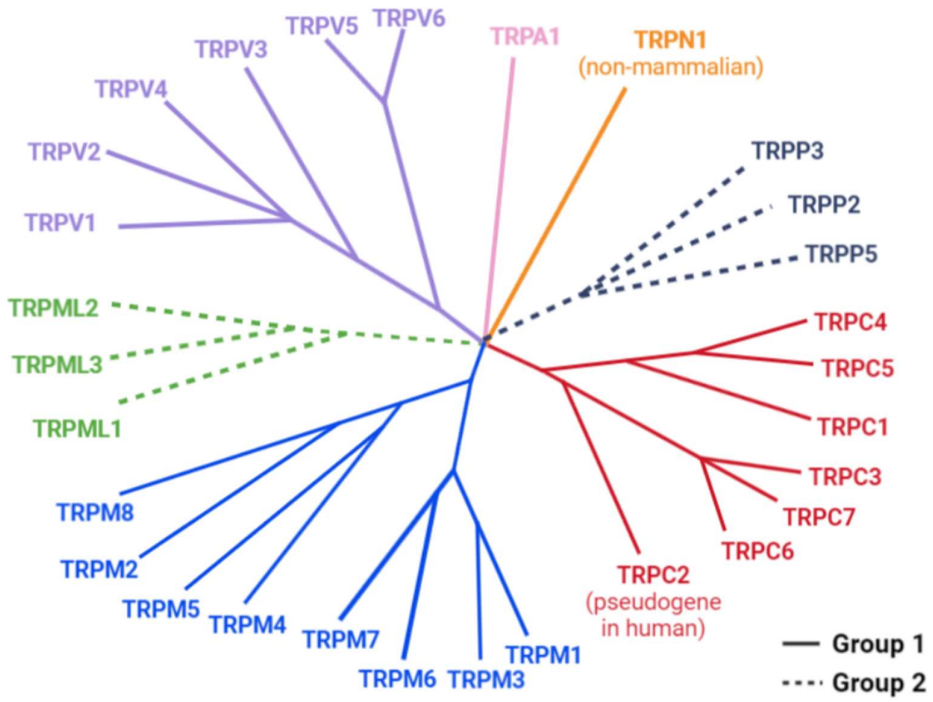

Figure 1.3 A phylogenetic tree of group 1 and 2 TRP channels

The 29 members of the TRP channel superfamily, colourised by subfamily as determined by sequence homology. Group 1 TRPs indicated by solid line: TRPC (canonical), TRPV (vanilloid), TRPM (melastatin), TRPCA (ankyrin) and TRPN (NOMPC-like), group 2 TRPs indicated by dashed line: TRPP (polycystin) and TRPML (mucolipin).

1.5.2. STRUCTURE AND ACTIVATION OF TRPC CHANNELS

The TRPC subfamily are non-selective cation channels displaying moderate selectivity for Ca^{2+} over monovalent cations[287]. Of the seven TRPC family members, amino-acid similarity classifies mammalian TRPCs into four groups: TRPC1, TRPC2 (pseudogene in humans), TRPC3/6/7, and TRPC4/5 (Figure 1.3). Overall, the seven homologs share ≥30% amino acid identity, whilst members of the TRPC3/6/7 subfamily share a high sequence homology of up to 80%[288]. These three subgroup members assemble to form both homo- and heteromeric TRPC channels[289] that are widely expressed across different human tissues, with some enrichment in the nervous system[282]. TRPC3 is the focus of this thesis, with the structure of the TRPC3 channel shown in Figure 1.4.

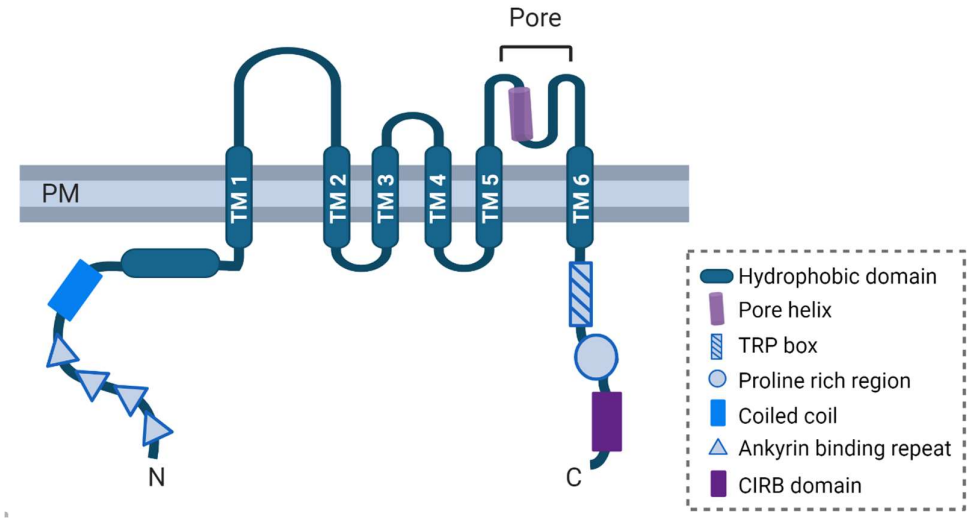

Figure 1.4 Proposed domain structure and transmembrane topology of TRPC3

TRPC3 contains six transmembrane core domains (TM1-TM6) with a pore-forming re-entrant loop between TM 5 and 6. At the cytoplasmic N-terminus, there are 4 ankyrin-like repeats, a coiled-coil domain and a hydrophobic domain preceding the first transmembrane segment. The cytoplasmic C-terminal region comprises the characteristic TRP domain and proline-rich region, followed by a calmodulin/IP_3 receptor binding domain (CIRB).

Structurally, the putative pore region of TRPC3 channels contains a conserved hydrophobic α-helix which is important for channel opening and selectivity[290-292]. At the cytoplasmic N-terminus, there are four ankyrin-like repeats which are a common protein binding domain, and interact with a number of proteins that mediate downstream TRPC3 function[293, 294]. The C-terminus is essential for TRPC3 regulation, comprising a highly conserved "TRP box" domain and proline-rich motif[282], followed by a calmodulin (CaM)/inositol 1,4,5-trisphosphate (IP_3) receptor binding (CIRB) region which confers TRPC3 channel sensitivity to internal Ca^{2+} store depletion[295]. According to the conformational coupling model, TRPC3 directly interacts with ER Ca^{2+} release channels (both IP_3 and ryanodine receptors) at this region, stimulating TRPC3-mediated store-operated Ca^{2+} entry (SOCE) in response to intracellular Ca^{2+} store depletion[296-299]. Alternatively, TRPC3 heteromerization partners, namely TRPC1, can mediate store depletion-dependent activation of TRPC3[300], or Ca^{2+} entry through associated Ca^{2+} channels such as Orai1 can trigger membrane recruitment of TRPC3 and increased conductance in response to store depletion[301]. TRPC3 channels can also be activated in response to stimulation of cellular phospholipase C (PLC), downstream of G protein-coupled receptor (GPCR) and receptor tyrosine kinase (RTK) activation by external stimuli at the PM[298, 302]. In so-called receptor-operated Ca^{2+} entry (ROCE), Gq-coupled activation of PLCβ, or RTK activation of PLCγ, cleaves phosphatidylinositol 4,5-

bisphosphate (PIP2) to generate diacylglycerol (DAG) and IP_3. IP_3 subsequently activates IP_3 receptors on the ER which stimulates store depletion, leading to TRPC activation through the mechanisms described[302, 303]. Therefore, whilst ROCE and SOCE represent two independent pathways of TRPC3-mediated Ca^{2+} entry, they are reciprocally regulated[304]. The other PLC product, DAG, can also stimulate TRPC3 Ca^{2+} influx by directly binding the channel, although this mechanism has only been demonstrated for the TRPC3/6/7 subgroup[305]. Hence, TRPC3 and its relatives TRPC6 and TRPC7 are considered as a unique family of lipid-sensitive cation channels.

Given the central role of TRPC3 channels in regulating Ca^{2+} homeostasis, dysregulation of TRPC3 channel activity is associated with a broad-spectrum of diseases[306]. Emerging evidence over the past decade has revealed that TRPC3 channels are frequently deregulated in cancer, and promote multiple pathophysiological cancer hallmarks [162].

1.5.3. TRPC3 IN CANCER

The TRPC channel family member TRPC3 is amplified in numerous cancers and promotes tumorigenesis through mediating sustained elevated Ca^{2+} [162]. Aberrant Ca^{2+} signalling deregulates Ca^{2+}-sensitive downstream effectors which control cell cycle progression, survival, apoptosis, migration and gene expression towards a cancer-promoting phenotype[307]. Namely, TRPC3 channels are key regulators of the cell cycle, therefore the overexpression and/or overactivity of TRPC3 is associated with cell cycle progression and proliferation in a number of cancer cell types[308-311]. Utilising the TRPC3-selective inhibitor Pyr3, numerous studies have demonstrated that inhibiting TRPC3 arrests the cell cycle, whilst simultaneously inducing apoptosis, leading to a significant reduction in overall cancer cell growth. In triple negative breast cancer cells, Pyr3 suppressed cell proliferation through sub-G1 accumulation, and by activating ERK 1/2, induced apoptosis via upregulation of cleaved caspase-3/7 and PARP[311]. Pyr3 also had an inhibitory effect on the cell proliferation, survival, migration, and G0/G1 phase transition in gastric cancer cell lines[309]. Interestingly, by forced expression of TRPC3, the authors demonstrated that TRPC3-mediated ROCE regulates cell cycle checkpoint, apoptosis cascade, and intracellular reactive oxygen species (ROS) production via activation of T cell 2 (NFATc2) nuclear translocation, which ultimately promoted gastric cancer tumorigenicity[309]. The pro-tumorigenic role of TRPC3 has also been demonstrated *in vivo,* as downregulation of TRPC3 expression, or administration of Pyr3, reduced tumour growth in mouse models of glioblastoma, gastric and ovarian cancer[308-310]. Indeed, a critical role for TRPC3 channels in the development of ovarian cancer (OC) has recently been identified. Utilising the non-selective TRPC blocker SKF96365 and TRPC3 knockdowns, Yang *et al.*[310] demonstrated that reduced activity/expression

of TRPC3 suppressed OC growth both *in vitro* in SKOV3 cells, and *in vivo* in nude mice injected with SKOV3 cells knocked down for TRPC3. *In vitro,* reduced TRPC3 activity arrested the cell cycle at M phase, suggesting TRPC3 promotes the proliferation of OC cells by contributing to metaphase exit. TRPC3 protein expression was also markedly increased in human OC compared to non-cancerous specimens. Further studies investigating the hormonal activation of TRPC3 validated the central role of TRPC3 in OC proliferation, as both FSH and oestrogen promoted OC proliferation through TRPC3 activation[312, 313]. These studies demonstrate a vital role for TRPC3 in the proliferation and cell-cycle progression of OC cells *in vitro* and *in vivo*.

The role of TRPC3 in other metastatic mechanisms of OC, such as migration and invasion, are yet to be investigated. Cell migration involves a variety of temporally and spatially coordinated Ca^{2+}-sensitive processes ranging from cell polarization, cell-cell and cell-basement membrane adhesions, as well as reorganisation of the cytoskeleton[314-316]. Ca^{2+} channels and transporters are therefore key regulators of cell migration, with several members of the TRP channel family implicated in promoting tumour cell motility[317], including TRPC3. Hitherto, TRPC3 has been shown to contribute to the migration of glioblastoma and melanoma cells, as well as cancerous and non-cancerous gastric cells[308, 309, 318]. In glioblastoma cells, inhibition of TRPC3 with Pyr3 reduced cell migration and invasion through impairing focal adhesion and cytoskeleton protein expression, namely focal adhesion kinase (FAK) and myosin light chains (MLC)[308]. Pyr3 also inhibited cell migration in melanoma cells by downregulating the secretion of proteolytic MMP9, which dissolves type IV collagen in basal membranes[319], thereby enhancing cellular migration ability[318]. Moreover, inhibition of TRPC1/3/6 has shown to mitigate EMT in gastric cancer cells[320]; a process by which cancer cells acquire a more motile and invasive phenotype (see Section 1.3.1). Additional studies have also implicated TRPC3 in mediating endothelial adhesion[321] and angiogenesis[313]. Together, these studies propose TRPC3 as an essential mediator of numerous metastatic mechanisms, that require further investigation in OC.

1.5.4. TRPC CHANNELS AND EV RELEASE

As discussed in Section 1.2, there is accumulating evidence to suggest that EVs may act as Ca^{2+}-driven downstream effectors in cancer progression. Indeed, EV release is stimulated by increases in intracellular Ca^{2+} in a variety of cancer cell types[143-145], with a number of molecules in the Ca^{2+} signalling cascade implicated in this response - including TRPC channels. For example, TRPC5 has shown to be required for EV release from chemoresistant breast cancer cells, and is enriched in EVs *in vitro* as well as in peripheral blood from breast cancer patients[112, 322]. TRPC6 and TRPC3 have likewise been identified within EVs from the OC cell line IGROV1[323] and

glioblastoma respectively[324], suggestive of their association with the biogenesis pathway. IP_3, and a number of GPCRs which regulate TRPC3-mediated Ca^{2+} entry, have also previously been implicated in the EV secretion pathway[143, 325].

Mutations in TRPC3 have also been linked with alterations in EV biogenesis pathways. A gain-of-function mutation (T635A) in TRPC3 in the ataxic *Moonwalker (Mwk)* mouse mutant promotes increased Ca^{2+} signalling upon overexpression in mouse neuronal cell lines as determined by assessing nuclear translocation of the Ca^{2+}-sensitive transcription factor NFAT, as well as *in vivo* in *Mwk* Purkinje cells[326, 327]. Microarray analysis conducted on the *Mwk* mouse mutant revealed that increased Ca^{2+} influx was coupled with significant alterations in lipid metabolism and vesicle fusion pathways, with several of the altered transcripts implicated in the biogenesis and/or secretion of EVs[326]. These included Unc13c, Smpd1, Snap23 and Tsg101. A pilot study conducted prior to the work presented in this thesis revealed that a number of these transcripts were likewise deregulated in human induced pluripotent stem cells (hiPSCs) which harboured a gain-of-function mutation (R762H) in the TRPC3 gene, derived from a patient diagnosed with a novel ataxic disorder termed spinocerebellar ataxia type 41 (SCA41)[328] (Figure 1.5 A). Notably, four of the six genes assayed followed the same pattern of deregulation as shown in the *Mwk* mouse model[326]. In addition, preliminary results demonstrated a detectable difference in EV release between TRPC3-mutant and control hiPSCs at 24 hours (Figure 1.5 B). Collectively, the existing literature reported here paired with these preliminary results proposes a direct link between TRPC3 and EV biogenesis, which forms the foundation of this project.

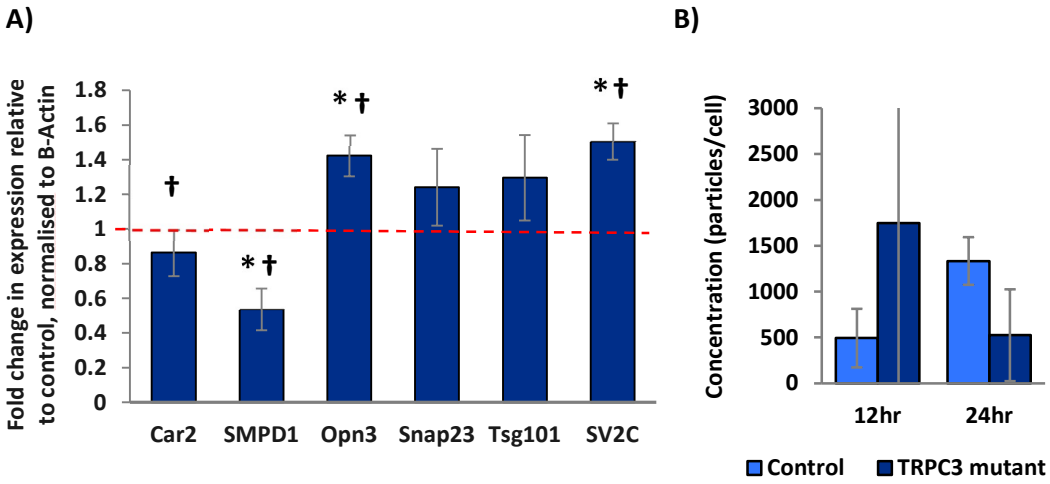

Figure 1.5 TRPC3 mutant hIPSCs display replicable expression changes in EV-related transcripts and a detectable difference in EV release

(A) *qRT-PCR analysis of TRPC3 mutant hiPSC gene expression, represented as fold change relative to control hiPSCs. All values normalised to β-actin expression. Data represents mean ± SEM of three independent experiments with statistical significance tested by students t-test: *P<0.05, † same trend as Mwk mouse. Error bars represent SEM of ΔCT values.* ***(B)*** *The total number of particles released per cell by control and TRPC3 mutant hiPSCs at 12- and 24-hour time points, as determined by NTA. Data representative of two biological replicates, with error bars representing the standard deviation between each replicate. Data author's own. qRT-PCR analysis performed in collaboration with Dr Lauren Watson.*

1.6. PROJECT AIMS AND OBJECTIVES

EVs are emerging as fundamental cell-cell communicators in cancer progression with roles identified in every stage of the metastatic cascade, and thus represent a potential node of therapeutic intervention in cancer. One of the main factors hindering our ability to engineer EV signalling for clinical applications is the lack of knowledge of molecular mechanisms underlying their formation and release, and how manipulating these mechanisms influences EV cargo and their metastatic capacity. An accumulating body of evidence highlights the role of Ca^{2+} and upstream GPCR stimulation in EV release - with preliminary data to suggest TRPC3 may facilitate Ca^{2+}-mediated EV biogenesis. This discovery, together with the emerging role of TRPC3 in the progression of OC, proposes that TRPC3-mediated EV release may contribute to the development of OC. The aims of this thesis were therefore to a) investigate the role of TRPC3 and TRPC3-mediated EV communication in OC and b) to investigate how TRPC3 activation, Ca^{2+} influx and upstream GPCR stimulation affect EV biogenesis and cargo. The specific objectives were to:

1. Assess how modulating TRPC3 activity influences the growth, migration and invasion of OC cells
2. Investigate a novel role for TRPC3-mediated EV communication in metastatic mechanisms of OC
3. Investigate the role of TRPC3, Ca^{2+} influx and GPCR stimulation in MVB-derived EV biogenesis using live single-cell imaging
4. Characterise the proteomic cargo of TRPC3 activator, Ca^{2+}, and GPCR-induced EVs to derive mechanistic insights into how these treatments influence EV biogenesis and cargo

Chapter 2

Materials and methods

2. Materials and methods

2.1. CELL CULTURE

2.1.1. CELL LINE MAINTENANCE

Human ovarian cancer cell lines SKOV3, OVCAR3, OVCAR5, IGROV1 and A2780 were initially employed in this study to measure endogenous expression of TRPC3 in OC lines of different cellular origins. SKOV3, a highly tumorigenic cell line derived from a non-serous carcinoma[329-332], was taken forward as the principal line of study in all further experiments. SKOV3, OVCAR3, OVCAR5 and IGROV1 were purchased from the National Cancer Institute, Frederick Cancer Division of Cancer Treatment and Diagnosis Tumour/Cell Line Repository (Bethesda, USA). The A2780 cell line was kindly gifted by Professor Robert Brown, Imperial College, London, UK. All cell lines were cultured in RPMI 1640 medium (Lonza) supplemented with 10% (v/v) heat-inactivated foetal bovine serum (FBS) (Gibco™). The cellular origin, cancer type and characteristics of each cell line are detailed in Table 2.1.

All cell lines were maintained in 75cm^2 or 175 cm^2 flasks in humidified incubators at 37°C and 5% CO_2. Cells were passaged twice per week at ~75% confluence, assessed by a Zeiss Primovert inverted microscope. During passage, cell media was aspirated and adherent cells were washed with 5ml Dulbeccos phosphate buffered saline (DPBS) (Gibco™) and dissociated with a sufficient volume of 0.33% (w/v) Trypsin-ethylenediamine tetra acetic acid (EDTA) (Gibco™) in PBS. Cells were incubated with Trypsin-EDTA for five minutes or until cells were fully detached. A 2X volume of fresh, pre-warmed media was then added to the cell suspension to inactivate the trypsin, and cells were pelleted by centrifugation at 1,300rpm for five minutes. Cell supernatant was then discarded, and the cell pellet re-suspended in 10ml fresh media. For general sub-culturing, cells were then seeded into new flasks at 1:4-1:8 dilution and returned to the incubator. For experiments, cells were seeded at set densities based on the well surface area of the plate used and required incubation period, detailed for each experiment. To calculate the cell volume required for each density, cell counts were conducted either manually using a haemocytometer or using a TC20™ automated cell counter (Bio-Rad).

For all experiments and cell types, cells were initially seeded in complete media (RPMI 1640 supplemented with 10% FBS). In experiments conducted in serum-free and EV-depleted FBS media, the media was switched as required once cells had reached ~70% confluence. EV-depletion of FBS was carried out by high-speed ultracentrifugation in open-topped tubes in a SW32Ti swing-bucket rotor (both Beckman Coulter) at 120,000g for 16hr at 4°C. After

ultracentrifugation, supernatant was pipetted off and filter sterilised with a 0.22µm filter and aliquoted for storage at -20˚C.

Table 2.1 The origin, type and characteristics of all ovarian cancer cell lines used in this project

Invasiveness assessed by Matrigel assay; migration assessed by wound healing assay at 30hr. High-grade serous carcinoma (HGSC).

Cell line	Type	Origin	Mutations	Doubling time (hr)	Invasiveness	Migration
SKOV3	Epithelial, non-serous carcinoma [331-333]	Ovary, ascites	PIK3CA; HRAS; ARID1A; Heterozygous loss of BRCA1, BRCA2; CTNNB1	27	High	>90%
OVCAR3	Epithelial, HGSC [331, 333, 334]	Ovary, ascites	Heterozygous loss of BRCA1, BRCA2	34.7	Moderate	~40%
OVCAR5	Epithelial, HGSC [329, 334]	Ovary, ascites	KRAS	48.8	High	~60%
IGROV1	Mixed: endometroid, serous, clear cell [332, 335]	Ovary, tumour tissue	ARID1A; BRCA1; BRCA2; PTEN; PIK3CA	27	Low	~20%
A2780	Epithelial, endometrioid [332, 333]	Ovary, tumour tissue	ARID1A; BRCA2; PTEN; PIK3CA	18	Low	<20%

2.1.2. FREEZING DOWN CELL STOCKS AND REVIVING CELLS FROM FROZEN

All cell stocks were made at an early passage (p 4-6) to ensure cell viability for future experiments. Confluent cells from a 75cm^2 flask were dissociated and pelleted as described in 2.1.1, and resuspended in 5ml of freezing medium (95% complete media + 5% dimethyl sulfoxide (DMSO) (Corning™)). The cell suspension was aliquoted in 1ml per cryovial (Thermofisher) and placed in a Mr Frosty™ freezing container (Nalgene™) at -80°C for 24hrs, before being transferred to liquid nitrogen for long-term storage.

Cell lines were kept in culture until ~p25, at which point a new cell stock was thawed. Cells were thawed from liquid nitrogen in a 37°C water bath until ice was almost melted, and transferred to a 15ml falcon tube containing 5ml pre-warmed complete medium to dilute the DMSO. Cells were then pelleted at 1000rpm for 3 minutes, the supernatant discarded, and cells re-suspended in 1ml of complete media. The full cell suspension was then seeded into a 25cm^2 flask containing 7ml complete media and placed in the cell culture incubator for 24hrs, at which point the cell media was changed or cells were split, depending on their confluence. In the first passage after thawing, 100% of cells were transferred to a 75cm^2 flask.

2.1.3. CELL TRANSFECTIONS

GFP-tagged NFAT

To assess Ca^{2+} signalling in SKOV3 cells, NFAT translocation assays were used. GFP-tagged NFAT constructs (Addgene, 11107 – Figure 2.1) were transiently transfected into SKOV3 cells. Cells were seeded in complete medium at a density of $0.6x10^5$ in 24-well plates on sterile, 13mm glass coverslips, and cultured to 50-70% confluency prior to transfection. 500ng NFAT-GFP DNA was diluted in Opti-MEM™ reduced serum medium (Gibco™), to which the FuGENE HD transfection reagent (Promega) was added at a 3:1 FuGENE to DNA ratio. Each tube was then briefly vortexed and incubated at room temperature (RT) for 10 minutes. In this time, cells were gently washed with PBS and the culture medium was refreshed. Following incubation, 50µl of the DNA/FuGENE mix was added to each well. Treatments were added to cells 24hrs post-transfection.

Figure 2.1 Plasmid map of the GFP-tagged NFAT construct transiently transfected into SKOV3 cells for NFAT translocation assays (Addgene, 11107)

CD81/CD63/CD9 pHluorin plasmids

CD81/CD63/CD9 pHluorin plasmids used to visualise MVB-PM fusion by TIRF microscopy (see Section 2.8) were kindly provided by Professor Aled Clayton, Cardiff University (see Figure 2.2 for plasmid maps). SKOV3 cells were seeded in complete medium at a density of $0.4x10^5$ in an 8 well glass bottom µ-slide (Thistle Scientific) and cultured to 50-70% confluency prior to transfection. 500ng pHluorin DNA was transfected into cells as above. Cells were imaged 24hrs post-transfection.

A)

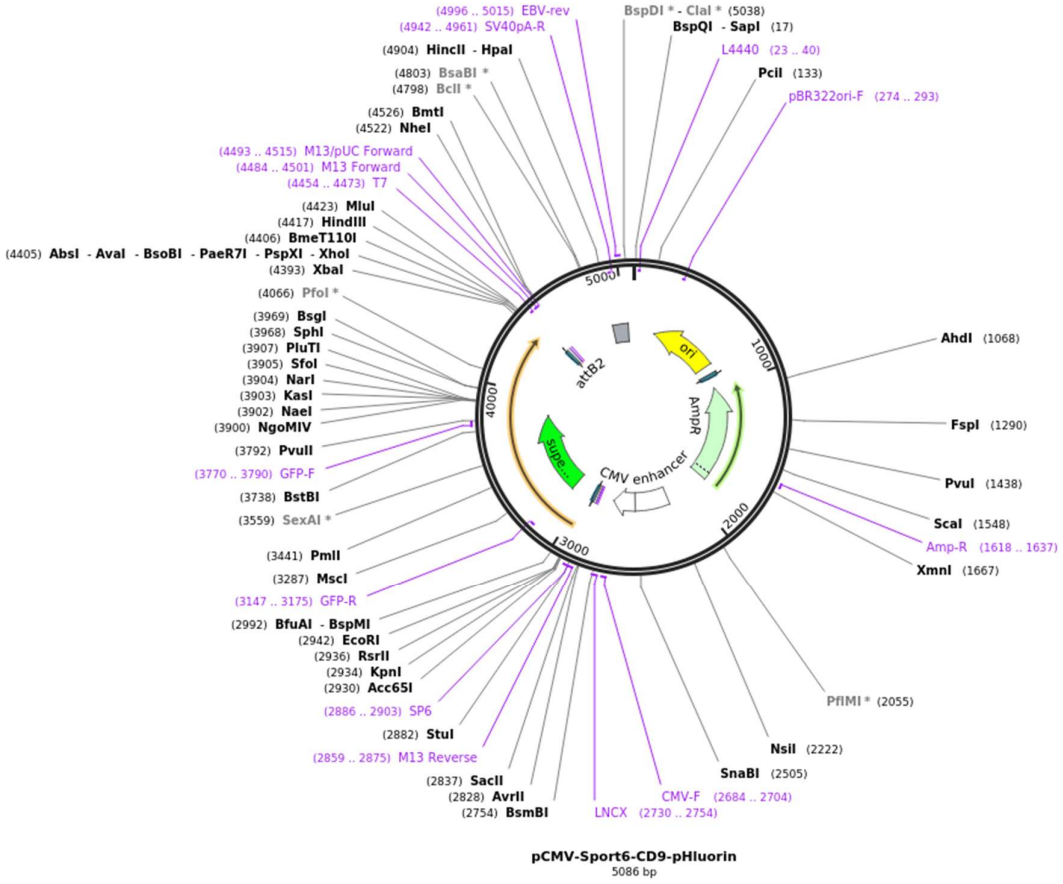

B)

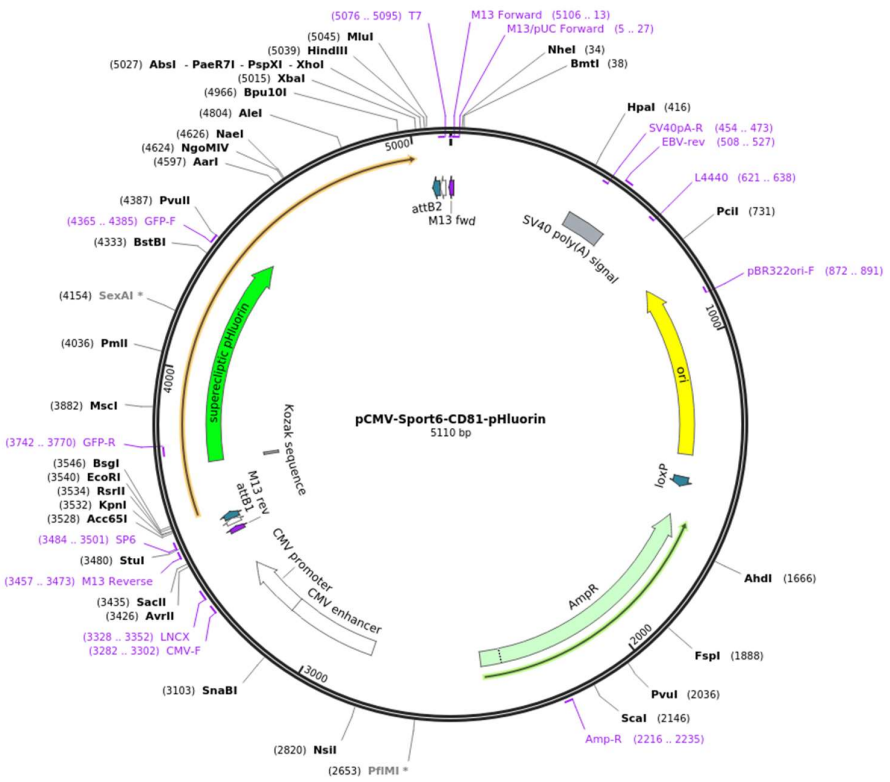

C)

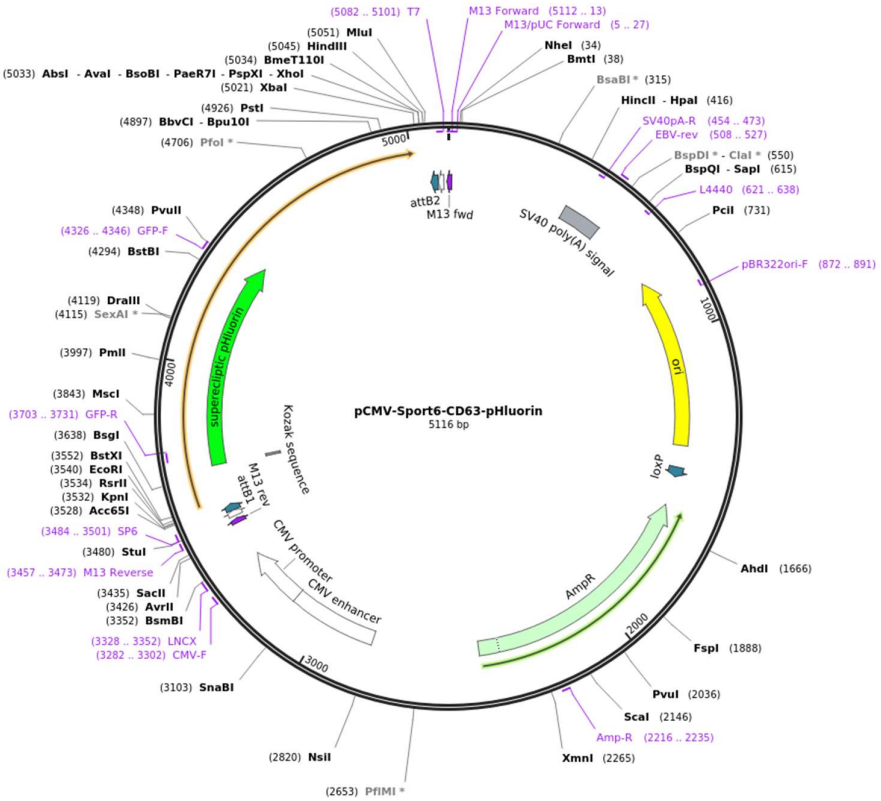

Figure 2.2 Plasmid maps for CD9, CD81 and CD63-pHluorin constructs transiently transfected into SKOV3 cells to visualise MVB-PM fusion by TIRF microscopy

(A) *CD9-pHluorin,* ***(B)*** *CD81-pHluroin,* ***(C)*** *CD63-pHluorin.*

Extracellular FLAG-TRPC3

For the detection of TRPC3 on SKOV3-EVs by the Exoview platform, SKOV3 cells were transfected with a WT TRPC3 construct that has a FLAG-tag on the extracellular domain of TRPC3, generated in-house by Dr Esther Becker: TRPC3 was cloned into the p3XFLAG-CMV™-7.1 expression vector (Sigma, E4026). Cells were transfected in Ca^{2+} free RPMI (Generon) supplemented with 5% FBS. To collect a large enough quantity of EVs for analysis, 2x 175cm^2 flasks of ~70% confluent SKOV3 cells were transfected with 38µg FLAG-TRPC3 DNA at a 3:1 FuGENE to DNA ratio, diluted in Opti-MEM™ as above. DNA concentration was calculated based on previous TRPC3 transfections in the lab carried out at 2µg DNA per well in a 6-well plate, and the surface area of a 175cm^2 flask is approximately 19x that of a 6-well. 24hrs post-transfection, the medium was switched to SFM, and transfected and non-transfected cells were conditioned for 48hrs prior to EV extraction.

2.2. CHEMICAL TREATMENTS

TRPC3 activator GSK 1702934A

The potent and selective TRPC3/6 activator GSK 1702934A[336] (Tocris) was solubilised in DMSO at a concentration of 1mM, and stored at -80°C in aliquots of 500µl to reduce cycles of freeze/thawing. At the time of treatment, an aliquot was thawed, and a serial dilution was prepared in either complete media for cell assays, serum-free media (SFM) to treat cells for EV extraction, or Tyrode's solution, pH 7.4 (2mM $CaCl_2$, 2.5mM KCl, 119mM NaCl, 2mM $MgCl_2$, 30mM glucose, 25mM HEPES) for TIRF imaging. Concentrations of 0.1-10µM were prepared in this manner, and used as stated for each experiment.

TRPC3 inhibitor Pyr3

The pyrazole compound Pyr3 (Sigma-Aldrich®), chemical name Ethyl-1-(4-(2, 3,3-trichloroacrylamide) phenyl)-5-(trifluoromethyl)-1H-pyrazole-4-carboxylate, potently and selectively antagonizes TRPC3 by binding to the extracellular side of the receptor[337]. Pyr3 was solubilised in DMSO at a concentration of 10mM and stored at 4°C as per the manufacturer's instructions. At the time of treatment, an aliquot was warmed at RT and serially diluted in the same manner as the TRPC3 activator for cell assays, EV extraction and TIRF imaging. Concentrations of 1-3µM were prepared and used as stated for each experiment.

Histamine

Histamine dihydrochloride (Sigma-Aldrich®) was stored in powder form at 4°C and prepared fresh prior to every experiment. Histamine was solubilised at a concentration of 10mM in complete medium for cell assays, SFM for EV extraction and Tyrode's solution, pH 7.4 for TIRF imaging. A final concentration of 100µM histamine was added to cells for all experiments, for the time period stated for each experiment.

Ionomycin

A ready-made solution of 1mM Ionomycin calcium salt in DMSO (Sigma-Aldrich®) was stored at -20°C in aliquots of 100µl. At the time of treatment, an aliquot was warmed at RT and serially diluted to a concentration of 1.25µM in complete medium for cell assays, SFM for EV extraction and Tyrode's solution, pH 7.4 for TIRF imaging. Cells were treated for the time period stated for each experiment.

DMSO

An equivalent concentration of DMSO was applied to control cells in all experiments where a compound solubilised in DMSO was used (TRPC3 activator, Pyr3, Ionomycin). Serial dilutions were performed side by side with the chemical compound in use. If variable concentrations of compounds were used within the same experiment, a concentration of DMSO equivalent to the highest concentration of compound was used. Final concentrations ranged between 0.01-1% DMSO.

2.3. PURIFICATION OF EVS

Prior to all EV extractions, SKOV3 cells were seeded into 175cm^2 flasks in complete medium and cultured to ~70% confluence. At this point, the media was switched to EV-depleted or serum-free medium (SFM) as required for each experiment. To extract SKOV3-EVs for initial comparisons between EV-depleted and serum-free media conditions, cells were cultured for 48hrs in either medium supplemented with 10% EV-depleted FBS (depleted as described in 2.1.1) or SFM. For SFM-EV characterisation, cells were cultured for 48hrs. For quantifying EVs extracted in SFM at various timepoints, SKOV3 cells were conditioned in SFM for 4, 8, 16, 24 and 48hrs. In all further experiments (functional analysis and proteomics), SKOV3 cells were conditioned in plain SFM or SFM supplemented with the appropriate treatment for 4hrs prior to extraction.

After the appropriate conditioning period, conditioned media was harvested and initially depleted of cells and debris by centrifugation at 300g for 5 minutes at RT, followed by 16,500g for 20 minutes at 4°C. Supernatant was then concentrated to 500µl in Vivaspin 20 100kDa concentrators (GE Healthcare) at 3000g in a swing bucket rotor. EVs were extracted from the concentrate by size exclusion chromatography (SEC) in pre-prepared columns (Biorad): columns were filled with 14ml Sepharose CL-28 (GE Healthcare) topped with PBS, and allowed to settle for at least three hours at RT to give a 10ml sepharose bed. After placing a column bed support above the resin, the column was washed three times through with PBS. The concentrate was then loaded onto the column and eluted in sterile PBS, and 20 fractions of 500µl flow-through were collected. Fractions 5-10 were enriched for EVs as determined by Nanoparticle tracking analysis (NTA). These fractions were pooled and further concentrated to the desired volume for experiments in Vivaspin 2 5kDa concentrators (GE Healthcare) at 3000g in a swing bucket rotor. For short-term storage (up to 4 days), samples were stored at 4°C, or at -80°C for long-term storage.

2.4. EV TREATMENT OF CELLS

For all EV functional analysis experiments (cell growth, migration and invasion), EVs were extracted from SKOV3 cells conditioned for 4hrs in plain SFM (untreated control), or SFM supplemented with 0.3µM TRPC3 activator, 3µM TRPC3 inhibitor or DMSO (0.03%). EVs were counted by nanoparticle tracking analysis (NTA) and cells were counted at the time of extraction as in 2.1.1 to calculate the number of EVs released per cell. Approximately 50 EVs per viable cell were counted at the time of EV extraction, therefore recipient cells were dosed with 50 particles per seeded cell at a 1x concentration, as well as two higher concentrations of 5x and 10x EVs/cell for cell growth and migration analysis. Only the 10x EV concentration was used for invasion analysis. An equivalent volume of PBS was applied to the no EV control for each concentration. Within each biological replicate for the cell growth and migration analysis, the same set of EVs were used for continuity and to reduce variability. All recipient cells were seeded in complete medium, and then switched to EV-depleted medium just prior to EV treatment to reduce contamination of FBS-EVs, whilst maintaining cell growth and viability.

2.5. CELL FUNCTIONAL ASSAYS

2.5.1. CELL COUNTS WITH TRYPAN BLUE

To assess the effect of SFM, TRPC3 activator/inhibitor and EV treatments on SKOV3 cell growth, cells were manually counted using a haemocytometer. In all experiments, SKOV3 cells were first

seeded into 12-well plates in complete medium at a density of $0.2x10^5$. For the analysis of different media conditions, the medium was switched to either complete medium, SFM or EV-depleted medium 24hrs after seeding. To evaluate the effect of TRPC3 activation/inhibition on SKOV3 cell growth, the medium was likewise switched to plain complete media (untreated control), or complete media supplemented with 0.1/03µM TRPC3 activator, 1/3µM TRPC3 inhibitor or DMSO equivalent. EV treatments were applied as detailed in 2.4. Cells were incubated in the respective treatment for 24, 48 or 72hrs. At each timepoint, cells were dissociated and pelleted as described in 2.1.1, and resuspended in 1ml of complete media. The cell suspension was mixed at a 1:2 ratio with trypan blue (Biorad) to distinguish live from dead cells, and pipetted onto the haemocytometer under a glass coverslip. A minimum of 3 wells were counted for every biological replicate in all experiments. Cell growth was also imaged just prior to dissociation by a Zeiss Primovert inverted microscope.

2.5.2. MTT VIABILITY ASSAY

Cell viability at increasing concentrations of TRPC3 activator was assessed using an MTT assay. 3(4,5–dimethylthiazol–2–yl)–2,5 diphenyl tetrazolium bromide (MTT) (Sigma-Aldrich®) is a yellow compound that is reduced to its insoluble purple derivate, formazan, by metabolically active cells. The purple precipitate is solubilised by adding MTT solvent (4mM HCl, 0.1% IGEPAL CA-630® (Sigma-Aldrich®) in isopropanol), and the absorbance of the solution is read at 570nm with a spectrophotometer. The intensity of the purple fluorescence is proportional to the number of viable cells present.

SKOV3 cells were seeded into a 48-well plate at a density of $0.5x10^5$, with 6 technical replicates per condition. At ~75% confluency, cells were treated with 0.3/1/10µM TRPC3 activator or DMSO equivalent for 4hrs, alongside untreated controls. MTT was solubilised to a concentration of 2mg/ml in complete medium, filtered through a 0.22µm filter, and added to each well at a working concentration of 1mg/ml. After 3hrs incubation with MTT, the media was pipetted out and replaced with 200µl MTT solvent. The plate was then shaken on low setting for 10 seconds and the absorbance was read on a SpectraMax i3x plate reader (Molecular Devices). To remove background absorbance from the media, the absorbance of wells containing only media and no cells was subtracted from that of experimental wells. The absorbance of experimental wells was normalised to that of untreated controls, and the percentage of viable cells extrapolated.

2.5.3. ANNEXIN V AND PROPIDIUM IODIDE APOPTOSIS ASSAY

Cell apoptosis in serum-free culture was analysed using an Annexin V-FITC and Propidium iodide Apoptosis Detection Kit (eBioscience™, Thermofisher). SKOV3 cells were seeded into 12-well plates in complete medium, and then switched to SFM or EV-depleted medium 24hrs later. After 24 and 48hrs incubation in the respective media type, cell medium was collected (to ensure dead, floating cells were analysed) and mixed with dissociated cells, collected as per 2.1.1. Cells were then processed according to the manufacturer's protocol. Analysis was conducted with a CytoFLEX S flow cytometer (Beckman Coulter) and CytExpert v2.1 software, with 10,000 events recorded per sample.

2.5.4. NFAT TRANSLOCATION ASSAY

To assess Ca^{2+} signalling in SKOV3 cells, cells were transiently transfected with GFP-tagged NFAT constructs as in 2.1.3. 24hrs post-transfection, cells were treated with 1.25µM ionomycin, 0.1/0.3/1/10µM TRPC3 activator, 100µM histamine, or a combination of histamine and 3µM TRPC3 inhibitor, alongside untreated and DMSO controls. In the combined treatment, cells were pre-treated with TRPC3 inhibitor for 30 minutes prior to histamine stimulation. After 2hrs incubation with the respective treatment, the cell media was aspirated, and cells were gently washed with PBS. Cells were then fixed for 20 minutes in 4% paraformaldehyde at RT, washed again three times in PBS to remove all fixing agent, and permeabilised with 0.4% Triton X-100 (Sigma Aldrich®) for 20 minutes at RT. The Triton X-100 was pipetted off and cells were then incubated with blocking solution (10% w/v skimmed milk powder and 1% v/v goat serum (Sigma Aldrich®) in tris-buffered saline with 0.2% Tween (Sigma Aldrich®) (TBST)) for 1hr at RT to prevent non-specific antibody binding. Next, cells were rinsed in PBS and incubated at 4°C overnight in rabbit polyclonal anti-GFP primary antibody (Novus Biologicals, NB600-308) diluted to 1:1000 in antibody carrier solution (3% w/v bovine serum albumin (BSA) plus 0.02% NaN_3 in TBST). Cells were washed three times in PBS and then incubated with secondary goat anti-rabbit IgG (H+L) Alexa Fluor 594 (Thermofisher, A-11012) diluted to 1:1000 in antibody carrier solution for 90 minutes at RT. Lastly, cells were washed three times in PBS and mounted onto glass slides with Prolong Gold Antifade 4',6-diamidin-2-fenilindolo (DAPI) mounting media (Thermofisher).

Slides were imaged on a Zeiss AxioImager 2 upright microscope with the 20x objective, with 5 images taken per coverslip, 3 biological replicates per condition, and 3 technical replicates per biological replicate. ≥100 cells per technical replicate were analysed using FIJI software (v2.3.0)[338] to calculate the mean nuclear intensity/mean cytoplasmic intensity (N/C) ratio for each cell by the manual ROI approach described by Kelley and Paschal (2018)[339].

2.5.5. WOUND HEALING ASSAY

A wound healing assay[340] was employed to study the motility of SKOV3 cells treated with TRPC3 activator/inhibitor and EV treatments over a 24hr time period. Prior to cell seeding, the bottom of a 12-well plate was marked with four parallel lines: two horizontal and two vertical in a cross format, so that the same 'wound' area in the centre of the cross was imaged at each time point. SKOV3 cells were seeded into 12-well plates at a density of $1x10^5$, with three wells per condition. Once cells had reached 90% confluency ~24hrs after seeding, they were serum starved for 24hrs before the cell monolayer was scratched down the centre of the well with a p1000 pipette tip. Each well was then washed twice with PBS to remove floating cells. Control media, or media containing 0.3µM TRPC3 activator/3µM TRPC3 inhibitor, DMSO or EV treatments was added to each well and cells were imaged immediately at timepoint 0 with a Zeiss Primovert inverted microscope. Cells were then placed back into the incubator and imaged again at 4, 8, 12 and 24hrs post-scratch.

The percentage of 'wound' closure over time was analysed using the FIJI[338] plugin "MRI Wound Healing Tool"[341] to measure the cell-free area in each image. To avoid bias in gap quantification due to unequal scratch widths, the migration area was calculated by subtracting the scratch area at each timepoint from the area at timepoint 0. The average of four biological replicates were combined for statistical analysis of TRPC3 activator/inhibitor treatments, and three for EV treatments.

2.5.6. MATRIGEL® INVASION ASSAY

To evaluate the invasiveness of SKOV3 cells treated with 0.3µM TRPC3 activator/3µM TRPC3 inhibitor, 100µM histamine, histamine and TRPC3 inhibitor combined or EV treatments, a Matrigel® invasion assay was used (depicted in Figure 2.3). The technique is based on a transwell invasion assay[342], with the addition of a thin layer of Matrigel® to mimic the ECM. BioCoat™ Matrigel® (Corning®) plates were thawed for 1hr at RT before inserts and wells were rehydrated with SFM for 2hrs in the cell culture incubator. The medium was then discarded, and SKOV3 cells were seeded into inserts at a density of $3x10^4$ in SFM supplemented with the respective chemical or EV treatment. For combined histamine and DMSO, or histamine and TRPC3 inhibitor treatments, cells were pre-treated with DMSO/TRPC3 inhibitor for 30 minutes prior to histamine stimulation. Complete medium was added into wells to act as a chemoattractant. The cells were then allowed to invade for 48hr.

Invaded cells were then stained and fixed as follows: all media was discarded, inserts and wells were washed with PBS and cells were stained with 10µM carboxyfluorescein succinimidyl ester (CFSE) (Sigma-Aldrich®) in PBS for 10 minutes in the cell culture incubator. Cells were washed again by adding PBS into both inserts and wells, and then fixed with 4% PFA for 20 minutes at RT. Next, cells were washed twice with PBS to remove all fixing agent, and a moistened cotton swab was used to wipe the top of the membranes to remove all non-invaded cells. The membranes were then cut from the inserts using a scalpel (Swann-Morton™) and mounted onto glass slides with Prolong Gold Antifade DAPI mounting media (Thermofisher). Images were taken of the entire surface area of each membrane on a Zeiss AxioImager 2 upright microscope with the 10x objective, with 3 technical replicates imaged per biological replicate. Invaded cells that were double stained for CFSE and DAPI were counted using the cell counter plugin in FIJI (v2.3.0)[338], and the percentage of invaded cells calculated by dividing the number of invaded cells by the number of seeded cells, multiplied by 100. Mean values of independent experiments were combined for statistical analysis.

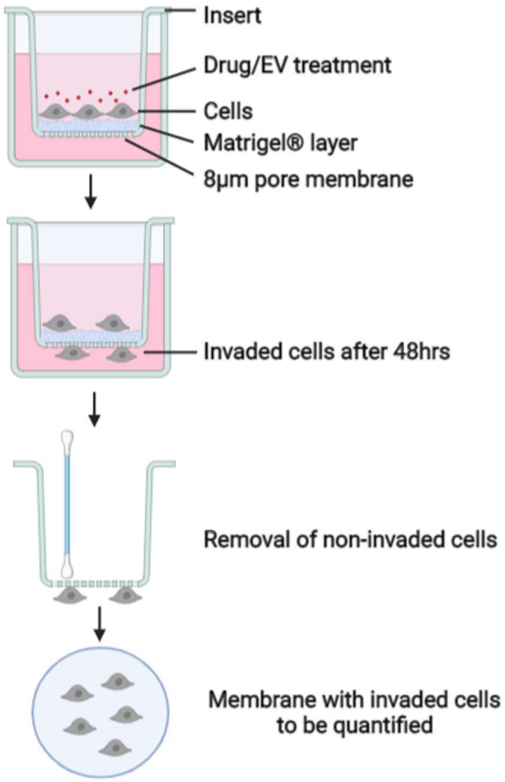

Figure 2.3 Schematic representation of Matrigel invasion assay

Cells are seeded into transwells which are pre-coated with a thin layer of Matrigel® that imitates the extracellular matrix. Cells are seeded in serum free medium with the appropriate drug or EV treatment and allowed to migrate and invade through the pores of the membrane over the following 48hrs. Non-invaded cells are then removed using a cotton swab and invaded cells are fixed, stained, and quantified.

2.6. WESTERN BLOTTING FOR OC CELLS

2.6.1. PROTEIN EXTRACTION

Endogenous TRPC3 protein expression was measured across a panel of OC cell lines by western blot. SKOV3, OVCAR3, OVAR5, IGROV1 and A2780 cells were seeded into 6-well plates and grown to ~90% confluency. For cellular protein extraction, cells were washed in PBS and lysed in 1X radioimmunoprecipitation assay (RIPA) buffer (Sigma-Aldrich®) in PBS supplemented with Halt™ protease inhibitor cocktail (1:1000 dilution) (Thermofisher). Cells were scraped in the lysis buffer, transferred to Eppendorf's and incubated on ice for 10 minutes before being pelleted by centrifugation at 14,000g for 20 minutes at 4°C. The protein concentration of lysates was determined by Pierce BCA Protein Assay Kit (Thermofisher) according to the manufacturer's protocol. Absorbance was read on a SpectraMax i3x plate reader (Molecular Devices) at 562nm.

2.6.2. WESTERN BLOTTING FOR TRPC3 EXPRESSION

Cell protein was reduced using 3x SDS sample buffer (187.5 mM Tris pH 6.8, 30% Glycerol, 6% SDS and 3mg Bromophenol Blue) containing 0.1M Dithiothreitol (DTT) at 95°C for 5 minutes. Samples were then stored at -20°C until further use. Just prior to gel electrophoresis, samples were re-heated at 95°C for 2 minutes and spun down. 50ug protein was loaded for each sample onto 8% hand cast polyacrylamide gels alongside 5µl ladder (Biorad), and run at 140V for 1hr in 1x SDS running buffer (10x stock: 60g Tris, 288g Glycine, 200ml SDS in 2L dH_2O) diluted in dH_2O. Proteins were then transferred to a nitrocellulose membrane (0.45µm pore, Amersham) through Biorad wet transfer apparatus for 90 minutes at 4°C, and run at 0.25A in 1x transfer buffer (10x stock: 60g Tris, 288g Glycine in 2L dH_2O) diluted in dH_2O and supplemented with 20% methanol. Membranes were then cut as required and blocked for 1hr at RT with 5% w/v skimmed milk powder in TBST (1% Tween (Sigma)) to prevent non-specific binding, followed by overnight incubation at 4°C with mouse anti-β-actin (1:10000) (Proteintech, 66009-1) and rabbit anti-TRPC3 (1:200) (Alomone labs, ACC-016) primary antibodies in 3% BSA in TBST. The following day, membranes were washed three times for 5 minutes in TBST and probed with horseradish peroxidase (HRP)-conjugated anti-mouse or anti-rabbit secondary antibodies (GE Healthcare) diluted to 1:10000 in 3% BSA in TBST, for 2hrs at RT. Washing steps were repeated and membranes were incubated for 5 minutes with ECL Prime (Millipore Sigma), and imaged by Syngene G:BOX Chemi XT4 gel system. Band intensity was quantified using ImageJ, and normalised to β-actin expression.

2.7. EV CHARACTERISATION

2.7.1. NANOPARTICLE TRACKING ANALYSIS

EV concentration and size distribution were characterized by nanoparticle tracking analysis (NTA), a method which allows detection of nanoparticles between 10nm to 1µm in suspension, based on Brownian motion. Laser light scatter is used to track and quantify individual particles within a known cell volume, and application of the Stokes-Einstein equation allows size determination of each particle. Here, NTA was conducted using a ZetaView PMX 110 (Particle Matrix) with NTA software v3.0. Prior to each experiment, the machine was calibrated with 100nm polymer microspheres (Applied Microspheres) at a concentration of 1:25,000. SEC fractions or pooled concentrate (see 2.3) were diluted to between 1:100 and 1:10,000 in 1ml PBS to fit the optimal range of detection, as indicated by the software. Each sample was run through the machine and PBS was washed through between each measurement. Data was acquired at RT with the following settings: sensitivity 80, frame rate 30 frames per second (fps), shutter speed 100, minimum brightness 25, maximum pixel size 1000 and minimum pixel size 5.

2.7.2. TRANSMISSION ELECTRON MICROSCOPY

Transmission electron microscopy (TEM) was used in this project to A) characterise the content of non-conditioned EV-depleted FBS and B) analyse SKOV3-EV size, morphology and immunogold labelling with CD81 and mGluR1. For A), carbon 300 mesh copper grids (TAAB, C267) and for B) carbon 300 mesh nickel grids (Agar Scientific) were glow-discharged for 20 seconds at 15mA. For objective A), 8µl of EV concentrate was pipetted onto grids and incubated for 2 minutes at RT. Grids were dabbed against filter paper to remove excess liquid and negatively stained with 10µl 2% uranyl acetate for 10 seconds, then dabbed again and left to airdry before storage. Immunogold labelling for objective B was conducted as described below. Immunogold-labelled and negative-stained EVs were imaged on a Jeol JEM-1400 Flash Transmission Electron Microscope, using a Gatan OneView 16 Megapixel camera at 100kV.

2.7.3. IMMUNOGOLD LABELLING OF SKOV3-EVS

For immunolabelling of EVs, 8µl of EV concentrate was deposited on glow-discharged, carbon-coated nickel grids for 2 minutes before grids were blocked in 1% BSA in PBS for 1hr at RT. Grids were then incubated with either mouse anti-CD81 (1:100) (Abcam, ab79559) or rabbit anti-mGluR1 (1:50) (Alomone labs, AGC-006) primary antibodies in 1% BSA in PBS for 1hr at RT. Grids were next washed three times for five minutes per wash in 1% BSA in PBS, before being incubated for 1hr at RT with 10nm gold-conjugated anti-mouse (Abcam, ab27241) or anti-rabbit

(Sigma-Aldrich®, G7402) secondary antibodies, both diluted to 1:50 in 1% BSA in PBS. After washing steps were repeated, samples were fixed in 2.5% glutaraldehyde (EM grade) in 0.1M phosphate buffer. Finally, grids were washed twice in ddH_2O, dabbed against filter paper to remove excess liquid, and negatively stained with 2% uranyl acetate as above. Grids with no EVs added (just PBS) were processed side-by-side with EV samples to assess non-specific antibody binding.

2.7.4. WESTERN BLOTTING FOR EV MARKERS

For EV protein extraction, EV samples were prepared and concentrated to 20-50µl as in 2.3. Non-conditioned SFM was processed in the same manner to be used as the media control. At the time of EV extraction, one 175cm^2 flask of conditioned SKOV3 cells was washed in PBS, pelleted as in 2.1.1 and snap frozen at -80°C for later cell protein extraction. Cell pellets and EVs were lysed with an equal volume of RIPA buffer (Sigma-Aldrich®) at a 1x concentration for cell pellets, and 2x concentration for EV samples. Lysates were incubated on ice for 10 minutes before being pelleted by centrifugation at 14,000g for 20 minutes at 4°C. The protein concentration of lysates was determined by Pierce BCA Protein Assay Kit) (Thermofisher) according to the manufacturers protocol. Absorbance was read on a SpectraMax i3x plate reader (Molecular Devices) at 562nm.

Western blots for EV markers were run using the Invitrogen NuPAGE system. For cell and EV, an equal concentration of 3-20ug total protein sample was prepared in 4x LDS NuPAGE sample buffer (Invitrogen), with or without 0.4mM DTT. As minimal protein was detected in the SFM media control, an equal volume to the EV sample was prepared in this manner. All samples were then boiled for 5 minutes at 95°C before loading onto 4-12% polyacrylamide Bis-Tris gels (Thermofisher) alongside 5µl ladder (Biorad), and run at 125V for 90 minutes in MES SDS buffer (Thermofisher), prepared as per the manufacturer's instructions. Proteins were transferred to a nitrocellulose membrane (0.45µm pore, Amersham) by wet transfer in the NuPAGE system for 2hrs at 4°C, run at 150V in 1x NuPAGE transfer buffer (Thermofisher) (20x stock solution diluted in dH_2O, and supplemented with 15% methanol). Membranes were checked for protein transfer with ponceau staining (Sigma), cut as required and blocked for 1hr at RT with 5% w/v skimmed milk powder in TBST (0.1% Tween). Next, membranes were incubated overnight at 4°C with primary antibodies (Table 2.2) diluted in blocking buffer, and then washed three times for 5 minutes in TBST before incubating in secondary antibodies (Table 2.2) for 1hr at RT. Washing steps were repeated and membranes were incubated for 5 minutes with ECL Prime (Millipore Sigma), and imaged by ChemiDoc MP Bio-Rad imaging system.

Antibody blocking

To assess non-specific binding for TRPC3 and mGluR1 antibodies, the blots were washed for 1hr shaking in TBST and re-probed with anti-TRPC3 and anti-mGluR1 antibodies preincubated with blocking peptides (mGluR1 blocking peptide Alomone labs, BLP-GC006; TRPC3 blocking peptide Alomone labs, BLP-CC016). For antibody blocking, 20µg antibody was added to 20µg blocking peptide diluted in blocking buffer as above, and incubated overnight rotating at 4°C. The final antibody dilution used for the western was the same as for non-blocked antibodies (1:200 for both anti-TRPC3 and anti-mGluR1). The western proceeded exactly as for non-blocked antibodies (detailed above), and membranes were exposed for the same amount of time as non-blocked antibodies on the imaging system.

Table 2.2 Specifications of all antibodies used in Western blotting for EV proteins

Target	Host	Manufacturer	Dilution	DTT?
TSG101	Mouse	Abcam, ab83	1:500	NO
TSG101	Rabbit	Abcam, ab30871	1:1000	NO
CD9	Rabbit	Cambridge Biosciences, EXOAB-CD9A-1	1:1000	NO
CD81	Mouse	Abcam, ab79559	1:1000	NO
CD63	Mouse	Novus Biologicals, NBP2-42225	1:1000	NO
Alix	Mouse	Abcam, ab117600	1:2500	NO
β-actin	Mouse	Proteintech 6609-1-Ig	1:5000	YES
Cytochrome C	Rabbit	Abcam, 79559	1:1000	YES
GM130	Rabbit	Abcam, ab52649	1:1000	YES
TRPC3	Rabbit	Alomone labs, ACC-016	1:200	YES
mGluR1	Rabbit	Alomone labs, AGC-006	1:200	YES
Rabbit IgG	Goat	Promega, W4011	1:5000	
Mouse IgG	Goat	Promega, W4021	1:20,000	

2.7.5. MACSPLEX EXOSOME ASSAY

The MACSPlex exosome assay is a multiplex bead-based flow cytometric assay which enables semi-quantitative detection of 37 different potential EV surface markers simultaneously. In this assay, EVs are incubated with a cocktail of 39 hard-dyed capture beads, 37 of which are coated with different monoclonal antibodies, and two internal isotype negative controls. Bead-captured EVs are subsequently detected by counterstaining with APC-conjugated CD9, CD63, and CD81 antibodies. Each bead has a unique fluorescent intensity, which can be distinguished by flow cytometry analysis. The technique is depicted in Figure 2.4. Here, the MACSPlex exosome assay was employed to initially characterise SKOV3-EVs extracted in SFM after 48hrs conditioning, and later to analyse differences in EV surface antigen expression following a 4hr treatment with SFM supplemented with 0.3µM TRPC3 activator or 3µM TRPC3 inhibitor, alongside untreated and DMSO controls. Non-conditioned SFM was used as a negative control in all experiments. At the time of EV extraction, an aliquot of 120µl conditioned medium was collected from each experimental condition following the first two centrifugation steps to deplete media of cells and debris (described in 2.3). Media samples were then processed according to the manufacturer's instructions (Miltenyi Biotec). The protocol allows users to select between specific APC detection of CD81, CD63 or CD9 expressing bead-captured EVs, or a combination of all three. In both experiments, bead-captured EVs were incubated with a cocktail of all three antibodies in order to detect most EV populations present. The samples were analysed with a CytoFLEX S flow cytometer (Beckman Coulter) and CytExpert v2.1 software, with at least 10,000 recorded events per sample. The mean fluorescence values were adjusted to the media control and normalized on CD63, CD81 and CD9 mean signal intensity as previously described [343]. For SKOV3-EV characterisation, data is represented as mean APC signal intensity of one biological replicate. For analysis of TRPC3 activator/inhibitor-induced EVs, data represents the mean fluorescence intensity values of antigens repeatedly detected across three biological replicates, normalized to CD63.

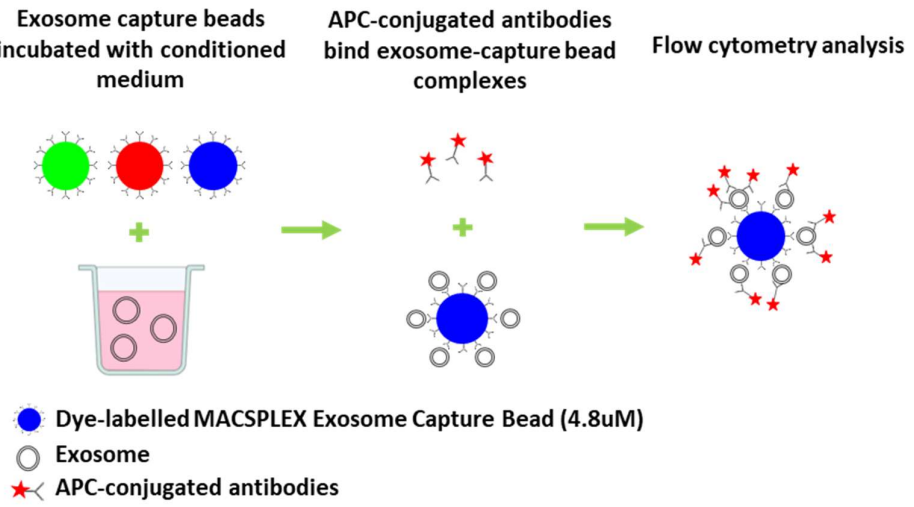

Figure 2.4 Overview of MACSPlex exosome assay

The bead-based assay consists of 37 exosome capture beads which are incubated with conditioned medium overnight. Capture beads bind with exosomes in the conditioned medium, excess material is washed away and APC-conjugated antibodies bind with CD81, CD63 and CD9 epitopes present on the surface of captured exosomes. APC fluorescence on distinguishable bead populations is then quantified by flow cytometry analysis.

2.7.6. EXOVIEW ANALYSIS

SKOV3-EV surface antigens were further characterised by the affinity-based platform Exoview®. In this novel assay, EVs are loaded onto an Exoview chip (NanoView Biosciences) arrayed with antibodies against tetraspanins CD81, CD63 and CD9, and mouse IgG1 as a negative control. Tetraspanin expressing EVs are captured on the respective antibody spot, and subsequently labelled with fluorescent antibodies against CD81 and CD9, or custom fluorescent antibodies of the users' choice. Quantification of EV fluorescence at each spot enables the detection of single and co-labelled EVs.

In this project, SKOV3-EVs extracted in SFM after 48hrs conditioning were analysed with manufacturer provided CD81 and CD9 fluorescent antibodies. In addition, APC-conjugated anti-TRPC3 (Alomone labs, ACC-016; APC conjugation kit from Abcam) (1:500) and DyLight 650-conjugated anti-FLAG (Abcam, ab117492) (1:500) antibodies were employed to enable the detection of TRPC3 expressing EVs. Anti-TRPC3 was conjugated to APC in-house with the Lightning-Link APC conjugation kit (ab201807), following the manufacturer's instructions. For anti-FLAG detection of TRPC3, SKOV3 cells were transfected with a WT TRPC3 construct that has a FLAG-tag on the extracellular domain of TRPC3 as in 2.1.1. 24hrs post-transfection, transfected and non-transfected cells were conditioned for 48hrs in SFM prior to EV extraction. EV samples

were diluted as appropriate to achieve a concentration within dynamic range of the Exoview assay. The assay was conducted by NanoView staff at an Exoview onsite demonstration as previously described[344]. The Exoview chip was imaged with the Exoview R100 reader (NanoView Biosciences) using the ExoScan v0.998 acquisition software. The data was analysed using Exoviewer v0.998 with sizing thresholds set to 50nm to 200nm diameter.

2.8. TIRF MICROSCOPY

Total internal reflection fluorescence (TIRF) microscopy uses an evanescent wave to selectively illuminate fluorophores in a <100nm depth adjacent to the glass coverslip. The technique enables highly sensitive detection of fluorescent signals at or near the PM, eliminating background fluorescence from outside of the focal plane and thus reducing signal-to-noise ratio, and ultimately improving the spatial resolution of the acquired event[345, 346].

2.8.1. CELL PREPARATION AND IMAGE ACQUISITION

In this project, TIRF microscopy was employed to image MVB-PM fusion in single cells with pH-sensitive tetraspanin-based (TSPAN) reporters developed by Sung *et al.* (2015)[235]. SKOV3 cells were transiently transfected with CD81, CD63 or CD9 pHluorin reporters as in 2.1.1. 24hrs post-transfection and just prior to imaging, cells were washed in Tyrode's solution, pH 5.5 (2mM $CaCl_2$, 2.5mM KCl, 119mM NaCl, 2mM $MgCl_2$, 30 mM glucose, 25mM MES) to remove structures such as focal adhesions or exocytosed exosomes from the coverslip. Cells were then imaged in Tyrode's solution, pH 7.4 in a 37°C humidified imaging chamber. After initial comparisons between CD81-, CD63- and CD9-pHluorin fusion characteristics, CD81-pHluorin was used exclusively to assess the effect of chemical treatments on MVB-PM fusion. For treatment conditions, Tyrode's solution, pH 7.4 was supplemented with 100µM histamine, 1.25µM ionomycin, 3µM TRPC3 inhibitor, 0.1/0.3/1µM TRPC3 activator or DMSO equivalent. For the analysis of histamine-induced MVB-PM fusion in TRPC3 inhibited cells, cells were pre-treated with TRPC3 inhibitor or DMSO equivalent for 30 minutes prior to histamine stimulation. Initially, MVB-PM fusion was quantified in 10-minute acquisitions from 0-40 minutes following histamine stimulation, and in 5-minute acquisitions from 0-35 minutes following TRPC3 activator/inhibitor treatment to determine the most appropriate timeframe for imaging. The effect of all treatments was immediate; therefore all further fusion events were quantified in 5-minute acquisitions immediately following stimulation. Cells expressing moderate levels of TSPAN-pHluorin were selected for imaging, with 1 cell in the field of view per acquisition. A minimum of 10 cells were imaged per treatment condition. Cells were imaged on an Olympus IX83 inverted

microscope, and images were captured with a Photometrics Evolve 512 Delta camera through a UAPON OTIRF 150x/1.45 objective. Images were acquired at 0.40 frames per second (fps) unless otherwise stated.

2.8.2. IMAGE ANALYSIS

All timeseries were analysed in FIJI (v2.3.0)[338] through a custom protocol. Initially, single channel image stacks were loaded into FIJI and formatted as 8-bit for use with the StackDifference Plugin[347]. The StackDifference Plugin was used to generate a sequence of difference images – each frame is the resultant subtraction of the next frame minus the previous frame. The gap between frames was set at 1. This method therefore selects for 'new' localised increases in fluorescence in every individual frame of the acquisition. The threshold was then adjusted to select for fluorescent events within the difference images stack, and the inbuilt 'Analyze Particles' function was employed to select and analyse fluorescent events above the set threshold. The fluorescence profile over-time of every event highlighted by the Analyze Particles function was assessed with the Time Series Analyzer V3 Plugin[348]. Events with minimal change in fluorescence, an irregular fluorescence profile and/or lateral movement of the fluorescence signal were excluded from the analysis. For graphs demonstrating quantity of events, each data point represents the number of events in one cell. For descriptive data graphs, each data point represents a single event. Mean fluorescence and circularity values were taken directly from the 'Analyze particles' data, and for circularity a value of 1 represents a circular object and 0 represents a linear object. Width values were generated by manually measuring the diameter of fluorescent events at peak fluorescence in FIJI[338]. The duration, localisation and synchronisation of fusion events were assessed by eye.

2.9. EV PROTEOMICS

2.9.1. SAMPLE PREPARATION

SKOV3 cells were seeded in a total of 65 175cm^2 flasks in complete medium, and cultured to ~80% confluency over the course of 2-3 days. On the day of EV extraction, all media was aspirated, and cells were washed twice with PBS. Sets of 13 flasks were then conditioned for 4hrs in either plain SFM (untreated control), or SFM supplemented with 100µM histamine, 1.25µM ionomycin, 0.3µM TRPC3 activator or 0.03% DMSO. EVs were then extracted from each set of flasks as described in 2.3, and fractions 5-10 were pooled together for each treatment group and concentrated to 20µl in PBS. At the time of EV extraction, two flasks of cells from each treatment group were counted with trypan blue as in 2.1.1 to ensure adequate cell viability. All

EV samples were stored at -80°C for up to one month, prior to downstream analysis. Four biological replicates were collected for all treatment groups. The samples were sent to the Discovery Proteomics Facility at the Target Discovery Institute, Oxford University, for mass spectrometry analysis. Protein extraction and liquid chromatography-mass spectrometry was conducted by Dr Svenja Hester, following the provided protocol below.

2.9.2. EV PROTEIN DIGESTION

An equal volume of 5% SDS plus protease inhibitors (x10) was added to 20µl EVs in PBS (complete Mini, EDTA free, Roche, Ref: 11836170001). Samples were then reduced by the addition of 1µl 500mM TCEP, and alkylated with 4µl 500mM IAA. Samples were made up to a final concentration of 1.2% with the addition of 4.5µl 12% phosphoric acid, and diluted 1:7 with 90% methanol in 100mM TEAB. Lastly, 1.5µg trypsin in 50mM TEAB was added to each sample prior to peptide separation and mass-spec analysis.

2.9.3. MASS-SPEC ANALYSIS

Peptides were resuspended in 5% formic acid and 5% DMSO and then trapped on an Acclaim™ PepMap™ 100 C18 HPLC Columns (5µm x 0.1mm x 20mm, Thermofisher) using solvent A (0.1% Formic Acid in water) at a pressure of 60 bar and separated on an Ultimate 3000 UHPLC system (Thermofisher) coupled to a QExactive mass spectrometer (Thermo Fischer Scientific). The peptides were separated on an Easy Spray PepMap RSLC column (75µm i.d. x 2µm x 50mm, 100 Å, Thermofisher) and then electrosprayed directly into an QExactive mass spectrometer (Thermofisher) through an EASY-Spray nano-electrospray ion source (Thermofisher) using a linear gradient (length: 60 minutes, 5% to 35% solvent B (0.1% formic acid in acetonitrile), flow rate: 250nL/min). The raw data was acquired on the mass spectrometer in a data-dependent mode (DDA). Full scan MS spectra were acquired in the Orbitrap (scan range 380-1800 m/z, resolution 70000, AGC target 3e6, maximum injection time 100ms). After the MS scans, the 15 most intense peaks were selected for HCD fragmentation at 28% of normalised collision energy. HCD spectra were also acquired in the Orbitrap (resolution 17500, AGC target 1e5, maximum injection time 128 ms) with first fixed mass at 100m/z.

The raw data files generated were processed using MaxQuant (Version 1.6.17.0), integrated with the Andromeda search engine. For protein groups identification, peak lists were searched against human database (UPR_Homo sapiens_9606_UP000005640_20200803.fasta) as well as list of common contaminants by Andromeda. Trypsin with a maximum number of missed cleavages of 2 was chosen. Deamidation (N, Q), Oxidation (M) were used as variable

modifications while Carbamidomethylation (C) was set as a fixed modification. Protein and PSM false discovery rate (FDR) were set at 0.01 and a minimum score of 30.

2.9.4. DATA PROCESSING

Label-free quantification (LFQ) intensity values were used for data processing through the Perseus (MaxQuant) software (v1.6.14.0). The dataset was initially filtered to remove proteins identified as "only identified by site", "reverse" or "potential contaminant". All identified proteins with a Q-value more than 0.01, razor + unique peptides of less than 1, and valid values of less than 1 were likewise removed from the dataset. LFQ values were log2 transformed, normalised by median subtraction and grouped by treatment group (n=4). Venn diagrams and UpSet plots were then generated to visualise the data distribution across treatment groups and replicates, respectively. Venn diagrams were generated manually from the Venn data generated in Perseus, and UpSet plots were generated through the online tool: https://intervene.shinyapps.io/intervene/. Based on this analysis, the dataset was filtered to only include proteins identifiable in at least three replicates of one or more treatment groups for all further analysis. Replicate three of the DMSO group was also excluded from all further analysis due to a high number of unique proteins. Missing values were then imputed from normal distribution for each column, with a width of 0.3 and down shift of 1.8 (default parameters). Following imputation, histograms were generated for each replicate and assessed by eye to ensure all values lied within the main distribution prior to statistical analysis.

2.9.5. DATA ANALYSIS

Initially, a multiple-sample ANOVA was run on all treatment groups with a threshold p-value of 0.05 to identify all differentially expressed proteins across the dataset. Differentially expressed proteins were then analysed by principal component analysis (PCA) and hierarchical clustering, generated in the Perseus software. Hierarchical clustering was performed on Z-scores and clustered by Euclidean distance, as per the default settings. The PCA plot was generated on protein intensity values. To clarify what proteins were specifically deregulated between each treatment group and their respective control (untreated for histamine, DMSO for ionomycin and TRPC3 activator), the mean fold change of each protein following treatment (LFQ intensity treatment – LFQ intensity control), and the p-value of this change was calculated for all treatment groups. These values were then plotted as Log_2 (fold change) against $-Log_{10}$ (p-value) in a volcano plot. Gene ontology (GO) analysis was performed using the online database DAVID[349, 350], with all proteins run against the full human genome as background. P-values were adjusted by Benjamini-Hochberg False Discovery Rate.

2.10. STATISTICAL ANALYSIS

All statistical analysis was performed in GraphPad Prism v6 software. Within the software, all data sets were assessed for normality using the Shapiro-Wilk test, and the recommended parametric or non-parametric alternative with multiple comparison test was conducted as follows. When comparing two sample means, a two-tailed paired t-test was used for the analysis of paired, parametric data, and for paired, non-parametric data, a Wilcoxon matched-pairs signed rank test was performed. An unpaired t-test with Welch's correction was used for unpaired, parametric data with no assumptions on SD. For the comparison of one variable (i.e., treatment group) between two or more independent groups when the data is parametric and unmatched, an ordinary one-way ANOVA and Tukey's multiple comparisons test was performed. For matched data, a Greenhouse-Geisser correction was applied. For non-parametric data, if the data were unmatched, a Kruskal-Wallis and Dunn's multiple comparisons test was performed, and matched data were assessed by a Friedman test with Dunn's multiple comparisons test. A two-way ANOVA and Tukey's multiple comparisons test was employed for the analysis of parametric, non-matched data with two variables. In some cases where comparisons between all means in the dataset was deemed unmeaningful, simple effects within each variable were assessed independently. Sidak's multiple comparisons test was used in replacement of a Tukey's test when comparing two variables between exactly two groups. All statistical tests are outlined in the figure legends. P-values in figures are shown as $p < 0.05$ *, $p < 0.01$ **, $p < 0.001$ *** and $p < 0.0001$ ****.

Chapter 3

Exploring the role of TRPC3 in ovarian cancer

3. Exploring the role of TRPC3 in ovarian cancer

3.1. BACKGROUND

3.1.1. CALCIUM DEREGULATION IN CANCER

Calcium (Ca^{2+}) is a ubiquitous intracellular signalling molecule that regulates diverse cellular functions such as cell cycle control, survival, apoptosis, migration and gene expression[307]. A large repertoire of Ca^{2+} permeable channels, exchangers, transporters and ion pumps act to maintain cytosolic Ca^{2+} homeostasis by regulating extracellular Ca^{2+} entry at the plasma membrane (PM) or facilitating release from internal stores[160, 161]. Mutations, dysregulation of activity or expression levels of Ca^{2+} channels and transporters are characterizing features of cancer, as distorted Ca^{2+} signalling deregulates Ca^{2+}-sensitive downstream effectors that, in turn, promotes pathophysiological cancer hallmarks such as enhanced survival, proliferation and invasion[162]. Indeed, altered channel activity and subsequent divergence in Ca^{2+} homeostasis is implicated in every stage of the metastatic cascade[351]. For example, overexpression of Ca^{2+} channels at the PM increases Ca^{2+} influx, subsequently promoting Ca^{2+}-driven proliferation through upregulation of MAPK/calmodulin-dependent pathways[352]. Cell motility is also tightly regulated by intracellular Ca^{2+} concentrations, and fluctuations in Ca^{2+} transport across the PM drive enhanced cell migration through cytoskeleton rearrangement and focal adhesion disassembly[353, 354]. A major family of Ca^{2+} permeant channels which are regarded as important players in cancer regulation are transient receptor potential (TRP) channels.

3.1.2. TRP CHANNELS IN CANCER

The TRP channel family are amplified in numerous cancers and promote tumorigenesis through mediating sustained elevated Ca^{2+} [162]. The canonical TRP channel subfamily (TRPC) includes various channels responsible for protein tyrosine kinase (RTK)- and G protein-coupled receptor (GPCR)-operated Ca^{2+} entry at the PM and from internal stores[355]. Of the seven TRPC family subtypes, amino-acid similarity classifies mammalian TRPCs into four groups: TRPC1, TRPC2 (pseudogene in humans), TRPC3/6/7, and TRPC4/5 (see Figure 1.3) – all of which have been implicated in cancer progression. For example, TRPC1 and TRPC5 mediate metastatic mechanisms in breast cancer cells by promoting epithelial to mesenchymal transition (EMT)[356] and tumour angiogenesis[357] respectively. TRPC6 likewise contributes to the proliferation of breast cancer cells[358], as well as prostate[359], hepatoma[360] and gastric cancer cells[361].

As TRPC3 shares approximately 75% homology with TRPC6, TRPC3 has since come under investigation for its potential role in cell proliferation. Mainly, altered TRPC3 activity has been studied in the context of ovarian cancer (OC). Utilising the non-selective TRPC blocker SKF96365 and TRPC3 knockdowns, Yang *et al.*[310] demonstrated that reduced activity/expression of TRPC3 suppressed OC growth both *in vitro* in SKOV3 cells, and *in vivo* in nude mice injected with SKOV3 cells knocked down for TRPC3. *In vitro,* reduced TRPC3 activity arrested the cell cycle at M phase, suggesting TRPC3 promotes the proliferation of OC cells by contributing to metaphase exit. TRPC3 protein expression was also markedly increased in human OC compared to non-cancerous specimens. Collectively, these results demonstrate a vital role for TRPC3 in the proliferation and cell-cycle progression of OC cells *in vitro* and *in vivo*. Further studies investigating the hormonal activation of TRPC3 validated the central role of TRPC3 in OC proliferation, as both follicle-stimulating hormone (FSH) and oestrogen promoted OC proliferation through TRPC3 activation[312, 313]. TRPC3 has since been identified as a direct driver of proliferation and migration in a number of cancers, including melanoma[318], lung[362], bladder[363] and breast[311].

With TRPC3 channels emerging as key contributors to cancer progression, particularly in OC, further investigation is required to assess how TRPC3-mediated Ca^{2+} entry influences other metastatic mechanisms of OC, such as their migration and invasion. To date, only an inhibitory effect of TRPC3 activity has shown to influence OC growth, notably using a non-selective TRPC inhibitor, therefore the role of TRPC3 upregulation and specific pharmacological inhibition in OC growth, migration and invasion are yet to be investigated. In addition, nothing is currently known about how TRPC3-mediated Ca^{2+} entry is regulated by OC cells. In a number of cell types, TRPC3 is activated downstream of histamine H_1 and H_2 GPCRs, and facilities histamine-induced Ca^{2+} entry[305, 364]. Independent studies report that histamine activation of the histamine H_1 receptor (H1HR) stimulates Ca^{2+} accumulation in both SKOV3 and OVCAR3 OC cell lines, and subsequently enhances their proliferation[365, 366]. Unpublished data from the lab likewise demonstrates that activation of H1HR increases the invasive capacity of SKOV3 cells, and that H1HR expression correlates with disease progression in clinical OC samples. Taken together, this proposes that TRPC3 may act downstream of H1HR to promote OC progression, although this link is yet to be investigated. Understanding how TRPC3 activity is regulated in OC, and how pharmacological modulators of TRPC3 influence OC progression may lead to the development of much-needed therapeutics for treating OC.

3.2. AIMS AND OBJECTIVES

TRPC3 protein expression is markedly increased in human OC compared to non-cancerous specimens, and plays a vital role in OC development *in vitro* and *in vivo.* To date, the non-selective TRPC blocker SKF96365 and TRPC3 knockdowns have been employed to demonstrate a role for TRPC3 in OC growth and cell cycle progression, as well as hormonal regulation of OC proliferation, migration and chemotherapy resistance. The aim of this chapter was to assess how modulating TRPC3 activity with the TRPC3-selective inhibitor Pyr3[337] and selective TRPC3/6 activator GSK 1702934A[336] influences the growth, migration and invasion of SKOV3 cells in the absence of hormonal stimulation. Mechanisms for TRPC3 activation by histamine stimulation, and ensuing effects on cell invasion were also assessed. The specific objectives were therefore to:

1. Characterise endogenous TRPC3 expression in ovarian cancer cell lines
2. Establish appropriate TRPC3 activator concentrations for increasing Ca^{2+} influx in SKOV3 cells without compromising cell viability
3. Assess how modulating TRPC3 activity effects the growth, migration and invasion of SKOV3 cells
4. Investigate the relationship between histamine and TRPC3 in Ca^{2+} signalling and SKOV3 invasion

3.3. RESULTS

3.3.1. TRPC3 IS EXPRESSED ACROSS A PANEL OF OVARIAN CANCER CELL LINES

In order to evaluate the role of TRPC3 in the progression of OC, and later in EV biogenesis, it was first necessary to measure endogenous expression of TRPC3 across a panel of epithelial OC cell lines: SKOV3, OVCAR3, OVCAR5, IGROV1 and A2780 (characteristics of each cell line detailed in Table 2.1). Endogenous TRPC3 was detected in all OC lines by western blot (Figure 3.1 A), with a predominant protein band at ~100kDa - consistent with the molecular weight reported in previous TRPC3 publications[310]. Double bands shown in the IGROV1 cell line and faintly in the A2780 cell line likely represents TRPC3/TRPC6 heteromeric channels, as TRPC3/6 subunits can assemble into both homomeric and heteromeric channels as reported in other cell lines[358, 367]. Quantification of band intensities normalised to β-actin expression revealed that TRPC3 expression is largely variable between OC lines (Figure 3.1 B). SKOV3 is a well-used cell line to study OC development, and was therefore selected as the principal line of study in this investigation.

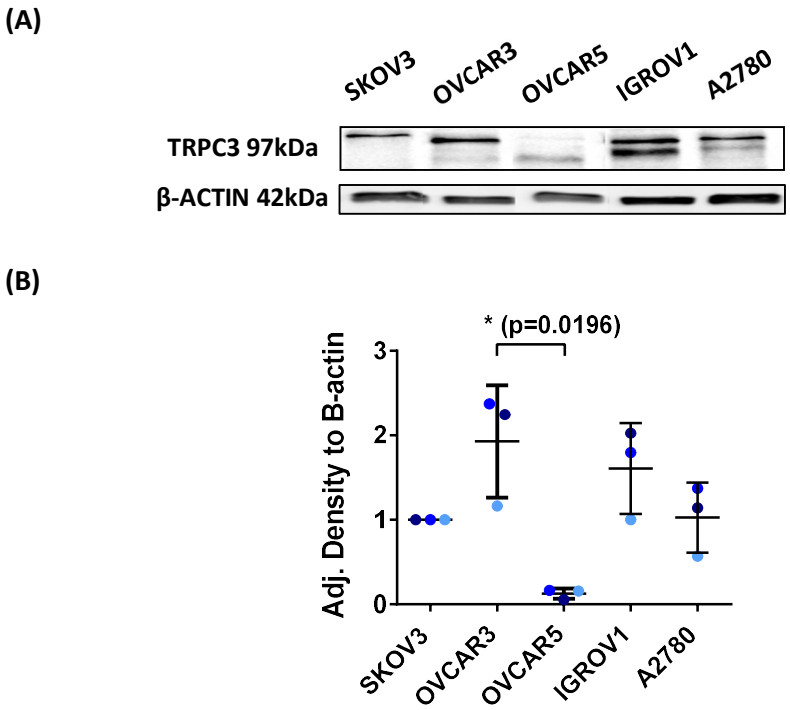

Figure 3.1 Characterising endogenous TRPC3 expression in ovarian cancer cell lines

(A) *Representative western blot of endogenous TRPC3 protein expression in five OC cell lines: SKOV3, OVCAR3, OVCAR5, IGROV1 and A2780. 50µg protein loaded for all samples.* ***(B)*** *Quantification of western blot data represented in (A). Relative density of TRPC3 expression to β-actin quantified using ImageJ software. Data represents mean ± SEM of three independent experiments with statistical significance tested by Friedman test and Dunn's multiple comparisons test: *P = 0.0196, if not indicated – not significant (p>0.05).*

3.3.2. CONCENTRATIONS OF TRPC3 ACTIVATOR UP TO 1µM DO NOT REDUCE SKOV3 CELL VIABILITY

The TRPC3 activator GSK 1702934A was employed in this chapter to assess the role of TRPC3 in OC progression, and later in EV biogenesis. Activating the TRPC3 channel increases Ca^{2+} influx into cells, and intracellular Ca^{2+} overload can lead to cell apoptosis[368]. Therefore, to study how upregulating TRPC3-mediated Ca^{2} entry influences cell behaviour without inducing cell death, optimal concentrations of TRPC3 activator which do not reduce cell viability must be determined for treating SKOV3 cells. SKOV3 cells were incubated with 0.3µM, 1µM and 10µM TRPC3 activator or DMSO equivalent for 4hrs, alongside untreated controls (-). Cell viability was then determined by MTT assay. The mean viability of SKOV3 cells treated with 0.3µM TRPC3 activator was 99.1% relative to untreated cells, which reduced to 93.4% at 1µM and 78.3% at 10µM TRPC3 activator (Figure 3.2). There was no significant difference in cell viability between 0.3µM and 1µM TRPC3 activator concentrations, although 10µM TRPC3 activator significantly reduced cell viability in comparison to both 0.3 and 1µM concentrations. Therefore, concentrations of up to 1µM TRPC3 activator do not reduce SKOV3 cell viability, and are suitable for downstream assessments of TRPC3 activity.

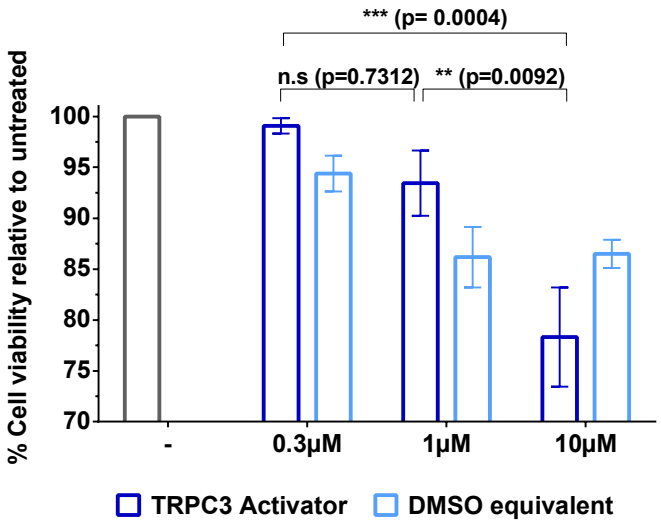

Figure 3.2 Concentrations of TRPC3 activator GSK 1702934A up to 1µM do not reduce SKOV3 cell viability

Percentage viability of SKOV3 cells by MTT following treatment with increasing concentrations of TRPC3 activator or DMSO equivalent for 4hrs, normalised to untreated cells (100). Mean ± SEM of three independent experiments, each independent experiment value the mean of six technical replicates. Statistical significance tested by two-way ANOVA and Tukey's multiple comparisons test. Only comparisons between TRPC3 activator concentrations shown.

3.3.3. TREATMENT WITH TRPC3 ACTIVATOR INCREASES Ca^{2+} SIGNALLING IN SKOV3 CELLS

Next, increasing concentrations of TRPC3 activator were trialled to evaluate the effect on Ca^{2+} signalling in SKOV3 cells, using a nuclear factor of activated T-cells (NFAT) translocation assay. NFAT is a Ca^{2+}-sensitive transcription factor which under normal conditions, resides in the cytoplasm inactive and phosphorylated. However, upon Ca^{2+} influx, NFAT is dephosphorylated by calcineurin and translocates to the nucleus where it activates gene expression[369] (see Figure 3.3 A for a schematic). Transfecting cells with GFP-tagged NFAT allows the subcellular location of NFAT to be visualised and quantified, providing an indirect measure of intracellular Ca^{2+} signalling downstream of activated TRPC3[327]. SKOV3 cells expressing GFP-tagged NFAT were treated with 1.25µM ionomycin (a Ca^{2+} ionophore) as a positive control, or 0.1/0.3/1/10µM TRPC3 activator alongside untreated (-) and DMSO controls. After 2hrs incubation, cells were fixed and subjected to indirect immunofluorescence using an anti-GFP antibody (Novus) and the DNA dye DAPI. Ionomycin markedly increased the nuclear localisation of GFP-tagged NFAT compared to untreated and DMSO controls as expected (Figure 3.3 B), demonstrating the utility of the assay. Although to a lesser extent, all concentrations of TRPC3 activator likewise increased the nuclear signal of GFP-tagged NFAT, indicative of increased Ca^{2+} signalling downstream of TRPC3 activation. To quantify NFAT localisation, the nuclear/cytosol (N/C) fluorescence intensity ratio was measured for each technical replicate in ImageJ, using the method described by Kelley and Paschal (2019)[339]. Indeed, ionomycin stimulated the most significant increase in NFAT nuclear translocation, and all concentrations of TRPC3 activator significantly increased the N/C ratio in comparison to DMSO (Figure 3.3 C). A dose-dependent response was apparent up to TRPC3 activator concentrations of 0.3µM, whereafter the effect on Ca^{2+} influx appeared to be saturated. Therefore, 0.1µM and 0.3µM TRPC3 activator are sufficient to upregulate TRPC3 channel activity and subsequently increase Ca^{2+} signalling in SKOV3 cells.

(A)

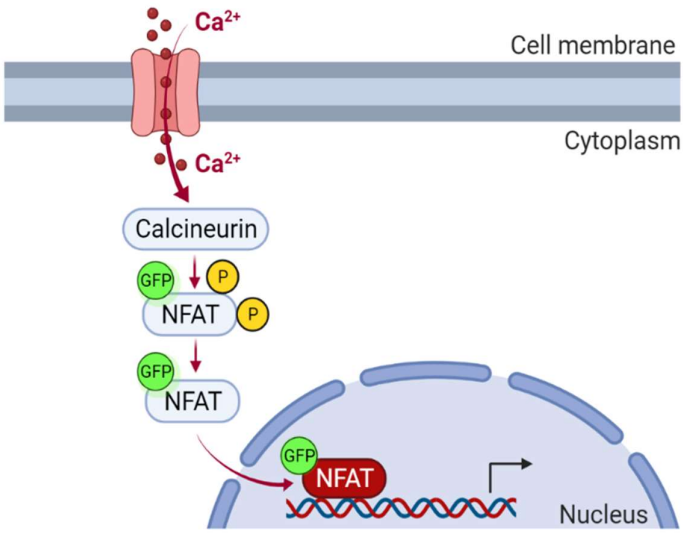

(B)

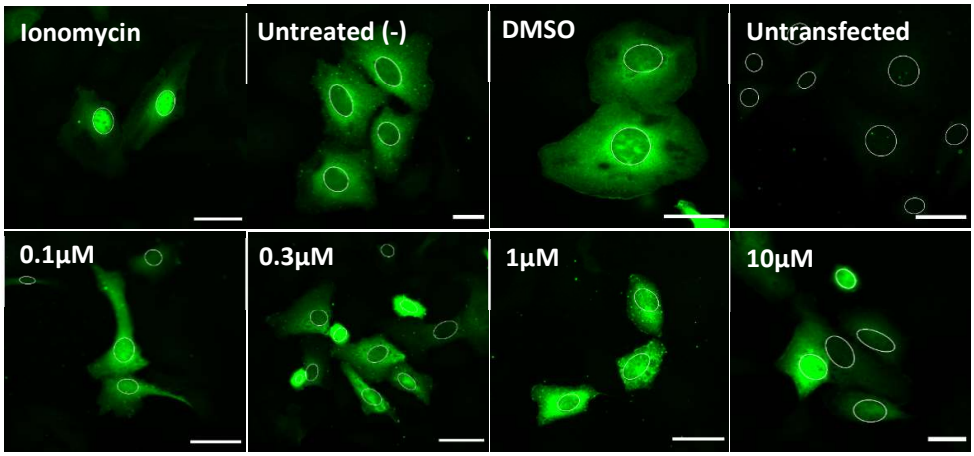

Scale bars 50µm

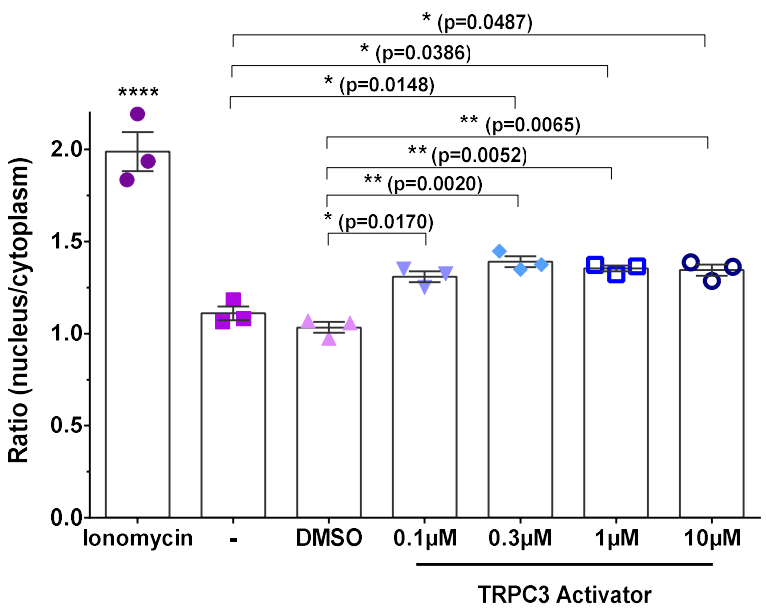

Figure 3.3 Treatment with TRPC3 activator GSK 1702934A increases Ca^{2+} signalling in SKOV3 cells

(A) *Schematic representation of NFAT translocation assay. A rise in intracellular calcium (Ca^{2+}) activates the phosphatase calcineurin, inducing dephosphorylation and nuclear translocation of NFAT which can be visualised by a GFP tag.* ***(B)*** *Representative images of NFAT translocation in SKOV3 cells expressing GFP-tagged NFAT following treatment with 1.25µM Ionomycin or 0.1/0.3/1/10µM TRPC3 activator, alongside untreated (-) and DMSO controls. Cells were treated for 2hrs, 24hrs post-transfection. Cells were then fixed and subjected to indirect immunofluorescence using an anti-GFP antibody (Novus). Nuclear regions are indicated. Scale bars 50µm.* ***(C)*** *Nuclear/cytosol fluorescence intensity ratio of treated cells shown in (B). Mean ± SEM of three independent experiments, n≥100 cells per condition, per experiment. Statistical significance tested by Ordinary one-way ANOVA and Tukey's multiple comparisons test, Ionomycin significance to all treatment conditions, **** P ≤ 0.0001. If not indicated – not significant (P > 0.05).*

3.3.4. CHEMICAL MODULATION OF TRPC3 ACTIVITY ALTERS THE GROWTH OF SKOV3 CELLS

Knocking down TRPC3 expression and non-specifically inhibiting TRPC channels suppresses OC growth, and attenuates hormone-induced proliferation[310, 312, 313]. To assess how modulating TRPC3 activity with the TRPC3-selective inhibitor Pyr3 and selective TRPC3/6 activator GSK 1702934A influences OC cell growth, OC cells were manually counted at 24, 48 and 72hrs following treatment with TRPC3 activator or inhibitor, using trypan blue to distinguish live from dead cells. A low and high dose concentration of TRPC3 activator and inhibitor were employed: 0.1µM and 0.3µM TRPC3 activator, and 1µM and 3µM TRPC3 inhibitor (Figure 3.4 A,B). Appropriate concentrations of TRPC3 activator were determined in Sections 3.3.2 and 3.3.3, and concentrations of TRPC3 inhibitor were based on results from Kiyonaka *et al.* who demonstrated complete inhibition of TRPC3 channel activity at 3µM Pyr3[337]. At both low and high dose

treatments, the number of TRPC3 activator treated cells was consistently higher than cells treated with TRPC3 inhibitor or DMSO equivalent, and the number of TRPC3 inhibitor treated cells was reduced in comparison to DMSO. In the low dose treatment, there was a significant difference in cell number between TRPC3 activator and inhibitor treatments at the 72hr timepoint. The higher dosage of TRPC3 activator significantly increased cell number in comparison to TRPC3 inhibitor at both 48 and 72hrs. Therefore, these results indicate that modulating TRPC3 activity with the TRPC3-selective inhibitor Pyr3 and selective TRPC3/6 activator GSK 1702934A alters the growth of SKOV3 cells at both low and high dose treatments.

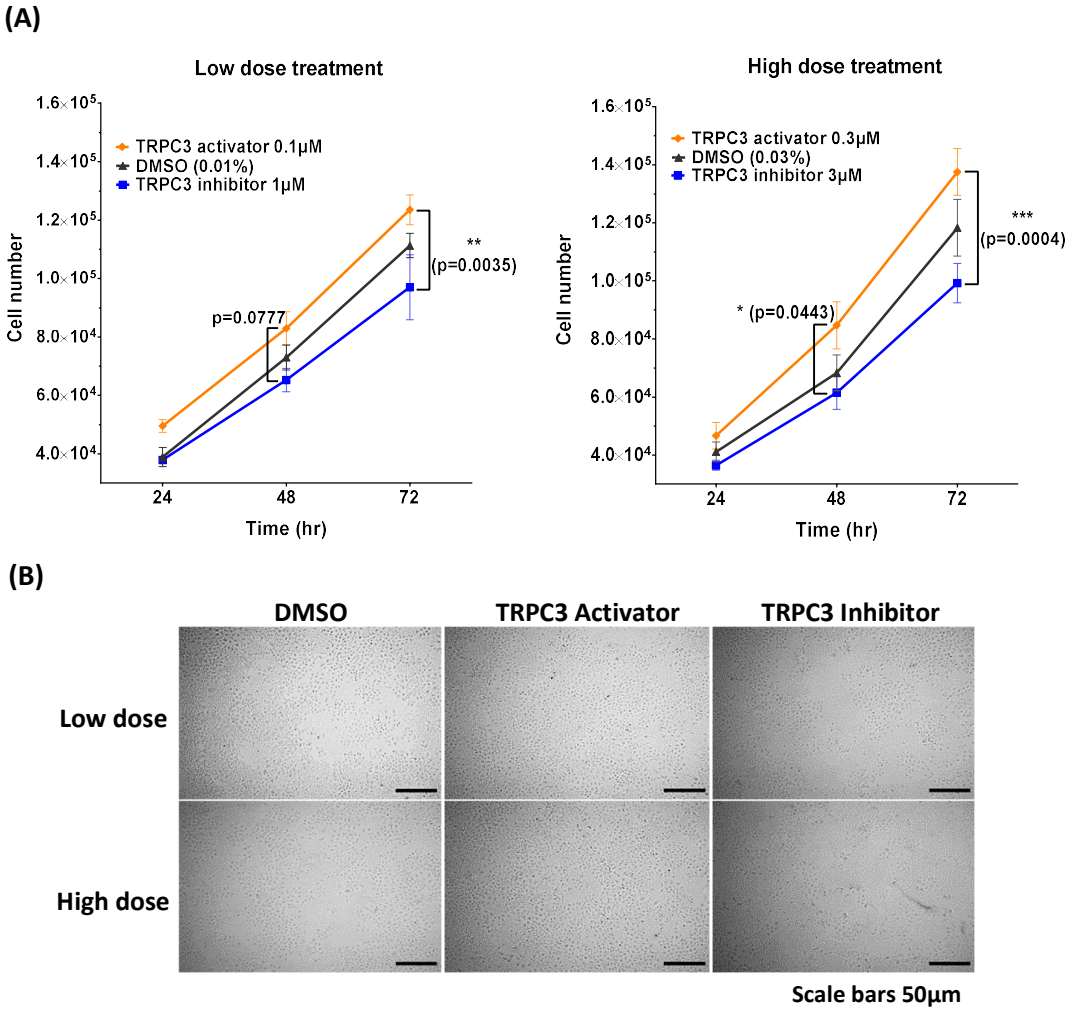

Figure 3.4 Modulating TRPC3 activity alters the growth of SKOV3 cells

(A) *Growth curves representing total cell number at 24, 48 and 72hr incubation with TRPC3 treatment or DMSO equivalent. Left: Low dose TRPC3 activator (0.1μM), low dose TRPC3 inhibitor (1μM), 0.01% DMSO. Right: high dose TRPC3 activator (0.3μM), high dose TRPC3 inhibitor (3μM), 0.03% DMSO. Data represents mean ± SEM of four independent experiments with statistical significance tested by two-way ANOVA and Tukey's multiple comparisons test, if not indicated – not significant ($p > 0.05$).* ***(B)*** *Representative images of SKOV3 cells in culture following 72hrs treatment with either low or high dose TRPC3 treatment or DMSO equivalent. Scale bars are 50μm.*

3.3.5. CHEMICAL MODULATION OF TRPC3 ACTIVITY ALTERS THE MIGRATORY CAPACITY OF SKOV3 CELLS

Inhibition of TRPC3 with Pyr3 reduces the migratory capacity of melanoma and glioblastoma cells, as determined by a wound healing assay[308, 318]. The role of TRPC3 in OC cell migration is yet to be investigated. Therefore, a wound healing assay was employed to study the motility of SKOV3 cells treated with TRPC3 activator or inhibitor over a 24hr time period. As a more pronounced effect was apparent in cell growth at the high dose treatment of 0.3µM TRPC3 activator and 3µM inhibitor, these concentrations were employed to assess cell motility and in all future experiments. Treatment was added immediately before the cell monolayer was scratched at timepoint 0, and gap closure was monitored at 4, 8, 12 and 24hrs (Figure 3.5 A-C). To avoid bias in gap quantification due to unequal scratch widths, the migration area was calculated by subtracting the scratch area at each timepoint from the area at timepoint 0. At 12 and 24hr timepoints, TRPC3 activator treated cells migrated significantly more than TRPC3 inhibitor treated cells across the scratch area (Figure 3.5 A). Untreated and DMSO treated cells showed the same rate of scratch closure over the 24hr period. The migration area for each treatment group was then normalised to the DMSO control (Figure 3.5 B). TRPC3 activator treated cells migrated significantly more than TRPC3 inhibitor treated cells at 4, 8 and 12hr timepoints, as well as untreated cells at 4hrs. These results demonstrate that modulating TRPC3 activity can influence the motility of OC cells, and identify a novel role for TRPC3 in OC cell migration.

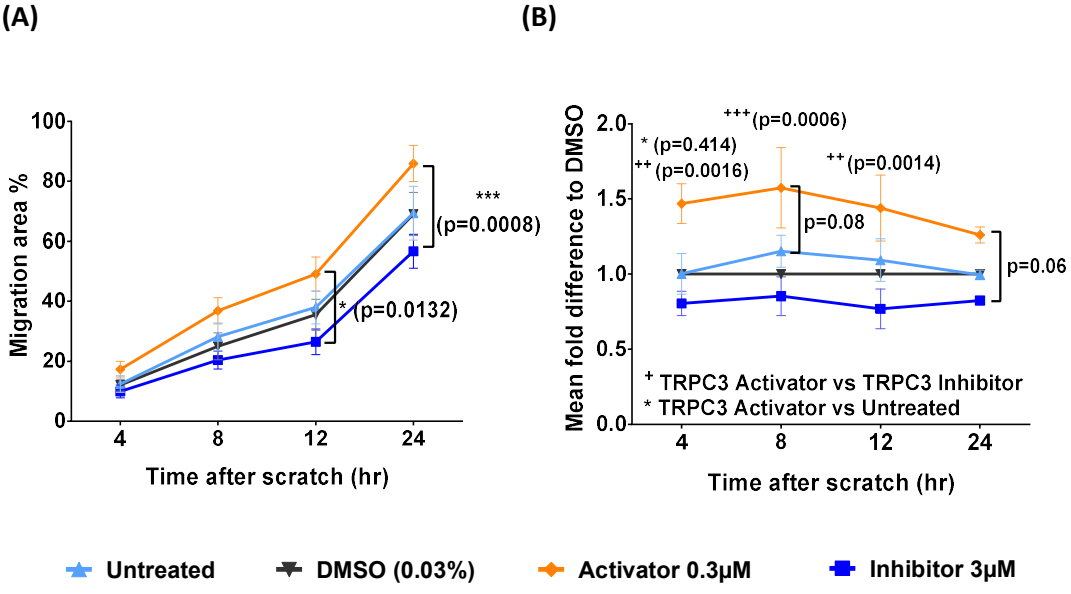

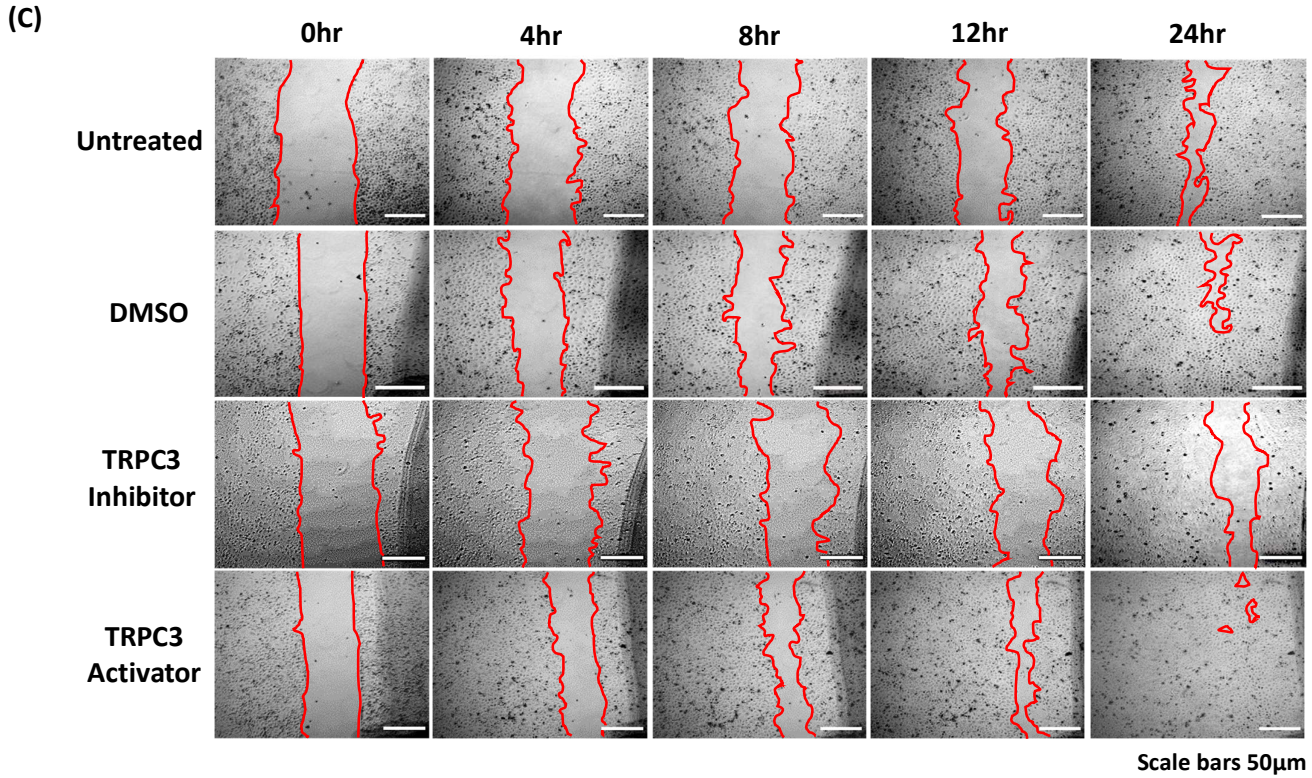

Figure 3.5 Modulating TRPC3 activity alters the migratory capacity of SKOV3 cells

(A) *A scratch assay was performed on SKOV3 cells treated with 0.3µM TRPC3 activator, 3µM TRPC3 inhibitor, DMSO equivalent or media control (untreated) and cell migration was monitored over a 24-hour period. Migration is represented as the percentage of scratch closure over time.* ***(B)*** *Cell migration in each treatment group was normalised to the DMSO control (=1). (A) and (B) represent mean ± SEM of four independent experiments with statistical significance tested by two-way ANOVA and Tukey's multiple comparisons test. *Significant difference in migration of TRPC3 activator and inhibitor treated cells, + significant difference in migration between TRPC3 activator and untreated cells: Unstated p-values ≥0.1.* ***(C)*** *Representative images of SKOV3 scratch assay used to quantify cell migration at 0, 4, 8, 12 and 24hr timepoints. Quantified area shown in red. Scale bars are 50µm.*

3.3.6. CHEMICAL MODULATION OF TRPC3 ACTIVITY DOES NOT INFLUENCE THE INVASIVENESS OF SKOV3 CELLS

So far, pharmacological modulation of TRPC3 activity has shown to influence the growth and migration of OC cells. To evaluate if the increased motility of SKOV3 cells under TRPC3 activation also increases their capacity to invade through the ECM, a Matrigel® invasion assay was performed. Cells were plated onto a Matrigel® layer in plain serum-free media, and serum-free media supplemented with 0.3µM TRPC3 activator, 3µM inhibitor or DMSO equivalent (0.03%). Cells were allowed to invade for 48hrs before invaded cells on the underside of the membrane were stained with carboxyfluorescein succinimidyl ester (CFSE) and the DNA dye DAPI, imaged and quantified to estimate the percentage of invasion (Figure 3.6 A,B). There was no detectable difference in invasion between untreated, DMSO treated, TRPC3 activator treated or TRPC3 inhibitor treated cells. Therefore, TRPC3 does not appear to contribute to the invasiveness of SKOV3 cells. As cell invasion reflects cell motility and their capacity to degrade the ECM, these results indicate that although TRPC3 activator treated cells are more motile, they may not possess sufficient proteolytic activity to degrade and penetrate the ECM.

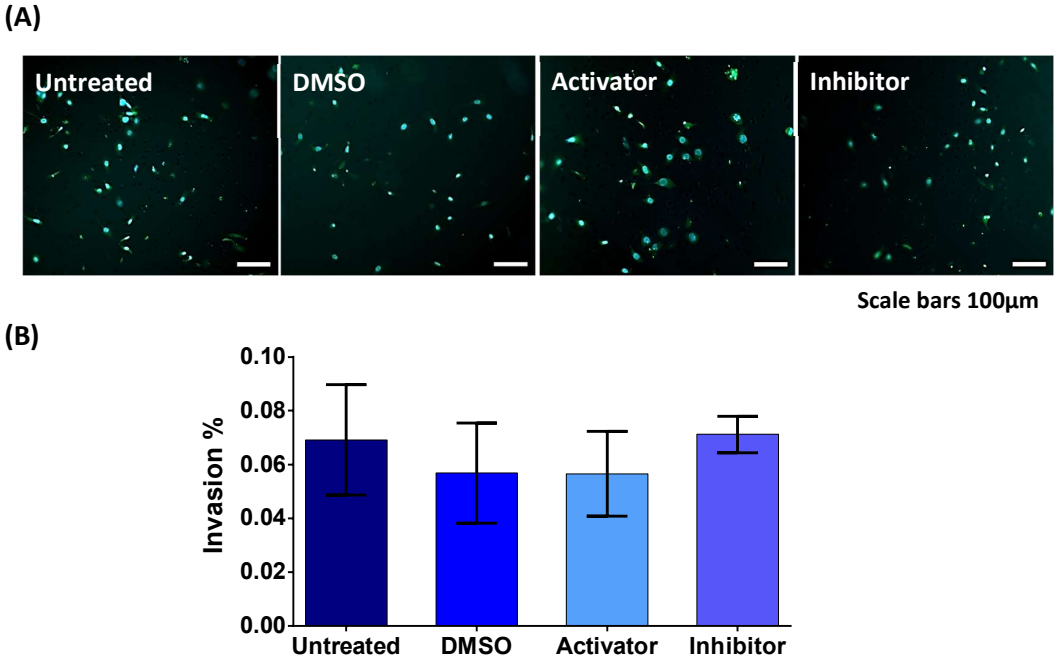

Figure 3.6 Matrigel® invasion assay shows modulating TRPC3 activity does not later the invasiveness of SKOV3 cells

(A) *Representative images of Matrigel® membranes used to quantify cell invasion. Cells were seeded onto membranes in plain media (untreated), or media supplemented with 0.3µM TRPC3 activator, 3µM TRPC3 inhibitor or DMSO equivalent and allowed to invade for 48hrs. Invaded cells were then stained with CFSE (green) and the DNA dye DAPI (blue), fixed and counted. Scale bars 100µm.* ***(B)*** *Percentage cell invasion through Matrigel® membranes shown in (A). Mean ± SEM of three biological replicates for each treatment. No statistically significant differences were observed between treatments as determined by ordinary one-way ANOVA and Tukey's multiple comparisons test.*

3.3.7. TRPC3 INHIBITION ATTENUATES HISTAMINE-INDUCED Ca^{2+} SIGNALLING

In a number of cell types, TRPC3 is activated downstream of histamine H_1 and H_2 GPCRs and facilitates histamine-induced Ca^{2+} entry[305, 364]. Histamine stimulation of the histamine H_1 receptor (H1HR) stimulates Ca^{2+} accumulation in both SKOV3 and OVCAR3 OC cell lines, and subsequently enhances their proliferation[365, 366]. This proposes that TRPC3 may act downstream of H1HR in OC. Mechanisms of TRPC3 activation in OC cells are yet to be investigated, but may represent important signalling pathways that contribute to OC progression. An NFAT translocation assay (depicted in Figure 3.3 A) was employed to decipher if histamine stimulation increases Ca^{2+} signalling in SKOV3 cells, and if this effect is mediated by TRPC3. SKOV3 cells expressing GFP-tagged NFAT were treated with 1.25µM ionomycin as a positive control, 100µM histamine or a combination of histamine and TRPC3 inhibitor, alongside untreated (-) and DMSO controls. In the combined treatment, cells were pre-treated with TRPC3 inhibitor for 30 minutes prior to histamine stimulation. Cells were then incubated with their respective treatment for 2hrs to mirror TRPC3 activator treatments in Figure 3.3. Following, cells were fixed and subjected to indirect immunofluorescence using an anti-GFP antibody (Novus) the DNA dye DAPI. Cells were then imaged and the N/C ratio for each technical replicate was calculated. Ionomycin and histamine significantly increased the nuclear localisation of GFP-tagged NFAT compared to untreated and DMSO controls, indicating that histamine stimulation increases Ca^{2+} signalling in SKOV3 cells (Figure 3.7 A,B). In histamine stimulated cells pre-treated with TRPC3 inhibitor, the effect of histamine was diminished, significantly reducing the N/C ratio to almost that of untreated and DMSO controls (Figure 3.7 B). Histamine-induced Ca^{2+} signalling is therefore attenuated in the presence of TRPC3 inhibitor, suggesting that TRPC3 acts downstream of histamine receptors in SKOV3 cells.

(A)

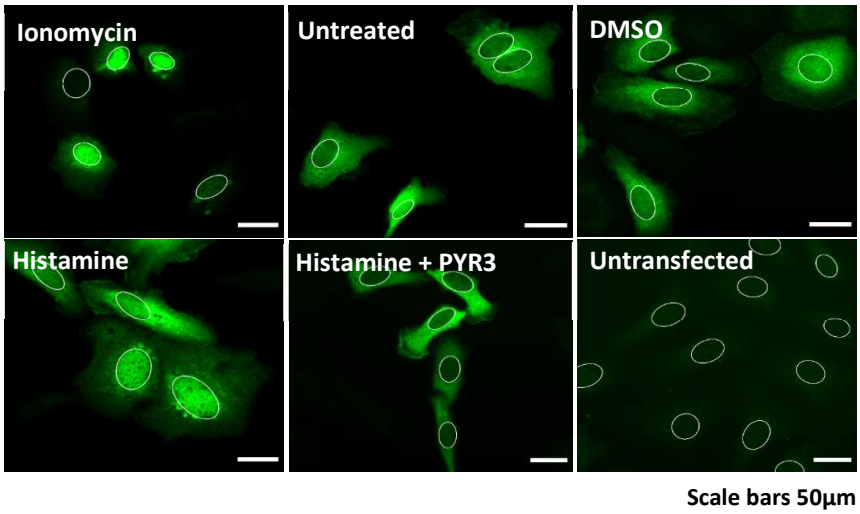

(B)

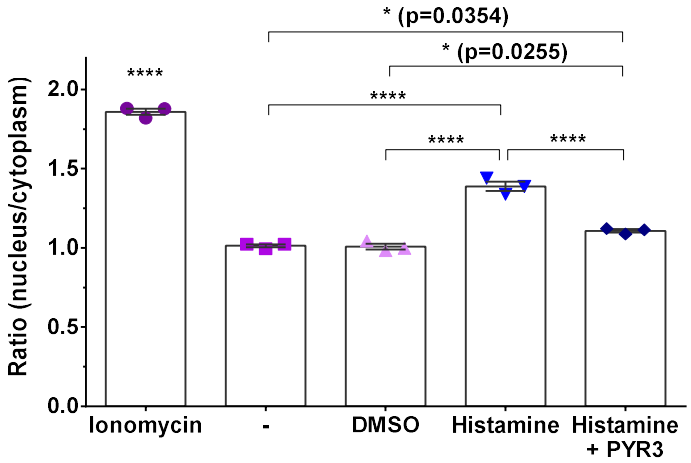

Figure 3.7 Increased Ca^{2+} signalling following histamine stimulation is blocked in the presence of TRPC3 inhibitor Pyr3

(A) *Representative images of NFAT translocation in SKOV3 cells expressing GFP-tagged NFAT following treatment with 1.25µM Ionomycin, 100µM histamine or 100µM histamine plus 3µM PYR3, alongside untreated (-) and DMSO controls. Cells were treated for 2hrs, 24hrs post-transfection. Histamine plus PYR3 treated cells were pre-treated with PYR3 for 30 minutes prior to histamine addition. Cells were then fixed and subjected to indirect immunofluorescence using an anti-GFP antibody (Novus). Nuclear regions are indicated. Scale bars 50µm.* ***(B)*** *Nuclear/cytosol fluorescence intensity ratio of treated cells shown in (A). Mean ± SEM of three independent experiments, n≥100 cells per condition, per experiment. Statistical significance tested by Ordinary one-way ANOVA and Tukey's multiple comparisons test, ionomycin significance to all treatment conditions. **** P ≤ 0.0001. If not indicated – not significant (P > 0.05).*

3.3.8. HISTAMINE TREATMENT ALONE OR IN COMBINATION WITH TRPC3 INHIBITOR DOES NOT SIGNIFICANTLY ALTER CELL INVASION

Histamine stimulation of H1HR stimulates Ca^{2+} accumulation in both SKOV3 and OVCAR3 OC cell lines, and subsequently enhances their proliferation[365, 366]. Unpublished data from the lab also demonstrates that histamine stimulation of H1HR increases the invasive capacity of SKOV3 cells (Supplementary Figure 1). Here, activation or inhibition of TRPC3 in unstimulated SKOV3 cells did not alter invasion (Figure 3.6). However, as demonstrated in Figure 3.7, TRPC3 inhibition attenuates histamine-induced Ca^{2+} signalling, and may therefore decrease the invasiveness of histamine-stimulated SKOV3 cells if the effect on invasion is Ca^{2+}-dependent. To test this hypothesis, a Matrigel® invasion assay was performed on SKOV3 cells which were pre-treated with TRPC3 inhibitor or DMSO equivalent for 30 minutes prior to histamine stimulation, alongside untreated cells and cells treated only with histamine. Cells were allowed to invade for 48hrs before invaded cells on the underside of the membrane were stained with CFSE and the DNA dye DAPI, imaged and quantified to estimate the percentage of invasion (Figure 3.8 A,B). Histamine did not significantly increase SKOV3 invasion in comparison to untreated cells as in previous experiments (Supplementary Figure 1). Therefore, whilst there is a trend for minimally increased invasion in histamine treated cells which is reduced under TRPC3 inhibition, the results of this experiment are inconclusive and the role of TRPC3 in histamine-stimulated SKOV3 invasion cannot be determined.

(A)

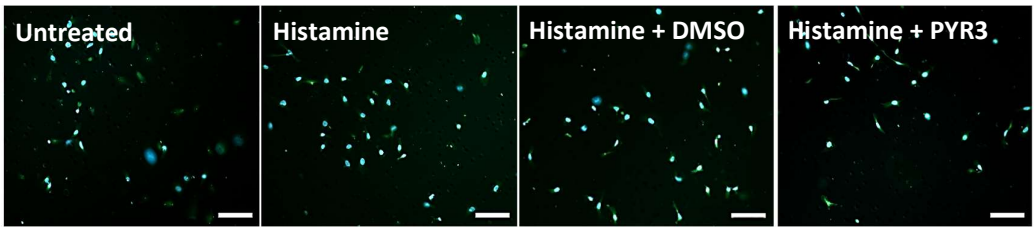

(B)

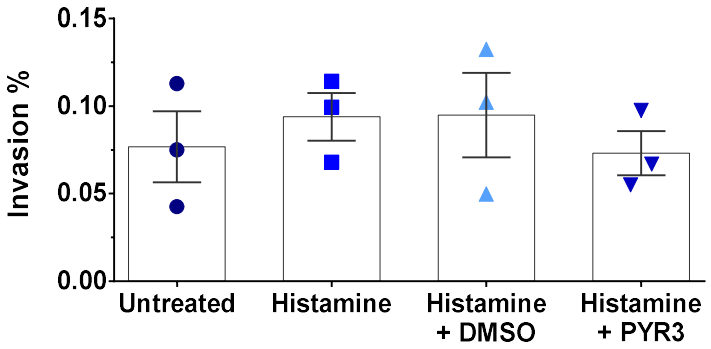

Figure 3.8 Matrigel® invasion assay shows histamine treatment alone or in combination with TRPC3 inhibitor PYR3 does not significantly alter cell invasion.

(A) *Representative images of Matrigel® membranes used to quantify cell invasion. Cells were seeded onto membranes in plain media or media supplemented with 100µM histamine, 100µM histamine plus DMSO (equivalent to PYR3) or 100µM histamine plus 3µM PYR3 and allowed to invade for 48hrs. Invaded cells were then stained with CFSE (green) and the DNA dye DAPI (blue), fixed and counted. Scale bare 100µm.* ***(B)*** *Percentage cell invasion through Matrigel® membranes shown in (A). Mean ± SEM of three technical replicates for each treatment. No statistically significant differences were observed between treatments as determined by ordinary one-way ANOVA and Tukey's multiple comparisons test.*

3.4. DISCUSSION

Previous studies have demonstrated that knocking down TRPC3 expression and non-specifically inhibiting TRPC channels suppresses OC growth, and attenuates hormonal regulation of OC progression[310, 312, 313]. This chapter aimed to extend these findings by investigating if modulating TRPC3 activity with a TRPC3-selective inhibitor and activator influences the progression of OC, using a range of *in vitro* assays to evaluate the different stages of the metastatic cascade. Initially, TRPC3 expression was characterised across a panel of epithelial OC cell lines, and TRPC3 activation in OC SKOV3 cells was found to increase Ca^{2+} signalling without compromising cell viability. The influence of TRPC3 modulation on cell growth, migration and invasion was then assessed: TRPC3 activation significantly increased SKOV3 cell growth and migration in comparison to TRPC3 inhibitor treated cells, whilst no detectable differences in cell invasion were observed. In addition, TRPC3 inhibition attenuated histamine-induced Ca^{2+} signalling, and whilst pathophysiological consequences on cell invasion were inconclusive, this proposes that TRPC3 is activated downstream of histamine receptors in SKOV3 cells.

3.4.1. TRPC3 EXPRESSION AND TARGETING IN OVARIAN CANCER

Initial experiments aimed to characterise endogenous expression of TRPC3 in a panel of OC cell lines. TRPC3 protein was detected in all OC lines by Western Blot (Figure 3.1), although expression was largely variable between OC lines. Previously, Yang *et al.*[310] compared TRPC3 protein expression in ovarian epithelial tumour samples and normal ovarian tissue, and found a marked increase in TRPC3 in human epithelial OC. The data presented here extends these findings by comparing TRPC3 expression amongst multiple OC cell lines. The variation in TRPC3 expression between OC lines likely reflects their different cellular origins: SKOV3 is derived from a non-serous carcinoma, OVCAR3 from high-grade serous carcinoma (HGSC), A2780 from an endometrioid adenocarcinoma and IGROV1 from serous cystadenocarcinoma[329-332], whilst the derivation of OVCAR5 cells is disputed. Originally, OVCAR5 cells were thought to stem from HGSC, however recent literature suggests this cell line may in fact originate from the gastrointestinal tract[370]. OVCAR5 had the lowest TRPC3 expression of all OC lines, which could be explained by their different histopathological origin. It would be interesting to assess if variations in TRPC3 expression between OC lines translates to differences in metastatic potential. There is currently limited available data comparing OC lines with regards to cancer traits such as proliferation, migration and invasion, though two publications do report that SKOV3 cells have a greater invasive capacity than OVCAR3[371, 372]. Based on this data, TRPC3 expression does not correlate with greater invasive potential in OC lines. Ideally, this panel of

OC cell lines would have been employed in downstream analysis of TRPC3 in different stages of the metastatic cascade to test this hypothesis and validate the role of TRPC3 in OC, although this was not possible due to time and budget constraints. Future experiments exploring the role of TRPC3 in metastatic mechanisms of different cell lines is key to characterising the emerging relationship between TRPC3 and OC.

As well as variations in the quantity of TRPC3 expression between OC lines, there were also differences in the number of detected protein bands at TRPC3 size which likely represent TRPC3/TRPC6 heteromeric channels, as TRPC3/6 subunits can assemble into both homomeric and heteromeric channels as reported in other cell lines[358, 367]. The possibility of TRPC3 heteromultimerization translates to issues with specific targeting of the TRPC3 channel, therefore the pathophysiological effects of TRPC3 modulation shown here may involve more than one TRPC channel. Although, the concentrations of TRPC3 inhibitor Pyr3 and activator GSK 1702934A were carefully considered to reduce off-target effects on heteromeric channels. GSK 1702934A is reported to selectively activate TRPC3 with an EC_{50} value of 0.08μM, and TRPC6 at 0.44μM[336]. Therefore, increases in Ca^{2+} signalling and ensuing effects on cell growth and migration at 0.1 and 0.3μM activator are likely attributable to upregulated activity of the TRPC3 channel, although the contribution of TRPC6 cannot be completely ruled out. In addition, concentrations of up to 3μM Pyr3 have shown to selectively inhibit TRPC3 without influencing TRPC6 activity[337]. Therefore, whilst higher concentrations of Pyr3 may have a more pronounced effect on cell proliferation and migration as seen in glioblastoma and melanoma cells treated with up to 20μM Pyr3[308, 318], the results presented here reflect specific regulation of the TRPC3 channel. These results also support the pharmaceutical potential of Pyr3 in treatment of TRPC3-related disease, including OC. There is currently no effective treatment for OC as the mechanism(s) by which OC develops remain largely unknown, and almost 45% of OCs gain a chemo-resistant phenotype following first line treatment with the chemotherapeutic agent cisplatin[262, 373]. TRPC3 poses as a potential therapeutic target for the treatment of OC, particularly in postmenopausal women with elevated FSH levels as knockdown of TRPC3 attenuated the anti-apoptotic effect of FSH following cisplatin treatment[313]. In addition, in a xenograft orthotopic model of glioblastoma, Pyr3 administration inhibited glioma tumour growth[308]. Further studies on the *in vivo* effects of Pyr3 are required to validate the utility of these compounds in treating OC.

3.4.2. TRPC3 IN SKOV3 CELL GROWTH

In this chapter, modulating TRPC3 activity with Pyr3 and GSK 1702934A altered the growth of SKOV3 cells. These results support previous findings that inhibiting or knocking down TRPC3 suppresses OC cell growth in culture and in nude mice, and reduces oestrogen and FSH-induced OC proliferation[310, 312, 313]. TRPC3 inhibition also reduces cell proliferation in additional cancer types, including glioblastoma, melanoma, breast and gastric tumours[308, 309, 311, 318]. In these studies, contradictory results suggest that reduced activity of the TRPC3 channel influences cell growth by inhibiting cell cycle progression and/or promoting apoptosis. For example, downregulation of TRPC3 arrested OC cells at M phase leading to inhibition of their growth without reducing cell viability, however under FSH stimulation, knockdown of TRPC3 was pro-apoptotic[310, 313]. In melanoma, gastric and breast cancers, Pyr3 induced cell-cycle blockade and apoptosis[309, 311, 318]. The trypan blue assay employed here indirectly measures cell growth by counting the number of viable cells, and cannot distinguish between changes in cell proliferation or apoptosis. To determine if altered OC cell growth is a result of proliferative or apoptotic pathways, or a combination of the two, the effect of TRPC3 modulation on BrdU uptake should be assessed to analyse cell-cycle progression, as well as annexin V/propidium iodide (PI) staining to quantify cellular apoptosis.

Future experiments should also focus on identifying the molecular pathways that mediate altered cell growth under TRPC3 modulation. TRPC3 appears to promote cancer cell growth by regulating both receptor-operated Ca^{2+} entry (ROCE) and store-operated Ca^{2+} entry (SOCE) in different cell types. TRPC3-mediated ROCE is stimulated in response to phospholipase C (PLC), downstream of GPCR and RTK activation by external stimuli at the PM[298, 302]. Various GPCRs have been reported to act upstream of TRPC3 in different cell types, including mGluR1[374], OXTR[375], ATR2[376] and histamine H_1/H_2 receptors[305, 364]. Here, TRPC3 inhibition attenuated histamine-induced Ca^{2+} signalling, proposing that TRPC3 is activated downstream of histamine receptors in SKOV3 cells. Interestingly, both TRPC3[310] and H1HR expression are upregulated in clinical OC samples, with H1HR expression correlating with disease progression (unpublished data, Carter lab). H1HR drives the proliferation of a number of cancer types including OC [365, 366], as well as breast[377], lung[378] and hepatocellular[379]. For example, H1HR inhibition in MDA-MD-231 and BT-549 breast cancer cell lines arrested the cell cycle at sub-G0 phase, with consequent suppression of cell proliferation and activation of the mitochondrial apoptosis pathway via ERK[377]. *In vivo,* injecting SNU368 hepatocellular carcinoma cells knocked down for H1HR into the lateral tail vein of nude mice markedly decreased the metastatic potential of SNU368 cells, whilst injection of

HLE hepatocellular carcinoma cells with H1HR overexpressed significantly increased the incidence of lung metastasis[379]. Further investigation is required to determine if TRPC3-mediated Ca^{2+} influx and subsequent OC growth is specifically regulated by H1HR, rather than $H_2/H_3/H_4$ histamine receptors, potentially by knocking down each receptor and analysing ensuing effects on histamine-induced Ca^{2+} signalling and TRPC3 channel activity. These experiments could identify a novel role for H1HR-TRPC3-mediated Ca^{2+} signalling in OC progression.

The ability of TRPC3 to regulate OC cell growth is likely due to a myriad of signalling pathways. In gastric cancer (GC) cells, use of a combination of ROCE and SOCE inhibitors revealed that TRPC3-mediated ROCE compensates for reduced SOCE and enhances cell proliferation, G1/S phase cell cycle transition and apoptosis resistance[309]. Interestingly, the authors also demonstrated that TRPC3-mediated ROCE activated NFAT nuclear translocation through the CNB2/GSK3β signalling cascade, which ultimately promoted GC tumorigenicity. CaMKIIα, a Ca^{2+}-activated transcriptional regulator involved in calcineurin/NFAT signalling[369, 380], was substantially inhibited when TRPC3 was downregulated in OC cells and reduced cell growth by decelerating metaphase exit[310]. Here, TRPC3 activation induced NFAT nuclear translocation in SKOV3 cells and was used as a measure of intracellular Ca^{2+} signalling. Activation of NFAT is frequently documented in fast-growing malignancies[381-383], and may therefore represent a downstream tumorigenic mechanism of TRPC3 in OC cell growth. In terms of SOCE, the Ca^{2+}/calmodulin/calcineurin/NFAT pathway has also shown to regulate TRPC3 expression based on Ca^{2+} store depletion in prostate cancer cells[384]. TRPC3 also acts as a SOCE channel in a Orai1:TRPC3 complex[385] in melanoma cells, whereby TRPC3-mediated SOCE regulates cell proliferation and apoptosis via activation of Akt and the JAK/STAT5 signalling pathway[318]. TRPC3 activation also regulates cell proliferation and apoptosis through the Ras-MAPK pathway, NF-kB activation and dysregulation of long-chain non-coding RNAs such as small nucleolar RNA host gene 3 (SNHG3)[311, 386, 387]. All of these pathways represent possible mechanisms by which TRPC3 modulation alters OC cell growth, and are to be explored further.

3.4.3. TRPC3 IN SKOV3 CELL MIGRATION

Cell migration is a central component of the metastatic cascade, and involves a variety of temporally and spatially coordinated Ca^{2+}-sensitive processes ranging from cell polarization, cell-cell and cell-basement membrane adhesions, as well as reorganisation of the cytoskeleton[314-316]. Ca^{2+} channels and transporters are therefore key regulators of tumour cell migration, with several members of the TRP channel family implicated in enhanced cell migration of numerous

cancer types[317]. Previous studies have demonstrated a role for TRPC3 in the migration of glioblastoma and melanoma cells, as well as cancerous and non-cancerous gastric cells and skin fibroblasts[308, 309, 318, 387]. Here, TRPC3 activation significantly increased SKOV3 cell migration in comparison to both untreated and TRPC3 inhibitor treated cells. This is the first demonstration of TRPC3 signalling mediating OC cell migration, and substantiates the role of TRPC3 in the progression of OC.

Many components of migration machinery are sensitive to alterations in Ca^{2+} signalling, therefore TRPC3 may mediate OC cell migration through several different mechanisms. In glioblastoma cells, inhibition of TRPC3 with Pyr3 reduces cell migration through impairing focal adhesion and cytoskeleton protein expression, namely focal adhesion kinase (FAK) and myosin light chains (MLC)[308]. FAK regulates cell migration by controlling the turnover of integrin adhesion sites at the leading lamellipodia of migrating cells and adhesion disassembly at the trailing edge, whilst MLC increases the contractility of the actin cytoskeleton to promote the cell protrusion and retraction essential for cell motility[388, 389]. In addition, Pyr3 inhibits cell migration in melanoma cells by downregulating the secretion of MMP9, a proteolytic enzyme which remodels the ECM and cleaves cell-cell adhesions to enhance the migratory capacity of cancer cells[319]. Interestingly, FAK, MLC and MMP9 are all upregulated in invasive OCs and play a functionally significant role in OC migration[390-392], proposing their involvement in TRPC3-mediated OC migration. Many studies have also shown low Ca^{2+} gradients at the leading edge of migrating cells provoke high sensitivity to SOCE, whereby SOCE-activated Ca^{2+} signalling is implemented in the mediation of actomyosin and focal adhesion assembly[354, 393]. Therefore, upregulation of TRPC3-mediated SOCE as demonstrated in melanoma cells may also facilitate increased OC migration.

Although the wound healing assay employed to evaluate OC cell motility is used in most studies of cancer cell migration including those discussed here, it does not consider the motility of individual cells, the effect of chemoattractant in the media or distinguish between cell division or motility. With regards to the latter, faster growing cells will close the wound area quicker than those with a low proliferation rate, therefore as TRPC3 modulation also influences OC cell growth, differences in the migration rates of TRPC3 activator and inhibitor treated cells may be a consequence of altered OC growth. Of note, there was no significant difference in OC cell growth at low or high concentrations of TRPC3 activator/inhibitor until 48hrs, whereas differences in cell migration were apparent from as early as 4hrs. This is consistent with the role of local and rapid Ca^{2+} signals in directional cell migration, and more prolonged transcriptional-

related changes in cell proliferation[161, 394]. SKOV3 cells were also serum starved 24hrs prior to the migration assay to suppress cell division. Collectively, this would suggest that the results of the wound healing assay are a true representation of altered OC cell migration under TRPC3 modulation, however the influence of cell proliferation cannot be completely ruled out. Repeating the wound healing assay with compounds that inhibit cell division such as mitomycin C as a control for cell proliferation would improve the reliability of these results[395]. In addition, a transwell migration assay or single cell tracking analysis would provide further information regarding cell behaviour in the presence of a chemoattractant and single cell locomotion.

3.4.4. TRPC3 IN SKOV3 CELL INVASION, AND OTHER MEASURES OF CANCER PROGRESSION

Enhanced cell motility drives tumour invasion into surrounding tissues and vasculature, enabling colonization at local and distant secondary sites[396, 397]. To evaluate if the increased motility of SKOV3 cells under TRPC3 activation also increases their capacity to invade through the ECM, a Matrigel® invasion assay was performed. There was no detectable difference in SKOV3 invasion under TRPC3 modulation, suggesting that TRPC3 does not contribute to the invasiveness of SKOV3 cells. As cell invasion reflects cell motility and their capacity to degrade the ECM, this indicates that although TRPC3 activator treated cells are more motile, they may not possess sufficient proteolytic activity to degrade and penetrate the ECM. Proteolytic enzymes released by tumour cells or the tumour microenvironment (TME) which aid ECM degradation include the urokinase form of the plasminogen activator (uPA), cathepsins and MMPs[186-188]. Contradictory to our results, secretion of MMP9 is regulated by TRPC3 in melanoma cells[318] and the related channel TRPC6 mediates the secretion of both MMP2 and MMP9 in prostate cancer cells[398]. To determine if TRPC3 modulation alters the expression of proteolytic enzymes in SKOV3 cells, a zymography assay could be used to visualise the breakdown of ECM-fluorescent labelled components by TRPC3 activator and inhibitor treated cells[399]. In addition, the Matrigel® invasion assay failed to replicate previous findings in the lab that histamine stimulation significantly increases the invasive capacity of SKOV3 cells. Although there was a trend for minimally increased invasion in histamine treated cells which was reduced under TRPC3 inhibition, further replicates are required to reduce the high variability between replicates and determine the role of TRPC3 in histamine-stimulated SKOV3 invasion. Besides its inherent variability, an important consideration of the Matrigel® invasion assay and indeed the other 2D assays employed in this chapter is that these assays study the behaviour of OC cells in isolation, and ignore the complex interactions with the TME which facilitate cancer progression *in vivo*[400]. Therefore, three-

dimensional assays such as a spheroid migration assay, or co-culture models with cells in the TME (stromal fibroblasts or ECM) could better encapsulate the role of TRPC3 in OC invasion *in vivo*.

To further explore the role of TRPC3 in OC progression, additional stages of the metastatic cascade should be evaluated. EMT is a key process in cancer metastasis whereby cancer cells acquire a more motile and invasive mesenchymal phenotype[178, 179]. The process of EMT is marked by the loss of epithelial markers such as E-cadherin and claudins in exchange for mesenchymal ones, such as vimentin, N-cadherin and MMPs[181]. A previous publication indicates that inhibition of TRPC1/3/6 in gastric cancer cells by SKF96365 and 2-APB increases the expression of E-cadherin and reduces levels of vimentin and α-SMA, thus mitigating the EMT process[320]. Therefore, evaluating the expression of EMT-key related genes may provide a clearer overall picture of how TRPC3 modulation is regulating OC cell migration and invasion. Another important measure of metastatic competence is the ability of tumour cells to adhere to the endothelial wall of lymphatic or blood vessels in order to intravasate and extravasate to distant sites[194, 401]. The expression of adhesion molecules by endothelial cells is regulated by Ca^{2+}-permeable ion channels including TRPC3, as overexpression of TRPC3 has shown to enhance TNFα-induced VCAM-1 expression[321]. The effect of TRPC3 activation/inhibition on OC cell adhesion could be assessed using a static adhesion assay[402]. TRPC3 has also been implicated in facilitating tumour neovascularisation in OC; a process whereby cancer cells release 'angiogenic activators' to activate surrounding endothelial cells to form new blood vessels to serve the growing mass and facilitate metastasis[173, 174]. Knockdown of TRPC3 in OC cells decreased the expression of angiogenic biomarkers survivin, HIF1α and VEGF[313], therefore evaluating the effect of Pyr3 on the expression of similar angiogenic markers may reveal a potential pharmaceutical role of Pyr3 as an angiogenesis inhibitor in OC.

3.5. KEY FINDINGS

- TRPC3 is variably expressed across a panel of OC cell lines.
- The selective TRPC3/6 activator GSK 1702934A increases Ca^{2+} signalling in SKOV3 cells without compromising cell viability.
- Modulating TRPC3 activity with the TRPC3-selective inhibitor Pyr3 and selective TRPC3/6 activator GSK 1702934A alters the growth of SKOV3 cells.
- TRPC3 activation significantly increases SKOV3 cell migration in comparison to both untreated and TRPC3 inhibitor treated cells, identifying a novel role for TRPC3 in OC cell migration.
- Modulating TRPC3 activity does not alter the invasiveness of SKOV3 cells.
- TRPC3 inhibition attenuated histamine-induced Ca^{2+} signalling, although pathophysiological consequences on cell invasion were inconclusive.

Chapter 4

The functional effects of TRPC3-mediated EV communication

4. The functional effects of TRPC3-mediated EV communication

4.1. Background

4.1.1. EVs in cancer progression

The process of cancer metastasis relies on complex intercellular interactions with the local and distant tumour microenvironment (TME)[2, 3]. Classically, cancer cells communicate via direct cell-cell interactions and the secretion of soluble factors such as cytokines, chemokines and growth factors[4-6]. In addition to these canonical secreted factors, EVs are emerging as fundamental cell-cell communicators in cancer progression, with roles identified in every stage of the metastatic cascade from promoting cell proliferation in primary tumours, to the migration, invasion and generation of pre-metastatic niches which permit their secondary metastasis[204, 205]. In serum samples from women diagnosed with OC, the concentration of circulating EVs is significantly elevated compared to benign disease or controls, and correlates with disease progression[163]. Similarly, SKOV3 cells release significantly more EVs than their less-invasive OC counterparts OVCAR3[372], and EVs from high-metastatic OC cells can promote the migration and invasion of recipient low-metastatic OC cells[403]. OC-derived EVs can also promote epithelial to mesenchymal transition (EMT), and the proliferation and migration of human peritoneal mesothelial cells (HPMCs), a common site for OC dissemination [404]. *In vitro* and *in* vivo, OC-derived EVs promote angiogenesis[405], and contain proteolytic MMPs which drive ECM degradation in OC invasion[406]. Although these examples demonstrate a substantial role for EVs within the OC TME, little is understood about the molecular mechanisms which contribute to the metastatic competence of OC-derived EVs.

4.1.2. A potential role for TRPC3-mediated EV communication in OC

TRPC3 protein expression is markedly increased in human OC compared to non-cancerous specimens, and plays a vital role in OC development *in vitro* and *in vivo*[310]. Indeed, the results presented in Chapter 3 demonstrate that pharmacological activation of TRPC3 significantly increases the growth and migratory capacity of SKOV3 cells. These metastatic mechanisms are likely mediated by divergences in Ca^{2+} homeostasis, as TRPC3 activation increases Ca^{2+} signalling in SKOV3 cells (Chapter 3). In a number of cell types, such increases in intracellular Ca^{2+} also induce EV release[143-145]. Further to this, EVs released by cancer cells with disrupted Ca^{2+} signalling show enhanced metastatic capacity compared to EVs secreted under normal conditions. For example, Ca^{2+} stimulation of the breast cancer cell line MDA-MB-231 induces a ~10-fold increase

in membrane type 1 MMP (MT1-MMP) EV release, which subsequently enhance ECM degradation[144]. In addition, EVs released by OC cells following chelation of extracellular Ca^{2+} induce biophysical and functional changes in OC-derived fibroblasts, and elicit a pronounced effect on recipient cell adhesion and migration[167]. Emerging evidence suggests that members of the TRPC family may mediate Ca^{2+}-induced EV release and subsequent metastatic mechanisms. TRPC5 has shown to be required for EV release from chemoresistant breast cancer cells, and through EV-mediated transfer of functional TRPC5 channels, upregulates Ca^{2+} influx in recipient chemosensitive cells to promote a chemoresistant phenotype[112, 322]. A gain-of-function mutation in TRPC3 has also been linked with alterations in EV biogenesis pathways in mouse purkinje cells, as increased Ca^{2+} influx was coupled with the deregulation of several transcripts related to EV biogenesis[326]. A number of these transcripts were likewise deregulated in human induced pluripotent stem cells (hiPSCs) harbouring a gain-of-function mutation in the TRPC3 gene, and preliminary results demonstrated a detectable difference in EV release between TRPC3-mutant and control hiPSCs at 24 hours (Figure 1.5 A,B). Moreover, in neurons, TRPC3 is a downstream effector of the GPCR metabotropic glutamate receptor 1 (mGluR1)[374], which has previously been implicated in mediating the release of EVs that increase the migration, invasion and growth of recipient melanoma cells[407]. Collectively, these results propose that disrupted Ca^{2+} signalling downstream of TRPC3 modulation in SKOV3 cells may induce the release of EVs with enhanced metastatic competence, potentially via the functional transfer of TRPC3 channels, or upstream regulators thereof. TRPC3-mediated EV release may therefore contribute to the increased growth and migration of SKOV3 cells observed in Chapter 3.

4.1.3. ISOLATING A PURE EV POPULATION FOR FUNCTIONAL ANALYSIS

As the EV field is new and in rapid evolution, there is currently no 'gold standard' method for their separation and isolation from other soluble factors in the cellular secretome, or from the culture medium itself. Culture medium is commonly supplemented with heat-inactivated foetal bovine serum (FBS) to provide additional growth factors and carrier proteins to support cell growth in culture[408]. However, serum in general - and FBS specifically - contains high concentrations of EVs which can interfere with quantitative and/or qualitative assessments of cell-culture-derived EVs[409]. Therefore, exogenous EVs are routinely removed from the culture medium prior to cell conditioning by high-speed ultracentrifugation (UC), although several publications report that this technique is not effective at depleting FBS-derived EVs from the medium, and persisting FBS-EVs can contaminate *in vitro* cell-derived EV analyses[409, 410]. Serum-free media (SFM) is increasingly used as a culture alternative to eliminate exogenous EV

contamination, though the effect of serum-free culture on cell growth and viability should be evaluated for each cell-type. In order to accurately assess the role of EVs in mediating metastatic mechanisms *in vitro*, the extraction culture conditions must be optimised for the cell line in use and the extent of potential contaminants quantified.

4.2. AIMS AND OBJECTIVES

As disrupted Ca^{2+} signalling can induce the release of EVs with enhanced metastatic competence, TRPC3-mediated EV release may contribute to the increased growth and migration of SKOV3 cells observed in Chapter 3. The aim of this chapter was to test this hypothesis by applying EVs from TRPC3 activator and inhibitor treated SKOV3 cells to naïve SKOV3 cells, and analysing ensuing effects on SKOV3 cell growth, migration and invasion. A schematic representation of the experimental procedure is illustrated in Figure 4.1. In addition, appropriate culture conditions were established to specifically assess the role of SKOV3-EVs in these metastatic mechanisms, and the effect of TRPC3 activation and inhibition on EV release and characteristics, as well as potential mechanisms of functional receptor transfer were assessed. The specific objectives were to:

1. Evaluate the effectiveness of FBS EV-depletion and optimise culture conditions for SKOV3-EV extraction
2. Characterise SKOV3-EVs and the effect of TRPC3 activation and inhibition on EV release and surface antigen expression
3. Assess if TRPC3 activator or inhibitor-induced EVs have the functional capacity to influence the growth, migration or invasion of naïve SKOV3 cells
4. Probe SKOV3-EVs for the expression of TRPC3 and its upstream regulator mGluR1

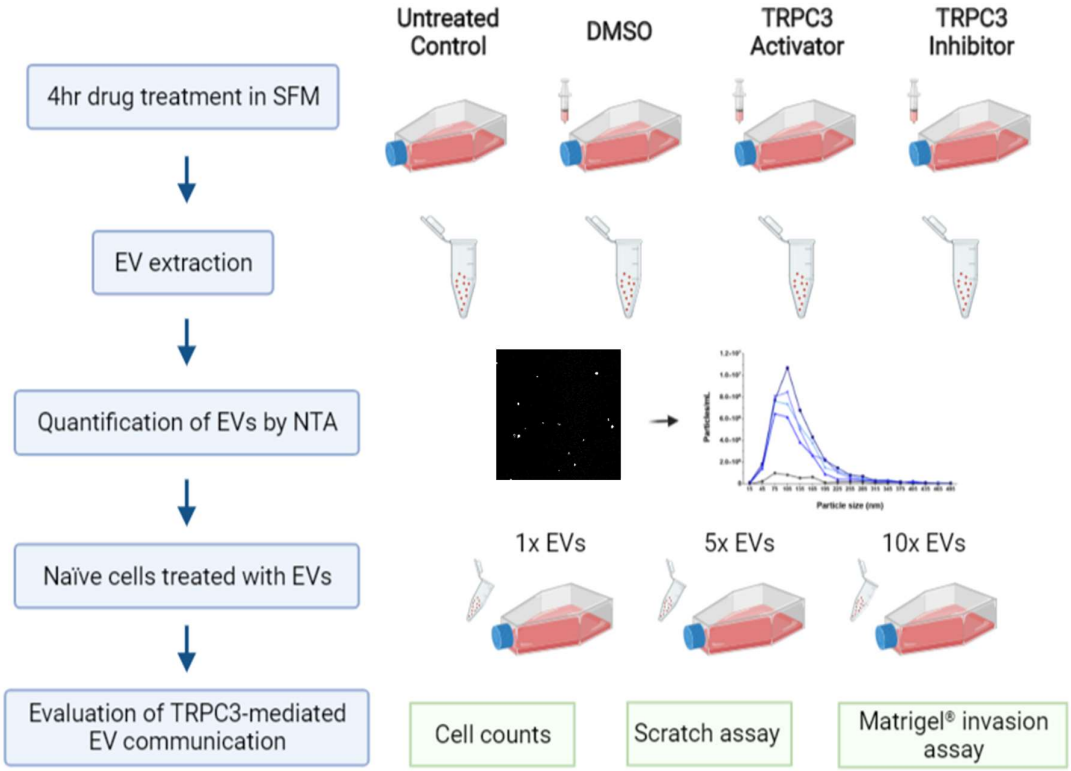

Figure 4.1 Illustrated overview of the experimental procedure used to assess TRPC3-mediated EV communication

Briefly, SKOV3 cells were grown to ~80% confluency in complete media, washed and treated with 0.3µM TRPC3 activator, 3µM TRPC3 inhibitor or DMSO equivalent in serum-free media (SFM) for 4 hours. EVs were then isolated from the conditioned media and quantified by NTA. 1x, 5x and 10x EV/cell concentrations were calculated from the untreated control and added to naïve cells in media supplemented with 10% EV-depleted FBS. Equivalent volumes of PBS were added to cells as a no EV control. Cell counts, scratch and Matrigel® invasion assays were used to assess the effects of TRPC3-mediated EV communication.

4.3. RESULTS

4.3.1. EV-DEPLETED FBS RETAINS PARTICLES DETECTABLE BY COMMON EV ASSAYS

To prevent contamination of quantitative and/or qualitative assessments of cell-derived EVs, bovine EVs were removed from the culture medium by high-speed UC. To assess the effectiveness of the EV depletion protocol and quantitate potential contamination, five independent EV-depleted FBS batches were assessed for particle count, size and protein concentration by NTA and BCA assay respectively. This showed that whilst there was a 76% (±11%) reduction in the number of particles, EV-depleted FBS retained high particle counts of $5.61x10^{10}$ $\pm 2.23x10^{10}$ per ml of FBS (Figure 4.2 A). Correspondingly, depletion reduced the protein content of FBS by 56% (±17%) but high protein concentrations of 28.5±10.5 µg/ml were still present (Figure 4.2 B). NTA size analysis demonstrated that the median size of the particles was reduced in the depleted FBS (Figure 4.2 C), suggesting the depletion protocol is more effective at removing larger particles. With evidence that depleted medium retains high particle and protein concentrations, and particles of EV size, the FBS was further assessed for the presence of EV markers by western blot. FBS samples pre- and post- depletion were void of EV protein markers CD63, CD9 and CD81, indicating that, whether due to the species specificity of antibodies or the absence of bovine EVs, detection of cell-derived EVs was specific (Figure 4.2 D). In contrast, a single band was present in all FBS samples for the EV marker TSG101, that was enriched in depleted FBS. This may represent antibody cross reactivity with the heavy chain of IgG which also migrates at ~50kDa, as two distinct bands were present in the positive EV control. Repeating with a different TSG101 antibody detected faint bands within the FBS that were absent following depletion, indicting specific detection (Figure 4.2 E). Actin however, showed high reactivity in all samples, and is therefore unsuitable for specific EV detection. These results together indicate that, whilst EVs could be specifically detected using optimised antibodies, medium depleted for EVs using a standard UC protocol retain high particle and protein concentrations and particles of EV size, which may interfere with cell-derived EV analysis.

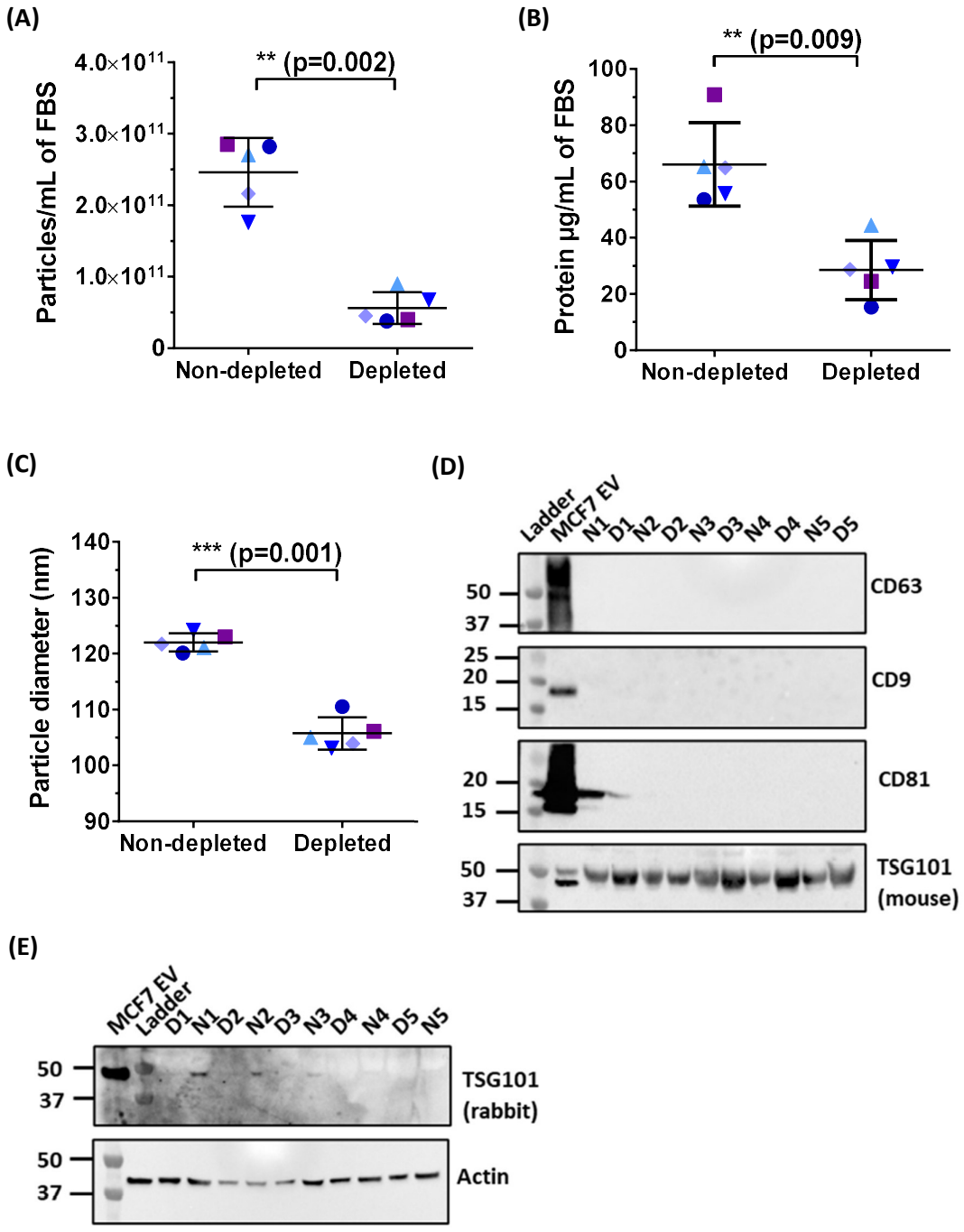

Figure 4.2 EV-depleted medium retains high particle and protein concentrations and particles of EV size

(A)-(C) *Five independent batches of FBS were analysed for (A) particle number, (B) protein concentration and (C) particle size pre- and post-EV depletion. Data representants mean ± SD, with each data point representing the mean of three replicate measurements. Statistical significance assessed with two-tailed paired t-test.* ***(D)*** *and* ***(E)*** *Western blotting of EV markers (CD63, CD9, CD81, TSG101, ACTIN) in FBS samples characterised in (A)-(C). N1-5 represent non-depleted FBS, and D1-5 EV depleted. Equivalent protein was loaded for each blot (20µg). All protein samples were run in non-reducing conditions, except for samples probed with ß-actin. Work done together with Dr Elizabeth Dellar.*

4.3.2. SERUM-FREE MEDIA IMPROVES ANALYSIS OF CELL-SPECIFIC EVS

In light of the results that EV-depleted FBS may contaminate quantitative and qualitative analysis of cell-specific EVs, SKOV3-EVs were next extracted in media supplemented with 10% depleted FBS (FBS EVs) and serum-free media (SFM EVs) to compare their elution, signal-noise ratio and suitability for downstream analysis. Non-conditioned media (NCM) controls were also assessed for comparison. NTA analysis of SEC fractions 5-10 indicated that particles from FBS EVs and FBS NCM eluted in the same manner, peaking at fraction 6 and declining thereafter (Figure 4.3 A). In this instance (mean of two biological replicates), there were in fact a higher concentration of particles at the elution peak for the NCM compared to FBS EVs, confirming that depleted FBS interferes with accurate EV quantification by NTA. In SFM, EVs eluted similarly over fractions 6 and 7 while minimal particles were detectable in SFM NCM. Calculation of the total particle content in five biological replicates confirmed a significant enrichment over NCM in SFM compared to FBS (Figure 4.3 B). SFM EVs and FBS EVs were next compared in terms of their protein content (Figure 4.3 C). Unsurprisingly, FBS EVs and FBS NCM had a significantly higher protein content than SFM EVs or SFM NCM. In contrast to the particle counts, FBS EV protein was significantly enriched over FBS NCM, indicating that the particles detected in NCM by NTA are largely nonspecific, low-protein molecules. There was no detectable difference in protein content between SFM EVs and SFM NCM, likely due to the minimal protein yield. Finally, transmission electron microscopy (TEM) was used to characterise the content of FBS NCM (Figure 4.3 D). Small, circular structures were abundant in FBS NCM - with some particle's indicative of EV morphology (cup-shaped, 40-150nm). These structures were absent in SFM NCM, indicating likely bovine origin. Collectively, these results verify that residual bovine particles in depleted medium contaminate the analysis of SKOV3-EVs, and propose SFM as an effective culture alternative for EV extraction.

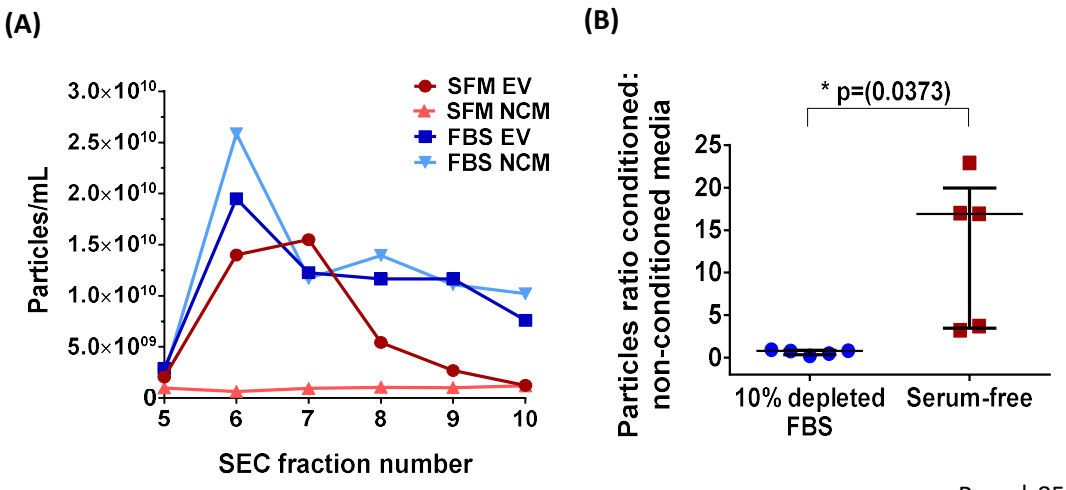

(C)

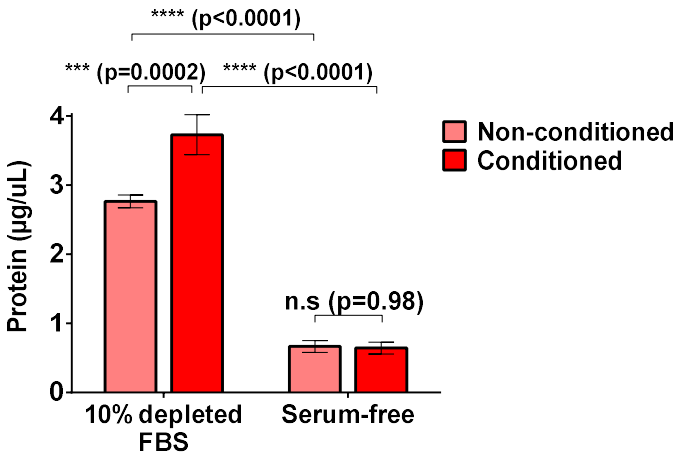

(D)

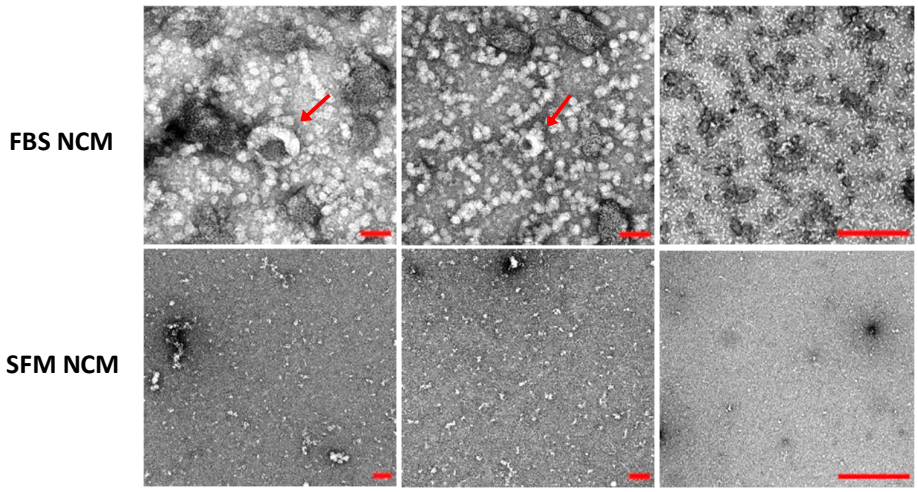

Figure 4.3 Serum-free media contains fewer small particles and less interfering protein

(A) *NTA particle counts for EV SEC fractions 5-10 collected from SKOV3 conditioned media containing 10% depleted FBS (FBS EV), SKOV3 conditioned serum-free media (SFM EV), and non-conditioned media controls (NC FBS and NC SFM respectively). Data represents mean of two biological replicates.* ***(B)*** *Ratio of particle counts in conditioned to non-conditioned media for media containing 10% depleted FBS and serum-free. Median and interquartile range shown for five biological replicates, with statistical significance tested by unpaired t-test with Welch's correction.* ***(C)*** *Protein concentration in media containing 10% depleted FBS and serum-free, comparing SKOV3 conditioned and non-conditioned samples. Mean ± SD of three replicate measurements, with statistical significance tested by two-way ANOVA with Sidak's multiple comparisons test.* ***(D)*** *Representative electron micrographs of small particles visible in non-conditioned media containing 10% EV-depleted FBS (FBS NCM), compared to serum-free media (SFM NCM). Arrows indicate EV-like structures. Scale bars 1000nm for far-right images, and 100nm for left and centre images.*

4.3.3. SERUM-FREE MEDIA IS A VIABLE ALTERNATIVE FOR CULTURING SKOV3 CELLS FOR EV EXTRACTION

As shown above, serum-free media improved the analysis of cell-specific EVs by eliminating exogenous EV contamination. However, serum starvation is often used as a method to induce cellular stress pathways[411] and is therefore not suitable for use with all cell types. To assess the capacity of serum-free conditions to support SKOV3 cell culture, SKOV3 cells were cultured for 24, 48 and 72hrs in SFM, and media supplemented with 10% EV-depleted or full FBS, and analysed for differences in cell growth and viability. Cell growth was reduced in depleted FBS and serum-free media at both 24 and 72hrs (Figure 4.4 A). Upon quantification, SKOV3 cell count in SFM was reduced to 60% (±15%) of full FBS media at 24hrs and 67% (±22%) at 48hrs, with depleted FBS cultured cell counts reduced to 88% (±11%) and 82% (±27%) at 24 and 48hrs respectively (Figure 4.4 B). No statistical significance was observed between SFM and depleted FBS cultured cell counts. To assess if lower cell counts in SFM and depleted FBS were due to reduced cell proliferation or enhanced apoptosis, an Annexin V apoptosis assay was used to quantify cellular apoptosis (Figure 4.3 C). Culture in SFM nor depleted FBS caused significant cell apoptosis at 24 or 48hrs, therefore SFM and depleted FBS reduce SKOV3 proliferation, but do not affect cell viability. After evaluating the suitability of SFM for SKOV3 culture, SKOV3-EVs were extracted from SFM at various timepoints to determine an appropriate conditioning period. In SFM, EVs were detectable above background by NTA after 4hrs, with a significant number of EVs detectable above background at 8hrs (Figure 4.4 D). Longer time periods >8hrs did not increase EV yield, with a reduction in detectable EVs at 16hrs. Taken together, SFM reduces SKOV3 proliferation in comparison to full FBS media but does not affect cell viability, and permits detection of SKOV3-EVs >4hrs conditioning. SFM is therefore suitable for culturing SKOV3 cells for EV extraction.

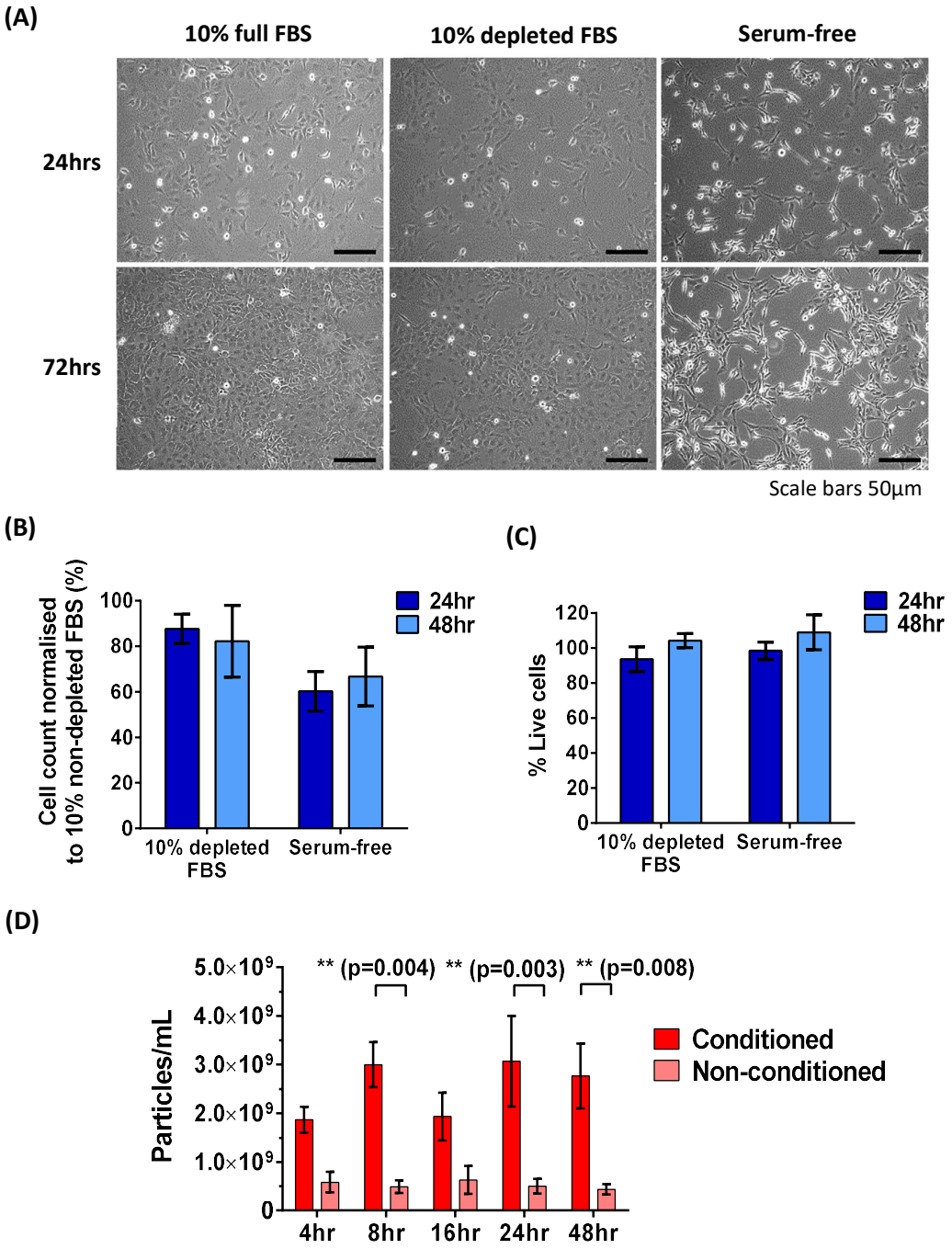

Figure 4.4 Serum-free media supports SKOV3 cell culture

(A) *Representative images of SKOV3 cells cultured in media supplemented with 10% non-depleted FBS (left), 10% depleted FBS (middle) and serum-free (right) at 24hr and 72hrs. Scale bars 50µm. Images taken by Dr Elizabeth Dellar.* ***(B)*** *Percentage of SKOV3 cell count after 24 and 48hr culture in media containing 10% depleted FBS or serum-free, normalised to culture in media containing 10% non-depleted FBS.* ***(C)*** *Percentage viability of SKOV3 cells cultured in media containing 10% depleted FBS or serum-free for 24 and 48hrs. (B) and (C) formed of mean ± SEM from three independent experiments with no statistical significance observed, as determined by two-way ANOVA and Sidak's multiple comparisons test.* ***(D)*** *Particle counts of SKOV3 conditioned and non-conditioned serum-free media after 4, 8, 16, 24 and 48hrs. Mean ± SEM of three independent experiments, with statistical significance determined by two-way ANOVA and Sidak's multiple comparisons test.*

4.3.4. SKOV3-EVs PRESENT TYPICAL EV MARKERS AND MORPHOLOGY

As demonstrated in Sections 4.3.2 and 4.3.3, culture conditions for SKOV3-EV extraction were optimised to reduce contaminants from the culture medium. However, cell-derived EVs also co-isolate with other soluble factors from the cellular secretome, therefore it is necessary to verify the origin and characteristics of extracted EVs prior to their use. A range of methods are used to characterise EVs including TEM to analyse single vesicle size and morphology, and immunocytochemistry techniques such as immunogold labelling, western blot, flow cytometry and affinity-based assays to assess the enrichment of EV markers[412]. Organelle markers are also assayed to evidence that the EV preparation is clear of cell contaminants[412]. Therefore, SKOV3-EVs were extracted from SFM after 48hrs conditioning and characterised in terms of their size, morphology and molecular composition using these techniques. The presence of EVs was initially confirmed by TEM, with the detection of negatively stained, 'cup-shaped' particles in the size range of 40-150nm (Figure 4.5 A). Using immunogold labelling in conjunction with TEM, these particles labelled positive for the EV marker CD81 – confirming their endosomal origin. Western blot analysis confirmed that SKOV3-EVs were enriched for CD81, as well as an array of recognised EV markers (CD9, TSG101 and ALIX) (Figure 4.5 B). SKOV3-EV lysates were clear of the mitochondrial marker cytochrome C and Golgi marker GM130, confirming the absence of cellular contamination in EV preparations. EV surface antigens were further analysed by the affinity-based platform Exoview®, whereby EVs are captured on antibody spots for CD81, CD63 and CD9 and subsequently labelled with fluorescent antibodies against CD81 and CD9. Quantification of EV fluorescence at each spot enables the detection of single and co-labelled EVs. In complement to the western blot analysis, CD81 and CD9 positive EVs were detected, as well as a subpopulation of CD81 and CD9 co-labelled EVs (Figure 4.5 C). Minimal CD63-positive EVs were detected. Lastly, SKOV3-EV surface antigen expression was analysed by flow-cytometry with the multiplexed MACSPlex assay. In this qualitative assay, SKOV3-EVs were mixed with 'exosome capture beads', each coated with different monoclonal antibodies against 37 potential EV surface antigens (depicted in Figure 2.4). Bead-captured EVs were subsequently detected by counterstaining with APC-conjugated CD9, CD63, and CD81 antibodies. Flow cytometry analysis of the APC signal detected the expression of 22 surface antigens, including all three tetraspanin markers (CD9, CD63, CD81) as well as additional proteins of interest CD29 (Integrin β1), SSEA-1 (Stage-specific embryonic antigen 1), CD105 (Endoglin), CD326 (EpCAM) and CD44 (Figure 4.5 D). Collectively, these results present a thorough characterisation of SKOV3-EVs, which are of typical EV size and morphology and comprise several proteins widely recognised as EV markers.

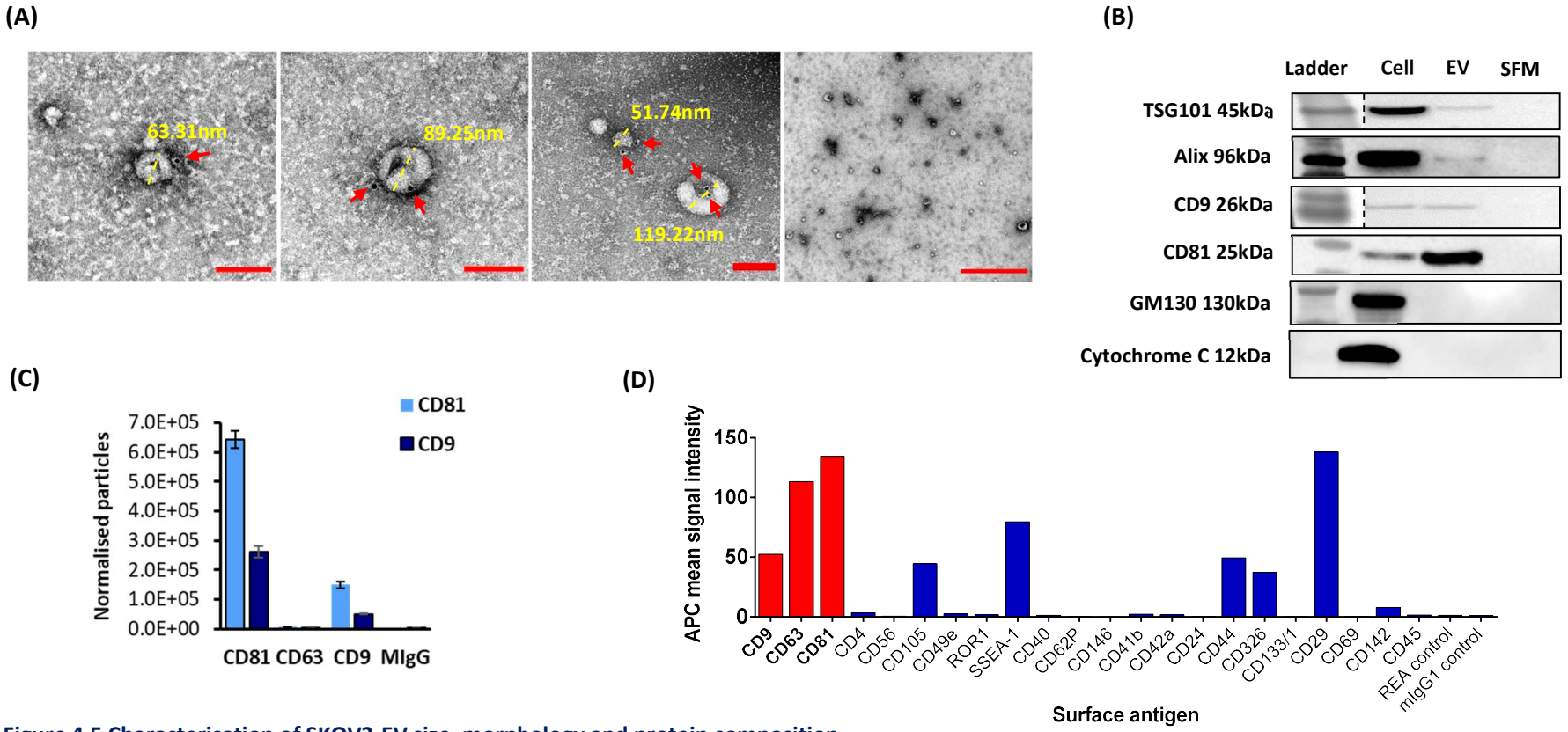

Figure 4.5 Characterisation of SKOV3-EV size, morphology and protein composition

(A) *Representative immunogold (anti-CD81) negative stained electron micrographs of SKOV3 EVs. Arrows indicate 10nm gold particles. Scale bars 100nm and 1000nm (far right image only).* ***(B)*** *Western blotting of EV protein markers (TSG101, Alix, CD9, CD81) in SKOV3 cell and EV. EV lysates were clear of negative protein markers GM130 and Cytochrome C. SFM: non-conditioned media control.* ***(C)*** *Exoview analysis detects CD81, CD63 and CD9 positive particles in SKOV3-EVs. Data represents mean ± SEM of repeated measurements from one independent experiment. Raw data not available for statistical analysis.* ***(D)*** *MACSPlex exosome assay data showing the mean signal intensities of 22 surface antigens and 2 isotype controls detected on SKOV3-EVs. EV markers CD9, CD63 and CD81 highlighted in red. APC fluorescence intensity adjusted to PBS blank. Results representative of one independent experiment.*

4.3.5. TRPC3 MODULATION INFLUENCES SKOV3-EV RELEASE AND SURFACE ANTIGEN EXPRESSION

The ultimate aim of this chapter is to test the hypothesis that disrupted Ca^{2+} signalling downstream of TRPC3 modulation induces the release of EVs with enhanced metastatic competence. To initially characterise the effect of TRPC3 modulation on SKOV3-EV release, EVs were extracted in SFM after 4hrs conditioning from 0.3µM TRPC3 activator and 3µM TRPC3 inhibitor treated cells, as well as untreated and DMSO controls, and analysed for differences in concentration and surface antigen expression by NTA and MACSPlex analysis respectively. NTA analysis demonstrated that TRPC3 activator-treated cells released significantly more EVs within the 100-120nm size range than untreated, DMSO and TRPC3 inhibitor-treated cells (Figure 4.6 A). To ensure increased EV release from TRPC3 activator-treated cells was not due to increased cell numbers (Figure 3.4), cells were counted at the time of EV extraction to calculate the number of EVs released per cell. Following this calculation, the increase in EV release from TRPC3 activator-treated cells was not significant compared to untreated, DMSO and TRPC3 inhibitor-treated cells, likely due to the large variability between replicates (Figure 4.6 B). These calculations were performed on total particle counts and therefore do not reflect the size-related increase shown in Figure 4.6 A. To assess if TRPC3 modulation also altered the expression of EV surface antigens, EVs were analysed by flow-cytometry with the MACSPlex assay as for the characterisation of SKOV3-EVs in Section 4.3.4. MACSPlex analysis (Figure 4.6 C, reported as mean fluorescence intensity values normalized to CD63) detected the expression of 17 surface antigens in all treatment groups across three biological replicates. EV markers CD63, CD9 and CD81 were detected in all samples, although the expression of CD9 was minimal across all groups. TRPC3 inhibition significantly reduced the expression of CD105 (Endoglin) compared to untreated and DMSO controls, and significantly increased the expression of CD41b (Integrin α-2b) compared to all groups. Conversely, TRPC3 activation significantly increased the expression of CD133.1 (Prominin-1) in comparison to all groups. These proteins represent potential downstream effectors of TRPC3, and their up- or down-regulation on the EV surface may hold functional significance for TRPC3-mediated EV communication in OC. In all, TRPC3 activation induced the release of 100-120nm EVs, and TRPC3 modulation in general altered the expression of EV surface antigens that may play a functional role in TRPC3-mediated EV communication.

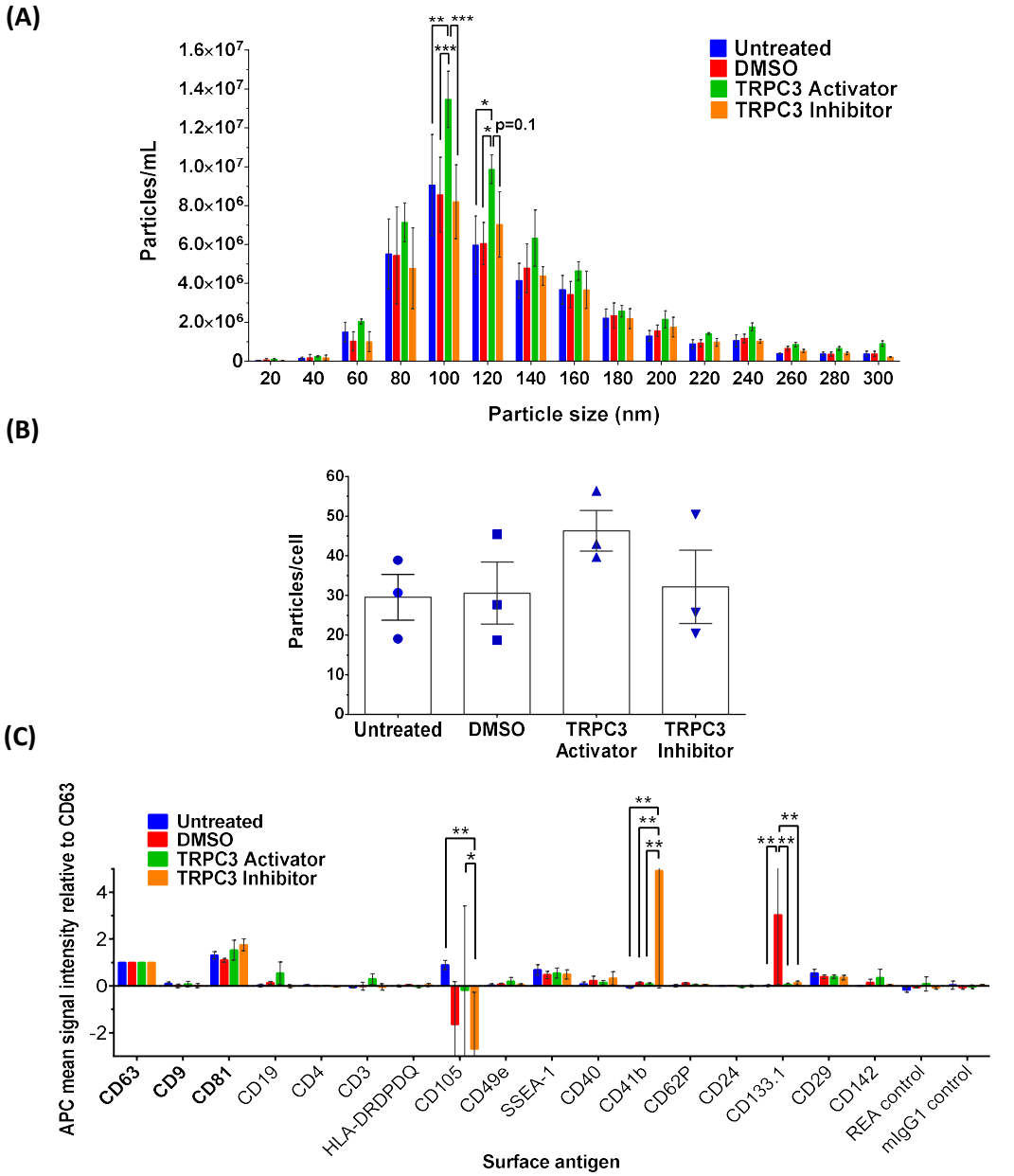

Figure 4.6 TRPC3 activator and inhibitor-induced EVs show detectable differences in concentration and surface antigens

(A) *NTA analysis of EV samples used to treat naïve cells in downstream assessments of TRPC3-mediated EV communication. Data shows the size-dependent concentration of particles isolated from untreated cells and cells treated with DMSO, TRPC3 activator and TRPC3 inhibitor. Mean ± SEM of three independent experiments with statistical significance tested by two-way ANOVA and Tukey's multiple comparisons test: *P ≤ 0.05, **P ≤ 0.01, ***P ≤ 0.001. Unstated p-values >0.1* ***(B)*** *The average particle concentration of EV samples from treatment groups and controls in (A) normalised to their respective cell counts. No statistically significant differences were observed between treatments as determined by ordinary one-way ANOVA with Greenhouse-Geisser correction and Tukey's multiple comparisons test.* ***(C)*** *MACSPlex exosome assay data showing the mean signal intensities of 17 surface antigens and 2 isotype controls detected from the conditioned media of all treatment groups in (A) across three biological replicates. Data normalised to CD63, with fluorescence intensity adjusted to non-conditioned media. Statistical significance tested by two-way ANOVA and Tukey's multiple comparisons test: *P≤0.05, ** P≤0.01, if not indicated – not significant (p ≥0.05).*

4.5.6. TRPC3 ACTIVATOR-INDUCED EVS INCREASE SKOV3 CELL GROWTH AT 48HRS

The work presented thus far demonstrates that increased Ca^{2+} signalling downstream of TRPC3 activation increases SKOV3 cell growth and migration, and induces the release of 100-120nm EVs. As disrupted Ca^{2+} signalling can induce the release of EVs with enhanced metastatic competence[144, 167], these results indicate that TRPC3 activation may induce the release of EVs that contribute to the increased growth and migration of SKOV3 cells. Therefore, EVs were extracted in SFM after 4hrs conditioning from 0.3µM TRPC3 activator and 3µM TRPC3 inhibitor treated cells, as well as untreated and DMSO controls, and applied to naïve SKOV3 cells to first assess their effect on cell growth. Recipient SKOV3 cells were manually counted at 24, 48 and 72hrs following EV treatment, using trypan blue to distinguish live from dead cells. To exclude the effect of TRPC3 activation on the quantity of EV release (see Figure 4.7 A,B) and identify whether the specific nature of the EVs was important, a set number of EVs were applied to recipient cells. Approximately 50 particles per viable cell were counted at the time of EV extraction (Figure 4.7 B), therefore recipient cells were dosed with 50 particles per seeded cell at a 1x concentration, as well as two higher concentrations of 5x and 10x particles/cell. Administered EVs were in PBS suspension, therefore an equivalent volume of plain PBS was applied to the no EV control for each concentration. Growth curves in Figure 4.7 represent recipient SKOV3 cell growth at 1x, 5x and 10x EV concentrations over the 72hr incubation period. Whilst no statistically significant differences in cell growth were apparent between EV treatments, there was a consistent trend for higher cell counts in the TRPC3 activator-EV treatment group at 48hrs, particularly at the 10x concentration. Therefore, recipient cell growth at 48hrs was normalised to the DMSO-EV control to assess if a dose-responsive effect of TRPC3 activator-EVs was apparent (Figure 4.7 B). TRPC3 activator-induced EVs increased recipient cell growth at all EV concentrations, and significantly so in comparison to TRPC3 inhibitor EVs and the no EV control at the 1x dosage, and in comparison to all treatment groups at the 10x dosage. Therefore, the effect of TRPC3 activator-EVs on recipient cell growth appeared to be dose-dependent. In addition, TRPC3 inhibitor-EVs consistently reduced recipient cell growth, although this effect was only significant in comparison to TRPC3 activator-EVs at the 1x and 10x dosage. Representative images of recipient SKOV3 cells at 48hrs are shown in Figure 4.7 C. These results indicate that TPRC3 activator-induced EVs possess the functional capacity to increase the growth rate of recipient SKOV3 cells, suggesting a novel role for TRPC3-mediated EV communication in the progression of OC.

(A)

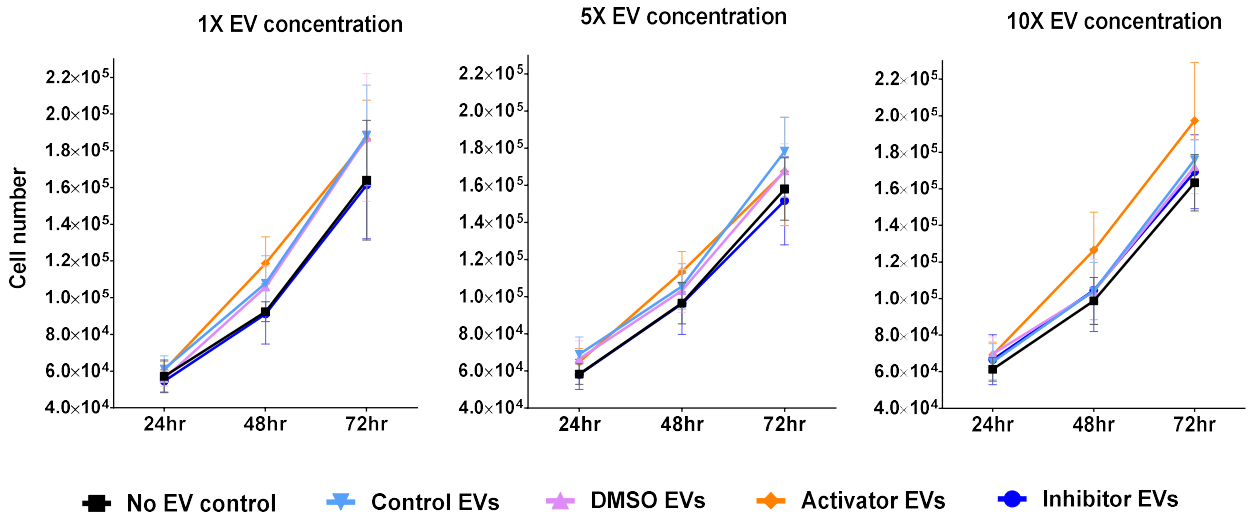
1X EV concentration
5X EV concentration
10X EV concentration
Cell number
2.2×10^5
2.0×10^5
1.8×10^5
1.6×10^5
1.4×10^5
1.2×10^5
1.0×10^5
8.0×10^4
6.0×10^4
4.0×10^4
24hr
48hr
72hr
No EV control
Control EVs
DMSO EVs
Activator EVs
Inhibitor EVs

(B)

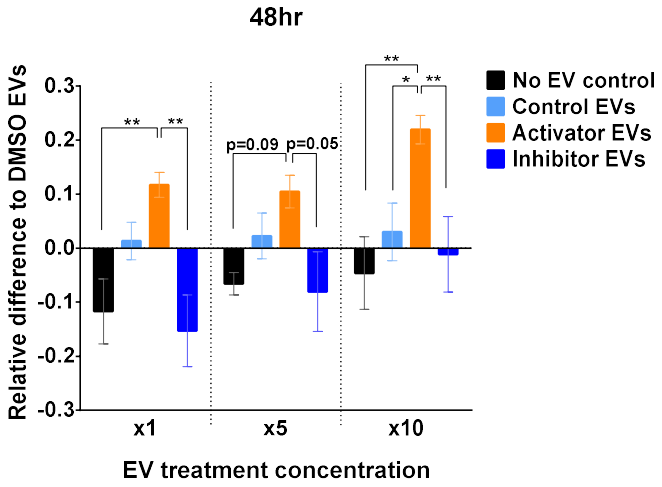
48hr
Relative difference to DMSO EVs
0.3
0.2
0.1
0.0
-0.1
-0.2
-0.3
**
**
p=0.09
p=0.05
**
*
**
x1
x5
x10
EV treatment concentration
No EV control
Control EVs
Activator EVs
Inhibitor EVs

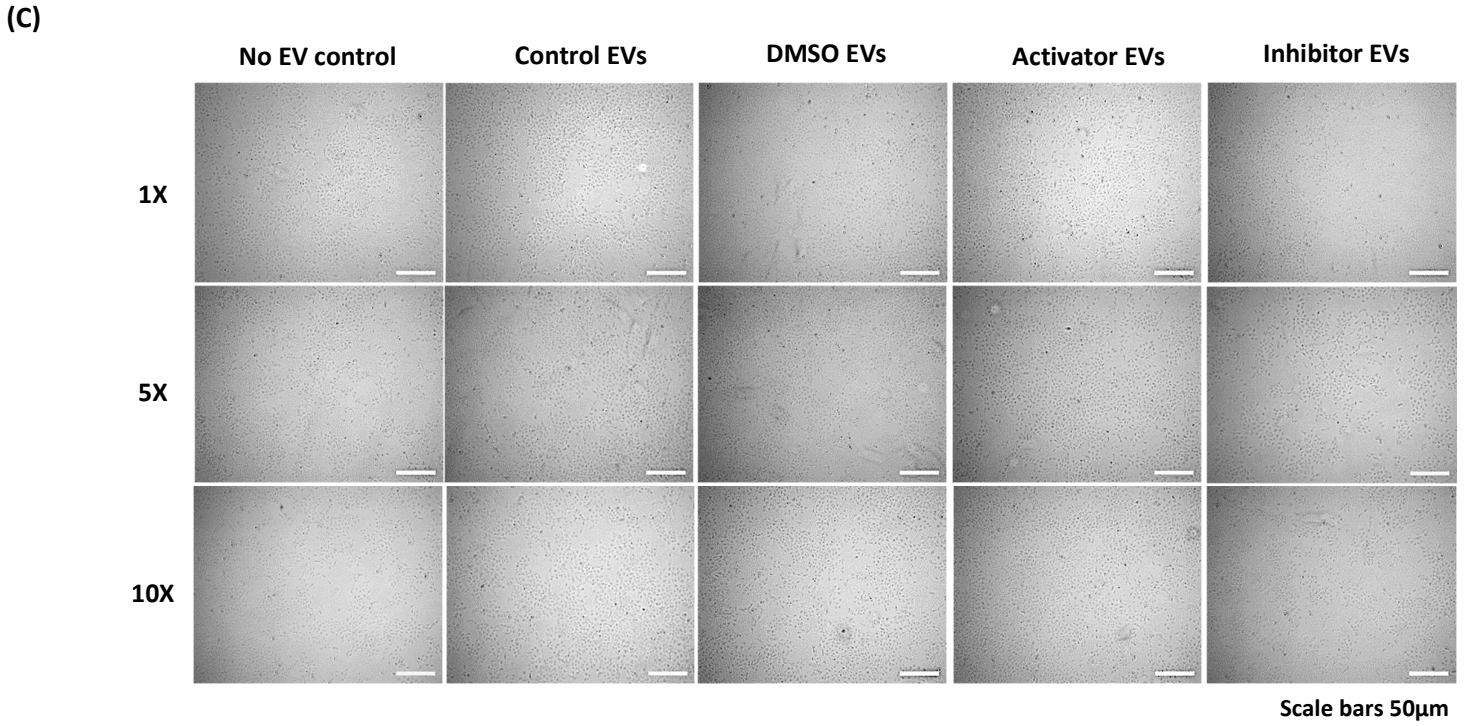

Figure 4.7 At 48hrs, TRPC3 activator-induced EVs increase recipient SKOV3 cell growth in a dose-dependent manner

(A) *Growth curves representing total cell number at 24, 48 and 72hr incubation with no EV control (PBS), control EVs, DMSO EVs, TRPC3 activator EVs or TRPC3 inhibitor EVs. Left to right: 1x, 5x and 10x EV treatment concentration. No statistically significant differences were observed between treatments as determined by two-way ANOVA and Tukey's multiple comparisons test.* ***(B)*** *The relative difference in total cell number at 48hrs between all treatment groups and DMSO EVs (0) at 1x, 5x and 10x EV treatment concentrations. (A) and (B) represent mean ± SEM of three independent experiments with statistical significance tested by two-way ANOVA and Tukey's multiple comparisons test: *P≤0.05, **P≤0.01. Unstated p-values ≥0.1.* ***(C)*** *Representative images of SKOV3 cells in culture at 48hrs following 1x, 5x and 10x EV treatments. Scale bars are 50µm.*

4.5.7. TRPC3-MEDIATED EV COMMUNICATION DOES NOT ALTER THE MIGRATORY CAPACITY OF SKOV3 CELLS

Next, the effect of TPRC3 inhibitor and activator-induced EVs on recipient SKOV3 migration was assessed. Within each biological replicate for the cell growth and migration analysis, the same set of EVs were used at the same concentrations for continuity and to reduce variability. Therefore, as before, EVs were extracted in SFM after 4hrs conditioning and recipient cells were dosed with 50 particles per seeded cell at a 1x concentration, as well as two higher concentrations of 5x and 10x particles/cell. An equivalent volume of PBS was applied to the no EV control for each concentration. A wound healing assay was employed to study the motility of recipient SKOV3 cells over a 24hr time period. EVs were added immediately before the cell monolayer was scratched at timepoint 0, and gap closure was monitored at 4, 8, 12 and 24hrs (Figure 4.8 A,B). To avoid bias in gap quantification due to unequal scratch widths, the migration area was calculated by subtracting the scratch area at each timepoint from the area at timepoint 0, and the migration area for each treatment group was then normalised to the according DMSO control. Relative migration rates for recipient cells treated with 1x, 5x and 10x EV concentrations are represented in Figure 4.8 A. Dissimilarly to the effect of TRPC3-induced EVs on recipient SKOV3 cell growth, no consistent trends were apparent for the effect of TRPC3 activator or inhibitor-induced EVs on recipient SKOV3 migration at any dosage. At the 10x EV dosage, TRPC3 inhibitor EVs and control EVs reduced recipient cell migration in comparison to the no EV control at 4hrs, although these effects did not reach significance. Representative images of the scratch assay used to quantify cell migration at the 10x EV treatment are shown in Figure 4.8 B. Overall, TPRC3 inhibitor and activator-induced EVs do not alter the migratory capacity of recipient SKOV3 cells, and therefore likely do not contribute to the deregulated cell migration observed downstream of TRPC3 modulation in Chapter 3.

(A)

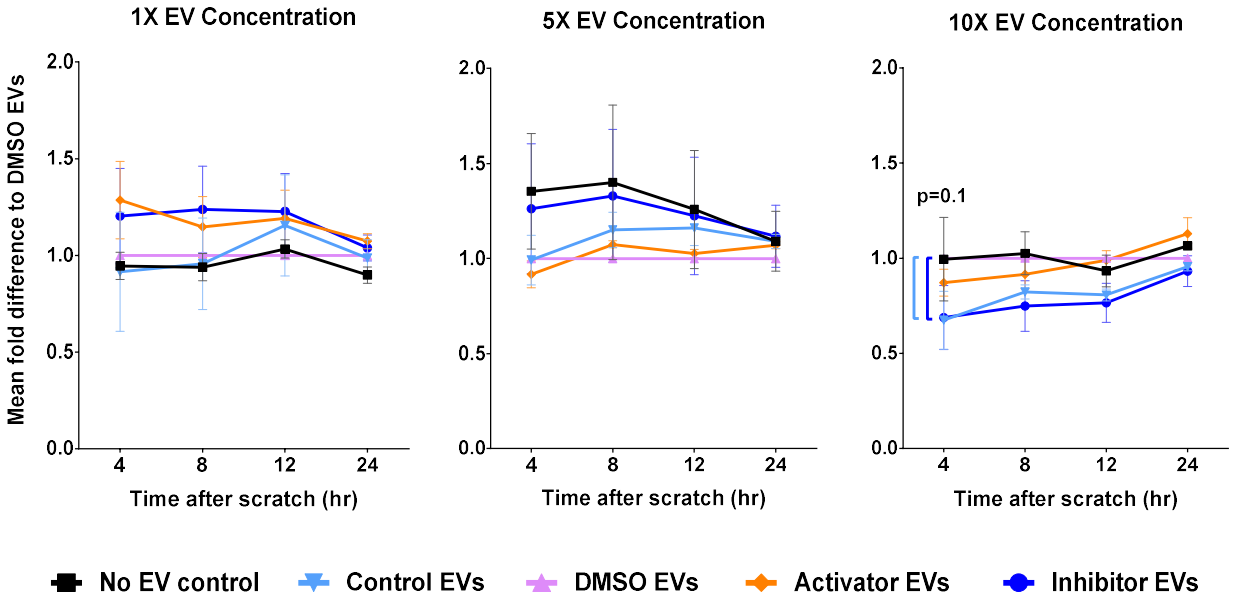
1X EV Concentration
5X EV Concentration
10X EV Concentration
Mean fold difference to DMSO EVs
2.0
1.5
1.0
0.5
0.0
4
8
12
24
Time after scratch (hr)
p=0.1
No EV control
Control EVs
DMSO EVs
Activator EVs
Inhibitor EVs

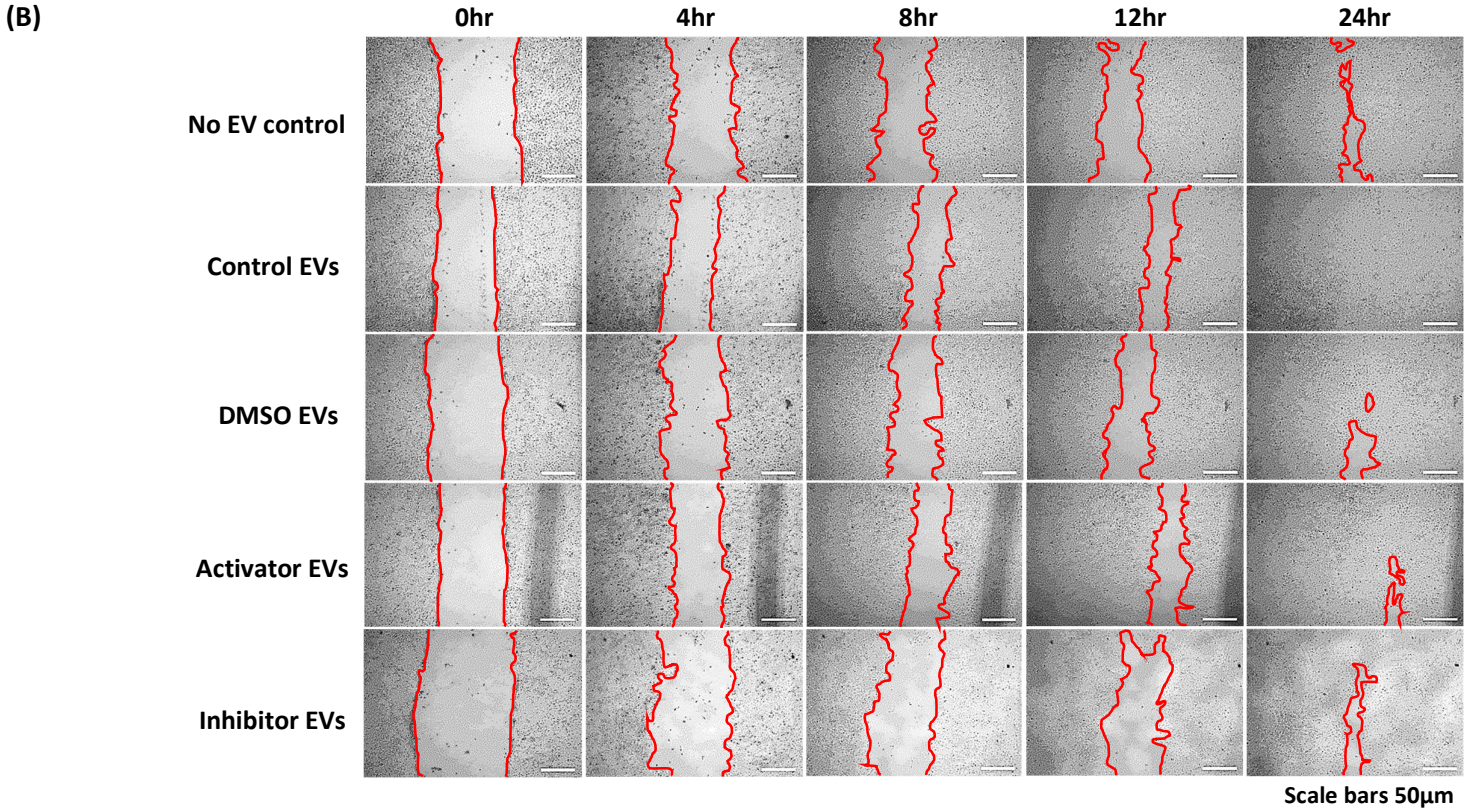

Figure 4.8 TRPC3 activator or inhibitor-induced EVs do not alter the migration rate of recipient SKOV3 cells

(A) *A scratch assay was performed on SKOV3 cells treated with no EV control (PBS), control EVs, DMSO EVs, TRPC3 activator EVs or TRPC3 inhibitor EVs and cell migration was monitored over a 24-hour period. Left to right: 1x, 5x and 10x EV treatment concentration. Cell migration in each treatment group was normalised to DMSO EVs (1). Data represents mean ± SEM of three independent experiments with statistical significance tested by two-way ANOVA and Tukey's multiple comparisons test. Unstated p-values >0.1.* ***(B)*** *Representative images of SKOV3 scratch assay used to quantify cell migration at 0, 4, 8, 12 and 24hr timepoints. 10x EV treatment images shown. Scale bars are 50µm.*

4.5.8. TRPC3-MEDIATED EV COMMUNICATION DOES NOT ALTER THE INVASIVENESS OF SKOV3 CELLS

The results presented thus far demonstrate that TRPC3 activator-induced EVs promote recipient SKOV3 cell growth, but bear no effect on their migratory capacity. Several papers report a functional role of EVs in OC cell invasion, mediated by their capacity to drive ECM degradation through releasing their proteolytic cargo of MMPs or by stimulating the expression or MMPs in recipient cells[228, 413, 414]. Therefore, in further assessment of the role of TRPC3-mediated EV release in metastatic mechanisms of OC, a Matrigel® invasion assay was performed to evaluate the effect of TRPC3 activator and inhibitor-induced EVs on recipient SKOV3 ECM degradation and invasion. EVs were extracted in SFM after 4hrs conditioning from TRPC3 activator and inhibitor treated cells, as well as untreated and DMSO controls, and applied to naïve SKOV3 cells plated onto a Matrigel® layer. Recipient cells were treated with a dosage of 10x EVs as this concentration elicited the most pronounced effect on cell growth (Figure 4.7). An equivalent volume of PBS was applied to the no EV control. Cells were allowed to invade for 48hrs following EV treatment, before invaded cells on the underside of the membrane were stained with CFSE and the DNA dye DAPI, imaged and quantified to estimate the percentage of invasion (Figure 4.9 A,B). SKOV3 EVs did not alter the invasiveness of recipient cells, regardless of TRPC3 activator or inhibitor treatment. Of note, this data is based on three technical replicates rather than biological, and therefore requires further replicates to confirm these results. However, the evidence presented thus far indicates that TRPC3 does not contribute to the invasiveness of SKOV3 cells directly (Figure 3.6) or indirectly through TRPC3-mediated EV communication.

(A)

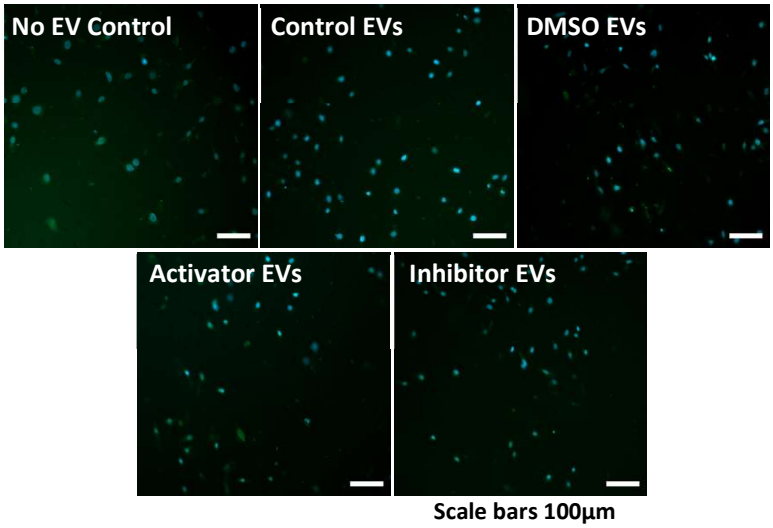

(B)

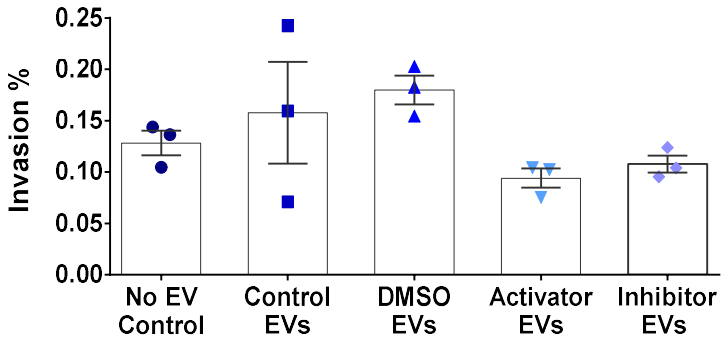

Figure 4.9 Matrigel® invasion assay showed no detectible difference in SKOV3 invasion following EV treatment

(A) *Representative images of Matrigel® membranes used to quantify cell invasion. Cells were seeded onto membranes with 10x EV/cell treatments: no EV control (PBS), control EVs, DMSO EVs, TRPC3 activator EVs or TRPC3 inhibitor EVs. Cells were allowed to invade for 48hrs. Invaded cells were then stained with CFSE (green) and the DNA dye DAPI (blue), fixed and counted. Scale bars 100µm.*
(B) *Percentage cell invasion through Matrigel® membranes shown in (A). Mean ± SEM of three technical replicates for each treatment. No statistically significant differences were observed between treatments as determined by ordinary one-way ANOVA and Tukey's multiple comparisons test.*

4.5.9. EVIDENCE OF TRPC3 AND MGLUR1 IN SKOV3-EVS

To conclude the assessments of TRPC3 in EV-mediated metastatic mechanisms in OC, SKOV3-EVs were probed for the expression of TRPC3 and its upstream regulator mGluR1. In neurons, TRPC3 is a downstream effector of the GPCR mGluR1[374], which has previously been implicated in mediating the release of EVs that increase the migration, invasion and growth of recipient melanoma cells[407]. As functional TRPC5 channels are incorporated into EVs derived from chemoresistant breast cancer cells[112, 322], here it was hypothesised that EV-mediated increases in SKOV3 cell growth observed in Figure 4.6 may be due to the intercellular transfer of TRPC3 and/or mGluR1. Therefore, SKOV3-EVs were extracted in SFM after 48hrs conditioning and probed with antibodies against TRPC3 and mGluR1 by western blot, immunogold TEM and Exoview® technology. The expression of TRPC3 and mGluR1 in SKOV3 cell and EV was initially confirmed by western blot, with CD81 and β-actin used as loading controls (Figure 4.10 A,B, left blots). The observed bands for SKOV3-cell correspond in length to TRPC3 (~97kDa)[310], and mGluR1α (~150kDa), mGluR1β (~100kDa) variants[415]. Predominant protein bands were also apparent in SKOV3-EV, although the detected bands varied in size in comparison to SKOV3-cell. Proteins are often modified upon incorporation into EVs by ubiquitination or glycosylation[416, 417], and may therefore exhibit different size profiles compared to cells. However, as both cell and EV also displayed significant non-specific binding, the blots were washed and re-probed with TRPC3 and mGluR1 antibodies preincubated with blocking peptides. The blocking peptide inhibits the detection of antibody-specific protein bands, and can therefore differentiate non-specific bands from antibody-specific bands. Whilst a faint band was detected at ~100kDa for TRPC3 in SKOV3-cell, likely due to insufficient washing prior to re-probing, SKOV3-EV was completely clear of protein bands for TRPC3 and mGluR1 (Figure 4.10 A,B respectively, right blots). With the presence of EVs confirmed by the β-actin loading control, this indicates that the detection of TRPC3 and mGluR1 in SKOV3-EV is specific.

To assess if mGluR1 is expressed on the surface of SKOV3-EVs, EVs were labelled by immunogold for the mGluR1 antibody and analysed by TEM (Figure 4.10 C). Immunogold TEM detected negatively stained, 'cup-shaped' particles in the size range of 40-150nm that labelled positive for mGluR1. This provides further evidence that mGluR1 may be expressed on the surface of SKOV3-EVs. As there are no commercially available antibodies for immunogold detection of TRPC3, the novel affinity-based platform Exoview® was employed to confirm the expression of TRPC3 on SKOV3-EVs. To enhance detection of TRPC3 on the EV surface, SKOV3 cells were transfected with a WT TRPC3 construct that has a FLAG-tag inserted into the extracellular

domain of TRPC3. 24hrs post-transfection, transfected and non-transfected cells were conditioned for 48hrs in SFM prior to EV extraction. APC-conjugated anti-TRPC3 and anti-FLAG antibodies were employed to enable the detection of TRPC3 positive EVs at CD81, CD63 and CD9 antibody spots (Figure 4.10 D). Endogenous TRPC3+ EVs were detected at the CD81 and CD9 antibody spots whilst there was no detectable signal at CD63, likewise to the detection of SKOV3-EVs in Figure 4.5 C. In contrast, minimal FLAG positive EVs were detected at CD81 and CD63 antibody spots, and were undetectable at CD9. This may reflect a poor transfection efficiency of the TRPC3-FLAG construct. Due to time constraints surrounding the use of the Exoview® platform, this analysis could not be replicated alongside positive and negative EV controls, therefore the results should be interpreted with caution. However, paired with the specific detection of TRPC3 and mGluR1 in SKOV3-EVs by western blot, and positive labelling of mGluR1 on the EV surface by immunogold TEM, there is tangible evidence to suggest that TRPC3 and mGluR1 are incorporated into SKOV3-EVs, and may therefore mediate recipient SKOV3 cell growth.

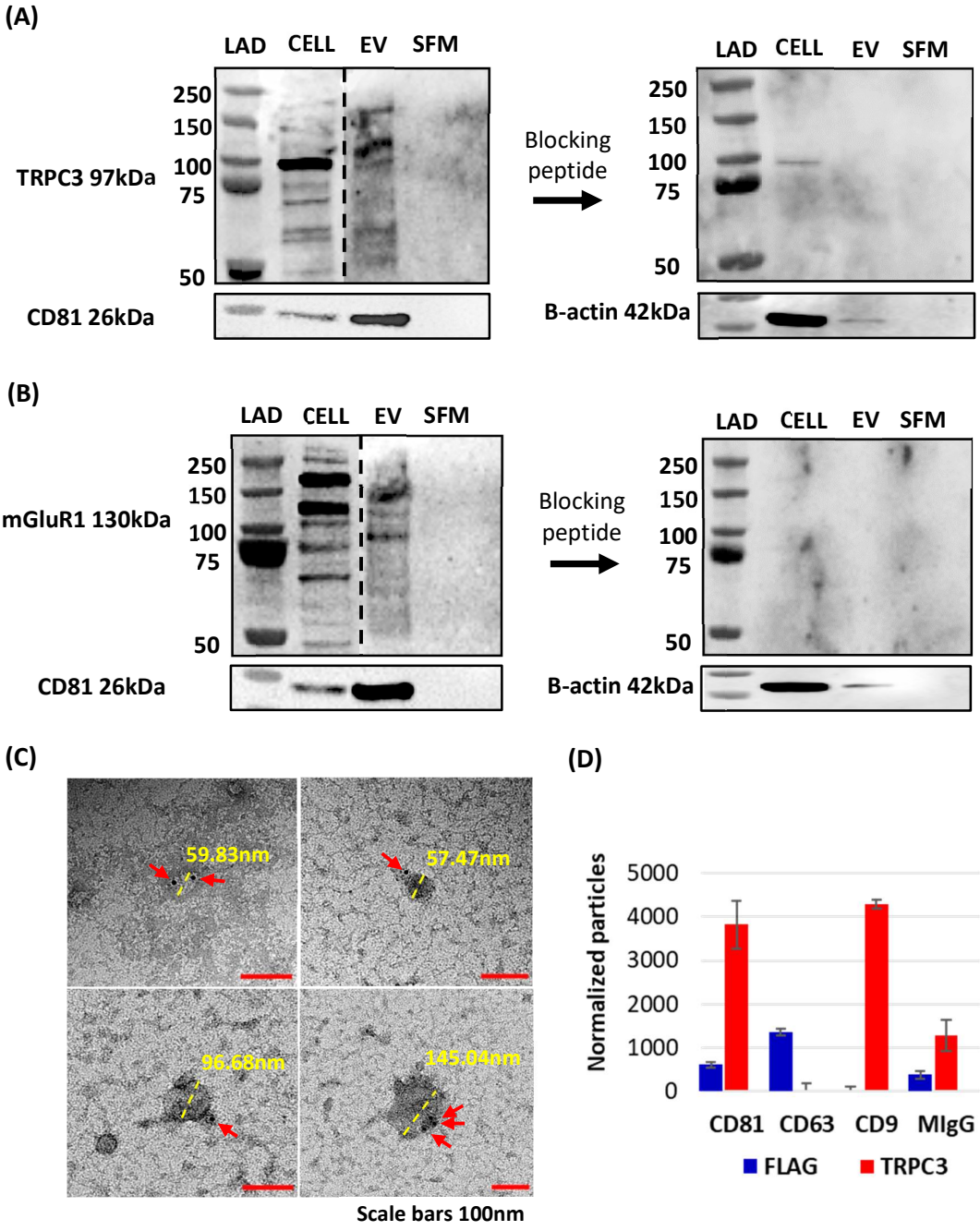

Figure 4.10 Evidence of TRPC3 and mGluR1 on EV surface by western blot, immunogold TEM and Exoview® technology

(A) *Western blotting of TRPC3 in SKOV3 cell and EV. Left membrane probed with TRPC3 antibody (Alomone labs) and CD81 as an EV loading control. Right membrane probed with same TRPC3 antibody that was preincubated with the negative control antigen, and β-actin as a loading control. Equivalent protein concentrations loaded on each membrane (4µg) in reducing conditions, except for CD81 ran non-reducing. SFM: non-conditioned media control.* ***(B)*** *As for (A), probing SKOV3 cell and EV with mGluR1 (Alomone labs).* ***(C)*** *Representative immunogold (anti-mGluR1) negative stained electron micrographs of SKOV3-EVs. Arrows indicate 10nm gold particles. Scale bars 100nm.* ***(D)*** *Exoview analysis detects both flag-tagged (Abcam) and endogenous TRPC3 (Alomone labs) positive particles in SKOV3-EVs. Data represents mean ± SEM of repeated measurements from one independent experiment. Raw data not available for statistical analysis.*

4.6. DISCUSSION

The focus of this chapter was to investigate a potential role for TRPC3 in EV-mediated metastatic mechanisms in OC. In Chapter 3, increased Ca^{2+} signalling downstream of TRPC3 activation increased SKOV3 cell growth and migration. As disrupted Ca^{2+} signalling can induce the release of EVs with enhanced metastatic competence[144, 167], it was hypothesised that modulation of TRPC3 activity may induce the release of EVs that contribute to the increased growth and migration of SKOV3 cells. To enable specific detection and analysis of SKOV3-EVs, EVs were extracted in SFM which proved a viable alternative for culturing SKOV3 cells and eliminated bovine contamination, yielding a purer population of EVs that present typical markers and morphology. In assessment of the chapter aim, TRPC3 activation induced the release of 100-120nm EVs with altered surface antigen expression that promote recipient SKOV3 cell growth, but bear no effect on SKOV3 motility or invasiveness. Lastly, preliminary results suggest that TRPC3 and its upstream regulator mGluR1 may be incorporated into SKOV3-EVs, and may therefore play a functional role in TRPC3-mediated EV communication in OC.

4.6.1. BOVINE CONTAMINATION IN THE ANALYSIS OF CELL-DERIVED EVS

Currently available techniques for EV isolation differentiate EVs from other soluble factors in the cell culture medium by size, density, and molecular composition. These methods include differential UC, SEC, precipitation-based methods, bead-based immunoaffinity capture, ultrafiltration and density gradients. Here, SEC was employed to isolate SKOV3-EVs as previous studies demonstrate that SEC EVs are capable of inducing greater functional changes in recipient cells[418], indicating that this method of isolation may be the most appropriate for analysing the functional activity of EVs. However, due to overlapping biophysical properties of human and bovine EVs, SEC or other isolation techniques are not capable of distinguishing between the two populations in FBS supplemented media. Depletion of FBS-EVs is commonly achieved by high-speed UC, however upon assessment of five independent batches of UC depleted FBS, EV-depleted medium was found to retain high particle and protein concentrations and particles of EV size, which contaminate the analysis of SKOV3-derived EVs. Previous publications echo these findings, likewise demonstrating by NTA that UC reduced particle counts by only 70% - with $7.9x10^9 \pm 0.34x10^9$ particles/mL retained following depletion[409]. A costly, commercially available EV-depleted FBS (Exo-FBS™) proved only marginally clearer with a 75% reduction in overall particle counts – comparable to the 76% reduction observed here. In addition, whilst the detection of cell-derived EVs by western blot was largely specific in this study except for β-actin, Kornilov *et al.*[410] detected the expression of EV markers CD63, CD71 and HSP70 in UC depleted

FBS. It is therefore apparent that current EV-depletion methods are not sufficient to ensure cell-derived EV preparations are clear from contaminants.

4.6.2. SERUM-FREE CULTURE FOR SKOV3-EV EXTRACTION

To eliminate bovine contamination and improve the analysis of cell-derived EVs, SKOV3-EVs were extracted in SFM which proved a viable alternative for culturing SKOV3 cells. However, whilst SFM was capable of maintaining SKOV3 viability up to 48hrs conditioning, SKOV3 proliferation was reduced in SFM in comparison to full FBS media. Reduced proliferation and metabolic activity have likewise been reported in additional cell lines cultured in SFM[410]. This is likely due to the absence of growth factors provided by FBS, as well as the lack of FBS-EVs which alone have shown to stimulate cell proliferation and differentiation[419]. Current research efforts are focused on engineering SFM with the necessary additives to rival the capacity of FBS to support cell growth and viability. In addition, further investigation is required to assess how serum-free culture may influence EV biogenesis. Previously, Li *et al.*[420] reported that whilst serum-free conditions did not alter the size or biophysical properties of EVs released from N2a neuroblastoma cells, several vesicular proteins implicated in EV biogenesis were differentially expressed in EVs isolated from SFM after 48hrs conditioning. These findings must be considered in downstream analysis of SKOV3-EVs isolated from SFM.

An additional benefit of isolating SKOV3-EVs in SFM was the detection of EVs above background from 4 hours conditioning. Extended conditioning periods of up to 72hrs are required to detect cell-derived EVs above the background of FBS-EVs in depleted medium, and here NTA failed to detect an increase in particles after 48hrs (Figure 4.3 A,B). As longer conditioning periods >8hrs did not increase EV yield in SFM, future SKOV3-EV extractions can be completed in a much smaller timeframe. Interestingly, this non-linear relationship between EV release and time has also been observed in human mammary epithelial and breast cancer cell cultures; whereby the concentration of EVs in the medium remained constant >9hrs[421]. The authors proposed that a dynamic equilibrium exists between EV release and uptake, influenced by the concentration of EVs present in the extracellular environment. This suggests that a similar feedback mechanism may regulate EV release by SKOV3 cells.

4.6.3. CHARACTERISING SKOV3-EVS

Evidencing EV size as well an array of markers is of particular importance to functional studies to understand the contributing EV subpopulations, as both small EVs (containing a mixture of exosomes and small MVs), and larger EVs/MVs are shown to have different oncogenic effects[20,

[422]. For example, a study by Keerthikumar and colleagues demonstrated that exosomes induced significant cell proliferation and migration in recipient cells compared to MVs[422]. Here, CD81+, 'cup-shaped' particles which are typical of EV morphology and size were initially detected by immunogold TEM. Western blot analysis confirmed that SKOV3-EVs were enriched for EV markers CD81, CD9, TSG101 and ALIX, and clear of markers indicative of cellular contamination (GM130 and cytochrome C). Classically, tetraspanins CD63, CD81 and CD9 have been used as markers of exosomes due to their accumulation in small EVs as compared to whole cell lysates, and to the steady-state accumulation of CD63 in MVBs[45, 423]. Likewise, ESCRT components and associated proteins TSG101 and ALIX are regarded as specific exosomal markers[424, 425]. This would therefore suggest that the isolated population of SKOV3-EVs presented here are of mainly endosomal origin, and qualify as exosomes. However, emerging and conflicting reports demonstrate a substantial overlap of protein markers between different EV subtypes, with CD81, CD9, TSG101 and ALIX all identified in additional EV populations[42, 422, 426, 427]. Using live intracellular tracking of tetraspanins in conjunction with quantitative proteomic analysis, Mathieu *et al.* recently demonstrated that CD9- and CD81-bearing EVs bud mainly from the PM of HeLa cells as MVs, whereas others bearing CD63 with little CD9 derive from internal cellular compartments, and qualify as exosomes[105]. Although MACSPlex analysis of SKOV3-EVs detected a population of CD63+ EVs, only CD81+ and CD9+ populations were detected by the Exoview® platform. The presence of CD63+ EVs should be validated by western blot and/or immunogold TEM, alongside syntenin-1 which has recently been identified as a putative universal biomarker of exosomes[428], to further characterise the origin of SKOV3-EVs. Therefore, whilst this chapter presents a thorough characterisation of SKOV3-EVs and evidences that SEC extractions from SFM yield a population of EVs characteristic of those reported in the literature[429], functional effects observed in downstream analysis cannot be attributed to an exact population of EVs.

4.6.4. A POTENTIAL ROLE FOR TRPC3 IN EV RELEASE

A number of studies demonstrate that increased intracellular Ca^{2+} induces EV release in cancerous cell types[143-145]. As TRPC3 activation increases Ca^{2+} signalling in SKOV3 cells, here it was hypothesised that TRPC3 modulation may induce the release of a unique population of EVs that contribute to the increased growth and migration of SKOV3 cells observed in Chapter 3. Indeed, TRPC3 activation induced the release of 100-120nm EVs with altered surface antigen expression. These findings are in line with a previous study demonstrating that TRPC5 is required for EV formation and release in Adriamycin-resistant human breast cancer cells[112]. Moreover, the differential expression of EV antigens may represent the metastatic competence of SKOV3

cells treated with TRPC3 activator or inhibitor, and their ability to convey this phenotype to recipient cells. For example, TRPC3 inhibition reduced EV expression of CD105 – known to play a pro-metastatic role in breast[430], ovarian[431], renal[432] and hepatocellular cancer[433]. Notably, excess CD105 expression promotes cell migration and intravasation in breast cancer patients, and is upregulated in EVs derived from these patients[430, 434]. As cell migration was reduced in TRPC3 inhibitor treated cells (Figure 3.5), this suggests that TRPC3 inhibition may downregulate CD105, as reflected in the EV content, reducing OC cell migration. In addition, TRPC3 activation increased EV expression of CD133, which is likewise enriched in EVs derived from metastatic melanoma cells, and enhances melanoma cell growth, motility and invasion[435-437]. This proposes CD133 as a potential downstream mediator of TRPC3 activator-induced SKOV3 cell growth, and may promote cell growth in EV recipient cells.

Notably, the increase in EV release induced by TRPC3 activation was detected by NTA. Whilst NTA provides a rough estimate of mean EV size and concentration, it has been criticised for its inaccuracy when comparing EV concentrations across different treatment groups[438, 439]. In addition, NTA analysis is unable to differentiate between different EV subtypes, and the 100-120nm TRPC3 activator-induced EVs overlap the reported size range for small EVs, MVs and apoptotic bodies[16]. Increasing concentrations of TRPC3 activator will increase Ca^{2+} influx into SKOV3 cells, therefore too high a concentration can result in intracellular Ca^{2+} overload and cell apoptosis[368]. Although the concentration of 0.3µM TRPC3 activator used to induce EV release did not reduce cell viability (Figure 3.2), the possibility that TRPC3 activation may initiate cell death and therefore the release of apoptotic bodies cannot be excluded. Direct analysis of EV secretion is therefore required to confirm a functional role for TRPC3 in EV biogenesis.

4.6.5. TRPC3-MEDIATED EV COMMUNICATION IN OC

Disturbances to cellular Ca^{2+} homeostasis in both breast and ovarian cancer cells induces the release of EVs with enhanced metastatic competence[144, 167]. Since TRPC3 activation increases Ca^{2+} signalling in SKOV3 cells and induces the release of a unique population of EVs, the effect of TRPC3 activator- and inhibitor-induced EVs on metastatic mechanisms in OC was investigated. Naïve SKOV3 cells were treated with EVs extracted from TRPC3 activator and inhibitor treated cells, as well as untreated and DMSO controls, and evaluated for changes in cell growth, migration and invasion. At 48hrs, TRPC3 activator-induced EVs increased recipient cell growth at all EV concentrations, suggesting a novel role for TRPC3-mediated EV communication in OC growth. Several publications likewise implicate OC-derived EVs in the proliferation and survival of OC cells, either by directly promoting the growth of less aggressive OC cells[403] or by inducing

a tumour-promoted phenotype in non-tumour cells within the TME which facilitate OC cell metastasis. For example, EVs derived from high-grade OCs promote the proliferation and migration of endothelial cells through intercellular transfer of their angiogenic cargo, including proteins ATF2, MTA1, and ROCK1/2[440]. EV-associated integrin α5β1 secreted from OC cells also promotes the proliferation, migration and EMT of HPMCs, a common site for OC dissemination[404]. In the same manner, non-tumour cell types in the TME release EVs that influence the survival of OC cells. Cancer-associated fibroblasts (CAFs) - key contributors to the TME – secrete EVs containing miRNA-21 which are taken up by SKOV3 cells in culture, and subsequently inhibit cell apoptosis and confer chemoresistance to OC cells by repressing the translation of the apoptosis protease-activating factor-1 (APAF1)[98]. It is possible that TRPC3 activation upregulates the loading of these proliferative and/or anti-apoptotic cargo into SKOV3-EVs which are transferred to recipient cells and enhance their metastatic phenotype. The data presented here also indicates that TRPC3 and its upstream regulator mGluR1 are incorporated into SKOV3-EVs released from control cells. Similarly, EVs released from chemoresistant breast cancer cells contain functional TRPC5 channels[112]. Uptake of TRPC5-containing EVs resultantly increased TRPC5 expression and Ca^{2+} influx in recipient chemosensitive cells. This proposes that if functional TRPC3/mGluR1 can be transferred in SKOV3-EVs, they may likewise increase Ca^{2+} influx in recipient cells leading to enhanced cell growth through the Ca^{2+}-sensitive pathways discussed in Section 3.4.2. Whether these proteins are intentionally loaded into EVs to alter the behaviour of recipient cells, or if they are simply 'pinched off' from the endosome or cell membrane in vesicle exocytosis is a hot topic of debate in EV research. Nonetheless, analysing the proteomic content of TRPC3 activator-induced EVs may provide some insight into the protein cargo which confers greater proliferative potential to recipient SKOV3 cells.

Whilst TRPC3 activator-induced EVs enhanced recipient SKOV3 cell growth, TPRC3 activator and inhibitor-induced EVs bared no effect on cell migration and invasion. In Chapter 3 there was likewise no detectable effect of TRPC3 modulation on SKOV3 cell invasion, indicating that TRPC3 does not contribute to the invasiveness of SKOV3 cells directly or indirectly through TRPC3-mediated EV communication. This could potentially be due to the highly invasive nature of SKOV3 cells, as attempting to increase the invasive capacity of an already highly invasive cell line may preclude any treatment effect. However, direct activation of TRPC3 significantly increased SKOV3 cell migration, hence it was hypothesised that TRPC3-induced EVs may contribute to this effect. Rather, the results presented here suggest that TRPC3 activation directly influences Ca^{2+}-sensitive processes that mediate cell migration through facilitating Ca^{2+} influx in SKOV3 cells, and that the effect of extracellular signals is minimal. This is also evident by the fact that EVs

released from control cells did not alter the migration of SKOV3 cells in comparison to the no EV control. This is contradictory to previous reports which demonstrate increased migration of EV treated cells. For example, Luga *et al.* showed that CAF-derived EVs activated Wnt-signaling pathways in breast cancer cells that increased cell protrusions and the rate of cell migration[234]. In OC, EVs secreted by hypoxic OC cells activated tumour-associated macrophages (TAMs) which in turn promoted OC proliferation and migration in a feedback loop[233]. OC-derived EVs also enhanced random and directional migration of CAFS by reducing focal adhesion strength[167]. Lastly, novel live-cell imaging techniques employed by Sung *et al.*[235, 236] revealed that EVs mediate the direction and speed of migrating cancer cells *in vivo*, stabilize leading-edge protrusions and leave a 'chemotactic' trail for migrating cells to follow.

It's possible that the wound healing assay employed here failed to detect EV-mediated increases in cell migration as the assay utilises a confluent layer of cells which do not secrete or uptake EVs in the same manner as dispersed cells[441]. Therefore, another motility assay such as the live-cell imaging technique employed by Sung *et al.*[235, 236], or a transwell migration assay would provide a more accurate measure of EV-mediated cell migration, and may yield different results. In addition, the wound healing assay does not consider the effect of EV communication between OC cells and cells in the TME. As discussed, numerous studies report that OC-derived EVs influence the migration of CAFs[167, 442], TAMs[233, 443] and mesenchymal stem cells (MSCs)[444], and vice versa[445-447]. Therefore, TRPC3-EVs may influence the migratory capacity of additional cell types in the OC TME. Directly treating these cell types with TRPC3-EVs, or using a co-culture model could better encapsulate the role of EVs and TRPC3-mediated EV communication in OC migration *in vivo.*

Finally, in the work presented here recipient cells were treated with a set dosage of EVs in order to control for the increase in EV release from TRPC3 activator treated cells. Recipient cells were dosed with 50 EVs per seeded cell at a 1x concentration, as well as two higher concentrations of 5x and 10x EVs/cell. Interestingly, recipient SKOV3 cell growth was most increased after 48hrs incubation with a dosage of 10x TRPC3 activator-induced EVs. The specificity of this timepoint may reflect mechanisms of EV uptake and cellular turnover, as discussed in Section 4.4.2. Given that the doubling time for SKOV3 cells is estimated between 27-36hrs[333, 448, 449], the 10x EV concentration corresponds to approximately 5x EVs/cell after 48hrs incubation. This dosage is within the range seen in the literature, ranging through 1.7x, 3x, and 10x doses to $1.5x10^7$ EVs per cell[94, 450-452]. The physiological relevance of these concentrations is unknown, as cells *in vivo* are exposed to a constant flow of EVs fluctuating in concentration from continual release and

uptake by surrounding cells. This may explain why no measurable effects of EV treatment were apparent on SKOV3 migration or invasion, and perhaps a higher concentration of EVs or longer incubation periods may yield different results. For example, Josson *et al.*[453] demonstrated that prostate cancer cells underwent EMT six weeks after incubation with stromal cell media. Likewise, repeated EV treatments or the use of fluidic devices would better mimic physiological conditions than the single bolus approach taken here and in other studies, and may be more likely to elicit measurable effects on SKOV3 cell migration and invasion.

4.7. KEY FINDINGS

- EV-depleted FBS retains high concentrations of bovine particles detectable by common EV assays.
- Serum-free extractions improve the analysis of SKOV3-EVs and yield a purer population of EVs that present typical markers and morphology.
- SFM maintains SKOV3 viability up to 48hrs and permits detection of EVs from 4hrs conditioning.
- TRPC3 activation induces the release of 100-120nm EVs with altered surface antigen expression.
- TRPC3 activator-induced EVs promote recipient SKOV3 cell growth, but bear no effect on cell migration or invasion.
- TRPC3 and mGluR1 may be incorporated into SKOV3-EVs.

Chapter 5

Analysing EV biogenesis using TIRF microscopy

5. Analysing EV biogenesis using TIRF microscopy

5.1. Background

5.1.1. Current methods for the analysis of EV biogenesis

As mounting evidence supports the functional role of EVs in numerous biological processes, there is a growing research effort to define mechanisms of EV biogenesis. Current approaches to study EV release in culture involve the collection of cell culture supernatant over extended time periods (24-72hr)[82]. EVs are then isolated by methods based on their size, density, immunoaffinity capture or precipitation, followed by downstream analysis of their physical and biochemical/compositional traits[454]. Due to the overlapping biophysical properties of EVs, both isolation and analytical techniques are unable to differentiate multivesicular body (MVB)-derived EVs from small plasma membrane (PM)-derived microvesicles, therefore inferences on EV biogenesis are based on a pooled, mixed population of EVs. These post-secretion-based types of analysis are also unable to monitor direct, real-time effects of potential modulators on MVB-PM fusion. The extended conditioning periods that are necessary to acquire sufficient material for conventional EV analysis allow secondary effects of treatments and/or negative-feedback loops to occur, concealing immediate or subtle treatment effects on biogenesis pathways. In order to define the factors which directly influence MVB-PM fusion and EV release, novel methods capable of capturing the distinct dynamics of MVB–PM fusion in real-time must be explored.

5.1.2. Tetraspanin-based pHluorin reporters for real-time visualisation of MVB-PM fusion

Tetraspanins CD81, CD63 and CD9 are highly enriched on intraluminal vesicles (ILVs) in late endosomal MVBs and are therefore routinely used as markers of MVB-derived EVs[455]. Many studies have used fluorescent labelling of these tetraspanins to track MVBs inside the cell[456-458], however detection of MVB-PM fusion was precluded by the bright fluorescence of internal endosomes. To overcome this problem, Verweij *et al.*[82] and Sung *et al.*[235] recently developed optical reporters in which tetraspanins are fused with a pH-sensitive GFP derivative, pHluorin. Within the acidic milieu of the MVB (pH~5.5), tetraspanin-pHluorin on the ILV surface is quenched and thus virtually nonfluorescent. Upon MVB-PM fusion, the pH in the MVB lumen is immediately neutralised (pH~7.4) and as ILVs are released into the extracellular space as exosomes, tetraspanin-pHluorin emits a bright, fluorescent signal that is detectable by live-cell

imaging (for a schematic, see Figure 5.1). This sensitive reporter system was employed by Verweij *et al.* to demonstrate a histamine inducible signalling pathway that triggers MVB-PM fusion in HeLa, HUVEC, SiHa and mesenchymal stem cells (MSCs)[82]. Likewise, Lu *et al.* (2018) used CD63-pHluorin to validate candidates from a genome-wide CRISPR-Cas9 screen for new players in MVB exocytosis[459]. Real-time visualisation of MVB-PM fusion also uncovered novel fusion dynamics in actively migrating cancer cells, as fusion at the leading cell edge directed cell movement[236]. These demonstrations evidence that tetraspanin-based pHluorin reporters can be used to assess the effects of fast-acting compounds on MVB-derived EV biogenesis and fusion.

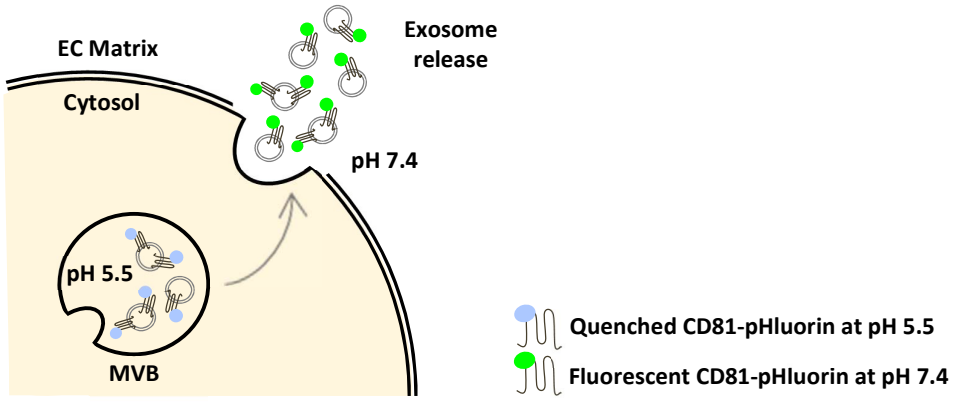

Figure 5.1 pH-sensitive tetraspanin-based reporters permit real-time visualisation of MVB-PM fusion in single cells

Schematic depicting the pHluorin reporter system: Within the acidic milieu of the MVB (pH~5.5), CD81-pHluorin on the ILV surface is quenched and nonfluorescent. Upon MVB-PM fusion and ILV release, MVB pH is immediately neutralised (pH~7.4) and CD81-pHluorin emits a bright, fluorescent signal.

5.1.3. A POTENTIAL ROLE FOR TRPC3 IN EV BIOGENESIS

The work presented thus far demonstrates that TRPC3 activation increases Ca^{2+} signalling and mediates cell growth and migration in SKOV3 cells (Chapter 3). Interestingly, increases in intracellular Ca^{2+} also induce EV release in a number of cell types[143-145]. Emerging evidence suggests members of the TRPC family may mediate EV biogenesis and subsequent metastatic mechanisms through facilitating Ca^{2+} influx[112, 322]. Here, TRPC3 activation induced the release of EVs capable of increasing the growth rate of recipient cells (Figure 4.7), suggesting a novel role for TRPC3 in EV biogenesis which should be investigated further.

5.2. AIMS AND OBJECTIVES

NTA analysis conducted in Chapter 4 demonstrated that TRPC3 activator-treated cells released more EVs within the 100-120nm size range than untreated, DMSO and TRPC3 inhibitor treated cells. TPRC3 activator-induced EVs also had the functional capacity to increase the growth rate of recipient cells, suggesting a novel role for TRPC3-mediated EV communication in the progression of ovarian cancer. Therefore, the ultimate aim of this chapter was to further investigate the role of TRPC3 in MVB-derived EV biogenesis and fusion. Using tetraspanin-pHluorin reporters, this analysis assessed the quantity, size, fluorescence, duration and localisation of MVB fusion events in SKOV3 cells treated with TRPC3 activator or inhibitor.

To validate imaging and analysis protocols, histamine and ionomycin were employed as well-established inducers of MVB-PM fusion[82, 144]. This analysis therefore examines if histamine and ionomycin stimulate MVB-PM fusion in OC cells for the first time, and likewise characterised histamine and ionomycin-induced MVB fusion dynamics. The specific objectives were to:

1. Establish image acquisition and analysis parameters capable of quantifying and characterising tetraspanin fusion events
2. Examine MVB-PM fusion in SKOV3 cells following stimulation with EV inducers histamine and ionomycin
3. Investigate the effect of TRPC3 activation and inhibition on MVB-PM fusion in SKOV3 cells

5.3. RESULTS

5.3.1. TETRASPANIN-BASED PHLUORIN REPORTERS PERMIT REAL-TIME VISUALISATION OF MVB-PM FUSION IN SINGLE CELLS BY TIRF MICROSCOPY

Current approaches to study EV release are limited in their capacity to capture the distinct dynamics of MVB-PM fusion. pH-sensitive tetraspanin-based reporters developed by Sung *et al.*[235] were employed to directly visualise and quantify MVB-PM fusion in single cells by total internal reflection fluorescence (TIRF) microscopy. To quantify MVB-PM fusion, an analysis workflow was developed in ImageJ which selects for 'new' localised increases in fluorescence above a set threshold in every individual frame of the acquisition (Figure 5.2 A). The fluorescence profile of all selected events was manually assessed, and events with minimal change in fluorescence, an irregular fluorescence profile and/or lateral movement of the fluorescence signal were excluded from the analysis. In SKOV3 cells expressing CD81-pHluorin, localized

increases in fluorescence were detected using this analysis protocol (Figure 5.2 B). The detectable fusion events resembled those previously reported by Verweij *et al.*[82], and likewise became more frequent upon stimulation with 100µM histamine (Figure 5.2 C). These analysis parameters were therefore capable of quantifying tetraspanin fusion events in SKOV3 cells, and were employed for all further downstream analysis.

(A)

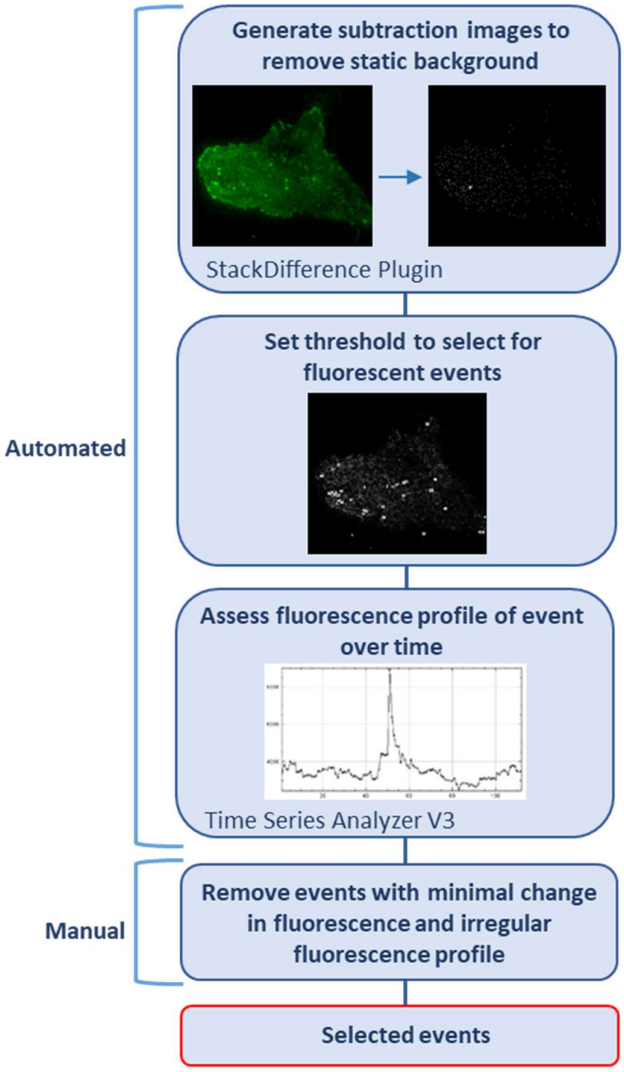

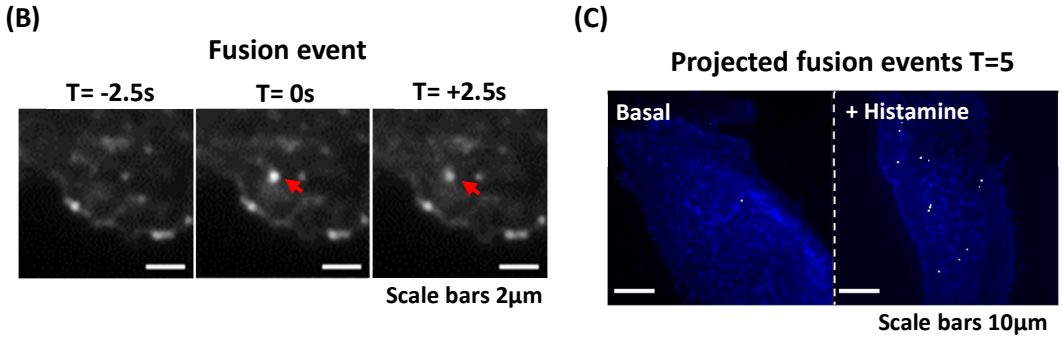

Figure 5.2 Analysis parameters were capable of quantifying tetraspanin fusion events in SKOV3 cells

(A) *Workflow for analysing fluorescent pHluorin events detected by TIRF microscopy using ImageJ.* ***(B)*** *Example of live CD81-pHluorin fusion event, indicated by red arrows. From left to right: one frame pre-fusion, moment of fusion and one frame post-fusion. Imaged at 0.4 frames per second (fps). Scale bars 2µm.* ***(C)*** *Projection of total fusion events at basal release (left) and histamine stimulated release (right) over a 5-minute time course. Pseudocoloured. Imaged at 0.4 fps. Scale bars 10µm.*

5.3.2. CD81, CD63 AND CD9-PHLUORIN EVENTS SHOW SIMILAR CHARACTERISTICS

Despite being regarded as classical markers of MVB-derived EVs, conflicting reports suggest that tetraspanins CD81, CD63 and CD9 represent sub-populations of MVB/PM-derived vesicles[104, 105, 460]. To assess if any detectable differences were apparent between tetraspanin fusion events, MVB-PM fusion in unstimulated cells was compared between CD81, CD63 and CD9-pHluorin reporters. To gain more information on their fusion dynamics, tetraspanin-pHluorin events were compared for their width, brightness and circularity as well as quantity. Overall, tetraspanin-pHluorin events exhibited similar characteristics across all four measurements (Figure 5.3 A-D), with the exception of CD9-pHlourin emitting a minimally brighter fluorescence signal (Figure 5.3 C). An average of 2-3 fusion events were emitted by all pHluorin-reporters over a 5-minute time course (Figure 5.3 A), similarly to fusion activity in unstimulated HeLa and HUVEC cells[82]. All pHluorin fusion events had a mean width of 0.4µm (Figure 5.3 B), in agreement with data from Verweij *et al.* and reported MVB size range (0.4–0.6µm)[82]. In addition, all tetraspanin fusion events averaged perfect circularity of 1 (Figure 5.3 D) – a parameter required by Bebelman *et al.*[461] to accept fluorescent events as bona fide MVB-PM fusion. Ultimately there appeared to be no detectable differences in MVB-PM fusion between CD81, CD63 and CD9-pHluorin reporters, and the fusion characteristics of all reporters were in keeping with those reported in the literature.

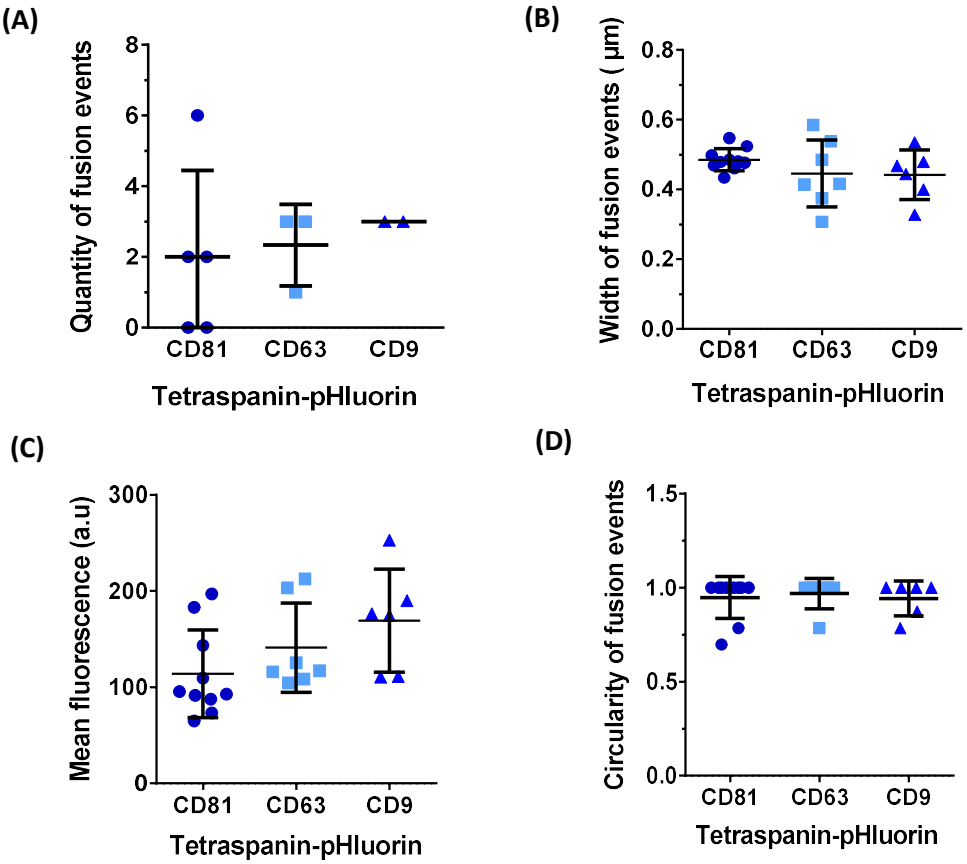

Figure 5.3 CD81, CD63 and CD9-pHlourin fusion events are similar in quantity, width, fluorescence and circularity

(A)-(D) *CD81, CD63 and CD9-pHluorin fusion events were analysed in untreated cells over a 5-minute time course for (A) quantity, (B) width (µm), (C) mean fluorescence (a.u) and (D) circularity. Mean ± SD shown for five, three and two transfected cells respectively in (A), and all fusion events in (B)-(D). Cells imaged at 0.4 fps. No statistically significant differences were observed as determined by Kruskal-Wallis and Dunn's multiple comparisons test.*

5.3.3. IMAGING AT 0.40FPS CAPTURES SUFFICIENT FUSION EVENTS WITHOUT INDUCING PHOTOBLEACHING OR PHOTOTOXICITY

In order to accurately assess the real-time effects of modulators on MVB-PM fusion, different frame rates were compared to establish an appropriate frame rate for imaging. Unstimulated cells were imaged over a 10-minute time course at 1.92 frames per second (fps), 1.01fps and 0.40fps. As shown in Figure 5.4 A, faster imaging captured more events – with an average of 19.7 events detected at 1.92fps, 16.5 at 1.01fps and 10.7 at 0.40fps. However, by the end of the 10-minute acquisition cells imaged at 1.92fps were visibly photobleached (Figure 5.4). Five static points were selected in cells imaged at each frame rate and the mean fluorescence of all points was plotted over the 10-minute time course (Figure 5.4 C). Faster imaging resulted in significant

photobleaching - with a decrease in mean fluorescence of 65.88% at 1.92fps and 46.45% at 1.01fps. As accurate analysis of MVB-PM fusion in this protocol relies on the assessment of fluorescence profiles, significant photobleaching can impede event analysis. Moreover, phototoxicity may affect fusion activity. To achieve a high signal-to-noise ratio, while avoiding photobleaching and phototoxicity, a frame rate of 0.40fps was used for all further imaging.

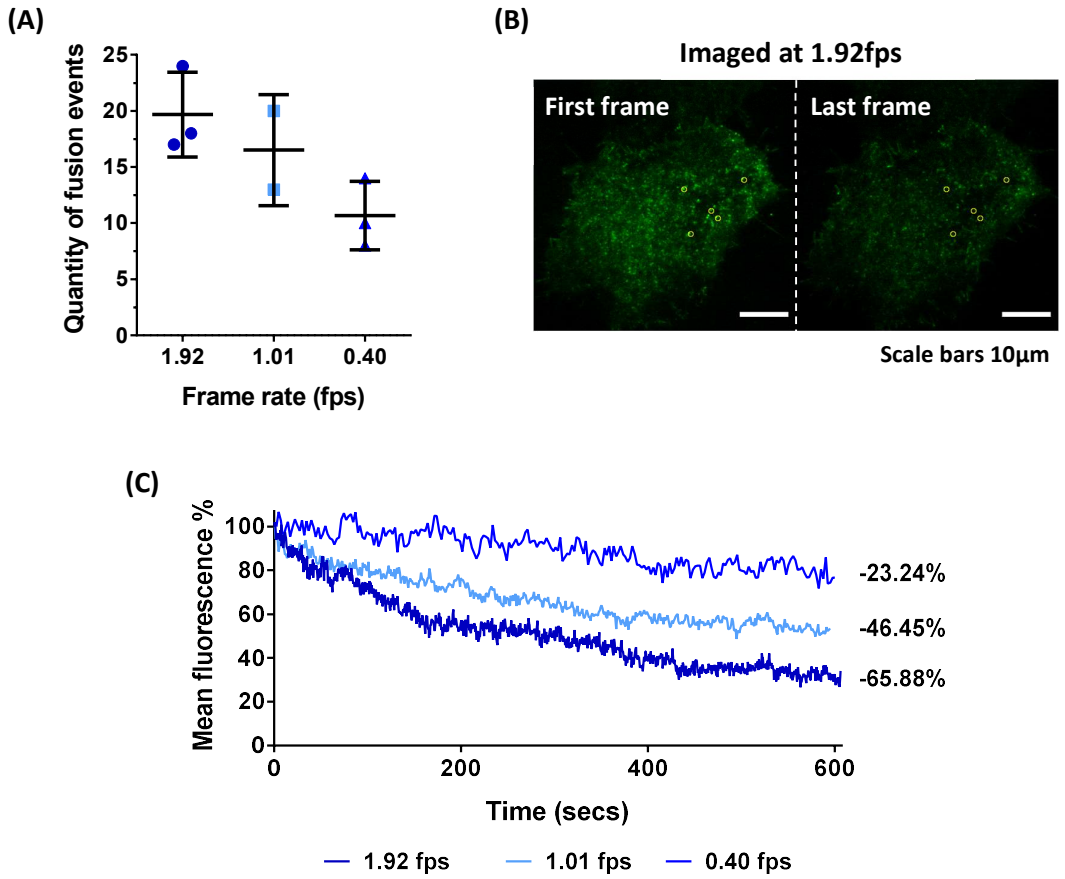

Figure 5.4 Faster imaging captures more events but causes significant photobleaching

(A) *Quantity of CD81-pHluorin events in untreated cells over a 10-minute time course captured at different frame rates: 1.92fps, 1.01fps and 0.40fps. Mean ± SD shown for three, two and three transfected cells respectively. FPS: frames per second.* ***(B)*** *Representative images showing the effect of photobleaching at 1.92fps on CD81-pHluorin fluorescence. First and last frame of acquisition shown. Selection of static points for analysis in* ***(C)*** *indicated by yellow circles. Scale bars 10µm. (C) Percentage of fluorescence bleaching over a 10-minute time course at 1.92fps, 1.01fps and 0.40fps. Data represents mean of five static points for each condition.*

5.3.4. HISTAMINE AND IONOMYCIN INDUCE MVB-PM FUSION IN SKOV3 CELLS

Histamine and Ionomycin are both well-established inducers of MVB-PM fusion in selected cell types[82, 144]. To validate imaging and analysis protocols and confirm that these compounds stimulate MVB-PM fusion in SKOV3 cells, CD81-pHluorin was employed to compare the frequency of basal MVB-PM fusion with histamine and ionomycin treated cells. Initially, fusion events were quantified in 10-minute acquisitions from 0-40 minutes following stimulation with 100µM histamine to determine the most appropriate timeframe for imaging. MVB-PM fusion markedly decreased from 20 minutes after histamine stimulation (Figure 5.5 A), indicating that the effect of histamine on MVB-PM fusion was immediate. CD81 fusion events were then quantified in untreated cells, and cells treated with either 100µM histamine or 1.25µM ionomycin in 5-minute acquisitions immediately following stimulation. Both ionomycin and histamine significantly increased the rate of CD81 fusion events compared to untreated controls (Figure 5.5 B,C). The established imaging and analysis parameters were therefore capable of detecting changes in MVB-PM fusion, and demonstrated that histamine and ionomycin act to increase EV release in SKOV3 cells.

(A)

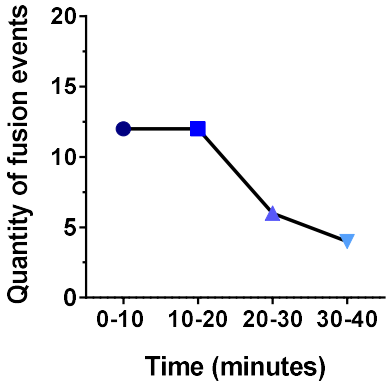

(B)

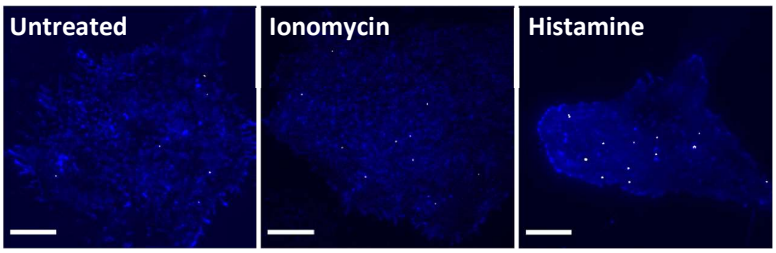

Projected fusion events T=5 mins
Scale bars 10µm

(C)

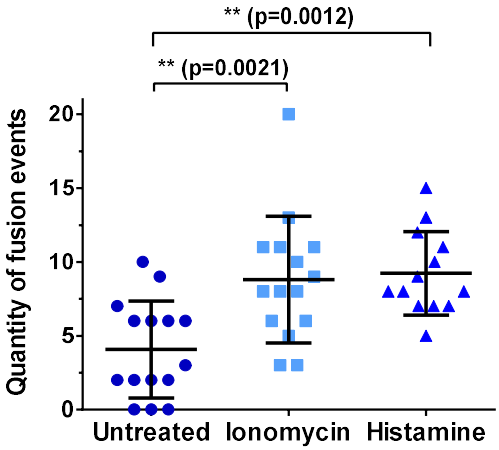

Figure 5.5 Histamine and ionomycin increase the rate of CD81 fusion events in SKOV3 cells

(A) *Quantity of CD81-pHluorin fusion events captured in cells treated with 100µM histamine in 10-minute acquisitions, from 0-40 minutes. Data represent fusion events in one cell per timeframe.*
(B) *Projection of total fusion events in untreated cells (left) and cells treated with 1.25µM ionomycin (middle) or 100µM histamine (right) over a 5-minute time course. Pseudocoloured. Scale bars 10µm.*
(C) *Quantity of CD81-pHluorin fusion events captured in untreated, ionomycin and histamine treated cells represented in (A) over a 5-minute time course (mean ± SD, n≥13). Statistical significance tested by one-way ANOVA and Tukey's multiple comparisons test.*

5.3.5. HISTAMINE AND IONOMYCIN INDUCE THE BIOGENESIS OF MVB-DERIVED EVS WITH DISTINCT CHARACTERISTICS AND FUSION DYNAMICS

To further characterise histamine and ionomycin-induced MVB-PM fusion in SKOV3 cells and gain more information on their fusion dynamics, all fusion events were assessed by size, mean fluorescence, circularity and duration. Indeed, analysis revealed discrete differences in the characteristics of histamine and ionomycin-induced fusion events (Figure 5.6 A-E). Histamine-induced fusion events were significantly larger and dimmer than both ionomycin stimulated and basal fusion events (Figure 5.6 A,B). Ionomycin-induced fusion events were also significantly dimmer than basal events, therefore unstimulated cells appear to emit the brightest CD81-pHluorin signal (Figure 5.6 B). All fusion events maintained a uniform circularity (Figure 5.6 C). Unexpectedly, there were also observed differences in the duration of fusion events which were classified into three event types: stay, fade and flash. All fusion events are characterised by a sudden increase in localised fluorescence, but the decay kinetics differ between event types (Figure 5.6 D). Typically, stay events do not decrease in fluorescence over the duration of the acquisition (5 minutes), fade events exponentially decay over time and flash events return to background fluorescence within a single frame. Interestingly, the proportions of observed event types differed under histamine and ionomycin stimulation (Figure 5.6 E). Basal MVB-PM fusion

consisted of largely flash event types (68%) with a smaller, and equal proportion of fade and stay events (~16%). Fade event types were most evident in ionomycin-stimulated cells (32%), with only 10% of ionomycin-induced fusion consistent with stay event types. Conversely, histamine-stimulated cells had the largest proportion of stay events (27%) and less than 50% flash event types. Taken together, this data demonstrates that histamine and ionomycin induce the biogenesis of MVB-derived EVs with distinct characteristics and fusion dynamics, possibly representing independent biogenesis pathways or EV sub-populations.

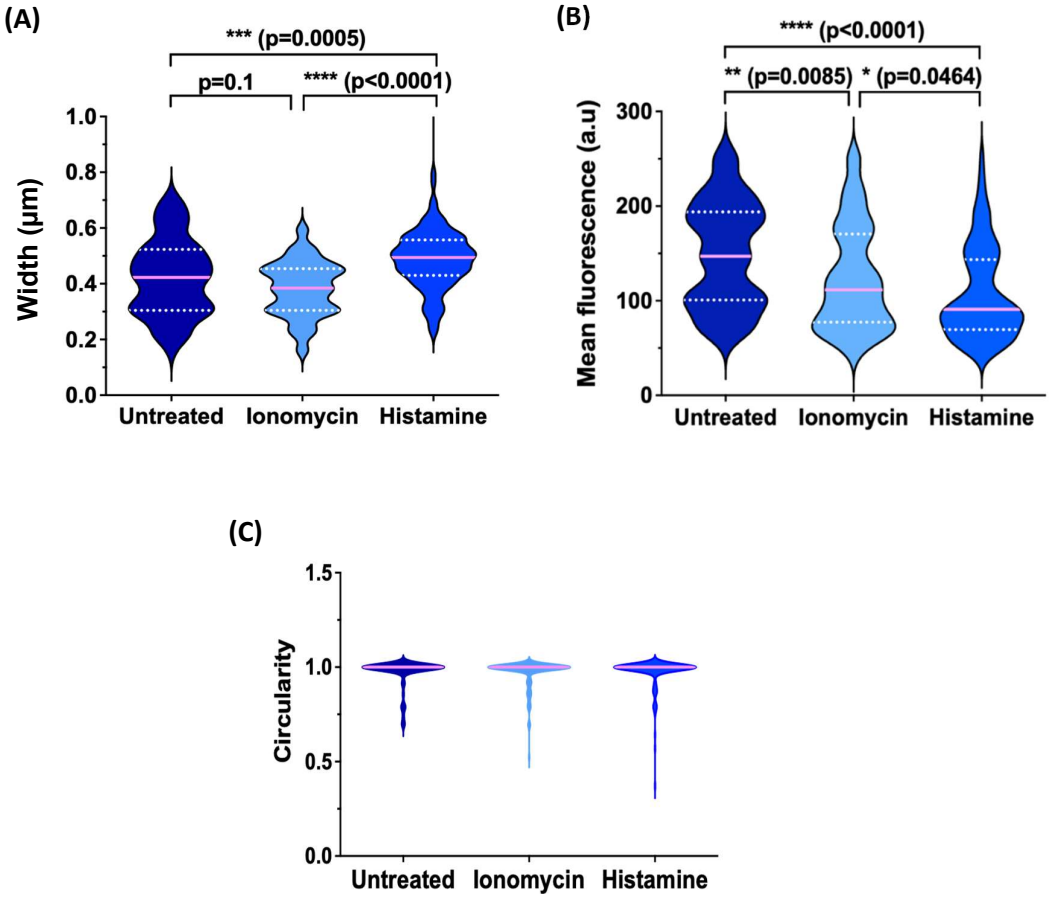

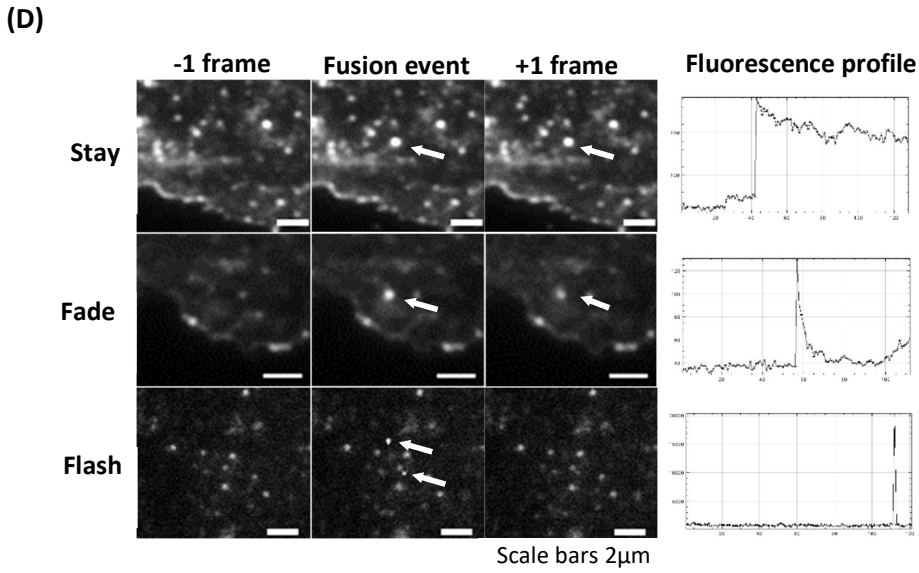

Figure 5.6 Histamine and ionomycin-induced fusion events differ in size, mean fluorescence and duration

(A)-(C) *The width (A), mean fluorescence (B) and circularity (C) of CD81-pHluorin fusion events were analysed in untreated, ionomycin and histamine treated cells represented in Figure 5.5 B. Violin plots show median and upper and lower quartiles, with statistical significance tested by Kruskal-Wallis and Dunn's multiple comparisons test.* ***(D)*** *Representative images demonstrating 'stay', 'fade' and 'flash' fusion event types over three consecutive frames, and their corresponding fluorescence profile over the total 5-minute time course. Red arrows indicate fusion events. Scale bars 2µm.* ***(E)*** *Percentage of 'stay', 'fade' and 'flash' fusion event types demonstrated in (D) in untreated, ionomycin and histamine treated cells over a 5-minute time-course. Data represents mean ± SEM, with no statistical significance observed between groups as determined by two-way ANOVA and Tukey's multiple comparisons test.*

5.3.6. TRPC3 ACTIVATION MEDIATES MVB-PM FUSION IN SKOV3 CELLS

With validated imaging and analysis protocols capable of quantifying and characterising inducible MVB-PM fusion, the CD81-pHluorin reporter was employed to address the chapter aim: to investigate the link between TRPC3 and MVB-PM fusion. Initially, SKOV3 cells were treated with 0.1µM TRPC3 activator or 1µM TRPC3 inhibitor (PYR3) and CD81 fusion events were quantified in 5-minute acquisitions from 0-35 minutes to determine the most appropriate timeframe for imaging. The rate of MVB-PM fusion was increased with TRPC3 activation compared to TRPC3 inhibition at five of the seven time points, with mean MVB-PM fusion equal at the further two time-intervals (Figure 5.7 A). There was a statistically significant overall treatment effect ($p=0.0118$), as determined by Ordinary two-way ANOVA. In addition, there was no effect of time on MVB-PM fusion under TRPC3 inhibition or activation, therefore it can be assumed that any effect of TRPC3 modulation is immediately translated to EV biogenesis. The experimental conditions were then extended to include untreated (-) and DMSO controls, as well as increasing concentrations of TRPC3 activator (0.1µM, 0.3µM, 1µM) to assess if MVB-fusion was affected in a dose-dependent manner. CD81 fusion events were quantified in 5-minute acquisitions immediately following stimulation. DMSO and PYR3 treated cells showed no difference in fusion activity compared to untreated cells (Figure 5.7 B,C). However, the rate of CD81 fusion activity increased in a dose-dependent manner following TRPC3 activation, with a significant increase in MVB-PM fusion at 0.3µM and 1µM concentrations in comparison to untreated and DMSO controls (Figure 5.7 B,C). Therefore, whilst TRPC3 inhibition does not affect MVB-PM fusion, activating TRPC3 stimulates MVB-PM fusion in a dose-dependent manner, identifying a novel role for TRPC3 in MVB-PM fusion and EV release in SKOV3 cells.

(A)

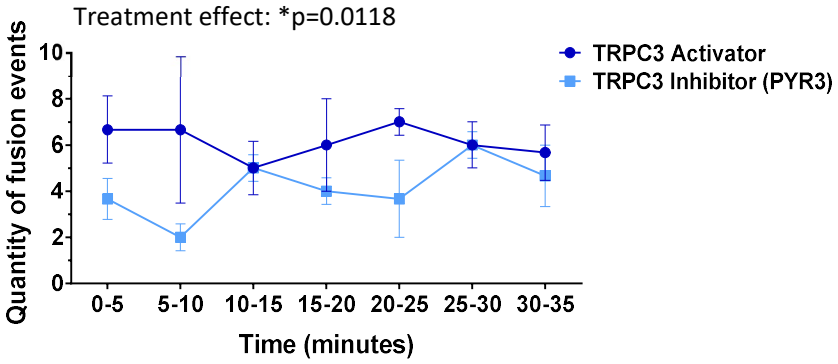

(B)

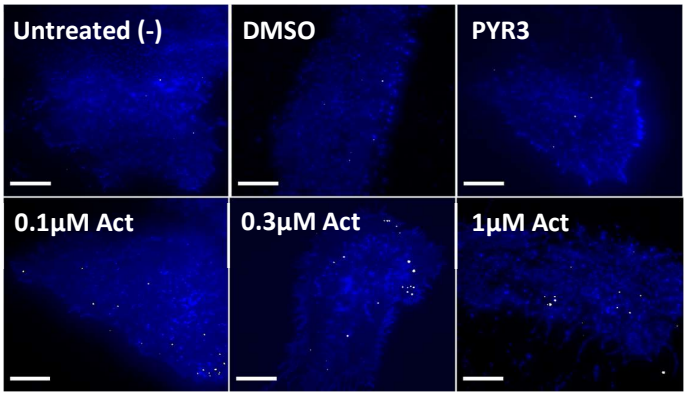

Projected fusion events T=5 mins
Scale bars 10µm

(C)

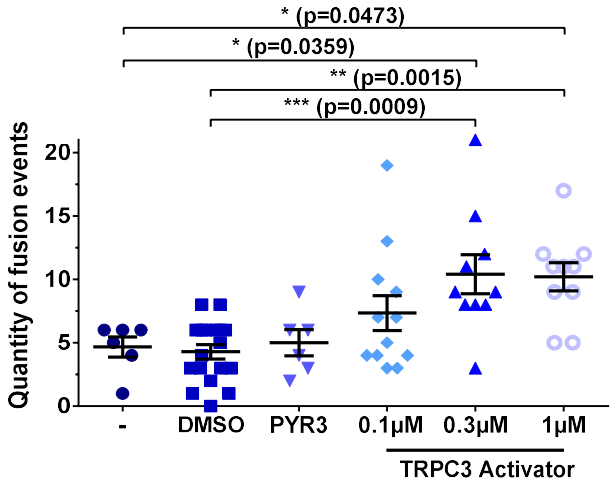

Figure 5.7 Activating TRPC3 stimulates MVB-PM fusion in a dose-dependent manner

(A) *Quantity of CD81-pHluorin fusion events captured in cells treated with either 0.1µM TRPC3 activator or 1µM TRPC3 inhibitor (PYR3) in 5-minute acquisitions, from 0-35 minutes. Data represents mean ± SEM of three cells per timepoint. The overall effect of treatment was determined statistically significant by two-way ANOVA, but no statistically significant differences were observed between groups by Sidak's multiple comparisons test.* ***(B)*** *Projection of total fusion events in control and treated cells over a 5-minute time course. Top row, left to right: untreated (-), DMSO (equivalent to highest concentration), 1µM PYR3. Bottom row, left to right: 0.1, 0.3 and 1µM TRPC3 activator (Act). Pseudocoloured. Scale bars 10µm.* ***(C)*** *Quantity of CD81-pHluorin fusion events captured in control and treated cells represented in (B) over a 5-minute time course (mean ±SEM, n ≥6). Statistical significance tested by one-way ANOVA and Tukey's multiple comparisons test.*

5.3.7. TRPC3 ACTIVATION INDUCES THE BIOGENESIS OF MVB-DERIVED EVS WITH DISTINCT CHARACTERISTICS AND FUSION DYNAMICS

Upon histamine and ionomycin stimulation, induced fusion events differed in size, fluorescence and duration. To understand how modulating TRPC3 activity may affect MVB characteristics and fusion dynamics, all fusion events were likewise assessed by size, mean fluorescence, circularity and duration. DMSO and PYR3 treatments demonstrated no effect on the quantity of detected fusion events in earlier analysis (Figure 5.7 B ,C), and likewise showed no effect on the size, mean fluorescence, circularity or duration of CD81 events (Figure 5.8 A-D). However, at increasing concentrations of TRPC3 activator and thus increasing rates of CD81 fusion activity (Figure 5.7 B,C), TRPC3 activator-induced fusion events were significantly larger and dimmer than DMSO-induced events in a dose-dependent manner (Figure 5.8 A,B). At the highest concentration of TRPC3 activator (1µM), MVB-PM fusion events were also significantly larger and dimmer than basal events. All fusion events maintain a uniform circularity (Figure 5.8 C). Fusion events were also classified into 'stay', 'fade' or 'flash' event types based on their duration, as described in Figure 5.6 D. The proportions of observed event types differ under TRPC3 modulation (Figure 5.6 E). Basal and DMSO-induced MVB-PM fusion mainly consisted of flash event types (63% and 84% respectively) with a smaller proportion of fade events, and no evident stay events in basal MVB-PM fusion. Stay event types were fairly consistent across all other treatment groups, varying between 7-14% of all captured events. Fade event types were the most variable amongst treatment groups, and were most evident in cells treated with 0.1µM TRPC3 activator (38%). In fact, there were significantly more fade event types and reciprocally significantly fewer flash events in 0.1µM TRPC3 activator treated cells compared to the DMSO control. Although, the effect of TRPC3 activation on MVB-fusion duration was not dose-dependent. Collectively these data characterise for the first time the effect of TRPC3 activation on MVB-PM fusion, demonstrating distinct TRPC3-induced MVB characteristics and fusion dynamics.

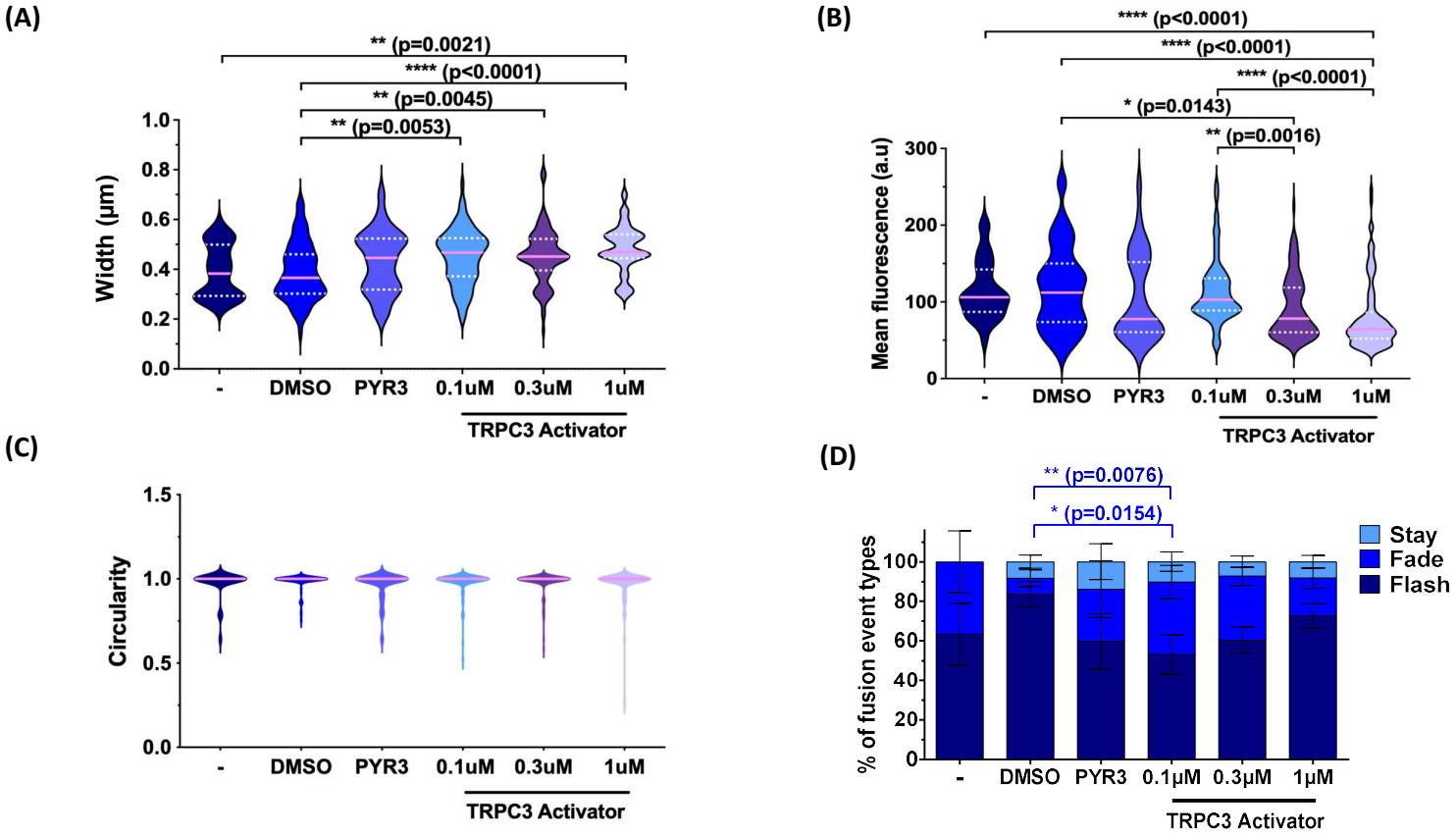

Figure 5.8 Activating TRPC3 alters the size, mean fluorescence and duration of MVB-PM fusion events

(A)-(C) *The width (A), mean fluorescence (B) and circularity (C) of CD81-pHluorin fusion events were analysed in untreated (-) and DMSO control cells, and cells treated with 1µM PYR3 or 0.1, 0.3, 1µM TRPC3 activator as represented in Figure 5.7 B. Violin plots show median and upper and lower quartiles, with statistical significance tested by Kruskal-Wallis and Dunn's multiple comparisons test.* ***(D)*** *Percentage of 'stay', 'fade' and 'flash' fusion event types as described in Figure 5.6 D, for control and treated cells represented in Figure 5.7 B over a 5-minute time-course. Data represents mean ± SEM, with statistical significance tested by two-way ANOVA and Tukey's multiple comparisons test.*

5.3.8. HISTAMINE INDUCES MVB-PM FUSION THROUGH ACTIVATION OF THE TRPC3 CHANNEL

Histamine stimulation increases cytosolic Ca^{2+} through activation of the histamine H_1 and H_2 GPCRs[462]. TRPC3 is activated downstream of both H_1 and H_2 receptors[305, 364], and may participate in histamine-induced Ca^{2+} entry. Indeed, the results presented in Chapter 3 demonstrate that increased Ca^{2+} signalling following histamine treatment is blocked in the presence of TRPC3 inhibitor Pyr3 (Figure 3.7 A,B). As both histamine and TRPC3 activation act to induce MVB-PM fusion (Figure 5.5 and 5.7), these results suggest that histamine may induce MVB-PM fusion through GPCR activation of the TRPC3 channel. To test this hypothesis, MVB-PM fusion was quantified in SKOV3 cells which were pre-treated with 3µM TRPC3 inhibitor Pyr3 for 30 minutes prior to 100µM histamine stimulation, alongside untreated cells, cells treated only with 100µM histamine, and cells pre-treated with an equivalent DMSO concentration for 30 minutes prior to histamine stimulation. This analysis replicated the results presented in Figure 5.5, confirming that histamine stimulation significantly increases the rate of CD81 fusion events compared to untreated controls (Figure 5.9 A,B). Pre-incubating cells with DMSO did not inhibit histamine-stimulated MVB-PM fusion, however in histamine stimulated cells pre-treated with TRPC3 inhibitor, the effect of histamine was diminished, significantly reducing MVB-PM fusion to that of the untreated control. These results therefore support that TRPC3 acts downstream of histamine GPCRs in SKOV3 cells, and indicate that histamine induces MVB-PM fusion through activation of the TRPC3 channel.

(A)

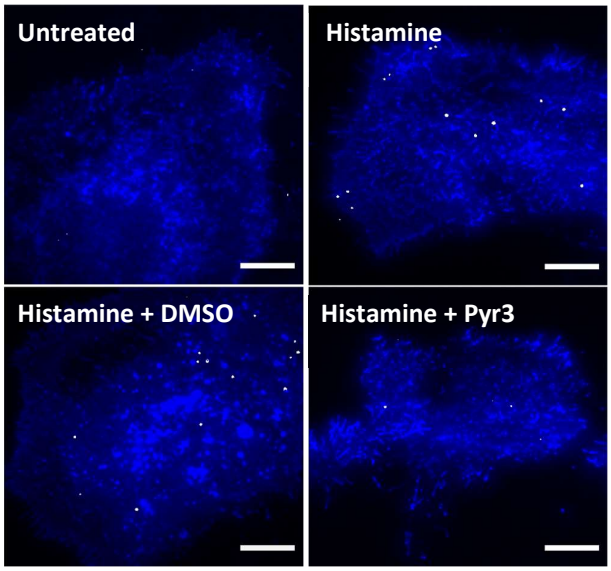

Projected fusion events T=5 mins
Scale bars 10µm

(B)

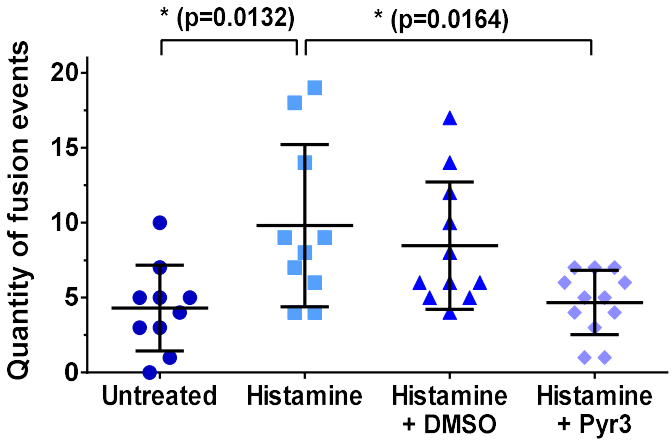

Figure 5.9 Pre-treatment with Pyr3 attenuates histamine stimulated MVB-PM fusion

(A) *Projection of total fusion events in untreated cells (top left) and cells treated with 100µM histamine (top right), 100µM histamine + 0.03% DMSO (bottom left) or 100µM histamine + 0.3µM Pyr3 (bottom right) over a 5-minute time course. Pseudocoloured. Scale bars 10µm.* ***(B)*** *Quantity of CD81-pHluorin fusion events captured in untreated cells, and cells treated with histamine, histamine + DMSO and histamine + Pyr3 represented in (A) over a 5-minute time course (mean ± SD, n≥10). Statistical significance tested by one-way ANOVA and Tukey's multiple comparisons test.*

5.3.9. INDUCED MVB-PM FUSION IN SKOV3 CELLS IS LOCALISED AND SYNCHRONISED

During the analysis of histamine, ionomycin and TRPC3 activator-induced MVB-PM fusion, it was noted that a number of fusion events occur within close proximity of one another – particularly in stimulated conditions. Examples of these localised fusion events are demonstrated in Figure 5.10 A. The distance between fusion events within the same cell was subsequently measured in all treatment conditions, and fusion events were considered localised if they occurred within 5µm of another event. Initially, the percentage of localised fusion events was quantified in untreated, and ionomycin and histamine stimulated cells (Figure 5.10 B). Although not significant, a higher proportion of fusion events were localised in ionomycin and histamine stimulated cells: on average 29% of basal MVB-PM fusion was localised, compared to 46% and 51% for ionomycin and histamine-induced fusion, respectively. Next, localised fusion events were quantified in cells treated with the TRPC3 inhibitor PYR3, 0.1µM, 0.3µM, or 1µM TRPC3 activator, and untreated (-) and DMSO controls (Figure 5.10 C). In untreated and DMSO-treated cells, an average of 28% and 30% of MVB-PM fusion was localised respectively, replicating unstimulated MVB-PM fusion in the histamine and ionomycin control population. Similar to histamine and ionomycin stimulated MVB-PM fusion, TRPC3 activation increased the number of localised fusion events in SKOV3 cells - peaking at 65% at 0.3µM activator, which is significantly increased in comparison to DMSO-induced MVB-PM fusion. Interestingly, although TRPC3 inhibition with PYR3 showed no effect on the quantity or characteristics of MVB-PM fusion, localised fusion is reduced to 9% in PYR3 treated cells. This is significantly reduced in comparison to both 0.3µM and 1µM TRPC3 activator treatments. Therefore, whilst TRPC3 inhibition induces diffuse fusion events in SKOV3 cells, stimulation with histamine, ionomycin and TRPC3 activator induces localised MVB-PM fusion.

An additional observation made during this analysis was the tendency for localised fusion events to occur simultaneously. The distance between all MVB-PM fusion events that appeared in the same frame was measured to assess what percentage of synchronised events were localised or diffuse. Indeed, significantly more localised fusion events appeared simultaneously compared to diffuse fusion - 24% to 13% respectively. This effect was not treatment dependent. Overall, these results demonstrate that histamine, ionomycin and TRPC3 activator induce localised and synchronised MVB-PM fusion in SKOV3 cells, proposing the idea of ‘EV hotspots’ within stimulated cells.

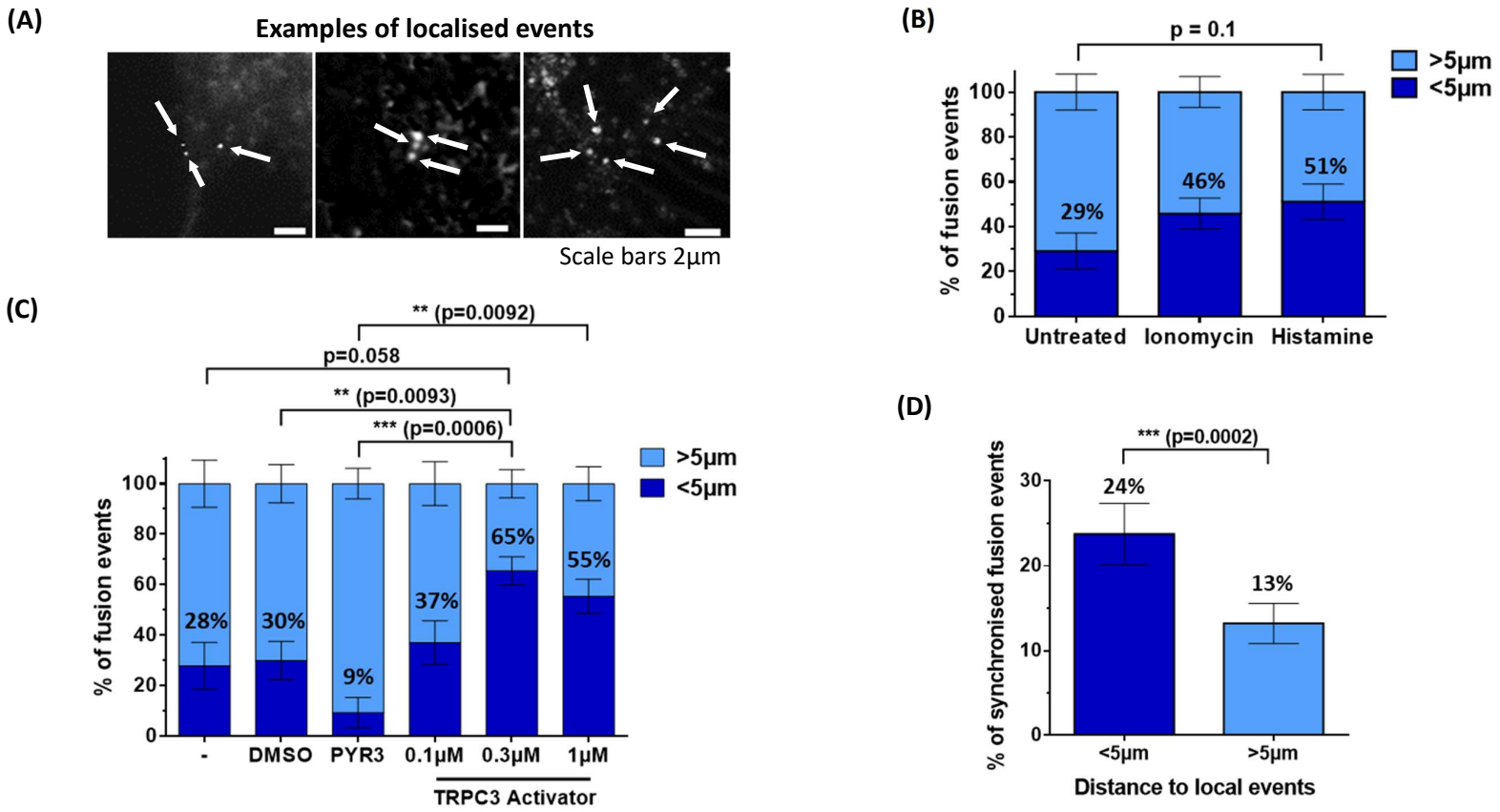

Figure 5.10 Histamine, ionomycin and TRPC3 activator increase localised and synchronised MVB-PM fusion in SKOV3 cells

(A) *Representative images demonstrating instances of localised CD81-pHluorin fusion events, indicated by red arrows. Scale bars 2µm.* ***(B)-(C)*** *Percentage of localised fusion events (defined as events occurring within 5µm (<5µm) of another fusion event in the same cell) in (B) untreated, ionomycin and histamine treated cells and (C) untreated (-), DMSO, PYR3 or 0.1, 0.3, 1µM TRPC3 activator treated cells. All data represents mean ± SEM (n≥6), with statistical significance tested by two-way ANOVA and Tukey's multiple comparisons test.* ***(D)*** *Percentage of synchronised events which occur within 5µm (<5µm) or further away than 5µm (>5µm) of another fusion event in the same cell. Data represents mean ± SEM of all imaged cells regardless of treatment condition, n=101. Statistical significance tested by Wilcoxon matched-pairs signed rank test.*

5.4. DISCUSSION

The aim of this chapter was to further investigate a novel role for TRPC3 in EV biogenesis. The results presented in Chapter 4 demonstrate that TRPC3 activation induced the release of EVs harbouring the functional capacity to increase the growth rate of recipient cells, suggesting a novel role for TRPC3-mediated EV biogenesis and communication in the progression of ovarian cancer. Using tetraspanin-pHluorin reporters, this chapter assessed the quantity, characteristics and fusion dynamics of MVB-PM fusion in SKOV3 cells treated with TRPC3 activator and inhibitor, alongside known inducers of MVB-PM fusion histamine and ionomycin. Initially, image acquisition and analysis parameters capable of characterising MVB-PM fusion were developed, and demonstrated that histamine and ionomycin act to increase MVB-PM fusion in SKOV3 cells. In assessment of the chapter aim, activating TRPC3 stimulated MVB-PM fusion in a dose-dependent manner, identifying a novel role for TRPC3 in MVB-PM fusion and EV release. This analysis also revealed treatment-induced differences in the physical characteristics of fusion events, and describes novel fusion dynamics including distinct fusion event types and localised, synchronised MVB-PM fusion.

5.4.1. IMAGING AND ANALYSIS PROTOCOLS FOR ASSESSING MVB-PM FUSION

In this analysis, image acquisition and analysis parameters were developed to assess MVB-PM fusion in SKOV3 cells. These protocols were guided by the methods paper published by Bebelman *et al.* detailing their recommended parameters for assessing CD63-pHluorin fusion events[461]. Although, some parameters were adapted to optimally quantify MVB-PM fusion in SKOV3 cells and to better fit the research aim. For example, Bebelman *et al.* recommends a fast-imaging speed of ≥2Hz - equivalent to 2 frames per second (fps) - and include a macro to correct for photobleaching in their analysis plug-in, AMvBE. However, imaging SKOV3 cells at 1.92fps resulted in significant photobleaching, which may impede event analysis by skewing the fluorescence profile of fusion events, or by directly affecting fusion activity through inducing phototoxicity. Therefore, a slower frame rate of 0.40fps was used to assess CD81-pHluorin fusion events in SKOV3 cells.

The analysis workflow developed here selects for 'new' localised increases in fluorescence above a set threshold in every individual frame of the acquisition. As recommended by Bebelman *et al.*; events with minimal change in fluorescence, an irregular fluorescence profile and/or lateral movement of the fluorescence signal were excluded from the analysis. These omissions prevent the analysis of fluorescent events which are not a consequence of MVB-PM fusion, such as tetraspanin-pHluorin-containing transport vesicles with neutral pH that move into the TIRF field

without fusing with the PM. However, Bebelman *et al.* also excludes events that do not follow a strict fluorescence profile; stating that the fluorescence signal must have a duration of ≥ 2s and decay exponentially. These fusion events are reminiscent of the 'fade' event types described here. The minimal signal duration for MVB-PM fusion is set at ≥ 2s as Verweij *et al.* demonstrate that short-lived fluorescence is associated with the release of soluble cargo (NPY) or membrane deposition (VAMP2)[82]. On this basis, these parameters exclude 'flash' event types from their analysis and suggest that these fusion events may not be associated with MVB-PM fusion. However, absolute fusion duration times will vary between cell types, temperature conditions, medium viscosity etc., therefore the relative fusion duration of VAMP2-pHluorin compared with CD81-pHluorin should be determined for each individual experiment. Moreover, they reason that fusion events with an extended signal duration may represent so-called 'kiss-and-run' events whereby the vesicle pore transiently opens and closes without fully collapsing into the PM, resulting in incomplete secretion or rapid reuptake of exocytosed EVs. Therefore the 'stay' event types described here may represent these kiss-and-run-like events. However, the focus of this chapter is to assess the effect of exogenous stimuli on MVB-PM fusion rather than the quantity of EV release, therefore these event types were not excluded from this analysis. Of note, another member of the lab used the AMvBE plug-in designed by Bebelman *et al.* to quantify MVB-PM fusion from the same set of untreated and histamine treated cells assessed here, and likewise demonstrated an increase in MVB-PM fusion upon histamine stimulation (Supplementary Figure 2). This indicates that despite differences in analysis parameters, both protocols yield comparable results in assessments of MVB-PM fusion.

5.4.2. HISTAMINE AND IONOMYCIN-INDUCED MVB-PM AND FUSION

Histamine and ionomycin induce MVB-PM fusion in a number of cell types[82, 144] and shown here for the first time, in OC cells. Limited research has been conducted into the mechanisms which mediate these inducible signalling pathways. Histamine stimulation induces MVB-PM fusion through GPCR signalling from the histamine H_1 receptor (H1HR), and subsequent phosphorylation of the exocytic t-SNARE, SNAP23[82]. As most GPCRs use Ca^{2+} as a second messenger, the authors investigated whether histamine-induced MVB-PM fusion events were linked to an increase in intracellular Ca^{2+}. The use of both intra- and extracellular Ca^{2+} chelators (BAPTA-AM and EGTA-AM, respectively) failed to reduce the number of histamine-induced MVB-PM fusion events, suggesting that histamine stimulates EV biogenesis through distinct mechanisms from Ca^{2+}-dependent, ionomycin-induced MVB-PM fusion. Indeed, it would appear that histamine and ionomycin are acting on different endosomal/exocytosis machinery to stimulate EV release: histamine-induced EV release is upregulated at the point of membrane

fusion by activation of PM-associated exocytic t-SNAREs, whereas ionomycin regulates MVB maturation through Ca^{2+}-dependent interactions with the SNAP receptor Munc13-4[144]. Here, histamine and ionomycin induced the biogenesis of MVB-derived EVs with discrete characteristics and fusion dynamics, supporting the notion of two distinct inducible signalling pathways.

Additional mechanisms may also contribute to the variable physical characteristics and fusion dynamics of induced MVB-PM fusion events. For example, histamine and ionomycin may influence the expression of tetraspanins, or the pathways which mediate their loading into EVs to generate dimmer fusion events as observed here. Or simply, if MVB maturation and PM fusion are upregulated but the rate of tetraspanin-internalisation remains constant, fewer tetraspanins will be incorporated into each MVB, thus resulting in a dimmer signal. With regards to histamine-induced fusion events which were both larger and dimmer than ionomycin stimulated and basal fusion events, larger MVBs may contain the same amount of CD81-positive ILVS, therefore the fluorescent signal is likely to appear more diffuse. Whilst Ca^{2+}-stimulated mechanisms have been shown to regulate MVB size[144, 147], the role of histamine in this process is as of yet unrecognised. The size and composition of treatment-induced MVBs may also impact signal duration upon fusion with the PM, with larger histamine-induced MVBs emitting more prolonged fluorescent 'fade' and 'stay' events than unstimulated MVB-PM fusion. It's also possible that histamine may alter the expression of proteins on the EV surface, making them 'stickier' and thus immobilizing them to the PM after MVB-PM fusion. Entrapment of tetraspanin-pHluorin EVs between cells and the coverslip, EV-EM interactions or aforementioned 'kiss-and-run-like' events may also account for differences in fluorescent signal duration.

5.4.3. TRPC3 ACTIVATOR-INDUCED MVB-PM FUSION

This chapter has identified a novel role for TRPC3 in EV biogenesis, and for the first time characterised TRPC3-induced MVB-PM fusion dynamics. Mainly, activating TRPC3 stimulated MVB-PM fusion in a dose-dependent manner. This may have important pathophysiological consequences in cancer, as TRP channels are amplified in numerous cancer types and contribute to tumorigenesis through enhancing cell survival, proliferation and invasion. TRPC3 in particular has been identified as a direct driver of proliferation and migration in a number of cancers, including melanoma[318], lung[362], bladder[363], breast[463] and ovarian[310]. In this work, TRPC3 activation increased the proliferation and migration of SKOV3 OC cells, and TRPC3 activator-induced EVs increased the growth rate of recipient cells (Chapters 3 and 4, respectively). Indeed, EVs are well-established mediators of tumour progression with roles identified in promoting cell proliferation, metastasis and the formation of the pre-metastatic niche [204]. Given the multiple

roles of EVs in cancer progression, the work presented here suggests increased TRPC3 activity in SKOV3 cells induces the release of EVs which may contribute to metastatic mechanisms downstream of increased Ca^{2+} signalling. In line with these findings, SKOV3 cells were found to release significantly more EVs than their less-invasive OC counterparts OVCAR3, carrying proteins involved in cell death and survival, cellular growth and proliferation[372,]. *In vivo*, the concentration of circulating EVs in serum samples from women diagnosed with OC is significantly elevated compared to benign disease or controls, and correlates with disease progression[163].

Deciphering the mechanisms by which TRPC3 mediates EV biogenesis and subsequent cancer pathways is limited due a lack of available data. As TRPC3 mediates sustained elevated Ca^{2+} in SKOV3 cells (Chapter 3), TRPC3 activator-induced EV release is likely to be Ca^{2+}-dependent. Ca^{2+}-regulated molecules are also likely to contribute to the increased size of TRPC3 activator-induced MVBs, such as Rab11 which generates Ca^{2+}-induced giant MVBs in K562 cells and Raw macrophages[147]. Current proposed models of Ca^{2+} induced EV biogenesis speculate that DAG/IP_3-mediated Ca^{2+} release from internal stores subsequently induces EV release[143, 325]. TRPC channels are activated downstream of GPCR stimulation in a Ca^{2+} signalling cascade involving phosphatidylinositol 4,5-biphosphate (PIP2) hydrolysis, generation of IP_3 and DAG, and IP_3-mediated Ca^{2+} release from internal stores[303]. Here, inhibiting TRPC3 attenuated histamine-stimulated Ca^{2+} entry and subsequent MVB-PM fusion, proposing that TRPC3 acts downstream of histamine GPCRs in SKOV3 cells and also mediates histamine induced MVB-PM fusion. Taken together, the results presented in this chapter propose that Ca^{2+} induced EV biogenesis in SKOV3 cells is mediated by a H_1/H_2HR-TRPC3-phosphatidylinositol signalling pathway. This pathway may act on EV biogenesis through a number of different mechanisms: firstly, Ca^{2+} stimulation could upregulate the endocytic pathway thereby increasing MVB biogenesis or maturation, or alternatively MVB-PM fusion could be upregulated at the point of membrane fusion. Available evidence suggests TRPC3 may facilitate EV biogenesis through the latter; as overexpression of TRPC3 enhances constitutive secretion from COS-7 cells by increasing vesicle fusion at the PM[464]. Proteomic analysis of TRPC3 activator-induced EVs conducted in Chapter 6 aims to further characterise this EV population and derive mechanistic insights into how TRPC3 mediates EV biogenesis pathways.

5.4.4. LOCALISED AND SYNCHRONISED MVB-PM FUSION

Histamine, ionomycin and TRPC3 activator induced localised and synchronised MVB-PM fusion in SKOV3 cells, proposing the idea of 'EV hotspots' within stimulated cells. Indeed, instances of localised and directional EV release have previously been reported in a number of cell types; in

the immunological synapse between T- and B cells[122], on the front end of migrating cancer cells[236] and on the apical and basolateral side of intestinal epithelial cells[465]. Regulated and localised MVB exocytosis may have important biological consequences *in vivo.* For example, lamellipodia of HT1080 cells show local concentrations of CD63-pHlourin fusion events at sites of adhesion assembly[235]. Considering TRPC3 activation enhances the migratory capacity of SKOV3 cells (Chapter 3), localised MVB exocytosis may represent sites of dynamic membrane structures promoting cell motility. In SKOV3 cells, localised fusion events were scattered across the PM with no obvious preferential sites for MVB exocytosis. Mapping these localised instances of MVB-PM fusion to subcellular structures could reveal pathophysiological roles for local MVB exocytosis. In addition, cell surface receptors/proteins can be tagged and imaged in conjunction with pHluorin reporters to assess if 'EV hotspots' co-localise with the expression of specific PM-associated complexes. Interestingly, GPCRs CCR5 and CXCR4 are recruited to the site of localised EV release at the immunological synapse[122, 466], proposing a similar mechanism for localised histamine-GPCR MVB-PM fusion. Likewise, localised TRPC3-induced MVB exocytosis may coincide with the location of TRPC3 channels in the PM. Further experiments characterising the sites of EV hotspots will improve understanding of their biological significance.

5.4.5. LIMITATIONS OF TETRASPANIN-PHLUORIN REPORTERS

Whilst the tetraspanin-pHluorin reporter system has provided valuable insights into inducible MVB-PM fusion in this work, there are various limitations associated with the technique. Firstly, tetraspanin-pHluorin fusion events report MVB-PM fusion rather than actual EV release. Therefore, in circumstances whereby MVB-PM fusion may not directly reflect EV exocytosis, vesicle release may be overestimated by this approach. For instance, MVBs may only transiently fuse with the PM resulting in incomplete secretion or rapid reuptake of exocytosed EVs as described for 'kiss-and-run like' events, or exocytosed EVs may remain stuck at the PM as observed for 'stay' event types. Exogenous stimuli may also influence tetraspanin-loading into EVs, distorting analysis of MVB-PM fusion. In addition, fluorescent signals from MVBs fusing with neutral vesicles adjacent to PM, or from late endo/lysosomal tetraspanins trafficked to the cell surface may interfere with accurate quantification of MVB-PM fusion. Secondly, whilst the ability to specifically analyse CD81+ EV release can be viewed as a strength of the method, EV subpopulations devoid of CD81 will inevitably be ignored. This includes CD81- EVs as well as MVs, exomeres and other EV-like vesicles[21]. Comparing MVB-PM fusion rates between CD81, CD63 and CD9-pHluorins, or potentially other EV-specific cargo reporters, will provide a clearer overall picture of EV release and the contributing sub-populations of EVs.

5.5. KEY FINDINGS

- MVB-PM fusion can be quantified and characterised in SKOV3 cells using tetraspanin-based pHluorin reporters and a novel, unbiased analysis protocol.
- Histamine and ionomycin induce the biogenesis of MVB-derived EVs with distinct characteristics and fusion dynamics in SKOV3 cells.
- Activation of the Ca^{2+} channel TRPC3 induces MVB-PM fusion in SKOV3 cells, demonstrating a novel role for TRPC3 in EV biogenesis.
- TRPC3 activator-induced EVs have distinct MVB characteristics and fusion dynamics.
- Inhibition of TRPC3 blocks the stimulatory effect of histamine on MVB-PM fusion.
- Induced MVB-PM fusion is localised and synchronised in SKOV3 cells.

Chapter 6

Proteomic profiling of treatment-induced EVs

6. Proteomic profiling of treatment-induced EVs

6.1. BACKGROUND

6.1.1. EV PROTEIN CARGO

The selective incorporation of proteins into EVs and their capacity to evoke phenotypic changes in recipient cells is one of the landmark discoveries in the EV field [12, 13, 91, 467]. Since, the proteomic cargoes of EVs have been characterised from a number of cell types and biological fluids during homeostatic and pathological states[468]. EV proteomes are reflective of their cellular and endosomal origin, and therefore exhibit divergent protein cargo under environmental stresses encountered during disease states. Analysis of EV-protein composition can therefore identify the site and pathology of their cellular origin, which has fuelled significant interest in exploiting EV protein cargo as putative biomarkers for disease diagnosis, prognosis and response to treatment[323].

EV-mediated intercellular transfer of these selectively loaded proteins is also implicated in a wide range of physiological and pathological processes including transduction of viral and bacterial infections, immune response and tumour metastasis[113-116]. Focusing on the latter, numerous roles for the transfer of functional EV proteins have been identified in every stage of the metastatic cascade (reviewed in [205]). For example, metastatic OC cells abundantly secrete EVs that express soluble E-cadherin, which functions to promote angiogenesis though binding VE-cadherin on recipient cells and activating β-catenin and NFκB signalling [405]. CD44, a cell surface glycoprotein, is also enriched in metastatic OC cell derived EVs, and its EV-mediated transfer promotes the migration, invasion and proliferation of low-metastatic OC cells[403]. Moreover, integrin expressing EVs direct organ-specific metastatic distribution to facilitate the establishment of secondary tumour sites in ovarian, breast and liver cell metastasis[113, 404]. Because of the many ways that EVs and their protein cargo contribute to tumour metastasis, understanding the factors which underly their formation and how these pathways can be promoted or inhibited, and the ensuing effects on their proteomic cargo holds significant therapeutic potential.

Knowledge of the proteomic composition of EVs can provide clues about the machinery involved in their biogenesis. EVs derived from different cellular origins sequester a common set of molecules which are likely involved in their formation, including chaperones (Hsp70, Hsp90), cytoskeletal proteins (actin, tubulin), tetraspanins (CD81, CD63, CD9), several components of

the ESCRT complex (TSG101, Alix) and proteins involved in vesicle transport and fusion (Rab7, Rab2, Annexins)[103]. The commonality of these proteins suggests there are conserved mediators of EV biogenesis, however the highly heterogenous nature of EVs and their cargo emphasises that there are multiple mechanisms involved[469]. This complexity impedes our ability to decipher the molecular pathways which underly EV formation and release.

6.1.2. The effect of external stimuli on EV biogenesis

In addition to pathological conditions and stresses, external cues can influence the biogenesis of EVs and their protein composition; including heat and oxidative stress[470], hypoxia[471] and pH[121], as well as molecular stimulants ceramide, histamine and ionomycin[82, 144, 472]. Observing how these external cues alter EV release has provided valuable insights into EV biogenesis pathways. For example, inducing EV release by increasing intracellular Ca^{2+} identified a Ca^{2+} stimulated MVB trafficking pathway dependent on Rab11 and the Rab binding protein Munc13-4[144, 147]. Verweij *et al.* [82 82 82 82 82 82 82 82 82 82 82 82 84] demonstrated that EV biogenesis is also induced by histamine stimulation through a Ca^{2+} independent pathway. Phosphoproteomics of HeLa cells following histamine stimulation determined that GPCR signalling from the histamine H_1 receptor (H1HR) via SNAP23, an exocytic t-SNARE, triggers MVB-PM fusion. These demonstrations of inducible signalling pathways highlight the interest in unravelling these mechanisms which function to trigger EV release, however a full proteomic screen of how these pathways influence EV cargo has, to our knowledge, never been conducted. As analysis of EV protein cargo can indicate their biogenesis machinery[103], characterising and comparing the protein compositions of induced EVs could improve our understanding of the biological processes and contributing molecules that underlie EV biogenesis.

6.2. Aims and Objectives

The results reported in Chapter five demonstrate that treating SKOV3 cells with histamine, ionomycin and TRPC3 activator induce the release of EVs with distinct characteristics and fusion dynamics. Treatment with TRPC3 activator also induces metastatic mechanisms in SKOV3 cells: acting to increase their proliferation and migration directly, and indirectly through the transfer of TRPC3 activator-induced EVs (detailed in Chapters 3 and 4, respectively). Within these experiments the number of EVs applied to recipient cells was consistent across treatment conditions, therefore these functional effects of EVs are attributable to changes in their cargo, not quantity.

The aim of this chapter was to characterise the proteomic cargo of histamine, ionomycin and TRPC3-activator-induced EVs and derive mechanistic insights into how these treatments

influence EV biogenesis pathways. This analysis also focused on identifying EV proteins and/or pathways which may mediate the functional effects observed on TRPC3-activator treated cells, and speculate a novel role for TRPC3-mediated EV communication in the progression of ovarian cancer. The specific objectives were to:

1. Characterise the protein content of basal and treatment-induced EVs
2. Assess the proteomic profiles of induced EVs for enriched proteins and gene ontology terms which may indicate biogenesis mechanisms
3. Identify candidate proteins which may mediate TRPC3-activator induced metastatic mechanisms in SKOV3 cells

6.3. RESULTS

6.3.1. BASAL AND INDUCED EVS EXTRACTED AFTER FOUR HOURS CONDITIONING HAVE TYPICAL AND REPLICABLE PROTEOMIC CARGO

Histamine, ionomycin and TRPC3 activator stimulate the immediate release of EVs with distinct characteristics and fusion dynamics (see Chapter 5). To assess if treatment-induced differences were also apparent in the proteomic cargo of EVs, label-free mass spectrometry was employed to analyse the protein content of EVs derived from SKOV3 cells following a 4hr treatment with 100µM histamine, 1.25µM ionomycin or 0.3µM TRPC3-activator, alongside untreated (histamine control) and DMSO (ionomycin and TRPC3 activator control). A 4hr conditioning period was selected to capture how the protein content of EVs is modified in response to these fast-acting mechanisms and proved a sufficient conditioning period to collect EV-protein for analysis (Supplementary Figure 3).

After filtering (detailed in Section 2.9), a total of 1198 proteins were quantified in the proteomic dataset; with 601 proteins identified in EVs derived from untreated cells, 922 for DMSO, 772 for histamine, 737 for ionomycin and 646 for TRPC3 activator (Figure 6.1 A). Of these, 469 proteins were shared across all treatment groups – equating to 39.1% of all identified proteins. A set of unique proteins were also identified for each group; with 18 proteins unique to untreated EVs, 169 to DMSO, 84 to histamine, 116 to ionomycin and 14 to TRPC3 activator (Figure 6.1 A). The Upset plots in Figure 6.1 B-F illustrate the distribution of proteins across the four biological replicates for each treatment group, representing untreated, DMSO, histamine, ionomycin and TRPC3 activator EVs respectively. For each treatment group bar DMSO, 45-49% of identified proteins were conserved across ≥3 biological replicates. As for DMSO EVs, 359 unique proteins (39% of all DMSO proteins) were identified in replicate three. As the expression of this high proportion of proteins was not replicable, replicate three of the DMSO group was excluded from

all further analysis. Although a smaller proportion, a number of proteins were only identifiable in one or two biological replicates for all treatment groups (Figure 6.1 B-F), demonstrating the highly heterogenous nature of EVs. Due to these discrepancies in overlapping protein expression across biological replicates, the dataset was filtered to only include proteins identifiable in at least three replicates of one or more treatment groups for all further analysis. This filtered dataset is represented in Figure 6.1 G: 410 proteins (81%) were shared across all treatment groups and the number of non-overlapping proteins was markedly reduced, indicating that the expression of the majority of unique proteins was not replicable. The 410 shared proteins were uploaded to DAVID[349, 350] for gene ontology (GO) analysis, and the most enriched cellular component term returned was 'extracellular exosome' (Figure 6.1 H). In addition, >80% of the top 100 EV marker proteins (list obtained from ExoCarta, accessed November 2021) were identified in EVs derived from all treatment groups (Supplementary Figure 4). Together, this data verifies that sample preparations for proteomic analysis represent an EV population, describes the protein content of EVs derived from all treatment groups and replicates, and justifies the data filtering. Therefore, the conclusions drawn in downstream analyses are deemed reliable.

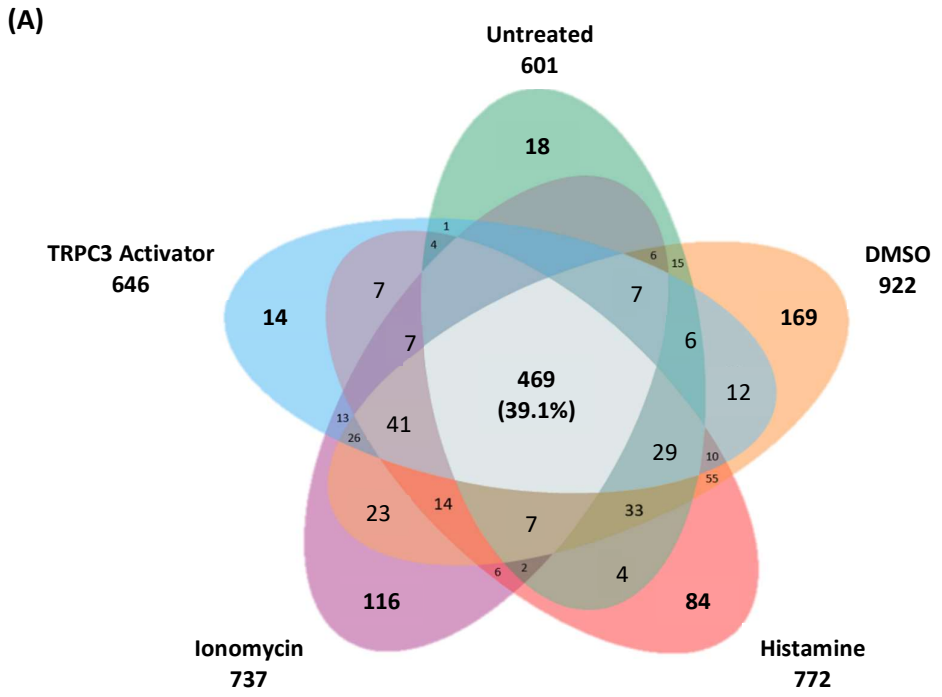

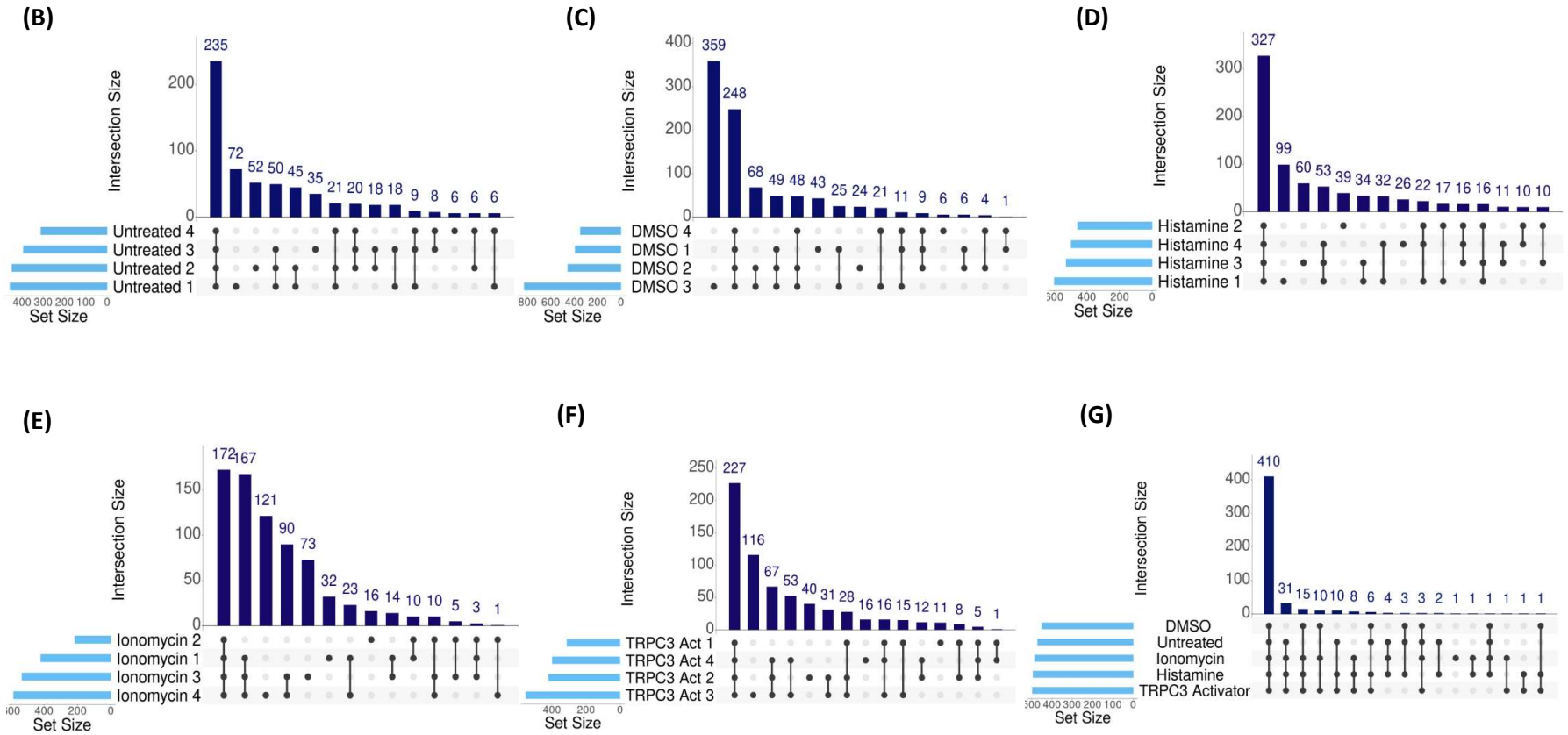
(B)
Intersection Size
235
72
52
50
45
35
21
20
18
18
9
8
6
6
6
Untreated 4
Untreated 3
Untreated 2
Untreated 1
Set Size
(C)
Intersection Size
359
248
68
49
48
43
25
24
21
11
9
6
6
4
1
DMSO 4
DMSO 1
DMSO 2
DMSO 3
Set Size
(D)
Intersection Size
327
99
60
53
39
34
32
26
22
17
16
16
11
10
10
Histamine 2
Histamine 4
Histamine 3
Histamine 1
Set Size
(E)
Intersection Size
172
167
121
90
73
32
23
16
14
10
10
5
3
1
Ionomycin 2
Ionomycin 1
Ionomycin 3
Ionomycin 4
Set Size
(F)
Intersection Size
227
116
67
53
40
31
28
16
16
15
12
11
8
5
1
TRPC3 Act 1
TRPC3 Act 4
TRPC3 Act 2
TRPC3 Act 3
Set Size
(G)
Intersection Size
410
31
15
10
10
8
6
4
3
3
2
1
1
1
1
1
DMSO
Untreated
Ionomycin
Histamine
TRPC3 Activator
Set Size

(H)

Top 10 cellular component GO terms for all shared proteins identified in the final dataset			
Cellular Component	**Fold enrichment**	**P-value**	**Benjamini**
Extracellular exosome	4.99	1.21E-242	6.60E-240
Focal adhesion	10.08	1.49E-88	4.06E-86
Cytosol	2.99	5.22E-86	9.49E-84
Membrane	3.54	2.73E-77	3.72E-75
Extracellular matrix	10.59	6.51E-72	7.10E-70
Cell-cell adherens junction	7.90	1.61E-47	1.46E-45
Melanosome	13.44	1.68E-35	1.31E-33
Proteasome complex	17.77	8.97E-33	6.11E-31
Ribosome	9.34	3.12E-32	1.89E-30
Myelin sheath	9.78	7.71E-32	4.20E-30

Figure 6.1 Characterising the protein content of basal and treatment-induced EVs

(A) *Venn diagram showing the total number of proteins identified in at least one replicate for untreated, DMSO, histamine, ionomycin or TRPC3 activator-induced EVs.* ***(B)-(F)*** *UpSet plots demonstrating the distribution of all identified proteins across biological replicates for each treatment group: (B) untreated, (C) DMSO, (D) histamine, (E) ionomycin and (F) TRPC3 activator.* ***(G)*** *UpSet plot of all proteins that were identified in ≥3 replicates of at least one treatment group shown in (A)-(F).* ***(H)*** *Gene ontology analysis of the 410 shared proteins that were identified in the final dataset represented in (G), against the full human genome as background. Ten most enriched cellular components shown, sorted for p-value after Benjamini-Hochberg correction. Fold enrichment is the number of genes annotated with that term divided by the number of genes expected by the software to be annotated with that term.*

6.3.2. TREATMENT-INDUCED EVS HAVE DISTINCT PROTEIN EXPRESSION PROFILES

Initial characterisation of the protein content of basal and induced EVs found replicable protein expression across biological replicates for each treatment group (Figure 6.1 B-F). To analyse the relatedness of biological replicates and discern if EV proteins were differentially expressed according to their treatment group, principal component analysis (PCA) and hierarchical clustering were performed. For this analysis, the proteomic dataset was filtered for only differentially expressed proteins ($p<0.05$). Across the proteomic dataset, 96 proteins were differentially expressed regardless of treatment group. Based on the expression of these 96 proteins, PCA indicated that EVs were distinguishable by their treatment group for most samples (Figure 6.2 A). The biological replicates for untreated and histamine-induced EVs clustered well within their treatment group, as did three of four replicates for ionomycin–induced EVs. Of note, the fourth replicate had a large number of missing values but remained within the normal distribution with imputed values, and was therefore not considered an outlier in this dataset. Discrimination between clusters was less obvious between DMSO and TRPC3 activator-induced EVs, suggesting much of the altered protein expression in TRPC3 activator-induced EVs is attributable to the effect of DMSO. Notably, the presence of DMSO in the conditioning media

was the strongest distinguishing component between all samples. As detailed in Section 2.2, ionomycin and TRPC3 activator compounds were reconstituted in DMSO prior to supplementation to serum-free media, whereas histamine was directly dissolved in serum-free media. This indicates that DMSO significantly alters the proteomic cargo of EVs. In line with the PCA, hierarchical clustering grouped biological replicates for untreated, histamine-induced and ionomycin-induced EVs based on differential protein expression, whereas DMSO and TRPC3-activator replicates were not distinguishable from one another (Figure 6.2 B). Hierarchical clustering also groups proteins with similar expression profiles, visualising protein expression patterns that contribute to the variance between samples in the PCA. See Supplementary Figure 5 for hierarchical clustering output with all protein names shown. Overall, these results demonstrate treatment-specific differences in EV protein expression.

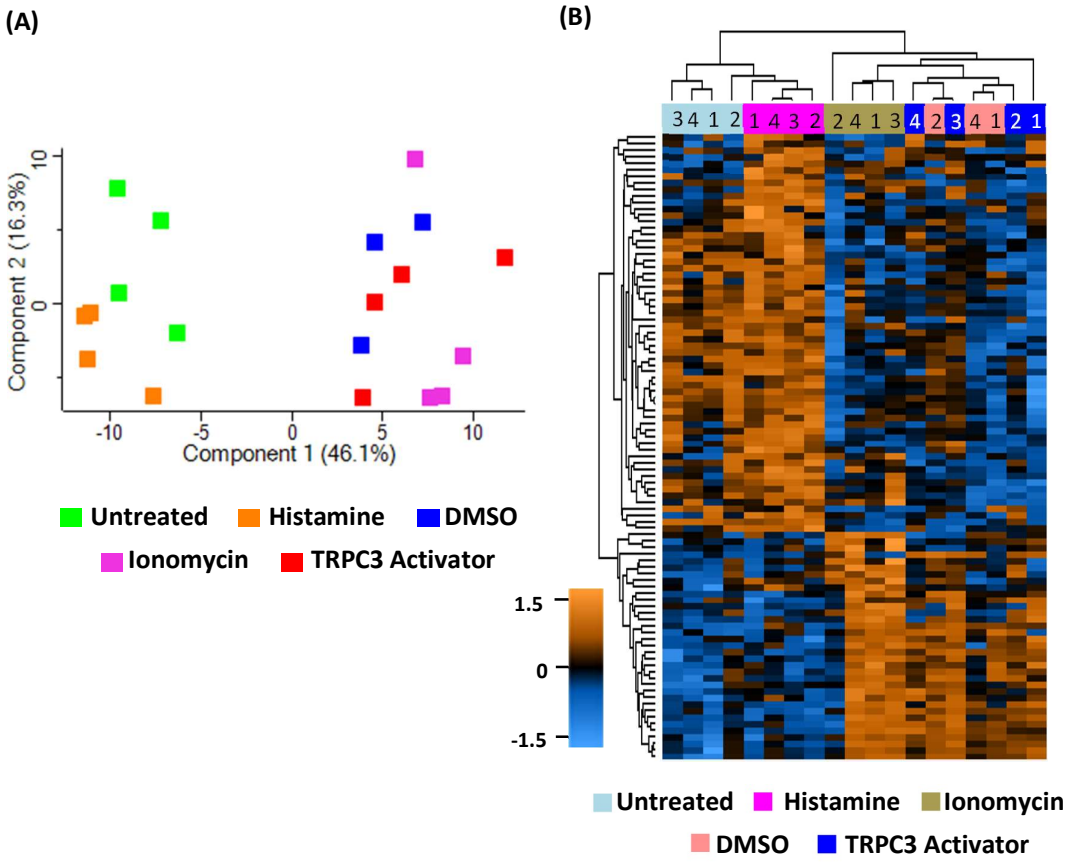

Figure 6.2 EV biological replicates cluster by treatment group in principal component analysis and hierarchical clustering

(A) *Principal component analysis of all differentially expressed proteins identified in untreated, histamine, DMSO, ionomycin and TRPC3 activator-induced EVs.* ***(B)*** *Hierarchical clustering of biological replicates for differentially expressed proteins in all treatment groups. Numbers represent replicate. Euclidean distance measure. (A) and (B) both generated with Perseus software (v1.6.14.0).*

6.3.3. HISTAMINE ALTERS THE PROTEOMIC CARGO OF EVS

Overall analysis of differential protein expression revealed treatment-induced differences in the proteomic cargo of EVs. To clarify what proteins were specifically deregulated in histamine-induced EVs, the mean fold change of each protein following histamine treatment (LFQ intensity histamine – LFQ intensity untreated), and the p-value of this change was calculated. These values were then plotted as Log_2 (fold change) against $-Log_{10}$ (p-value) in a volcano plot (Figure 6.3 A). The volcano plot in Figure 6.3 A represents all identified proteins: proteins in orange had a 2-fold change either up (right) or down (left), proteins in red had a p-value of less than 0.05 and proteins in green had both. Of all identified proteins, 112 were upregulated by 2-fold or more in histamine-induced EVs, and 21 of these had a p-value of less than 0.05. A total of 23 proteins were downregulated by 2-fold or more, but notably none of the downregulated proteins had a significant p-value. This would suggest that histamine acts to induce pathways that upregulate protein-loading into EVs, or induce a sub-population of EVs with different proteomic cargo. All proteins with a 2-fold change and a p-value of less than 0.05 are listed in Figure 6.3 B, alongside their corresponding fold change and p-value. All deregulated proteins listed in Supplementary Figure 6. Of note, the most upregulated protein in histamine-induced EVs was the tetraspanin and EV marker CD81 (Figure 6.3 A). Although the p-value was determined non-significant, its high expression in histamine-induced EVs suggests CD81 is directly involved in histamine-stimulated EV biogenesis, and accounts for the increase in CD81 fusion events observed by TIRF microscopy (Chapter 5, Figure 5.4). In summary, histamine induces the release of CD81-rich EVs with significantly upregulated protein cargo, possibly representing a sub-population of EVs.

(A)

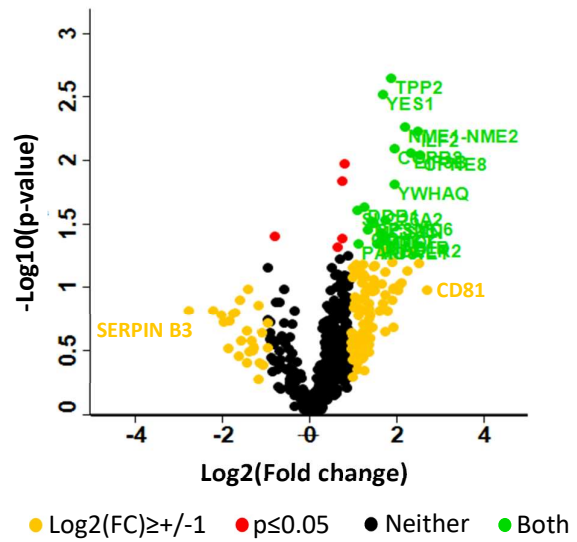

(B)

Significantly upregulated proteins in histamine-induced EVs		
Gene names	**Fold Change**	**p-value**
CPNE8	5.74	9.10E-03
ILF2	5.52	5.84E-03
EIF3B	4.94	8.74E-03
NME1-NME2;NME2;NME2P1;NME1	4.51	5.47E-03
YWHAQ	3.88	1.53E-02
COPB2	3.83	8.05E-03
TPP2	3.61	2.26E-03
PSMC6	3.30	2.95E-02
CAD	3.27	4.19E-02
YES1	3.20	3.00E-03
MYOF	3.16	3.75E-02
PTK7	3.15	3.73E-02
KDELR2	3.14	4.37E-02
MAP1B	3.13	4.08E-02
HUWE1	2.94	4.55E-02
NCSTN	2.78	3.12E-02
RPS25	2.65	2.97E-02
GGH	2.52	3.49E-02
DDB1	2.38	2.31E-02
PAICS	2.19	4.57E-02
SLC26A2	2.12	2.48E-02

Figure 6.3 Histamine induced-EVs exhibit significantly upregulated protein cargo

The mean fold change of each protein following histamine treatment was calculated and p-values were generated using a two tailed t-test. ***(A)*** *Volcano plot displaying the Log_2 of fold change of each protein against -Log_{10} of the p-value resulting from the t-test. Proteins with a fold change ≤ 0.5 or ≥ 2 are orange, proteins with a p-value of ≤ 0.05 are red and proteins that have both are green and labelled. The single most up and down-regulated proteins are also labelled.* ***(B)*** *Gene names for the 21 proteins identified with a 2-fold change and a p-value of ≤ 0.05, with corresponding fold change and p-value. Proteins sorted by fold change value.*

6.3.4. GENE ONTOLOGY ANALYSIS IDENTIFIED POTENTIAL MEDIATORS OF HISTAMINE-INDUCED EV BIOGENESIS

Having identified a number of deregulated proteins in histamine-induced EVs, GO analysis was carried out through DAVID to understand if the combination of these proteins represents an enrichment of biological processes, cellular components or molecular functions in histamine-induced EVs that could provide clues on their biogenesis. The gene names for all proteins with a 2-fold increase and a p-value of less than 0.05 were uploaded to the DAVID analysis tool. Overall, the submitted gene list returned 27 terms for biological process, 8 for cellular component and 10 for molecular function. The top ten most significant GO terms returned for each category are represented in Table 6.1, alongside their corresponding fold enrichment and adjusted p-value (Benjamini corrected). Terms with an adjusted p-value less than 0.05 are highlighted in red. Of note, the most enriched cellular component term returned was 'extracellular exosome' (Table 6.1), confirming the origin of the samples used for this analysis. Intriguingly, seven of the ten most significant biological processes over-represented in histamine-induced EVs were related to the synthesis or metabolism of nucleoside trisphosphates, specifically UTP, CTP and GTP. Terms of interest related to the latter include 'GTP biosynthetic process', 'purine nucleotide metabolic process', 'nucleoside triphosphate biosynthetic process' and 'nucleoside diphosphate phosphorylation'. These terms are of particular interest as GTP and nucleoside-diphosphate kinases (NDPKs) which mediate these processes are essential for signal transduction by G-protein coupled receptors (GPCRs)[473], implicated in the release of histamine-induced EVs through activation of the histamine receptor H1HR (a GPCR)[82]. In addition, the most enriched molecular function term returned was 'nucleoside diphosphate kinase activity' - further supporting a role for NDPKs in histamine-induced EV biogenesis. Other molecular function terms of interest include 'ATP binding' and 'protein histidine kinase activity': NDPKs can act as protein histidine kinases that directly activate G-proteins through a GPCR-independent pathway[473], and ATP binding is essential for ESCRT-III membrane budding and scission in EV biogenesis[474]. This exploratory analysis has generated valuable insights into the biological processes and contributing molecules that underlie histamine-induced EV biogenesis which should be explored in future work.

Table 6.1 Gene ontology terms associated with significantly upregulated protein expression in histamine-induced EVs

A total of 21 proteins identified with a 2-fold increase following histamine treatment and a p-value of less than 0.05 were uploaded to the DAVID analysis tool, and ran against the full human genome as background. The top ten most significant GO terms returned for biological process, cellular component, and molecular function are shown, sorted for p-value after Benjamini-Hochberg correction. Terms with an adjusted p-value less than 0.05 are highlighted in red. Fold enrichment is the number of genes annotated with that term divided by the number of genes expected by the software to be annotated with that term.

GO terms for significantly upregulated proteins in histamine-induced EVs		
Biological process	**Fold Enrichment**	**Adjusted p-value**
UTP biosynthetic process	304.20	2.30E-07
Pyrimidine nucleotide metabolic process	324.48	1.65E-05
Purine nucleotide metabolic process	292.03	1.65E-05
CTP biosynthetic process	243.36	2.26E-05
GTP biosynthetic process	224.64	2.35E-05
Nucleoside triphosphate biosynthetic process	208.60	2.49E-05
Negative regulation of myeloid leukocyte differentiation	547.57	2.97E-04
Positive regulation of neuron projection development	32.81	5.46E-03
Nucleoside diphosphate phosphorylation	121.68	5.83E-03
Cellular response to fatty acid	95.23	8.64E-03
Cellular component	**Fold Enrichment**	**Adjusted p-value**
Extracellular exosome	5.13	2.72E-09
Cytosol	3.44	2.50E-04
Focal adhesion	9.71	3.39E-02
Membrane	3.11	7.77E-02
Intermediate filament	20.16	1.35E-01
Cytoplasm	1.89	1.87E-01
Cell periphery	38.94	4.85E-01
Nucleus	1.68	4.85E-01
Molecular function	**Fold Enrichment**	**Adjusted p-value**
Nucleoside diphosphate kinase activity	146.79	1.75E-04
ATP binding	4.91	2.27E-03
Protein histidine kinase activity	733.96	7.03E-02
Intermediate filament binding	146.79	2.62E-01
Fatty acid binding	77.26	3.97E-01
Protein binding	1.42	5.41E-01
Endopeptidase activity	27.18	6.44E-01
Enzyme binding	6.61	6.44E-01
Identical protein binding	3.92	6.44E-01
Drug binding	19.31	7.66E-01

6.3.5. CONSTITUTIVE AND HISTAMINE-INDUCED EV RELEASE REPRESENT SEPARATE POPULATIONS

GO analysis was also conducted on downregulated proteins identified in histamine-induced EVs to explore what terms were under-represented. As no downregulated proteins had a p-value of less than 0.05, all proteins identified as downregulated by 2-fold or more were included in the GO term analysis. Overall, the submitted gene list returned 42 terms for biological process, 20 for cellular component and 13 for molecular function. The top ten most significant GO terms returned for each category are represented in Table 6.2. As expected, the most enriched cellular component term returned for downregulated proteins was 'extracellular exosome' (Table 6.2). Compared to the cellular component terms returned for upregulated protein expression in histamine-induced EVs, there is an enrichment of terms associated with nucleosomes in downregulated proteins, including 'nucleosome' 'nuclear nucleosome', 'nucleus', and 'nuclear chromatin'. Nucleosomes and other histone-rich non-vesicular nanoparticles are actively secreted by cells and co-isolate with EVs, owing to their overlapping size range[24, 475]. Another unique cellular component term returned was 'cornified envelope'. The cornified envelope (CE) is a heavily cross-linked matrix of proteins and extracellular lipids that lies beneath the PM. Notably, biological process terms associated with the formation of the CE are also under-represented in histamine-induced EVs, including 'keratinization', 'keratinocyte differentiation' and 'peptide cross-linking' (Table 6.2). These PM-associated molecular activities and structures likely represent the release of an MV population, whereby they are 'pinched' off into MVs upon budding from the PM. None of the biological process or molecular function terms associated with upregulated protein expression in histamine-induced EVs overlap with the identified terms for downregulated proteins (Table 6.1 and 6.2), supporting the notion of two separate populations. Collectively, these results suggest that non-vesicular nanoparticles and MVs represent a large proportion of constitutive EV release that is exceeded by exosomes following histamine stimulation.

Table 6.2 Gene ontology terms associated with downregulated protein expression in histamine-induced EVs

A total of 23 proteins identified with a 2-fold decrease following histamine treatment were uploaded to the DAVID analysis tool, and ran against the full human genome as background. The top ten most significant GO terms returned for biological process, cellular component, and molecular function are shown, sorted for p-value after Benjamini-Hochberg correction. Terms with an adjusted p-value less than 0.05 are highlighted in red. Fold enrichment is the number of genes annotated with that term divided by the number of genes expected by the software to be annotated with that term.

GO terms for downregulated proteins in histamine-induced EVs		
Biological process	**Fold Enrichment**	**Adjusted p-value**
Nucleosome assembly	36.10	7.11E-11
Chromatin silencing	69.42	2.06E-09
Antibacterial humoral response	53.25	6.93E-06
Innate immune response in mucosa	78.10	2.77E-05
Keratinocyte differentiation	25.69	2.05E-03
Platelet aggregation	38.10	6.51E-03
Keratinization	32.54	8.84E-03
Peptide cross-linking	31.24	8.84E-03
Innate immune response	6.36	1.95E-02
Defense response to Gram-positive bacterium	18.38	3.35E-02
Cellular component	**Fold Enrichment**	**Adjusted p-value**
Extracellular exosome	5.73	2.01E-23
Nucleosome	72.14	4.75E-23
Nuclear nucleosome	105.95	7.43E-17
Extracellular space	5.03	2.30E-06
Nucleus	2.35	2.30E-06
Nuclear chromatin	15.37	5.98E-05
Blood microparticle	16.73	2.58E-04
Cytoplasm	1.87	9.16E-03
Extracellular region	2.90	2.40E-02
Cornified envelope	27.64	3.62E-02
Molecular function	**Fold Enrichment**	**Adjusted p-value**
Protein heterodimerization activity	15.20	2.00E-14
DNA binding	4.69	1.25E-07
RAGE receptor binding	107.07	5.67E-03
Calcium ion binding	4.93	5.67E-03
Immunoglobulin receptor binding	45.30	2.57E-02
Cadherin binding involved in cell-cell adhesion	6.77	6.48E-02
Toll-like receptor 4 binding	196.29	9.63E-02
Arachidonic acid binding	157.03	1.05E-01
Myosin heavy chain binding	98.15	1.49E-01
Protein-glutamine gamma-glutamyltransferase activity	87.24	1.51E-01

6.3.6. IONOMYCIN ALTERS THE PROTEOMIC CARGO OF EVS

Ionomycin is an evidenced inducer of EV release in a number of cell types[144, 145]; including SKOV3 OC cells as identified in this thesis (Chapter 5, Figure 5.4). To understand what biogenesis mechanisms are stimulated by ionomycin and how this influences the proteomic cargo of EVs, the mean fold change of each protein following ionomycin treatment (LFQ intensity ionomycin – LFQ intensity DMSO), and the p-value of this change was calculated. These values were then plotted as Log_2 (fold change) against -Log_{10} (p-value) in a volcano plot (Figure 6.4 A). The volcano plot in Figure 6.4 A represents all identified proteins: proteins in orange had a 2-fold change either up (right) or down (left), proteins in red had a p-value of less than 0.05 and proteins in green had both. Of all identified proteins, 66 were upregulated by 2-fold or more in ionomycin-induced EVs, and 10 of these had a p-value of less than 0.05. A total of 48 proteins were downregulated by 2-fold or more, and 7 of these had a p-value of less than 0.05. All proteins with a 2-fold change and a p-value of less than 0.05 are listed in Figure 6.4 B, alongside their corresponding fold change and p-value. All deregulated proteins listed in Supplementary Figure 7. Of note, the most upregulated protein in ionomycin-induced EVs was PDCD6 - also known as apoptosis-linked gene 2 (ALG-2) - the partner protein of the ESCRT accessory protein and EV marker Alix (Figure 6.4 A,B). A Ca^{2+}-dependent ALG-2 interaction activates the MVB sorting function of ALIX[150], which then regulates the biogenesis of EVs through interactions with syndecan-4 (SDC4) and syntenin-1 (SDCBP)[73], which are also both significantly upregulated in ionomycin-induced EVs (Figure 6.4 A,B). These results suggest that ionomycin induces the release of EVs with divergent proteomic cargo through the Ca^{2+}-dependent syndecan-syntenin-ALIX axis.

(A)

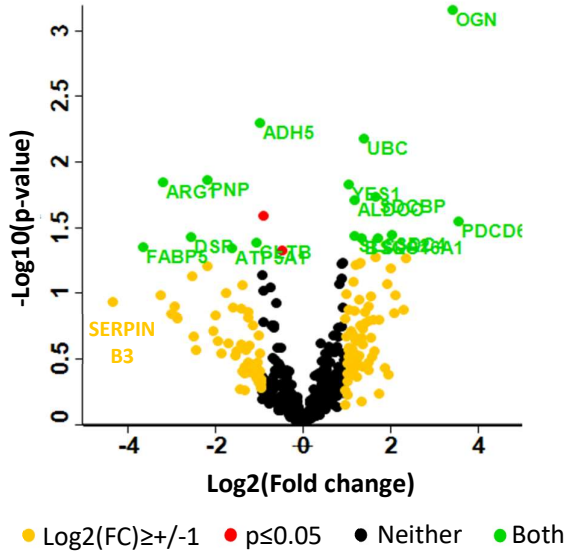

(B)

Significantly upregulated proteins in ionomycin-induced EVs		
Gene names	**Fold Change**	**p-value**
PDCD6	11.52	2.82E-02
OGN	10.64	6.95E-04
SDC4	4.07	3.58E-02
SLC16A1	3.26	3.78E-02
SDCBP	3.12	1.83E-02
UBC;UBB;RPS27A; UBA52	2.58	6.63E-03
BSG	2.52	3.79E-02
ALDOC	2.27	1.94E-02
SLC3A2	2.23	3.64E-02
YES1	2.07	1.47E-02
Significantly downregulated proteins in ionomycin-induced EVs		
Gene names	**Fold Change**	**p-value**
FABP5	0.08	4.40E-02
ARG1	0.11	1.41E-02
DSP	0.17	3.69E-02
PNP	0.22	1.38E-02
ATP5A1	0.33	4.52E-02
CLTB	0.48	4.07E-02
ADH5	0.50	5.01E-03

Figure 6.4 Ionomycin-induced EVs exhibit divergent protein cargo

The mean fold change of each protein following ionomycin treatment was calculated and p-values were generated using a two tailed t-test. ***(A)*** *Volcano plot displaying the Log_2 of fold change of each protein against -Log_{10} of the p-value resulting from the t-test. Proteins with a fold change ≤ 0.5 or ≥ 2 are orange, proteins with a p-value of ≤ 0.05 are red and proteins that have both are green and labelled. The single most up and down-regulated proteins are also labelled.* ***(B)*** *Gene names for the 17 proteins identified with a fold change ≤ 0.5 or ≥ 2 and a p-value of ≤ 0.05, with corresponding fold change and p-value. Proteins sorted by fold change value.*

6.3.7. IONOMYCIN-INDUCED EVS MAY BE GENERATED THROUGH THE ENDOCYTIC PATHWAY

To derive further mechanistic insights into ionomycin-induced EV biogenesis, GO analysis was performed on upregulated protein cargo to identify biological process, cellular component and molecular function terms that were enriched in ionomycin-induced EVs. All proteins with a 2-fold increase and a p-value of less than 0.05 were uploaded to the DAVID analysis tool. Overall, the submitted gene list returned 80 terms for biological process, 16 for cellular component and 4 for molecular function. As none of the molecular function terms returned were significant following Benjamini correction, the uploaded gene list for molecular function terms was extended to include all proteins with a 2-fold increase. The top ten most significant GO terms returned for each category are represented in Table 6.3. As expected, the most enriched cellular component term returned was 'extracellular exosome' (Table 6.3), followed by 'endocytic vesicle membrane', 'plasma membrane' and 'endosome membrane'. Both terms relating to the endocytic pathway were highly enriched (Table 6.3), and are not represented in the cellular component terms for other EV samples. This would suggest that ionomycin-induced EVs are specifically generated through the endocytic pathway, and are released upon fusion of MVBs with the PM as exosomes. Although not listed in Table 6.3, 'endosomal transport' was identified as a significantly enriched biological process term (p=6.75E-05) – further supporting this notion. Notably, 'positive regulation of extracellular exosome assembly' had the highest fold enrichment of all returned biological process terms (645.85), with a significant p-value of 8.10E-03. Co-occurring significant biological process terms include 'positive regulation of exosome secretion' (p=2.86E-02) and 'positive regulation of epidermal growth factor receptor signalling pathway' (Table 6.3). These terms encompass an enrichment of endosomal and ESCRT molecular activities, and likewise indicate that ionomycin-induced EVs are predominantly formed through these mechanisms. The identified molecular function term 'calcium-dependent protein binding' (Table 6.3) suggests that Ca^{2+} mediates these mechanisms of EV biogenesis, of which there is evidence for[144, 150]. As ionomycin acts to increase intracellular Ca^{2+}, these results cumulatively propose that ionomycin activates Ca^{2+}-dependent interactions within the endocytic pathway and ESCRT machinery that ultimately induces MVB-PM fusion for exosome release.

Table 6.3 Gene ontology terms associated with upregulated protein expression in ionomycin-induced EVs

For biological process and cellular component terms, 10 proteins identified with a 2-fold increase following ionomycin treatment and a p-value of less than 0.05 were uploaded to the DAVID analysis tool. The uploaded gene list for molecular function terms was extended to include all proteins with a 2-fold increase. All gene lists were ran against the full human genome as background. The top ten most significant GO terms returned for biological process, cellular component, and molecular function are shown, sorted for p-value after Benjamini-Hochberg correction. Terms with an adjusted p-value less than 0.05 are highlighted in red. Fold enrichment is the number of genes annotated with that term divided by the number of genes expected by the software to be annotated with that term.

GO terms for upregulated proteins in ionomycin-induced EVs		
Biological process	**Fold enrichment**	**Adjusted p-value**
Virion assembly	430.56	3.77E-06
Regulation of necrotic cell death	430.56	3.77E-06
MyD88-independent toll-like receptor signalling pathway	397.44	3.77E-06
Regulation of type I interferon production	397.44	3.77E-06
Error-prone translesion synthesis	271.94	8.50E-06
Error-free translesion synthesis	271.94	8.50E-06
Stress-activated MAPK cascade	246.04	9.67E-06
Nucleotide-excision repair, DNA duplex unwinding	234.85	9.67E-06
Nucleotide-excision repair, DNA damage recognition	224.64	9.67E-06
Positive regulation of epidermal growth factor receptor signalling pathway	215.28	9.67E-06
Cellular component	**Fold enrichment**	**Adjusted p-value**
Extracellular exosome	6.48	9.60E-09
Endocytic vesicle membrane	84.96	2.63E-04
Plasma membrane	3.40	2.86E-03
Endosome membrane	30.31	2.86E-03
Extracellular space	6.24	1.21E-02
Focal adhesion	14.34	1.49E-02
Melanosome	41.64	1.49E-02
Membrane raft	20.42	5.26E-02
Cytosol	2.96	7.33E-02
Cell-cell adherens junction	13.02	9.93E-02
Molecular function	**Fold enrichment**	**Adjusted p-value**
Protein heterodimerization activity	5.90	2.96E-04
Poly(A) RNA binding	3.55	3.23E-04
Calcium-dependent protein binding	21.83	4.62E-04
Protein binding	1.39	9.49E-03
Neutral amino acid transmembrane transporter activity	57.55	4.30E-02
Protein homodimerization activity	3.18	6.48E-02
Structural constituent of ribosome	5.70	9.80E-02
DNA binding	2.14	9.80E-02
Transition metal ion binding	105.51	3.84E-01
Collagen binding	10.55	5.98E-01

6.3.8. CONSTITUTIVELY RELEASED EVS REPRESENT A MIXED POPULATION

As for the analysis of histamine-induced EVs, GO terms were assessed for downregulated proteins identified in ionomycin-induced EVs to explore what terms were under-represented. Only 7 of the proteins downregulated by 2-fold in ionomycin-induced EVs had a p-value of less than 0.05, which when submitted to the DAVID analysis tool returned no significant GO terms except for the cellular component term 'extracellular exosome' (p=0.016). The GO term analysis was therefore repeated on all proteins downregulated by 2-fold or more. Overall, the submitted gene list returned 55 terms for biological process, 27 for cellular component and 25 for molecular function. The top ten most significant GO terms returned for each category are represented in Table 6.4. Of note, GO analysis returned no significant terms for molecular functions. Following 'extracellular exosome', general cellular component terms associated with the extracellular space and cytosol were enriched in downregulated proteins, including 'extracellular matrix', 'extracellular space', 'cytosol' and 'cytoskeleton' (Table 6.4). This is in contrast to the specific endocytic terms returned for upregulated proteins in ionomycin-induced EVs (Table 6.3). Cellular component terms 'desmosome' and 'cornified envelope' are also under-represented in ionomycin-induced EVs. Desmosomes are intercellular junctions exposed on the lateral side of the PM, and cross-link with the CE. Notably, biological process terms associated with the formation of desmosomes and the CE are also under-represented in ionomycin-induced EVs, such as 'keratinocyte differentiation', 'keratinization' and 'peptide cross-linking' (Table 6.4). Likewise to downregulated protein expression in histamine-induced EVs, these PM-associated molecular activities and structures likely represent an MV population. Collectively, these results indicate that SKOV3 cells constitutively release a mixed population of EVs that is dominated by exosomes following ionomycin stimulation.

Table 6.4 Gene ontology terms associated with downregulated protein expression in ionomycin-induced EVs

A total of 48 proteins identified with a 2-fold decrease following ionomycin treatment were uploaded to the DAVID analysis tool, and ran against the full human genome as background. The top ten most significant GO terms returned for biological process, cellular component, and molecular function are shown, sorted for p-value after Benjamini-Hochberg correction. Terms with an adjusted p-value less than 0.05 are highlighted in red. Fold enrichment is the number of genes annotated with that term divided by the number of genes expected by the software to be annotated with that term.

GO terms for downregulated proteins in ionomycin-induced EVs		
Biological process	**Fold enrichment**	**Adjusted p-value**
Keratinocyte differentiation	24.55	1.47E-03
Retina homeostasis	38.87	1.47E-03
Single organismal cell-cell adhesion	18.47	2.15E-03
Epidermis development	18.29	1.47E-02
Response to reactive oxygen species	31.89	1.99E-02
Keratinization	25.91	2.97E-02
Peptide cross-linking	24.88	2.97E-02
Defense response to bacterium	10.72	5.58E-02
Cell redox homeostasis	16.15	8.12E-02
SRP-dependent cotranslational protein targeting to membrane	13.23	1.18E-01
Cellular component	**Fold enrichment**	**Adjusted p-value**
Extracellular exosome	5.52	6.41E-27
Desmosome	84.37	4.33E-07
Extracellular matrix	12.54	4.78E-07
Extracellular space	4.51	4.12E-06
Cytosol	2.75	7.42E-06
Cytoskeleton	7.28	1.95E-03
Focal adhesion	6.90	2.31E-03
Cornified envelope	29.35	5.00E-03
Cytoplasm	1.81	6.99E-03
Nucleus	1.75	1.15E-02
Molecular function	**Fold enrichment**	**Adjusted p-value**
RAGE receptor binding	85.26	5.98E-02
Structural molecule activity	7.59	5.98E-02
Calcium ion binding	3.92	5.98E-02
Antioxidant activity	46.89	5.98E-02
Poly(A) RNA binding	3.05	6.47E-02
Cysteine-type endopeptidase inhibitor activity	27.58	9.93E-02
Structural constituent of ribosome	7.04	9.93E-02
Protein kinase C inhibitor activity	208.41	1.58E-01
Toll-like receptor 4 binding	156.31	1.76E-01
Protein binding	1.32	1.76E-01

6.3.9. TRPC3 ACTIVATION ALTERS THE PROTEOMIC CARGO OF EVS

The work presented in this thesis has identified a novel role for TRPC3 in EV biogenesis and mediating metastatic mechanisms in SKOV3 cells, which are partially driven through the transfer of TRPC3 activator-induced EVs (detailed in Chapters 3-5). To gain insight into how TRPC3 is acting on EV biogenesis and identify candidate proteins which may mediate the effect of TRPC3 activation on the metastatic capacity of SKOV3 cells, the mean fold change of each protein following TRPC3 activator treatment (LFQ intensity TRPC3 activator – LFQ intensity DMSO), and the p-value of this change was calculated. These values were then plotted as Log_2 (fold change) against $-Log_{10}$ (p-value) in a volcano plot (Figure 6.5 A). The volcano plot in Figure 6.5 A represents all identified proteins: proteins in orange had a 2-fold change either up (right) or down (left), proteins in red had a p-value of less than 0.05 and proteins in green had both. Of all identified proteins, 39 were upregulated by 2-fold or more in TRPC3 activator-induced EVs, and 7 of these had a p-value of less than 0.05. A total of 26 proteins were downregulated by 2-fold or more, and only 1 of these had a p-value of less than 0.05. All proteins with a 2-fold change and a p-value of less than 0.05 are listed in Figure 6.5 B, alongside their corresponding fold change and p-value. All deregulated proteins listed in Supplementary Figure 8. A number of significantly upregulated proteins are calcium-binding proteins (EHD4, TPM4, NUCB1), whose upregulation is likely linked to increased intracellular Ca^{2+} following TRPC3 activation. These Ca^{2+}-binding proteins are abnormally expressed in a number of cancer types[476]. Upregulated proteins ACLY, HSP4A, YES1 and S100A4 are likewise implicated in mediating metastatic mechanisms. The most significantly upregulated protein EHD4 is an endosomal protein which regulates early endosomal transport and fission of endosome-derived vesicles[477, 478], and has recently been recognised as a specific-exosomal marker[104, 479]. Taken together, this data suggests that TRPC3 activation upregulates the expression of Ca^{2+}-binding and metastasis-related proteins, which are packaged into EVs through stimulation of the endosomal pathway.

(A)

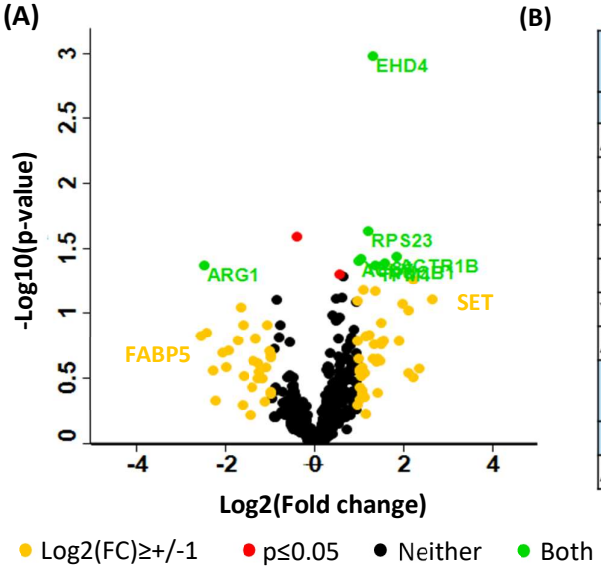

(B)

Significantly upregulated proteins in TRPC3 activator-induced EVs		
Gene names	**Fold Change**	**p-value**
ACTR1B	3.60	3.64E-02
NUCB1	2.99	4.12E-02
TPM4	2.58	4.30E-02
EHD4	2.48	1.05E-03
RPS23	2.31	2.30E-02
YES1	2.06	3.80E-02
ACLY	1.98	3.96E-02
Significantly downregulated proteins in TRPC3 activator-induced EVs		
Gene names	**Fold Change**	**p-value**
ARG1	0.18	4.29E-02

Figure 6.5 TRPC3 activator-induced EVs exhibit divergent protein cargo

The mean fold change of each protein following treatment with TRPC3 activator was calculated and p-values were generated using a two tailed t-test. ***(A)*** *Volcano plot displaying the Log_2 of fold change of each protein against $-Log_{10}$ of the p-value resulting from the t-test. Proteins with a fold change ≤ 0.5 or ≥ 2 are orange, proteins with a p-value of ≤ 0.05 are red and proteins that have both are green and labelled. The single most up and down-regulated proteins are also labelled.* ***(B)*** *Gene names for the 8 proteins identified with a fold change ≤ 0.5 or ≥ 2 and a p-value of ≤ 0.05, with corresponding fold change and p-value. Proteins sorted by fold change value.*

6.3.10. GENE ONTOLOGY ANALYSIS IDENTIFIES AN ENRICHMENT OF TERMS ASSOCIATED WITH METASTASIS IN TRPC3 ACTIVATOR-INDUCED EVS

To explore what terms were enriched in TRPC3 activator-induced EVs that could mediate the effect of TRPC3 activation on metastatic mechanisms and EV biogenesis, GO analysis was performed on all proteins identified in TRPC3 activator-induced EVs with a 2-fold increase and a p-value of less than 0.05. Due to the small number of submitted proteins (7), no significant GO terms were returned except for the cellular component terms 'membrane' (p=5.79E-03) and 'extracellular exosome' (p=9.56E-03). The GO term analysis was therefore repeated on all proteins upregulated by 2-fold or more. Overall, the submitted gene list returned 60 terms for biological process, 35 for cellular component and 20 for molecular function. The top ten most significant GO terms returned for each category are represented in Table 6.5. Following 'extracellular exosome' as the most enriched cellular component term, a number of terms associated with cell motility, migration and actin remodelling were enriched in upregulated proteins, including 'lamellipodium' and 'actin filament' (Table 6.5), as well as significant terms outside of the top ten: 'filopodium' (p=0.014), 'actin cytoskeleton' (p=0.042) and 'actomyosin, actin portion' (p=0.049). Notably, 'mesenchyme migration' had the highest fold enrichment of all returned biological process terms, with co-occurring but non-significant terms 'movement of cell or subcellular component' (p=0.067) and 'positive regulation of epithelial cell proliferation' (p=0.21). All of these terms represent molecular activities and structures implicated in metastatic processes. In addition, seven of the ten most significant biological process terms are also significantly enriched in upregulated protein expression in histamine-induced EVs (Table 6.1), suggesting TRPC3 activation and histamine act to induce EV biogenesis through similar mechanisms. Collectively, these terms suggest that TRPC3 activator-induced EVs capture upregulated metastatic pathways in SKOV3 cells, and are likely induced through similar mechanisms as histamine induced-EVs.

Table 6.5 Gene ontology terms associated with upregulated protein expression in TRPC3 activator-induced EVs

A total of 39 proteins identified with a 2-fold increase following TRPC3 activator treatment were uploaded to the DAVID analysis tool, and ran against the full human genome as background. The top ten most significant GO terms returned for biological process, cellular component, and molecular function are shown, sorted for p-value after Benjamini-Hochberg correction. Terms with an adjusted p-value less than 0.05 are highlighted in red. Fold enrichment is the number of genes annotated with that term divided by the number of genes expected by the software to be annotated with that term.

GO terms for upregulated proteins in TRPC3 activator-induced EVs		
Biological process	**Fold enrichment**	**Adjusted p-value**
Nucleosome assembly	45.44	7.93E-23
Mesenchyme migration	227.69	8.25E-05
Pyrimidine nucleotide metabolic process	126.49	4.57E-04
Purine nucleotide metabolic process	113.84	4.89E-04
UTP biosynthetic process	94.87	5.95E-04
CTP biosynthetic process	94.87	5.95E-04
GTP biosynthetic process	87.57	6.61E-04
Nucleoside triphosphate biosynthetic process	81.32	7.34E-04
Negative regulation of myeloid leukocyte differentiation	213.46	3.30E-03
Innate immune response in mucosa	45.54	3.61E-03
Cellular component	**Fold enrichment**	**Adjusted p-value**
Extracellular exosome	5.16	5.44E-25
Nuclear nucleosome	98.28	2.58E-21
Nucleosome	42.72	5.49E-15
Lamellipodium	19.31	6.06E-08
Focal adhesion	8.69	1.02E-05
Actin filament	28.51	4.33E-05
Membrane	2.81	5.47E-04
Cytosol	2.33	5.47E-04
Extracellular space	3.44	9.29E-04
Nucleus	1.83	1.75E-03
Molecular function	**Fold enrichment**	**Adjusted p-value**
Protein heterodimerization activity	10.46	2.94E-10
Histone binding	16.42	2.34E-04
Nucleosomal DNA binding	31.10	7.66E-04
DNA binding	3.08	9.41E-04
Nucleoside diphosphate kinase activity	57.22	1.05E-03
ATP binding	2.87	8.77E-03
Actin filament binding	10.84	1.95E-02
Structural constituent of cytoskeleton	10.40	9.53E-02
Protein histidine kinase activity	286.12	9.53E-02
Cadherin binding involved in cell-cell adhesion	4.93	2.19E-01

6.3.11. NEGATIVE REGULATORS OF CANCER DISSEMINATION AND METASTASIS ARE UNDER-REPRESENTED IN TRPC3 ACTIVATOR-INDUCED EVS

As analysis of upregulated protein expression in TRPC3 activator-induced EVs identified an enrichment of metastasis related terms, GO terms were also assessed for downregulated protein expression to explore what terms were under-represented in TRPC3 activator-induced EVs. As only one downregulated protein had a p-value of less than 0.05, all proteins identified as downregulated by 2-fold or more were included in the GO term analysis. Overall, the submitted gene list returned 17 terms for biological process, 18 for cellular component and 9 for molecular function. The top ten most significant GO terms returned for each category are represented in Table 6.6. Of note, GO analysis returned no significant terms for molecular functions. Again, 'extracellular exosome' was the most enriched cellular component term. Similar to ionomycin-induced EVs, a number of cellular component terms associated with the extracellular space and cytosol were enriched in downregulated proteins, including 'extracellular space', 'extracellular matrix', 'cytosol' and 'cytoplasm' (Table 6.6). Cellular component terms 'desmosome' and 'cornified envelope' and biological processes associated with their formation were also under-represented in TRPC3 activator-induced EVs. These terms are associated with downregulated protein expression in all treatment groups, suggesting they represent constitutive release of a mixed EV population. In addition to these shared terms, unique biological processes associated with negative regulation of cancer dissemination and metastasis were also under-represented in TRPC3 activator-induced EVs, including 'negative regulation of endopeptidase activity' (Table 6.6), and non-significant terms 'negative regulation of peptidase activity' (p=0.56) and 'negative regulation of proteolysis' (0.64). Paired with the terms identified for upregulated protein expression in TRPC3 activator-induced EVs (Table 6.5), these terms suggest that not only does TRPC3 activation induce the release of EVs containing proteins associated with increased metastatic potential, but also decreases the loading into EVs of negative regulators of cancer pathways. These findings support observations that TRPC3 activation mediates metastatic mechanisms in SKOV3 cells (detailed in Chapters 3 and 4).

Table 6.6 Gene ontology terms associated with downregulated protein expression in TRPC3 activator-induced EVs

A total of 26 proteins identified with a 2-fold decrease following TRPC3 activator treatment were uploaded to the DAVID analysis tool, and ran against the full human genome as background. The top ten most significant GO terms returned for biological process, cellular component, and molecular function are shown, sorted for p-value after Benjamini-Hochberg correction. Terms with an adjusted p-value less than 0.05 are highlighted in red. Fold enrichment is the number of genes annotated with that term divided by the number of genes expected by the software to be annotated with that term.

GO terms for downregulated proteins in TRPC3 activator-induced EVs		
Biological process	**Fold enrichment**	**Adjusted p-value**
Keratinization	53.82	6.76E-03
Peptide cross-linking	51.67	6.76E-03
Keratinocyte differentiation	33.99	1.58E-02
Single organismal cell-cell adhesion	25.58	2.74E-02
Negative regulation of endopeptidase activity	21.35	3.71E-02
Cell envelope organization	430.56	1.84E-01
Epidermis development	22.79	2.50E-01
Bundle of His cell-Purkinje myocyte adhesion involved in cell communication	215.28	2.76E-01
Regulation of ventricular cardiac muscle cell action potential	117.43	4.40E-01
Negative regulation of telomere maintenance via telomerase	107.64	4.40E-01
Cellular component	**Fold enrichment**	**Adjusted p-value**
Extracellular exosome	5.52	8.20E-13
Desmosome	112.49	2.05E-04
Extracellular space	5.01	1.68E-03
Extracellular matrix	11.40	1.54E-02
Cornified envelope	44.02	3.12E-02
Cytosol	2.44	4.95E-02
Cytoplasm	1.94	6.90E-02
Intermediate filament	17.92	1.12E-01
Fascia adherens	134.99	1.23E-01
Cytoskeleton	7.28	1.23E-01
Molecular function	**Fold enrichment**	**Adjusted p-value**
Cell adhesive protein binding involved in bundle of His cell-Purkinje myocyte communication	225.08	5.03E-01
Protein-glutamine gamma-glutamyltransferase activity	150.05	5.03E-01
Telomerase RNA binding	84.41	5.93E-01
RNA binding	4.94	6.27E-01
Cysteine-type endopeptidase inhibitor activity	39.72	6.27E-01
Structural molecule activity	8.20	6.27E-01
Cadherin binding involved in cell-cell adhesion	6.99	7.15E-01
Poly(A) RNA binding	2.99	7.17E-01
Cell adhesion molecule binding	21.78	7.42E-01

6.3.12. DMSO ALTERS THE PROTEOMIC CARGO OF EVs

PCA of differential protein expression across treatment groups demonstrated a tangible effect of DMSO on the proteomic cargo of EVs (Figure 6.2 A). To identify what EV proteins were specifically deregulated by DMSO, the mean fold change of each protein following DMSO treatment (LFQ intensity DMSO – LFQ intensity untreated), and the p-value of this change was calculated. These values were then plotted as Log_2 (fold change) against $-Log_{10}$ (p-value) in a volcano plot (Figure 6.6 A). The volcano plot in Figure 6.6 A represents all identified proteins: proteins in orange had a 2-fold change either up (right) or down (left), proteins in red had a p-value of less than 0.05 and proteins in green had both. Of all identified proteins, 74 were upregulated by 2-fold or more following DMSO treatment, and 20 of these had a p-value of less than 0.05. A total of 80 proteins were downregulated by 2-fold or more, and 30 of these had a p-value of less than 0.05. All proteins with a 2-fold decrease or increase and a p-value of less than 0.05 are listed in Figure 6.6 B and C respectively, alongside their corresponding fold change and p-value. All deregulated proteins listed in Supplementary Figure 9. As noted in the PCA, DMSO induced the largest divergence in the EV proteome of any treatment group. Low concentrations of DMSO can induce an array of molecular and cellular processes through structural changes in proteins and membrane lipids[480]. The diversity of these cellular effects is reflected in the proteome of DMSO-induced EVs, as they pertain to a range of seemingly unrelated processes including cell adhesion (FERMT3, LOXL2, LAMB3), integrin signalling (ILK, PARVB, TGFB1), endocytosis (LRP1) and remodelling of the cytoskeleton (TUBA4A, COTL1, PLEK). Despite their functional variation, the majority of upregulated proteins are associated with the PM, ECM or extracellular region as secreted proteins, suggesting these proteins may be a by-product of the effect of DMSO on cell membranes rather than representing altered EV proteomic cargo. Regardless, DMSO induces the release of significantly altered protein cargo - emphasising the need for appropriate controls in the analysis of cell-derived EVs.

(A)

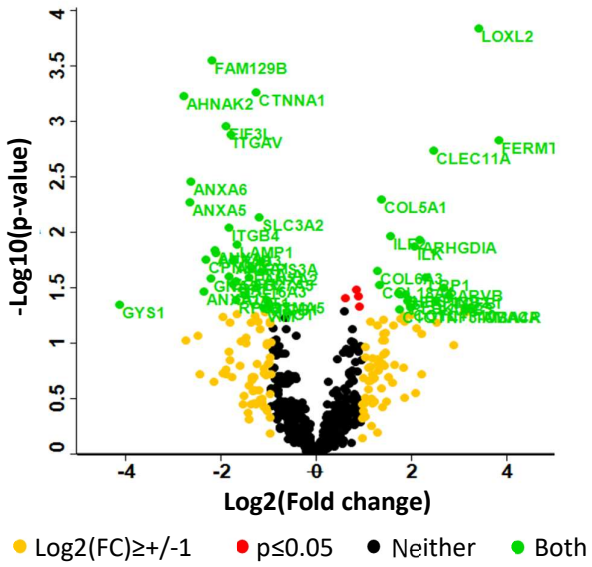

(B)

Significantly downregulated proteins in DMSO-induced EVS		
Gene names	Fold Change	p-value
GYS1	0.06	4.48E-02
AHNAK2	0.15	5.89E-04
ANXA5	0.16	5.36E-03
ANXA6	0.16	3.48E-03
ANXA11	0.19	3.41E-02
CPNE1	0.20	1.77E-02
GNAS	0.22	2.60E-02
FAM129B	0.22	2.81E-04
ANXA4	0.23	1.45E-02
ATP1B3	0.23	1.55E-02
EIF3L	0.27	1.10E-03
EGFR	0.28	2.49E-02
ITGB4	0.28	9.02E-03
ITGAV	0.29	1.33E-03
ANXA1	0.30	1.82E-02
SLC16A3	0.30	2.95E-02
RPS27	0.31	4.12E-02
RALY	0.31	2.78E-02
LAMP1	0.32	1.30E-02
VAT1	0.35	3.73E-02
SLC7A5	0.38	2.55E-02
HLA-A;HLA-H	0.39	2.07E-02
CTNNA1	0.42	5.46E-04
SLC3A2	0.43	7.40E-03
ANXA2;ANXA2P2	0.45	2.26E-02
RPS3A	0.45	1.84E-02
VIM	0.47	4.85E-02
PSMA5	0.49	4.12E-02
XPO1	0.50	4.65E-02
ITGB1	0.50	4.24E-02

(C)

Significantly upregulated proteins in DMSO-induced EVs		
Gene names	Fold Change	p-value
FERMT3	14.22	1.47E-03
LOXL2	10.54	1.45E-04
TUBA4A	9.42	4.97E-02
F10	8.74	4.76E-02
TGFBI	6.85	3.74E-02
PARVB	6.40	3.19E-02
LAMB3	5.63	4.23E-02
CLEC11A	5.53	1.84E-03
LRP1	4.91	2.54E-02
ARHGDIA	4.50	1.18E-02
ILK	4.14	1.34E-02
COTL1	3.91	4.79E-02
PLEK	3.77	4.20E-02
SERPINE2	3.65	3.61E-02
C1QTNF3-AMACR; C1QTNF3	3.37	4.95E-02
THBS1	3.32	3.55E-02
ILF2	2.94	1.09E-02
COL5A1	2.58	5.07E-03
COL18A1	2.52	3.01E-02
COL6A3	2.43	2.23E-02

Figure 6.6 DMSO alters the proteomic cargo of EVs

The mean fold change of each protein following treatment with DMSO was calculated and p-values were generated using a two tailed t-test. ***(A)*** *Volcano plot displaying the Log_2 of fold change of each protein against -Log_{10} of the p-value resulting from the t-test. Proteins with a fold change ≤ 0.5 or ≥ 2 are orange, proteins with a p-value of ≤ 0.05 are red and proteins that have both are green and labelled.* ***(B)*** *Gene names for the 20 proteins identified with a 2-fold decrease and a p-value of ≤ 0.05, and* ***(C)*** *30 proteins identified with a 2-fold increase and a p-value of ≤ 0.05. (B) and (C) listed with corresponding fold change and p-value. Proteins sorted by fold change value.*

6.3.13. GENE ONTOLOGY ANALYSIS OF DEREGULATED PROTEIN EXPRESSION IN EVS DERIVED FROM DMSO TREATED CELLS

DMSO induced the largest divergence in the secreted proteome of any treatment group. GO term analysis was subsequently performed on deregulated protein expression to understand what molecular activities and structures were associated with these changes: are these proteins intentionally captured and released by EVs, or do they represent a co-isolated by-product of the structural effect of DMSO on cell membranes? The gene names for all proteins with a 2-fold increase or decrease and a p-value of less than 0.05 were uploaded to the DAVID analysis tool. Significant GO terms ($p<0.05$) for each category for up- and down-regulated proteins are represented in Table 6.7, alongside their corresponding fold enrichment and adjusted p-value (Benjamini corrected). Overall, the submitted gene list of upregulated proteins returned 21 terms for biological process, 13 for cellular component and 6 for molecular function. The downregulated gene list returned 27 terms for biological process, 35 for cellular component and 22 for molecular function. As recognised in the analysis of individual upregulated proteins (6.3.12), DMSO-induced EVs are enriched for terms associated with a variety of largely unrelated molecular activities and structures, from 'cell adhesion' to 'collagen trimmer' and 'endoplasmic reticulum lumen'. Notably, 'extracellular exosome' which is the most enriched cellular component term for all EV protein expression regardless of direction, is only the seventh most enriched term for upregulated protein expression in DMSO-induced EVs. Terms associated with the ECM and extracellular region are markedly more enriched, including 'extracellular matrix', 'extracellular region' and 'extracellular space' (Table 6.7 A). In contrast, 'extracellular exosome' is the most enriched cellular component term for downregulated protein expression, and the terms are generally more similar to those identified for other EV samples (Tables 6.1-6.7). Ultimately these results demonstrate that even at low concentrations, DMSO induces the secretion of soluble proteins which co-isolate with EVs and have the potential to skew interpretations of EV-based assays. This is the first demonstration of the effect of DMSO on EV proteomes.

Table 6.7 Gene ontology terms associated with deregulated protein expression in DMSO-induced EVs

Following DMSO treatment, 20 proteins with a 2-fold increase and 30 proteins with a 2-fold decrease were identified with a p-value of less than 0.05 and uploaded to the DAVID analysis tool. Proteins were run against the full human genome as background. Significant GO terms ($p \leq 0.05$) *for biological process, cellular component, and molecular function are shown, sorted for p-value after Benjamini-Hochberg correction. Fold enrichment is the number of genes annotated with that term divided by the number of genes expected by the software to be annotated with that term.*

GO terms for significantly upregulated proteins in DMSO-induced EVs		
Biological process	**Fold Enrichment**	**Adjusted p-value**
Cell adhesion	14.63	1.01E-04
Extracellular matrix organization	25.70	2.57E-04
Positive regulation of cell migration	22.82	3.88E-03
Cellular component	**Fold Enrichment**	**Adjusted p-value**
Extracellular matrix	23.45	1.15E-06
Extracellular region	6.47	6.28E-06
Collagen trimer	47.16	5.91E-05
Extracellular space	5.80	6.49E-04
Endoplasmic reticulum lumen	22.60	6.49E-04
Basement membrane	43.94	9.04E-04
Extracellular exosome	3.09	1.48E-02
Proteinaceous extracellular matrix	12.95	2.38E-02
Molecular function	**Fold enrichment**	**Adjusted p-value**
Integrin binding	42.31	2.67E-04
GO terms for significantly downregulated proteins in DMSO-induced EVs		
Biological process	**Fold Enrichment**	**Adjusted p-value**
Leukocyte migration	25.81	1.18E-03
Antigen processing and presentation of exogenous peptide antigen via MHC class I, TAP-dependent	33.32	4.53E-02
Cellular component	**Fold Enrichment**	**Adjusted p-value**
Extracellular exosome	4.46	1.18E-08
Melanosome	45.11	2.36E-08
Membrane	4.40	4.99E-06
Cell surface	10.51	6.59E-06
Focal adhesion	13.11	6.59E-06
Plasma membrane	2.76	1.07E-04
Sarcolemma	33.50	2.77E-04
Cell-cell adherens junction	12.34	2.89E-04
Perinuclear region of cytoplasm	6.42	9.30E-03
Integrin complex	63.28	1.39E-02
Molecular function	**Fold Enrichment**	**Adjusted p-value**
Calcium-dependent phospholipid binding	72.76	1.27E-09
Phospholipase inhibitor activity	239.79	2.02E-07
Calcium-dependent protein binding	45.48	1.63E-04
Cadherin binding involved in cell-cell adhesion	12.73	4.16E-04
Poly(A) RNA binding	4.67	3.63E-03
Calcium ion binding	5.89	5.78E-03
Protein binding	1.56	1.79E-02

6.4. DISCUSSION

The results presented through Chapters 3-5 of this thesis identify a novel role for TRPC3 in EV biogenesis and mediating metastatic mechanisms in SKOV3 cells, and demonstrate that histamine, ionomycin and TRPC3 activator induce the release of EVs with distinct characteristics and fusion dynamics. In this chapter, label-free mass spectrometry was employed to analyse the protein content of histamine, ionomycin and TRPC3 activator-induced EVs to derive mechanistic insights into how these treatments influence EV biogenesis, and identify candidate proteins which may mediate TRPC3 activator-induced metastatic mechanisms. This data represents the first characterisation and comparison of EV proteomes following treatment with different chemical inducers. EVs isolated in serum-free media after 4hrs conditioning showed typical and replicable proteomic cargo that was differentially expressed according to treatment group. The proteomes of induced EVs were subsequently compared with untreated or DMSO controls, revealing previously unappreciated roles for CD81, NDPKs and Ca^{2+}-dependent interactions with the syndecan-syntenin-ALIX axis in EV biogenesis. This analysis also evidenced the endosomal origin and enriched metastatic potential of TRPC3 activator-induced EVs, as well as presenting novel characterisation of the effect of DMSO on EV proteomes.

6.4.1. EV EXTRACTION CONDITIONS AND MASS SPEC PROTEOMIC ANALYSIS

As identified in the initial characterisation of the protein content of basal and induced EVs (Section 6.3.1), a number of EV proteins were only detectable in one or two biological replicates for each treatment group. Whilst these discrepancies somewhat represent the highly heterogenous nature of EVs, it also reflects the limitations of the data dependent acquisition mass spec (DDA-MS) technique used. In DDA-MS, fragmentation data is acquired from a predefined set of selected precursor ions which tend to represent only the most abundant peptides[481]. This stochastic selection leads to a high number of missing values, resulting in a well-documented inability to reproducibly identify the same set of proteins across replicate experiments[482, 483]. In contrast, data independent acquisition mass spec (DIA-MS) fragments all detected precursor ions, significantly improving the reproducibility and sensitivity of the mass spec analysis. Due to the variably low expression of EV proteins, future quantification with DIA-MS would increase the range and reproducibility of identified EV proteins. In demonstration of this, DIA-MS was recently employed in the analysis of urinary EVs and identified highly replicable protein cargo from small sample volumes[484].

For mass spec analysis of EV proteomic cargo, induced-EVs were extracted by SEC following a 4hr conditioning period in either plain or treatment-supplemented serum-free media (SFM). The utility of SEC to isolate EVs from SFM with minimal contamination was demonstrated in Figure 4.5. However, whilst SFM eliminates bovine contamination which can interfere with proteomic analysis of cell-derived EVs[411], the effect of serum-free culture on the EV proteome must be considered. Previously Li *et al.* reported that several vesicular proteins implicated in EV biogenesis were differentially expressed in EVs isolated from SFM after 48hrs conditioning, and that SFM EVs were enriched for stress-related proteins[420]. Indeed, cellular stress is reflected in the protein content of EVs[485] and serum starvation is often used as a method to induce cellular stress pathways[411]. However, the effect of serum starvation is cell-type dependent, and the viability of SKOV3 cells did not reduce up to 48hrs conditioning in SFM (Figure 4.3) or after 4hrs conditioning in SFM supplemented with DMSO, histamine, ionomycin or TRPC3 activator (Supplementary Figure 10). Whilst these assessments indicate that up-or-down regulated protein expression identified in induced-EVs are not a by-product of apoptotic pathways, mining the proteomic dataset for stress-related proteins would provide further assurances that EV proteomic cargo is not impacted by serum-free culture.

A further consideration of the culture conditions for EV proteomic analysis is the conditioning period used. TIRF analysis demonstrated that histamine, ionomycin and TRPC3 activator induce EV release with immediate effect (Figures 5.5 and 5.6), therefore a 4hr conditioning period was employed to capture the proteomic profile of induced-EVs. Over longer, classically used conditioning periods, the population of induced-EVs may degrade or be taken up by neighbouring cells, and therefore devoid from proteomic analysis. However, how inducing EV biogenesis pathways translates to qualitative differences in their proteomic cargo and how long this process takes is unknown. Recently published work by Mathieu *et al.* compared EV proteomes from 3hr and 24hr conditioning periods, and identified marked differential expression of lysosomal, endosomal and PM associated proteins[105]. Therefore, extending the length of the conditioning period for EV proteomic analysis would likely yield different outcomes.

6.4.2. THE EFFECT OF DMSO ON THE SECRETED PROTEOME

First noted in the PCA, the presence of DMSO in the cell conditioning media was the strongest distinguishing component between all EV samples (Figure 6.2 A). Further analysis comparing the proteome of basal EVs to DMSO induced-EVs highlighted a number of significantly deregulated proteins – 74 were upregulated by 2-fold or more in DMSO-induced EVs and 20 of these were

significant ($p<0.05$), and 80 proteins were downregulated by 2-fold or more with 30 having a p-value <0.05. This represents the largest divergence in EV proteome of any treatment group. Upregulated proteins in DMSO induced-EVs seem to pertain to a wide range of unrelated processes with minimal links to EVs. This is likewise reflected in the GO analysis, as DMSO-induced EVs were enriched for terms associated with a variety of molecular activities and structures with 'extracellular exosome' – the most enriched cellular component term for all other EV samples - only appearing as the seventh most enriched term. Instead, upregulated proteins and terms associated with the ECM, PM and extracellular region were markedly enriched.

Through changing the secondary structure and binding properties of proteins and membrane lipids, DMSO can increase membrane fluidity and dysfunction[486, 487]. The accurate analysis of EV proteomics relies on the integrity of the PM; therefore if this is compromised, the secreted proteome is likely to be contaminated with non-specific membrane shedding. However, the majority of these membrane effects are only apparent at high concentrations of DMSO after long periods of exposure, whereas DMSO induced-EVs were derived from cells treated for a 4hr period with a concentration of 0.03% - well within the recommended vehicle range (≤1.5%)[480]. This is the first demonstration of how exposing cells to low concentrations of DMSO for short time periods can affect their secreted proteome. Nevertheless, a concentration of 0.03% was employed in all cell-based assays within this thesis and demonstrated no effect on the migration, proliferation or invasion of SKOV3 cells either directly or through the transfer of DMSO induced-EVs (Chapters 3 and 4 respectively). Importantly, DMSO also had no effect on the quantity, size or dynamics of CD81-EV release (Figures 5.4-5.9). This would suggest that the upregulated protein expression induced by DMSO is unlikely to represent functionally relevant EV protein cargo, and may be a by-product of its interaction with cell membranes. However, these findings must be considered in future analysis of EV proteomics as if the appropriate vehicle controls are not performed, inaccurate conclusions could be drawn. Other solubilising agents such as ethanol may be more appropriate for reconstituting compounds used to treat cells for EV analysis.

6.4.3. Analysis of Histamine-induced EVs identified potential mediators of EV biogenesis

Histamine stimulation induces MVB-PM fusion in SKOV3 cells (Figure 5.4) as well as HeLa, HUVECs and MSCs as previously reported[82]. This suggests that the histamine-stimulated signalling pathway may act an essential mediator of EV biogenesis. Using phosphoproteomics, Verweij *et al.* determined that histamine induces MVB-PM fusion through GPCR signalling from

the histamine receptor H1HR, and subsequent phosphorylation of SNAP23 via the H1HR–$G\alpha_q$–PKC pathway [82]. Here, a full proteomic screen of EV cargo identified significantly upregulated protein expression in histamine-induced EVs – 112 proteins were upregulated by 2-fold or more and 21 of these were significant ($p<0.05$), whereas none of the 23 proteins downregulated by 2-fold or more had a p-value <0.05. Amongst the upregulated proteomic cargo are a number of proteins either directly implicated in or associated with recognised pathways of EV biogenesis, implying a novel role for them in histamine-induced EV release.

The most upregulated protein in histamine-induced EVs was the tetraspanin and EV marker CD81 (Figure 6.3 A). Tetraspanins associate in lipid-rich membrane microdomains which are readily internalised by cells and processed through the endosomal pathway, hence their enrichment in MVB-derived EVs[45, 488]. Although the specificity of CD81 as an exosomal marker is disputed[105, 426], its high expression in histamine-induced EVs confirms TIRF analysis that histamine stimulates EV release through the endocytic pathway. In addition, these tetraspanin-enriched microdomains (TEMs) together with CD81 play a key role in EV biogenesis and protein loading into EVs[455]. It's reported that 45% of the EV proteome corresponds to the expression of tetraspanins and their associated proteins in TEMs[489], suggesting a large proportion of the upregulated protein cargo in histamine-induced EVs interact with CD81-rich TEMs. Interestingly, GPCRs and G protein subunits $G\alpha_{11}$, $G\alpha_q$ and $G\beta$ associate specifically with CD81, but not with other tetraspanins[490]. It's thought that through CD81-GPCR complexes, CD81 may act to enhance ligand binding and downstream signalling. This ties in with the enrichment of biological process and molecular function terms related to G-protein activation in upregulated protein expression in histamine-induced EVs, such as 'GTP biosynthetic process', 'purine nucleotide metabolic process', 'nucleoside diphosphate kinase activity' and 'protein histidine kinase activity'. All of these terms relate to the activity of NDPKs which control G-protein signalling by regulating the availability of GTP, as well as directly activating G-proteins through a GPCR-independent pathway[473]. Interestingly, NDPKs also regulate the activity of the mTOR complex 1 (mTORC1)[491] – an emerging mediator of EV biogenesis[492]. This analysis has therefore identified previously unappreciated roles for CD81, NDPKs and their associated proteins in histamine-induced EV release - contributing to a growing body of work implicating GPCR signalling in EV biogenesis[459, 493].

Aside of GPCR signalling, a number of upregulated proteins identified in histamine-induced EVs are also likely to contribute to their biogenesis and protein loading. With regards to the latter, E3 ubiquitin-protein ligase HUWE1, 26S proteasome regulatory subunit 10B (PSMC6) and

tripeptidyl-peptidase-2 (TPP2) are all mediators of protein ubiquitination - a prerequisite for protein recognition by the ESCRT machinery and incorporation into EVs[494]. Likewise, myoferlin (MYOF) is recognised as a determining factor for the proteomic diversity of EVs[495]. In terms of EV biogenesis, 14-3-3 protein theta (YWHAQ) regulates small GTPase mediated signalling; partly in its role as a Rab effector protein[496]. Small GTPases - specifically Rab proteins and their effectors - play a multitude of roles in the formation, intracellular transport and secretion of EVs[78, 497]. The upregulated coatomer subunit beta (COPB2) is also an essential regulator of vesicular trafficking[498], whilst copine-8 (CPNE8) is a Ca^{2+}-dependent membrane-binding protein which regulates molecular events at the interface of the cell membrane and cytoplasm[499]. Although a number of these proteins are not currently recognised as mediators of EV biogenesis, their associations with the molecular processes that govern EV biogenesis suggest a novel role for them in the formation of histamine-induced EVs. Of course, the expression of these proteins would need to be validated to support such conclusions.

6.4.4. IONOMYCIN INDUCES EV RELEASE THROUGH THE SYNDECAN-SYNTENIN-ALIX AXIS

By employing Ca^{2+} ionophores such as ionomycin, a number of studies demonstrate that increased intracellular Ca^{2+} concentrations induce EV release - including the work presented here (Chapter 5, Figure 5.4). Hitherto, Ca^{2+} regulated mechanisms thought to mediate EV release include a Munc13-4-Rab11 MVB trafficking pathway[144], synaptotagmins which function as Ca^{2+} sensors[148] and second messenger inositol 1,4,5-trisphosphate (IP^3)[143]. To further characterise the downstream mechanisms which mediate Ca^{2+}-induced EV release, a full proteomic screen of ionomycin-induced EVs was conducted here. A number of proteins were deregulated in ionomycin-induced EVs - 66 proteins were upregulated by 2-fold or more and 10 of these were significant ($p<0.05$), and 48 proteins were downregulated by 2-fold or more with 7 having a p-value <0.05. Of these, the Ca^{2+} binding protein PDCD6 (known as ALG-2) exhibited the highest expression in ionomycin-induced EVs (Figure 6.4 A,B). Through a Ca^{2+}-dependent interaction, ALG-2 induces a conformational change in ALIX that enables its association with ESCRT machinery[150]. The function of ALIX and thus ALG-2 is critical for ESCRT-dependent MVB formation. For example, ALIX bridges together the ESCRT-III and ESCRT-I complexes through its association with ESCRT-III and TSG101[500], and assembles ESCRT-III and Vps4 complexes which mediate endosomal membrane budding and abscission of MVBs[151, 152]. ALIX also facilitates MVB sorting and formation through its interactions with syndecan-4 and syntenin-1[73], which are likewise significantly upregulated in ionomycin-induced EVs (Figure 6.4 A,B). The syndecan–syntenin–ALIX mechanism is estimated to control around 50% of EV secretion in unstimulated

MCF-7 cells[73]. Considering the function of ALIX is regulated through Ca^{2+}-dependent interactions with ALG-2, the syndecan–syntenin–ALIX axis may account for the biogenesis of a larger proportion of vesicles following ionomycin stimulation. Therefore, the results presented here suggest that ionomycin induces the release of EVs through Ca^{2+}-dependent interactions with the syndecan-syntenin-ALIX axis.

EVs formed through the syndecan-syntenin-ALIX axis originate from endosomal membranes and the fusion of MVBs with the cell surface[73]. GO analysis of upregulated proteins in ionomycin-induced EVs returned an enrichment of terms related to the endocytic pathway, including 'endocytic vesicle membrane', 'endosome membrane' and 'endosomal transport', supporting the notion that ionomycin-induced EVs are predominantly formed through these mechanisms. This is in line with increased MVB-PM fusion events detected by TIRF microscopy following ionomycin stimulation (Chapter 5, Figure 5.4). However, the cellular component term 'plasma membrane' was also significantly enriched in upregulated protein expression in ionomycin-induced EVs. This would suggest that ionomycin likewise induces the release of PM-derived EVs. Indeed, an increase in intracellular Ca^{2+} can disrupt PM-cytoskeleton anchorage, resulting in increased MV biogenesis through outward budding from the PM[156, 501]. The PM protein basigin (BSG) and its interacting partner solute carrier family 3 member 2 (SLC3A2) are both significantly upregulated in ionomycin-induced EVs (Figure 6.4 A,B), and in a recent study assessing the specificities of MVB and PM-derived EVs, BSG and SLC3A2-containing EVs were primarily released from the PM[105]. Cumulatively, these results propose that through increasing intracellular Ca^{2+}, ionomycin stimulates the release of MVB-derived EVs through the syndecan-syntenin-ALIX axis as well as a PM-derived EV population.

6.4.5. TRPC3 ACTIVATOR-INDUCED EVS ARE ENRICHED WITH METASTATIC POTENTIAL

Increased activity of TRPC3 contributes to the progression of ovarian cancer through mediating sustained elevated Ca^{2+} [310]. Despite extensive research into the expression of TRP channels in cancer and their pathological consequences, roles for Ca^{2+}-dependent effectors are poorly understood. Here, TRPC3 activation induced the biogenesis of an EV population capable of communicating metastatic mechanisms to recipient cells (detailed in Chapters 4 and 5). To gain insight into how TRPC3 is acting on EV biogenesis and what cargo may mediate the metastatic capacity of SKOV3 cells, the proteome of TRPC3 activator-induced EVs was assessed. TRPC3 activator-induced EVs exhibited a smaller divergence in proteomic cargo than histamine, ionomycin or DMSO-induced EVs: 39 proteins were upregulated by 2-fold or more and 7 of these were significant ($p<0.05$), and 26 proteins were downregulated by 2-fold or more with only 1

having a p-value <0.05. This suggests that it may be the increased release of this deregulated protein cargo, in combination with other soluble factors or EV cargo (RNA, DNA, lipids), that mediates the effect of TRPC3 activation on the metastatic capacity of SKOV3 cells.

However, within the upregulated proteomic cargo of TRPC3 activator induced-EVs are Ca^{2+}-binding proteins that are abnormally expressed in a number of cancer types and implicated in mediating metastatic mechanisms. For example, tropomyosin-4 (TPM4) enhances the migration of lung cancer cells[502] and has utility as a potential early diagnosis marker in lung, breast and oesophageal squamous cell cancer[503]. TPM4 is also highly expressed in ovarian tumour tissue[504] and is identified in EVs from pancreatic cancer cells[505]. Of particular interest here is the S100 calcium-binding protein A4 (S100A4). S100A4 is highly expressed in numerous cancers and promotes tumour progression and metastasis through EMT induction[506]; including in ovarian cancer cells where it increases tumour cell invasiveness, and is suggested as a prognostic biomarker[507]. S100A4 is upregulated in EVs derived from highly metastatic hepatocellular carcinoma (HCC) cells as well as leukaemia-associated-mesenchymal stem cells[508, 509]. In both pathologies, EV-mediated transfer of S100A4 enhanced the metastatic potential of recipient cells by driving their proliferation, migration and invasion. Also of interest is nucleobindin-1 (NUCB1): again, NUCB1 expression is elevated in numerous cancer types and is recognised as a candidate biomarker for ovarian cancer[510]. In a recent study from Vignesh *et al.*[511], NUCB1 is specifically packaged into tumour-EVs derived from several cancer cell lines, and thereby induces EMT in recipient cells, and augments the migration of non-tumour cells[511]. In TRPC3 activator-induced EVs, these metastatic proteins are upregulated alongside the specific-exosomal marker EHD4[104, 479] and dynactin subunit ACTR1B, which together regulate endocytic transport[512, 513]. This would indicate that metastatic proteins are packaged into EVs through stimulation of the endosomal pathway, and subsequent TRPC3-mediated EV communication may therefore contribute to metastatic mechanisms in SKOV3 cells. Although, the transfer and uptake of this proteomic cargo needs to be validated.

The GO terms for upregulated protein expression in TRPC3 activator-induced EVs were also enriched for molecular activities and structures implicated in metastasis, such as cell motility, migration and proliferation. These terms included ‘mesenchyme migration’, ‘lamellipodium’, ‘actin filament’, ‘movement of cell or subcellular component’ and ‘positive regulation of epithelial cell proliferation’. In contrast, terms related to the negative regulation of cancer dissemination and metastasis were under-represented in TRPC3 activator-induced EVs, including ‘negative regulation of endopeptidase activity’, ‘negative regulation of peptidase

activity' and 'negative regulation of proteolysis'. Endopeptidases such as asparagine endopeptidase (AEP) and prolyl endopeptidase (PEP) are association with increased metastatic potential in several cancers including breast[514, 515], prostate[516], and colorectal[517, 518]. Likewise, the activity of peptidases and proteolytic enzymes is key for degradation of the ECM and basement membrane in cancer cell invasion[519, 520]. Therefore, these terms suggest that not only does TRPC3 activation induce the release of EVs containing proteins associated with increased metastatic potential, but also decreases the loading into EVs of negative regulators of cancer pathways.

This exploratory analysis has generated valuable insights into the biological processes and contributing molecules that underlie induced EV biogenesis and confer TRPC3 activator-induced EVs enriched metastatic potential. In addition to the focus of this project, the presented proteomic dataset can be of use to wider groups interested in the role of TRPC3 in ovarian cancer, EV biogenesis or the mechanisms of histamine and Ca^{2+}-mediated EV release. Of course, to confirm the conclusions drawn here further work needs to be conducted to validate protein expression, and examine how manipulating the proposed signalling pathways effects EV release.

6.5. KEY FINDINGS

- EVs extracted in serum-free media after 4hrs conditioning show typical and replicable proteomic cargo.
- Inducing EV release with chemical stimulants histamine, ionomycin and TRPC3 activator significantly alters the EV proteome.
- CD81, NDPKs and their associated proteins may contribute to histamine-induced EV release through the GPCR signalling pathway.
- Ionomycin stimulates the release of MVB-derived EVs through Ca^{2+}-dependent interactions with the syndecan-syntenin-ALIX axis, as well as a PM-derived EV population.
- TRPC3 activation upregulates the expression of Ca^{2+}-binding and metastasis-related proteins, which are packaged into EVs through stimulation of the endosomal pathway.
- Short-term exposure to low concentrations of DMSO (0.03%) can influence the secreted proteome.

Chapter 7

General discussion and future directions

7. General discussion and future directions

Despite a significant research effort, the molecular mechanisms underlying EV formation and release remain poorly understood. This is in part due to the highly heterogenous nature of EVs, issues with culture medium contaminants in *in vitro* cell-derived EV analyses, and a lack of available techniques to monitor direct, real-time effects of potential modulators on EV release. As mounting evidence supports the functional role of EVs in cancer progression, understanding the factors that underly EV biogenesis and how these pathways can be manipulated, and the ensuing effects on their cargo and metastatic capacity holds significant therapeutic potential. This is particularly relevant to cancers with poor response rates to current therapeutics, such as OC, in which almost 45% of cases gain a chemoresistant phenotype following first line treatment[262, 373]. In this thesis, an array of *in vitro* assays, optimised media conditions, proteomic analysis and a novel live single-cell imaging technique was employed to investigate the role of the Ca^{2+} channel TRPC3 in EV biogenesis and OC progression. This analysis demonstrated that pharmacological activation of TRPC3 significantly increased Ca^{2+} signalling and OC growth and migration, and induced the release of MVB-derived EVs with distinct characteristics and metastatic proteomic cargo that increased the growth rate of recipient OC cells. Analysis also revealed novel roles for Ca^{2+} influx and GPCR stimulation by histamine in MVB-derived EV biogenesis in OC, and identified candidate proteins which provide mechanistic insights into how these treatments influence EV biogenesis pathways. Through this work, several methodological aspects of importance have also been demonstrated, including bovine contamination in the analysis of cell-derived EVs, and novel characterisation of the effect of DMSO on EV proteomes. The implications of these results, and future directions will be discussed herein.

7.1. The role of TRPC3 in the development of OC

Initial experiments demonstrated that endogenous TRPC3 protein was highly expressed across a panel of five OC cell lines of different cellular origins. This data extends previous findings by Yang *et al.*[310] who found a marked increase in TRPC3 protein expression in human ovarian epithelial tumour samples compared to normal ovarian tissue. The expression of TRPC3, and notably other TRPC channels including TRPC1/4 /6, has also been confirmed at the mRNA level in SKOV3 OC cells, whilst TRPC5 and 7 were undetectable by both RT-PCR and western blot[521]. This study by Zeng *et al.* also reported on the specific TRPC isoforms that were expressed in SKOV3 cells, showing that the TRPC3 splice variant TRPC3a with an extended N-terminus was co-expressed with variants TRPC1β, TRPC4β, TRPC4γ, and TRPC6 with exon 3 and 4 deletion[521].

In human embryonic kidney (HEK) cells, stable expression of TRPC3a gave rise to both Gq-PLCβ mediated ROCE and thapsigargin triggered SOCE[522], suggesting that TRPC3 activation may increase Ca^{2+} signalling in SKOV3 cells as presented here, through both of these pathways. Indeed, overexpression of TRPC isoforms by Zeng *et al.* significantly increased OC colony growth, suggesting that not only TRPC3a, but additional TRPC channels 1/4/6 and their spliced variants are important for OC development. However, in human ovarian adenocarcinoma tissues, this study reported that TRPC1/3/4 and 6 were expressed at lower levels in undifferentiated ovarian cancer tissues (grade III) compared to well-differentiated tissues (grade I, grade II)[521], suggesting that whilst TRPC3 may be biologically relevant to oncogenic processes in OC, its expression alone is not representative of disease outcome. However, this analysis was only conducted on ovarian tumours from six patients (three undifferentiated, three well-differentiated), therefore further clinical studies and more extensive bioinformatic analysis are required to validate how TRPC3 expression correlates with OC disease progression and survival.

After validating the expression of TRPC3 in OC cell lines, the TRPC3-selective inhibitor Pyr3 and selective TRPC3/6 activator GSK 1702934A were employed to assess how pharmacological modulation of TRPC3 influences Ca^{2+} signalling and the growth, migration and invasion of SKOV3 cells. TRPC3 activation amplified Ca^{2+} signalling in SKOV3 cells, and significantly increased cell growth and migration, but did not affect cell invasion. Importantly, whilst previous studies demonstrate a role for TRPC3 in the proliferation and cell-cycle progression of OC cells[310], this is the first demonstration of TRPC3 signalling mediating OC cell migration, and substantiates the role of TRPC3 in the progression of OC. Similar findings have been reported for other cancer cell lines, such as glioblastoma and melanoma cells[308, 318], whereby inhibition of TRPC3 with Pyr3 reduced cell migration through impairing focal adhesion and cytoskeleton protein expression, and the secretion of proteolytic MMP9. The expression of Ca^{2+}-sensitive cytoskeletal and adhesion molecules should be assessed downstream of TRPC3 activation in SKOV3 cells to gain further insight into how TRPC3 is regulating OC cell motility. In addition, the effect of TRPC3 modulation on other metastatic mechanisms in OC should be evaluated. A previous publication indicates that inhibition of TRPC1/3/6 mitigates EMT in gastric cancer cells[320], therefore evaluating the expression of EMT-key related genes may provide a clearer overall picture of how TRPC3 modulation is regulating OC progression.

The expression of additional TRPC channels in SKOV3 cells as reported by Zeng *et al.*[521] is an important consideration for the effects of pharmacological modulation of TRPC3 activity presented in this thesis. Whilst concentrations of the TRPC3 inhibitor Pyr3 and activator GSK

1702934A were carefully selected to reduce off-target effects on other TRPC channels, the contribution of other TRPC channels, namely the highly related TRPC6, cannot be completely ruled out. Indeed, siRNA-mediated knockdown of TRPC6 in SKOV3 cells by Zeng *et al.*[521] reduced cell proliferation, and TRPC6 overexpression significantly increased OC colony growth[521]. To ensure the effects on OC cell growth and migration reported in this thesis are specifically due to deregulated TRPC3 activity, siRNA-mediated knockdowns, or preferably CRISPR/Cas9 knockouts, should be employed against TRPC3 and other TRPC channels and assessments of cell growth and migration repeated. These experiments are also required to rule out effects of the TRPC3 activator and inhibitor that are not directly related to modulation of TRPC3 activity. In triple-negative breast cancer cells, administration of Pyr3 induced mitochondrial fragmentation and nuclear condensation[311], suggesting that Pyr3 may induce general DNA damage and apoptosis rather than/in addition to specifically inhibiting TRPC3-mediatied proliferation.

Further experiments exploring the role of TRPC3 in different OC cell lines are also required to validate TRPC3 as an essential regulator of OC. Thus far, this thesis and the majority of investigations studying TRPC3 in OC have been conducted in SKOV3, an epithelial OC line derived from a highly invasive non-serous carcinoma[331-333]. *In vivo*, ovarian tumours are highly heterogenous and often comprise a mixed cell population[332], therefore repeating the findings of this thesis in additional OC lines would better encapsulate the role of TRPC3 in heterogenous *in vivo* ovarian tumours. Moreover, despite SKOV3 being one of the most commonly used cell lines to model OC *in vitro*[331], it does not reflect key characteristics of high-grade serous carcinomas (HGSCs), which represent 80% of OCs[332]. For example, SKOV3 cells have a flat copy-number profile and lack TP53 mutations, whereas HGSC is defined by TP53 mutations (95% of samples) and substantial copy-number changes, with the median fraction of the genome altered as large as 46% in HGSC[331]. This suggests that OC cell lines which more closely resemble HGSC, such as OVCAR3[331] that also expressed high levels of TRPC3, may be a more appropriate model to study TRPC3 in OC *in vitro*. Indeed, analysis of OC cell invasion may yield different results in OVCAR3 cells which are less invasive than SKOV3[333], as attempting to increase the invasive capacity of an already highly invasive cell line may preclude treatment effects on OC invasion which may otherwise be apparent.

7.2. TRPC3 IN EV BIOGENESIS AND EV-MEDIATED METASTATIC MECHANISMS

Preliminary results obtained from hIPSCs harbouring a gain-of-function mutation in TRPC3 suggested that overactivity of TRPC3 may be linked to alterations in EV biogenesis pathways. Indeed, elevated intracellular Ca^{2+} acts to induce EV release in a number of cancer cell types[143-

[145], and here, TRPC3 activation increased Ca^{2+} signalling in SKOV3 cells. Given the multifaceted roles of EVs in cancer progression, it was hypothesised that pharmacological modulation of TRPC3 may induce the release of EVs that contribute to the increased growth and migration of SKOV3 cells. To specifically assess the role of SKOV3-EVs in mediating metastatic mechanisms *in vitro*, it was first necessary to ensure the EV extraction culture medium was void of contaminating bovine-EVs from supplemented FBS. In these assessments, it was discovered that FBS depleted for EVs by standard UC retained high particle and protein concentrations and particles of EV size, which contaminated the analysis of SKOV3-derived EVs. Previous publications echo these findings, likewise demonstrating by NTA that both UC EV-depleted FBS and commercially available EV-depleted FBS retained high particle concentrations[409]. The incomplete removal of bovine EVs is likely to have significant implications for all *in vitro* cell-specific EV investigations, and brings into question the validity of publications which utilise depleted FBS. This was recently illustrated in a publication which reported that the retention of RNA species in EV-depleted FBS had resulted in inadvertent false-positive reporting of extracellular RNA in numerous publications[523]. Experimental guidelines published by the International Society for Extracellular Vesicles (ISEV) do not currently advise authors to evidence that their cell-culture-derived EV assessments are devoid of contamination from bovine EVs if the media has been 'depleted'[412]. The data presented here paired with akin publications denote that these guidelines should be adjusted accordingly.

Serum-free media (SFM) proved a viable alternative for culturing SKOV3 cells and eliminated bovine contamination, yielding a purer population of EVs that presented typical markers and morphology. Therefore, all further EV extractions were performed in SFM. However, as SFM was shown to reduce SKOV3 proliferation in comparison to FBS-supplemented media, it should be noted that not all cellular assays were conducted in SFM. This includes the analysis of TRPC3 expression in OC cell lines, and assessments of SKOV3 cell growth and migration. A previous study by Rashid and Coombs[524] demonstrated that growing A549 human lung epithelial cells in serum-reduced media (Opti-MEM) dysregulated cellular protein expression of chloride intracellular channel protein 1 (CLIC1), proteasome subunit alpha Type 2 (PSMA2) and heat shock 70kDa protein 5 (HSPA5). This suggests that TRPC3 expression in SKOV3 cells may be altered in SFM, therefore EVs extracted from TRPC3 activator and inhibitor treated cells in SFM may not necessarily represent the activity of EVs released by cells directly treated with TRPC3 activator/inhibitor in full media, as for the initial assessments of TRPC3 in SKOV3 growth and migration. Therefore, SKOV3 TRPC3 expression should be assessed in SFM to validate assessments of TRPC3-mediated EV communication.

Once appropriate culture conditions for EV extraction had been established, the role of TRPC3 in EV biogenesis and EV-mediated metastatic mechanisms was investigated. Initially, EVs extracted from TRPC3 activator and inhibitor treated SKOV3 cells were analysed for differences in concentration and surface antigen expression by NTA and MACSPlex analysis respectively. TRPC3 activation induced the release of 100-120nm EVs, and TRPC3 modulation significantly altered the expression of EV surface antigens CD105, CD41b and CD133.1. Notably, both CD105 and CD133 are associated with metastatic phenotypes in other cancer cell lines, and were likewise identified in EVs released from these cell types[430, 434-437]. The differential expression of these antigens may represent the metastatic competence of SKOV3 cells treated with TRPC3 activator or inhibitor, and their ability to convey this phenotype to recipient cells. However, the MACSPlex assay is bias in the fact that it only detects EV surface antigens which are co-expressed with EV markers CD81, CD63 and CD9. Initial characterisation of SKOV3-EVs detected variable expression of these markers across different assays, and due to the heterogeneity of EVs, very little is understood about co-expression of EV surface markers. Therefore, whilst the MACSPlex assay is a useful multiplex tool for the analysis of multiple EV surface antigens, these results should be validated by an unbiased approach such as western blot or proteomic analysis.

Due to the technical limitations associated with NTA, EV release by TRPC3 activator and inhibitor treated SKOV3 cells was further analysed by TIRF microscopy using a CD81-pHluorin reporter. This sensitive reporter of MVB-PM fusion has been employed by a number of groups to assess the effects of fast-acting compounds on MVB-derived EV biogenesis and release[82, 459], and was therefore an ideal system for assessing EV release in response to pharmacological modulation of TRPC3. TIRF analysis confirmed that TRPC3 activation induces EV release in SKOV3 cells, notably in a dose-dependent manner, whilst TRPC3 inhibition did not affect the rate of EV release. These results suggest that the increased population of 100-120nm EVs detected by NTA represent MVB-derived EVs, known as exosomes. This is the first direct demonstration of TRPC3 involvement in EV biogenesis, and specifically exosome release. Interestingly, both NTA and TIRF analysis detected a size-dependent increase in EV release following TRPC3 activation; as by NTA the increase was specifically in EVs sized 100-120nm, and by TIRF analysis TRPC3 activator-induced EVs were significantly larger than DMSO-induced EVs in a dose-dependent manner. This could be indicative of the mechanisms by which TRPC3 activation mediates EV release. For example, it could suggest that TRPC3 activator-induced EV release is Ca^{2+}-dependent, involving Ca^{2+}-regulated molecules such as Rab11 which generates Ca^{2+}-induced giant MVBs in K562 cells and Raw macrophages[147]. Alternatively, it could suggest that TRPC3 activation influences the release of a specific EV subpopulation. This has previously been demonstrated for other

modulators of EV release, namely GW4869, an inhibitor of neutral sphingomyelinase, which inhibited the release of small EVs (50-100nm) while increasing the release of larger EVs (100-200nm)[105, 525]. By TIRF microscopy, the effect of TRPC3 activation on EV release was exclusively analysed in a CD81-positive EV population. Indeed, a study comparing two EV subpopulations with different size distributions reported that CD81 was enriched in larger exosome-like vesicles with a median size of ~140nm, compared to smaller vesicles of ~80nm[526]. Whilst the biological significance of EV size is unknown, collectively the results presented here suggest TRPC3 activation induces the release of larger, CD81-enriched exosomes, likely through a Ca^{2+}-dependent pathway. To assess if TRPC3 activation increases the release of additional, or indeed all subpopulations of EVs, dual-labelling TIRF microscopy using different tetraspanin reporters or a combination of tetraspanin and EV cargo proteins, should be employed.

As TRPC3 activation both stimulates EV release and increases OC growth and migration, the contribution of TRPC3-mediated EV release to these metastatic mechanisms was assessed. EVs were extracted from TRPC3 activator and inhibitor treated SKOV3 cells and applied to naïve SKOV3 cells, and ensuing effects on cell growth, migration and invasion were analysed. After 48hrs incubation, TRPC3 activator-induced EVs increased recipient cell growth at all EV concentrations, whilst no effects on cell migration or invasion were apparent. Numerous studies similarly report that cancer cell-derived EVs can promote tumour growth by upregulating proliferative signalling and increasing resistance to growth suppressors and apoptosis in recipient cells[33, 206-217]. However, the results presented here are also contradictory to reports which demonstrate that cancer cell-derived EVs promote recipient cell migration and invasion[228, 232, 233, 440]. Opposing roles of EVs in tumorigenesis have previously been reported; for example, in oesophageal cancer cells, exposure to autologous EVs inhibited cell proliferation, but enhanced cell migration[527]. Again, this could be indicative that TRPC3 activation influences the release of a specific EV subpopulation. Functional analyses of two EV subpopulations by Lee *et al.*[526] revealed that one population enhanced the proliferation of human cell cultures, whilst the other had no effect on proliferation, but enhanced exosome production. Together, these findings suggest that TPRC3 activation induces the release of a subpopulation of EVs that possess the functional capacity to increase the growth rate of recipient SKOV3 cells, suggesting a novel role for TRPC3-mediated EV communication in the progression of OC.

A key question that arises from these results is *how* TRPC3 activator-induced EVs promote OC cell growth. Here, two possible mechanisms were investigated. Firstly, it was hypothesised that functional TRPC3 channels and potentially an upstream GPCR mGluR1 may be incorporated into

SKOV3-EVs and transferred to the membrane of recipient cells, as reported for EV-mediated transfer of TRPC5 from chemoresistant breast cancer cells[112]. In this study, uptake of TRPC5-containing EVs increased TRPC5 expression and Ca^{2+} influx in recipient chemosensitive cells. Therefore, intercellular transfer of TRPC3/mGluR1 may likewise increase Ca^{2+} influx in recipient SKOV3 cells leading to Ca^{2+}-driven cell proliferation. Preliminary results supported this hypothesis, with tangible evidence from western blots, TEM and Exoview technology to suggest that TRPC3 and mGluR1 are present in SKOV3-EVs. Of note, this analysis was conducted on endogenous EVs, and should therefore be repeated on TRPC3-activator induced EVs. In order to validate this hypothesis a number of additional experiments are required, including the analysis of EV uptake by recipient cells. Lipid binding dyes such as PKH67 and PKH26 could be employed to label EVs and quantitate their uptake through confocal microscopy or flow cytometry analysis. Subsequently, the expression and functional activity of TRPC3 should be assessed in recipient cells before and after the addition of TRPC3 activator-induced EVs. This could be achieved by western blot to assess TRPC3 expression, and an NFAT assay - as employed in this thesis - to analyse changes in Ca^{2+} signalling.

The second proposed mechanism by which TRPC3 activator-induced EVs may increase recipient SKOV3 cell growth is through transfer of their metastatic cargo. Therefore, the proteomic cargo of TRPC3 activator-induced EVs was analysed by label-free mass spectrometry to provide some insight into what proteins may be deregulated in TRPC3 activator-induced EVs, and confer greater proliferative potential to recipient SKOV3 cells. This analysis identified a number of upregulated Ca^{2+}-binding proteins in TRPC3 activator-induced EVs that are abnormally expressed in different cancer types including OC, and implicated in mediating tumour growth, migration and invasion. These included TPM4, S100A4, and NUCB1. In addition, the non-receptor protein tyrosine kinase and proto-oncogene YES1 was significantly upregulated in TRPC3 activator-induced EVs compared to the DMSO control population. YES1 is explicitly implicated in regulating cell growth, survival, apoptosis and cell cycle progression in a number of cancer types, and is therefore an attractive therapeutic target[528-532]. According to both the ExoCarta and Vesiclepedia databases (accessed March 2022), YES1 has not been identified in EVs derived from any cancer cell line or biofluid, suggesting the upregulation of YES1 in EVs is specific to upregulated TRPC3 activity, and therefore poses as a potential mediator of recipient SKOV3 cell growth. A potent YES1 inhibitor CH6953755 developed by Hamanaka *et al.*[533] inhibited cell growth in YES1-amplified cancers *in vitro* and *in vivo,* and could therefore be employed in this study to inhibit YES1 in both parental and recipient SKOV3 cells to test the hypothesis that YES1 mediates TRPC3 activator-induced SKOV3 proliferation.

In further support of the enriched metastatic cargo of TRPC3 activator-induced EVs, GO term analysis of upregulated protein expression returned molecular function and cell component terms associated with cell proliferation, motility and migration. In contrast, terms related to the negative regulation of cancer dissemination and metastasis were under-represented in TRPC3 activator-induced EVs, including 'negative regulation of endopeptidase activity', 'negative regulation of peptidase activity' and 'negative regulation of proteolysis'. Proteomic analysis of other cancer cell-derived EVs identified peptidase and endopeptidase inhibitors such as tissue inhibitor of metalloproteinases (TIMP) 1/2/3, which reduced the invasiveness of recipient cells[20, 534-536]. The under-representation of these terms in TRPC3 activator-induced EVs suggests that conversely, upregulated TRPC3 activity decreases the loading of these proteins into EVs, enhancing their metastatic capacity. Although TRPC3 activator-induced EVs did not increase the invasiveness of recipient SKOV3 cells in this thesis, further analysis of their proteolytic activity through a zymography assay, or collagen degradation assay, could validate these findings.

Collectively, proteomic analysis suggests that TRPC3 activation modulates EV cargo, overall increasing their metastatic capacity. To validate if the intercellular transfer of this metastatic cargo is responsible for increasing recipient SKOV3 cell growth, a number of additional experiments are required. Firstly, the results of the proteomic analysis need to be confirmed by western blot, or through more advanced multiplex techniques such as the Exoview platform. Cellular expression of these proteins should also be assessed, as this will indicate whether TRPC3 activation deregulates protein expression specifically in EVs, or if EVs capture upregulated metastatic pathways in TRPC3 activator treated cells. In addition, uptake of TRPC3 activator-induced EVs by recipient cells needs to be confirmed, potentially through labelling EVs with lipid binding dyes and quantifying their uptake by confocal microscopy or flow cytometry analysis. Similarly, specific cargo proteins identified by proteomic analysis could be fluorescently labelled, and their uptake by recipient cells assessed. These experiments will potentially validate a novel role for TRPC3-mediated EV communication in OC growth.

7.3. HISTAMINE AND Ca^{2+} IN OC EV BIOGENESIS

In this thesis, histamine and the Ca^{2+} ionophore ionomycin were employed as well-established inducers of EV biogenesis to validate TIRF imaging and analysis protocols. This analysis revealed for the first time that both histamine and ionomycin increase MVB-PM fusion in OC cells. Previous analysis of histamine and Ca^{2+}-induced EV release in additional cancer cell lines suggest that they stimulate EV biogenesis through two distinct signalling pathways. In breast carcinoma cells, ionomycin induced MVB-PM fusion through a Ca^{2+}-dependent MVB trafficking pathway

involving Rab11 and the Rab binding protein Munc13-4[144]. Conversely, histamine stimulation induced MVB-PM fusion in HeLa cells through GPCR signalling from the histamine H_1 receptor (H1HR), and subsequent phosphorylation of SNAP23 via the H1HR–$G\alpha_q$–PKC pathway[82]. The authors suggested that histamine-induced MVB-PM fusion was not mediated by Ca^{2+} signalling downstream of H1HR stimulation as intra- and extracellular Ca^{2+} chelators had no effect on the rate of MVB-PM fusion. However, these chelators were employed independently, therefore it cannot be excluded that in response to intracellular Ca^{2+} chelation, Ca^{2+} entry at the PM was upregulated thus inducing EV release, and vice versa. Here, ionomycin, histamine and TRPC3 activation increased Ca^{2+} signalling and MVB-PM fusion in SKOV3 cells, suggesting that Ca^{2+} signalling may underly all three mechanisms of EV biogenesis. TIRF imaging of CD81-pHluorin could be combined with fluorescent Ca^{2+} indicators to analyse in real-time, how intracellular Ca^{2+} concentrations fluctuate in response to histamine, ionomycin and TRPC3 activation, and how this coincides with MVB-PM fusion events.

In addition, evidence presented in this thesis suggests that TRPC3 may mediate histamine-induced MVB-PM fusion in SKOV3 cells, as inhibiting TRPC3 attenuated histamine-stimulated Ca^{2+} entry and subsequent MVB-PM fusion. This is in line with previous studies that demonstrate TRPC3 is activated downstream of histamine H_1 and H_2 GPCRs and facilities histamine-induced Ca^{2+} entry, albeit in other cell lines[305, 364]. This proposes that histamine and TRPC3 activator-induced EV biogenesis may represent a shared, Ca^{2+}-dependent pathway, mediated by H_1/H_2HR-TRPC3-phosphatidylinositol signalling (Figure 7.1). Indeed, proteomic analysis of histamine and TRPC3 activator-induced EVs revealed a significant overlap in GO biological process terms, and induced fusion event types were similar by TIRF microscopy (larger, and dimmer than basal fusion), supporting the notion of a shared, inducible signalling pathway. Further investigation is required to determine the exact histamine GPCR involved, potentially by knocking down each receptor and analysing ensuing effects on histamine-induced MVB-PM fusion. Likewise, inhibitors against PKC and the IP_3 receptor could be employed to elucidate the downstream signalling pathway at play. In addition, the proteomic analysis conducted here characterised for the first time the effect of histamine and ionomycin stimulation on EV protein cargo. This analysis identified a number of candidate proteins which, following validation, could contribute to a growing body of work on GPCR and Ca^{2+} signalling in EV biogenesis. For example, histamine-induced EVs were enriched for CD81 and NDPKs which interact with and regulate GPCR signalling[473, 490], and ionomycin-induced EVs were enriched for ALG-2, syndecan-4 and syntenin-1, suggesting Ca^{2+}-regulated EV biogenesis is mediated through the syndecan-syntenin-ALIX axis[73, 150]. Further to their potential role in EV biogenesis, the upregulated proteomic cargo of

histamine and ionomycin-induced EVs may be significant to the development of OC. In both breast and ovarian cancer cells, disturbances to cellular Ca^{2+} homeostasis induced the release of EVs with enhanced metastatic competence[144, 167]; capable of increasing cell invasion, adhesion and migration. Although outside the scope of this thesis, mining the upregulated protein cargo of histamine and ionomycin-induced EVs for metastasis-related proteins, and analysing functional effects on recipient SKOV3 cells, may reveal novel roles for histamine and Ca^{2+}-mediated EV release in OC progression.

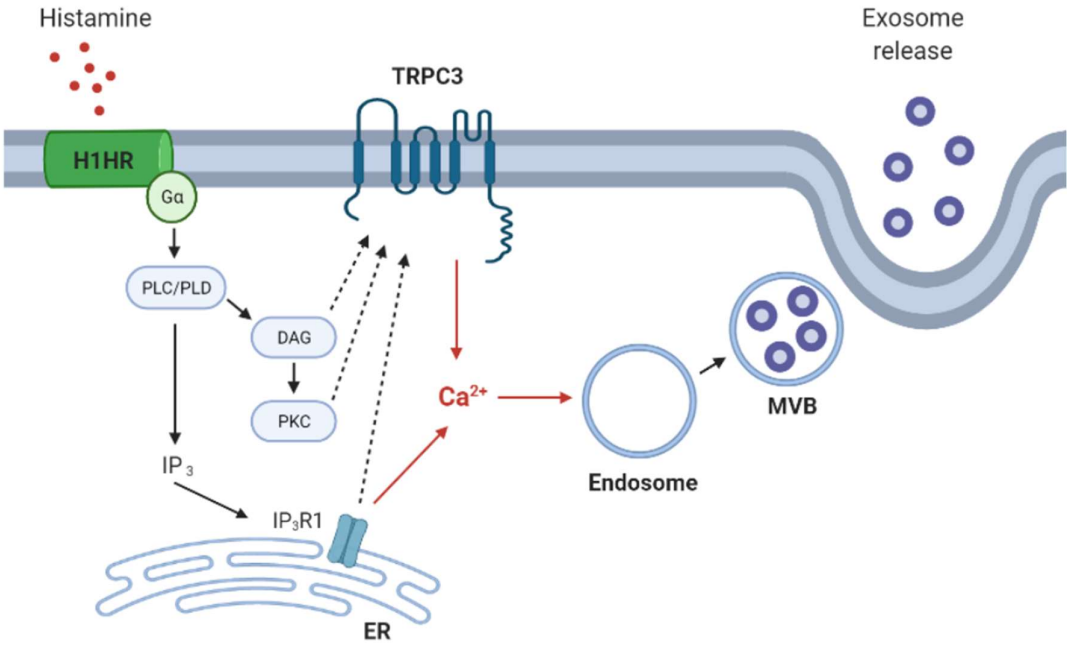

Figure 7.1 Proposed model of TRPC3-mediated EV biogenesis

GPCR stimulation, potentially of histamine receptor H1HR, initiates the phosphatidylinositol signalling pathway via Gα protein: activated PLC cleaves PIP2 into DAG and IP_3. IP_3 subsequently binds to its receptor IP3R1 in the endoplasmic reticulum (ER), stimulating the release of Ca^{2+} which in turn induces EV biogenesis. TRPC3 can be regulated downstream of GPCR stimulation by DAG, input from IP3R1 and inhibitory phosphorylation by PKC (dashed lines).

7.4. FUTURE DIRECTIONS AND NOVEL CONTRIBUTIONS

The work presented in this thesis provides a novel contribution to our understanding of the molecular mechanisms and dynamics which underly EV biogenesis, mainly identifying a novel role for TRPC3-mediated EV biogenesis in OC. The conclusions drawn in this thesis are based on the analysis of a single OC cell line, therefore to confirm if these findings translate to heterogenous *in vivo* ovarian tumours, this analysis should be repeated in additional OC cell lines, or potentially an *in vivo* mouse model. Further work is required to validate if the effects of

pharmacological modulators reported herein are specifically due to deregulated TRPC3 activity, and the potential contribution of other TRPC channels, namely the highly related TRPC6, should be investigated. This could be achieved by employing siRNA-mediated knockdowns, or CRISPR/Cas9 knockouts, against TRPC3 and other TRPC channels and assessments of pharmacological activation/inhibition repeated. These results could support the pharmaceutical potential of TRPC3 inhibition by Pyr3 in treatment of TRPC3-related disease, including OC. Moreover, this project could be extended by characterising the pathways which act downstream of TRPC3 activation in OC growth, migration and EV biogenesis, as well as additional metastatic mechanisms in OC. And lastly, validation of the vast proteomic analysis conducted in this work could yield novel insights into the biological processes and contributing molecules that underlie EV biogenesis, and EV-mediated communication in OC. Hopefully the data presented here will serve as a basis for future hypothesis generation, leading to significant advances in the EV field.

Finally, the novel contributions of this thesis are:

- TRPC3 mediates Ca^{2+} signalling in SKOV3 cells and contributes to cell growth and migration, but does not regulate cell invasion
- Histamine, ionomycin and TRPC3 activation stimulate the biogenesis of MVB-derived EVs with distinct characteristics and fusion dynamics, including localised and synchronised EV release
- TRPC3-mediated EV release promotes recipient SKOV3 cell growth potentially through transfer of their metastatic cargo, but bears no effect on cell migration or invasion
- Inhibiting TRPC3 attenuates histamine-stimulated Ca^{2+} entry and MVB-PM fusion, indicating that TRPC3 is activated downstream of histamine GPCRs in SKOV3 cells
- CD81 and NDPKs, and Ca^{2+}-dependent interactions with the syndecan-syntenin-ALIX axis, may contribute to histamine and ionomycin-induced EV release, respectively
- EV-depleted FBS retains high concentrations of bovine particles detectable by common EV assays
- Short-term exposure to low concentrations of DMSO can influence the secreted proteome

Supplementary materials

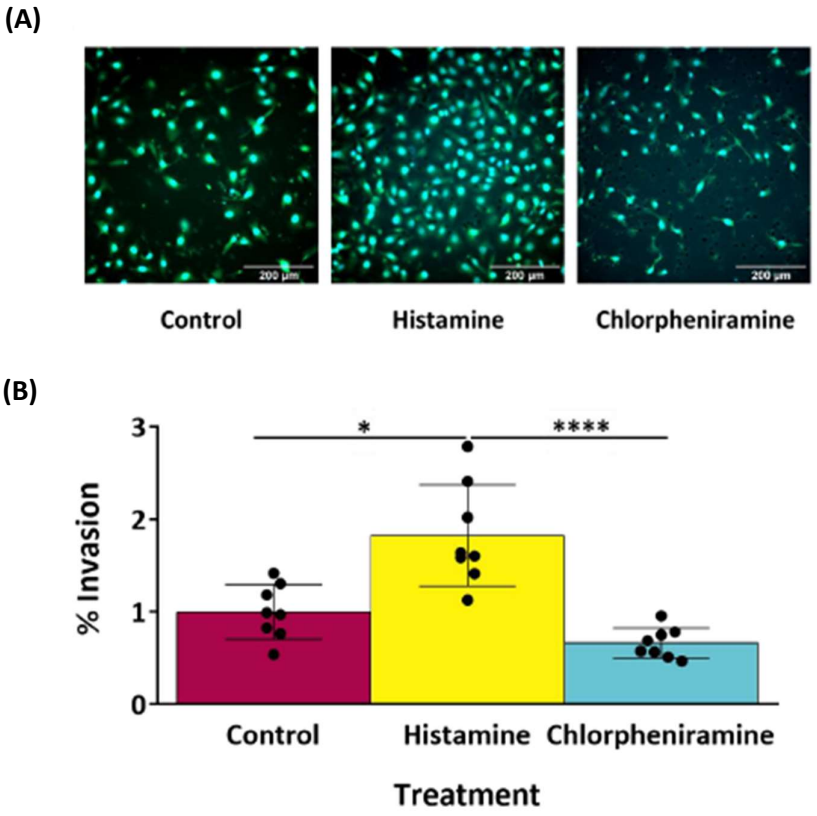

Supplementary Figure 1. Matrigel® assay of histamine-induced SKOV3 invasion

(A) *Representative images of Matrigel® membranes used for quantifying SKOV3 invasion. Cells were stained with DAPI (blue) and CFSE (green). Scale bare 200µm.* ***(B)*** *Percentage of invasion was calculated for SKOV3 control, treated with histamine or chlorpheniramine (anti-histamine). Two independent experiments were combined, each one with four technical replicates. Kruskal-Wallis test followed by Dunn's correction was used for statistical analysis. Error bars 1X SD; *P<0.05, ****P<0.0001. Work conducted by Dr Emanuela Carollo.*

(A)

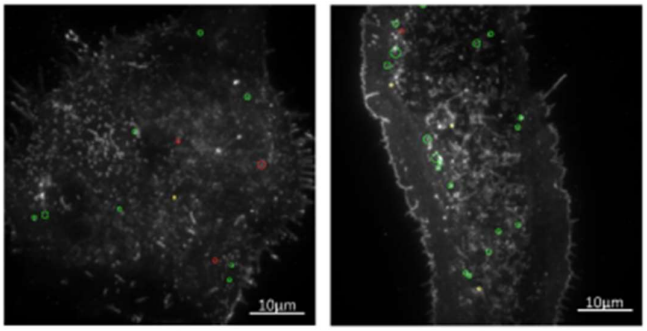

(B)

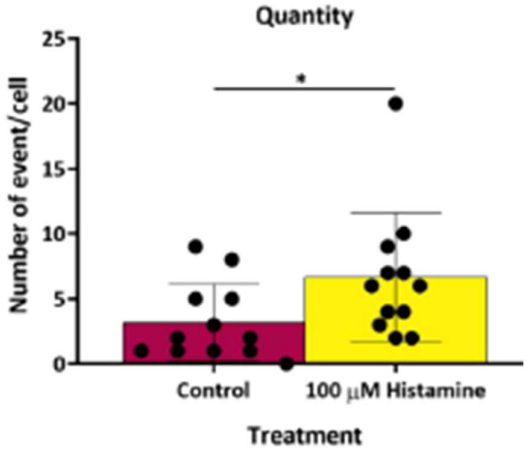

Supplementary Figure 2. Quantification of histamine-induced MVB-PM fusion using the AMvBE analysis plug-in

(A) *Representative images of total projected MVB-PM fusion events in control cell (left) and histamine treated cell (right). Positive events detected by the plug-in are circled in green; yellow and red circles indicate events that did not satisfy one or more parameters determined by the plug-in, respectively. Scale bar 10µm.* ***(B)*** *Quantity of CD81 MVB-PM fusion events per cell in cells treated with control media or 100µM histamine (n=12), as determined by AMvBE analysis. Statistical differences were calculated with the Mann-Whitney test. Error bars, 1X SD. * P<0.05. Analysis conducted by Dr Emanuela Carollo.*

(A)

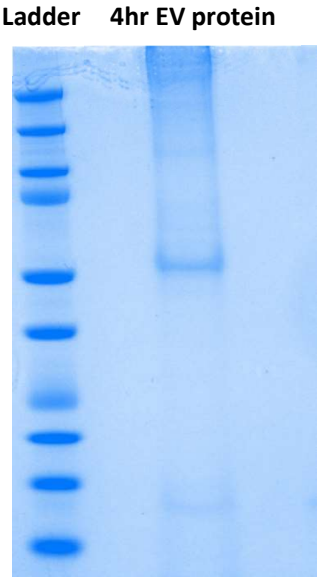

(B)

Sample	Protein conc. (µg/µl)	Conc. in 40µl sample (µg)
4hr EV	0.75	30

Supplementary Figure 3. Coomassie stain and micro-BCA quantification of EV protein from SKOV3 cells conditioned for 4hrs in serum-free media

(A) *Coomassie stain showing protein ladder and EV protein collected from SKOV3 cells after 4hrs conditioning in serum-free media. EVs concentrated to 20µl in PBS, and lysed in 20µl RIPA, total sample volume 40µl. 27µl sample loaded to blot. Coomassie stain with Pierce Imperial™ Protein Stain, Thermo Scientific. Performed according to manufacturer's protocol.* ***(B)*** *Quantification of EV protein sample shown in (A) with micro-BCA assay: Thermo Scientific™ Pierce Micro BCA Protein Assay. Performed according to manufacturer's protocol.*

Gene symbol	Number of times identified (ExoCarta)	Identified in EV sample				
		Untreated	DMSO	Histamine	Ionomycin	Activator
PDCD6IP	399	X	X	X	X	X
GAPDH	377	X	X	X	X	X
HSPA8	363	X	X	X	X	X
ACTB	350	X	X	X	X	X
ANXA2	337	X	X	X	X	X
CD9	328	X	X	X	X	X
PKM	327	X	X	X	X	X
HSP90AA1	327	X	X	X	X	X
ENO1	327	X	X	X	X	X
ANXA5	313	X	X	X	X	X
HSP90AB1	306	X	X	X	X	X
CD63	306				X	X
YWHAZ	301	X	X	X	X	X
YWHAE	300	X	X	X	X	X
EEF1A1	295					
PGK1	291	X	X	X	X	X
CLTC	283	X	X	X	X	X
PPIA	278	X	X	X	X	X
SDCBP	277	X	X	X	X	X
ALDOA	275	X	X	X	X	X
EEF2	274	X	X	X	X	X
ALB	274					
TPI1	270	X	X	X	X	X
VCP	269	X	X	X	X	X
CFL1	268	X	X	X	X	X
MSN	266	X	X	X	X	X
ATP1A1	266	X	X	X	X	X
PRDX1	263	X	X	X	X	X
MYH9	262	X	X	X	X	X
EZR	262	X	X	X	X	X
CD81	262	X	X	X	X	X
ANXA6	260	X	X	X	X	X
FLOT1	259	X	X	X	X	X
YWHAB	258	X	X	X	X	X
LDHB	258	X	X	X	X	X
SLC3A2	257	X	X	X	X	X
GNB1	257	X	X	X	X	X
PFN1	256	X	X	X	X	X
TSG101	255	X	X	X	X	X
YWHAQ	254		X	X	X	X
GNAI2	252	X	X	X	X	X
CLIC1	251	X	X	X	X	X
ANXA1	251	X	X	X	X	X
ITGB1	250	X	X	X	X	X
LDHA	249	X	X	X	X	X
FASN	248	X	X	X	X	X
CDC42	248			X	X	X
RAP1B	242	X	X	X	X	X
CCT2	242	X	X	X	X	X
YWHAG	240	X	X	X	X	X
GNB2	240					

Gene symbol	Number of times identified (ExoCarta)	Identified in EV sample				
		Untreated	DMSO	Histamine	Ionomycin	Activator
ACTN4	240	X	X	X	X	X
RAB5C	239	X	X	X	X	X
C3	239	X	X	X	X	X
RAB10	236	X	X	X	X	X
HIST1H4A	234	X	X	X	X	X
KRT1	233					
FN1	233	X	X	X	X	X
AHCY	233	X	X	X	X	X
A2M	232				X	
BSG	230	X	X	X	X	X
ACTN1	229	X	X	X	X	X
ANXA7	228	X	X	X	X	X
ACLY	228	X	X	X	X	X
HIST1H4B	227					
GDI2	227	X	X	X	X	X
FLNA	227	X	X	X	X	X
UBA1	226	X	X	X	X	X
GNAS	226	X	X	X	X	X
GSN	225				X	
CCT4	225	X	X	X	X	X
RAN	222	X	X	X	X	X
PRDX2	222	X	X	X	X	X
RHOA	220	X	X	X	X	X
CCT3	220	X	X	X	X	X
RAC1	219					
LGALS3BP	219	X	X	X	X	X
TCP1	218	X	X	X	X	X
KRT10	218					
CAP1	218	X	X	X	X	X
RAB7A	217	X	X	X	X	X
TUBB4B	216	X	X	X	X	X
HSPA5	215	X	X	X	X	X
IQGAP1	214	X	X	X	X	X
GPI	214	X		X		X
RALA	213	X		X	X	
KPNB1	212	X	X	X	X	X
HIST1H4I	212					
TFRC	211	X	X	X	X	X
EIF4A1	211	X	X	X	X	X
HIST4H4	210					
CCT8	210	X	X	X	X	X
TLN1	209	X	X	X	X	X
HIST1H4K	209					
HIST1H4H	209					
CCT6A	209	X	X	X	X	X
ANXA11	209	X	X	X	X	X
HIST1H4J	208					
HIST1H4F	208					
HIST1H4D	208					
	Total:	**81**	**80**	**83**	**85**	**83**

Supplementary Figure 4. Top 100 EV proteins identified in proteomic samples

*List of top 100 proteins that are most commonly identified in EVs through mass-spec, sorted by occurrence. EV sample groups labelled with **'X'** if protein is present. List obtained from ExoCarta, accessed November 2021 from: http://exocarta.org/exosome_markers_new*

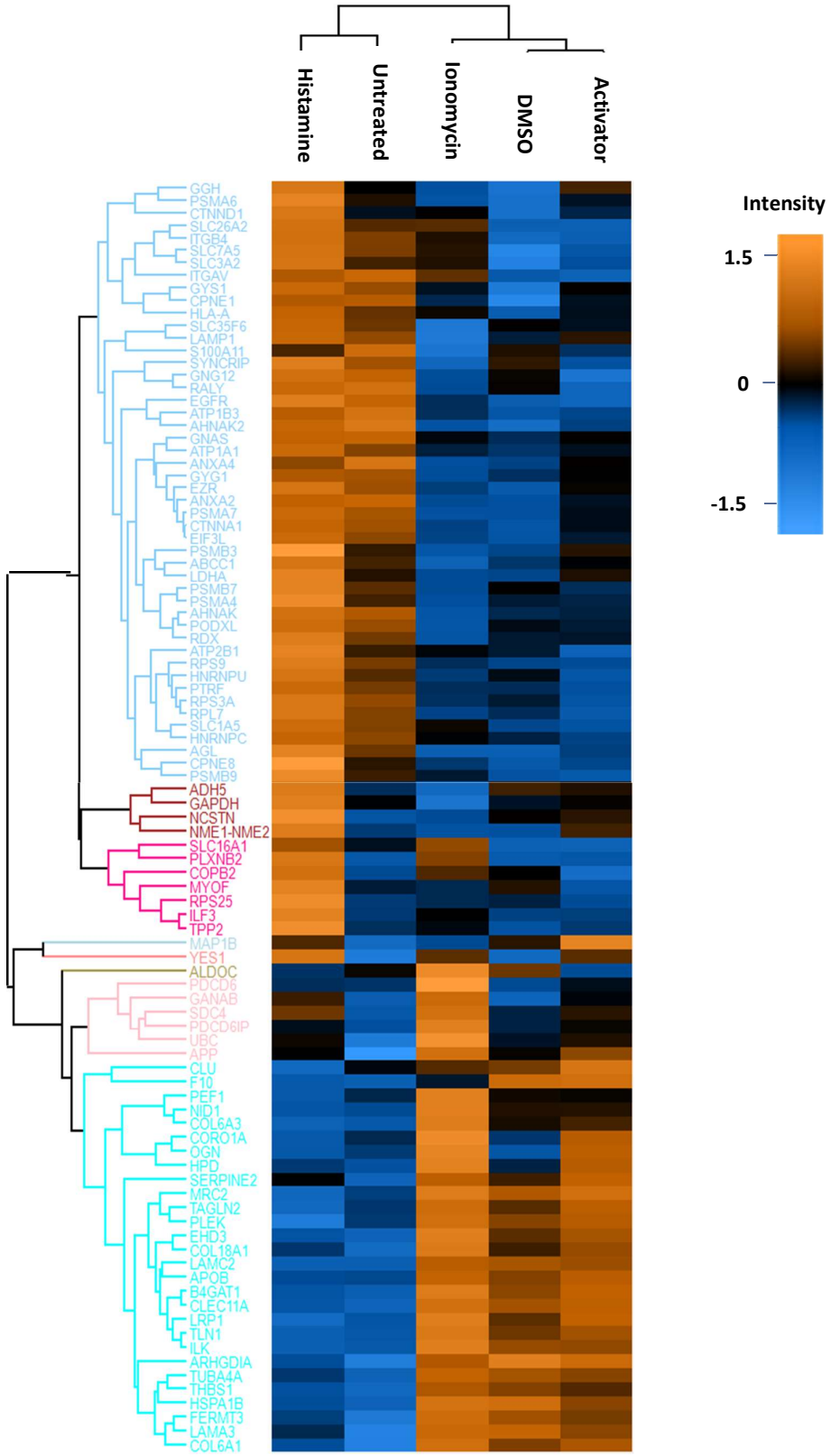

Supplementary Figure 5. Hierarchical clustering of EV proteomic samples

Hierarchical clustering of EV proteomic biological replicates, grouped by treatment. All differentially expressed proteins shown. Euclidean distance measure. Generated with Perseus software (v1.6.14.0).

(A) Upregulated proteins in histamine-induced EVs

Gene names	Fold change	p-value
CD81	6.60	1.05E-01
CPNE8	5.74	9.10E-03
RPL13a;RPL13A;RPL13AP3	5.71	6.41E-02
ILF2	5.52	5.84E-03
EEA1	5.10	5.21E-02
EIF3B	4.94	8.74E-03
SDC4	4.70	7.38E-02
NME1-NME2;NME2;NME2P1;NME1	4.51	5.47E-03
RPL36	4.27	9.18E-02
UBR4	4.12	9.49E-02
AGL	4.04	1.05E-01
YWHAQ	3.88	1.53E-02
COPB2	3.83	8.05E-03
LGALS1	3.79	2.06E-01
NT5E	3.77	1.03E-01
PYGB	3.74	1.02E-01
APP	3.72	6.27E-02
COL12A1	3.69	1.25E-01
TPP2	3.61	2.26E-03
RPS14	3.42	1.53E-01
PRKDC	3.33	2.19E-01
ITGA6	3.32	1.13E-01
PSMC6	3.30	2.95E-02
ILF3	3.30	7.46E-02
CAD	3.27	4.19E-02
PSMB9	3.25	5.15E-02
YES1	3.20	3.00E-03
LOXL2	3.20	1.32E-01
MYOF	3.16	3.75E-02
PTK7	3.15	3.73E-02
KDELR2	3.14	4.37E-02
MAP1B	3.13	4.08E-02
CD9	3.12	9.26E-02
ACTR3	3.05	1.53E-01
HUWE1	2.94	4.55E-02
CD44	2.83	9.26E-02
SERPINE2	2.79	1.05E-01
CD70	2.78	6.64E-02
NCSTN	2.78	3.12E-02
NTN4	2.76	6.87E-02
APLP2	2.74	8.65E-02
TRIM28	2.73	2.03E-01
HNRNPU	2.72	9.67E-02
PSMD1	2.72	1.08E-01
RPS25	2.65	2.97E-02
RPS6	2.63	2.49E-01
EIF3A	2.61	1.66E-01
COL4A2	2.57	1.75E-01
PSM8;PSMB8	2.56	1.33E-01
EIF3F	2.56	1.60E-01
FLNB	2.56	1.48E-01
FERMT3	2.55	3.24E-01
CD47	2.55	2.03E-01
TFRC	2.55	2.79E-01
TKT	2.53	9.81E-02
GGH	2.52	3.49E-02

(B) Downregulated proteins in histamine-induced EVs

Gene names	Fold change	p-value
MYL12A;MYL12B;MYL9	0.47	4.04E-01
PFN1	0.47	2.27E-01
TGM3	0.45	3.93E-01
PLEK	0.44	1.39E-01
FABP5	0.44	5.24E-01
HIST1H4A	0.42	2.97E-01
CSTA	0.40	3.12E-01
HIST1H2AJ;HIST1H2AH;H2AFJ;HIST1H2AG;HIST1H2AD;HIST1H2AB;HIST3H2A;HIST1H2AC	0.40	2.63E-01
HIST1H2BN;HIST1H2BL;HIST1H2BM;HIST1H2BH;HIST2H2BF;HIST1H2BC;HIST1H2BD;H2BFS;HIST1H2BK;HIST1H2BA	0.39	3.19E-01
FAM129B	0.38	1.02E-01
CASP14	0.37	2.21E-01
S100A8	0.37	3.90E-01
LTF	0.34	2.66E-01
S100A16	0.33	1.26E-01
SFN	0.33	3.47E-01
TGM1	0.31	1.59E-01
CLIC1	0.30	1.61E-01
S100A9	0.28	1.85E-01
S100A7	0.28	3.01E-01
C3	0.25	1.88E-01
IGHG1;IGHG3	0.24	1.63E-01
IGHA1	0.22	1.51E-01
SERPINB3	0.15	1.52E-01

(A) Cont.

PDIA3	2.52	1.92E-01
EEF1G	2.52	9.83E-02
WDR1	2.50	2.16E-01
COL6A1	2.46	2.77E-01
UGDH	2.46	2.05E-01
GNA11	2.45	2.59E-01
CSF1	2.43	8.22E-02
ACLY	2.42	1.07E-01
COPA	2.41	2.60E-01
FLOT2	2.39	3.28E-01
ACTC1;ACTG2;ACTA2;ACTA1	2.39	4.45E-01
LMAN2	2.39	1.18E-01
DDB1	2.38	2.31E-02
ADAM10	2.37	2.24E-01
GANAB	2.36	1.26E-01
S100A6	2.35	3.56E-01
RPS13	2.34	1.94E-01
SLC2A1	2.34	2.44E-01
UBA1	2.33	1.49E-01
EPB41L2	2.33	7.77E-02
NPM1	2.33	2.32E-01
RPS15A	2.33	6.50E-02
RPL21	2.32	2.21E-01
PSMB5	2.31	9.12E-02
KIAA0368;ECM29	2.30	8.17E-02
PSMD6	2.29	2.55E-01
NID2	2.29	3.64E-01
RPS11	2.26	2.66E-01
NUCB1	2.25	2.53E-01
EPHX1	2.23	2.86E-01
CLDN1	2.23	3.70E-01
SERPINH1	2.22	2.67E-01
PGAM1	2.21	2.44E-01
ABCC1	2.21	7.56E-02
STARD3	2.20	2.42E-01
PAICS	2.19	4.57E-02
GNAI3	2.17	3.39E-01
COL4A1	2.17	1.64E-01
ACTN4	2.13	6.91E-02
TPM4	2.13	2.40E-01
ATP2B1	2.12	1.22E-01
SLC26A2	2.12	2.48E-02
ATP1B1	2.12	2.59E-01
PFKP	2.12	1.41E-01
HLA-B	2.12	3.93E-01
CALR	2.11	2.37E-01
PSMB2	2.11	4.36E-01
PSMB6	2.10	6.60E-02
ALCAM	2.07	7.73E-02
ACTN1	2.05	1.18E-01
DYNC1H1	2.05	3.30E-01
KTN1	2.05	2.89E-01
VARS	2.05	1.34E-01
SET;SETSIP	2.04	3.33E-01
ACTR1B	2.03	3.00E-01
IPO7	2.02	1.43E-01

Supplementary Figure 6. All proteins up-or down-regulated by 2-fold in histamine-induced EVs

(A) *Gene names for all proteins identified with a fold change ≥ 2 and* ***(B)*** *with a fold change ≤ 0.5 (LFQ intensity histamine – LFQ intensity untreated), with corresponding fold change and p-value. Proteins sorted by fold change value.*

(A) Upregulated proteins in ionomycin-induced EVs

Gene names	Fold change	p-value
PDCD6	11.52	2.82E-02
OGN	10.64	6.95E-04
GANAB	5.07	5.40E-02
HIST1H2BN;HIST1H2BL;HIST1H2BM;HIST1H2BH;HIST2H2BF;HIST1H2BC;HIST1H2BD;H2BFS;HIST1H2BK;HIST1H2BA	4.84	1.34E-01
SET;SETSIP	4.27	1.04E-01
PLOD1	4.22	1.41E-01
SDC4	4.07	3.58E-02
CORO1A	3.98	6.38E-02
ANXA11	3.85	4.12E-01
IST1	3.75	8.52E-02
AGRN	3.63	3.70E-01
PEF1	3.32	1.59E-01
HBA1	3.30	5.80E-01
SLC16A1	3.26	3.78E-02
ADAM10	3.13	5.24E-02
SDCBP	3.12	1.83E-02
CPNE3	3.06	2.76E-01
NUCB1	3.02	1.59E-01
CD9	2.96	3.03E-01
PTGFRN	2.90	2.19E-01
PDCD6IP	2.89	1.06E-01
B4GAT1	2.83	3.36E-01
COL6A2	2.82	1.26E-01
ANPEP	2.80	3.86E-01
HPD	2.79	1.63E-01
EPHA2	2.64	1.38E-01
NAP1L1	2.64	1.69E-01
UBC;UBB;RPS27A;UBA52	2.58	6.63E-03
ACTR1B	2.57	1.86E-01
NTN4	2.57	3.60E-01
RPS27	2.55	2.43E-01
BSG	2.52	3.79E-02
RPL11	2.52	2.16E-01
ACTC1;ACTG2;ACTA2;ACTA1	2.50	6.59E-01
ASS1	2.48	1.73E-01
TOM1L1	2.47	5.85E-02
SLC1A5	2.44	1.11E-01
CD81	2.43	5.91E-02
CD70	2.41	2.98E-01
SERPINH1	2.33	3.22E-01
PRKDC	2.32	4.33E-01
CD44	2.31	6.11E-02
RPS15A	2.28	2.19E-01
CPNE8	2.28	2.30E-01
ALDOC	2.27	1.94E-02
CPNE2	2.25	2.15E-01
TSG101	2.23	1.35E-01
SLC3A2	2.23	3.64E-02
NPM1	2.23	3.65E-01
NT5E	2.21	2.79E-01
PSMD11	2.20	4.14E-01
SLC7A5	2.19	8.07E-02
UBR4	2.17	2.00E-01
TFRC	2.16	2.63E-01
APP	2.14	1.91E-01

(B) Downregulated proteins in ionomycin-induced EVs

Gene names	Fold change	p-value
RPS14	0.50	2.07E-01
EPB41L2	0.49	4.71E-01
LTF	0.49	3.77E-01
AGL	0.48	4.26E-01
PDIA3	0.48	3.33E-01
CLTB	0.48	4.07E-02
RPL18A	0.47	4.40E-01
EEF2	0.46	3.48E-01
TPI1	0.45	1.75E-01
S100A6	0.43	3.97E-01
DSG1	0.43	2.48E-01
LCN1	0.42	3.36E-01
CAT	0.42	1.39E-01
SLC35F6	0.42	1.52E-01
MVP	0.40	2.67E-01
F10	0.40	5.47E-01
TGM1	0.40	4.03E-01
AZGP1	0.40	3.63E-01
RAB6A;RAB6B	0.38	3.92E-01
PRDX2	0.38	8.65E-02
TXN	0.38	2.45E-01
CDSN	0.37	1.30E-01
S100A8	0.37	5.37E-01
LAMP1	0.35	2.77E-01
RPL13	0.35	2.95E-01
CLTA	0.33	1.29E-01
ATP5A1	0.33	4.52E-02
LGALS7	0.31	2.38E-01
SERPINB12	0.29	9.90E-02
S100A9	0.27	2.87E-01
DCD	0.26	2.31E-01
S100A11	0.25	1.46E-01
CASP14	0.24	1.93E-01
PNP	0.22	1.38E-02
JUP	0.22	6.15E-02
S100A7	0.18	2.70E-01
SFN	0.18	2.13E-01
HSPB1	0.17	7.38E-02
DSP	0.17	3.69E-02
TGM3	0.14	1.55E-01
IGHG1;IGHG3	0.13	1.48E-01
CSTA	0.13	1.25E-01
DSC1	0.12	1.44E-01
ARG1	0.11	1.41E-02
PKP1	0.10	1.04E-01
FABP5	0.08	4.40E-02
SERPINB3	0.05	1.16E-01

(A) Cont.

S100A4	2.13	3.81E-01
APLP2	2.08	3.45E-01
COL4A2	2.07	1.33E-01
YES1	2.07	1.47E-02
AKR1A1	2.06	3.01E-01
ACHE	2.05	2.60E-01
XPO1	2.04	2.69E-01
PIP	2.01	4.67E-01
RPL21	2.01	5.87E-01
MAPRE2	2.00	4.09E-01

Supplementary Figure 7. All proteins up-or down-regulated by 2-fold in ionomycin-induced EVs

(A) *Gene names for all proteins identified with a fold change ≥ 2 and* ***(B)*** *with a fold change ≤ 0.5 (LFQ intensity ionomycin – LFQ intensity DMSO), with corresponding fold change and p-value.*
Proteins sorted by fold change value.

(A) Upregulated proteins in TRPC3 activator-induced EVs

Gene names	Fold change	p-value
SET;SETSIP	6.24	7.79E-02
ACTC1;ACTG2;ACTA2;ACTA1	5.09	2.63E-01
AGRN	4.64	3.06E-01
OGN	4.59	5.47E-02
RPL34	4.29	9.51E-02
GYS1	4.26	2.87E-01
NPM1	3.95	8.40E-02
PSMB6	3.72	1.62E-01
ACTR1B	3.60	3.64E-02
NUCB1	2.99	4.12E-02
NT5E	2.94	1.63E-01
HSPA4	2.80	1.72E-01
NAP1L1	2.79	1.17E-01
ATP1B1	2.79	1.64E-01
B4GAT1	2.76	2.30E-01
H3F3B;H3F3A;HIST2H3A;HIST3H3;HIST1H3A	2.65	4.08E-01
S100A4	2.63	2.20E-01
FLOT1	2.62	2.33E-01
TPM4	2.58	4.30E-02
NME1-NME2;NME2;NME2P1;NME1	2.56	6.66E-02
CORO1A	2.50	1.71E-01
EHD4	2.48	1.05E-03
GPC1	2.45	2.23E-01
GGH	2.33	1.47E-01
RPS23	2.31	2.30E-02
ARPC2	2.20	1.49E-01
ANPEP	2.19	5.90E-01
PIP	2.19	4.40E-01
WDR1	2.17	2.83E-01
APLP2	2.12	6.56E-02
HIST1H2BN;HIST1H2BL;HIST1H2BM;HIST1H2BH;HIST2H2BF;HIST1H2BC;HIST1H2BD;H2BFS;HIST1H2BK;HIST1H2BA	2.10	3.93E-01
RPL27A	2.09	4.13E-01
LRP1	2.08	2.59E-01
PLOD1	2.06	3.00E-01
YES1	2.06	3.80E-02
RRAS2	2.03	4.59E-01
EPHA2	2.02	2.82E-01
ACTR3	2.01	3.68E-01

(B) Downregulated proteins in TRPC3 activator-induced EVs

Gene names	Fold change	p-value
SERPINB12	0.50	1.91E-01
RPL18	0.48	1.24E-01
RHOA	0.47	2.59E-01
RPL21	0.46	4.74E-01
TPI1	0.44	3.18E-01
TGM3	0.42	2.82E-01
CKB	0.41	2.37E-01
HNRNPC	0.41	3.15E-01
JUP	0.40	1.56E-01
C1QTNF3-AMACR;C1QTNF3	0.38	2.29E-01
IGHA1	0.38	3.69E-01
BSG	0.37	5.97E-01
PNP	0.33	1.22E-01
CSTA	0.33	3.02E-01
SFN	0.33	5.04E-01
DSP	0.32	8.95E-02
S100A16	0.30	1.61E-01
CASP14	0.26	1.91E-01
DSC1	0.25	2.59E-01
TGM1	0.24	1.99E-01
SERPINB3	0.21	4.69E-01
C3	0.20	2.75E-01
PKP1	0.19	1.41E-01
ARG1	0.18	4.29E-02
FABP5	0.17	1.49E-01

Supplementary Figure 8. All proteins up-or down-regulated by 2-fold in TRPC3 activator-induced EVs

(A) *Gene names for all proteins identified with a fold change ≥ 2 and* ***(B)*** *with a fold change ≤ 0.5 (LFQ intensity TRPC3 activator – LFQ intensity DMSO), with corresponding fold change and p-value. Proteins sorted by fold change value.*

(A) Upregulated proteins in DMSO-induced EVs

Gene names	Fold change	p-value
FERMT3	14.22	1.47E-03
LOXL2	10.54	1.45E-04
TUBA4A	9.42	4.97E-02
COL6A1	8.78	5.29E-02
F10	8.74	4.76E-02
APOB	7.33	1.05E-01
TGFBI	6.85	3.74E-02
PARVB	6.40	3.19E-02
ARG1	5.73	6.49E-02
LAMB3	5.63	4.23E-02
CLEC11A	5.53	1.84E-03
LRP1	4.91	2.54E-02
NID2	4.62	1.92E-01
APP	4.60	8.31E-02
ARHGDIA	4.50	1.18E-02
YWHAQ	4.28	7.39E-02
CD81	4.21	2.81E-01
ILK	4.14	1.34E-02
HTRA1	3.93	5.59E-02
COTL1	3.91	4.79E-02
PLEK	3.77	4.20E-02
SERPINE2	3.65	3.61E-02
LAMA3	3.62	6.38E-02
FABP5	3.62	3.08E-01
LAMC2	3.54	5.72E-02
WDR1	3.53	1.67E-01
FBLN2	3.38	5.99E-02
C1QTNF3-AMACR;C1QTNF3	3.37	4.95E-02
THBS1	3.32	3.55E-02
RAB6A;RAB6B	3.11	1.56E-01
AHCY	3.09	6.93E-02
FBLN1	3.04	2.29E-01
ILF2	2.94	1.09E-02
PDIA3	2.85	2.03E-01
PGAM1	2.75	3.37E-01
PFKP	2.72	1.22E-01
EHD3	2.71	8.07E-02
MRC2	2.69	9.51E-02
YWHAE	2.68	1.60E-01
FN1	2.66	6.21E-02
TLN1	2.64	8.24E-02
ADAMTS13	2.64	1.27E-01
CNTN1	2.62	9.37E-02
UGDH	2.62	1.53E-01

(B) Downregulated proteins in DMSO-induced EVs

Gene names	Fold change	p-value
AHNAK	0.50	1.55E-01
ITGB1	0.50	4.24E-02
XPO1	0.50	4.65E-02
ITGA3	0.49	1.04E-01
EIF3C;EIF3CL	0.49	4.06E-01
PSMA5	0.49	4.12E-02
GNG12	0.49	1.01E-01
ERBB2	0.48	1.96E-01
PSMD11	0.48	3.85E-01
EHD4	0.48	5.23E-02
LAMP2	0.47	3.75E-01
VIM	0.47	4.85E-02
RPL8	0.47	1.68E-01
ACTR1B	0.47	1.88E-01
S100A4	0.46	3.14E-01
PFN1	0.45	3.41E-01
RPS3A	0.45	1.84E-02
PIP	0.45	3.46E-01
ANXA2;ANXA2P2	0.45	2.26E-02
HIST1H2BN;HIST1H2BL;HIST1H2BM;HIST1H2BH;HIST2H2BF;HIST1H2BC;HIST1H2BD;H2BFS;HIST1H2BK;HIST1H2BA	0.45	3.23E-01
EPRS	0.44	7.41E-02
RPS24	0.43	2.64E-01
SLC3A2	0.43	7.40E-03
HNRNPC	0.43	6.44E-02
RAB35	0.43	1.55E-01
KTN1	0.42	3.56E-01
CTNNA1	0.42	5.46E-04
ATP1A1	0.41	5.65E-02
PSMA1	0.41	2.64E-01
RPL13a;RPL13A;RPL13AP3	0.41	3.47E-01
RAB7A	0.40	2.04E-01
NUCB1	0.40	2.73E-01
RPLP2	0.40	2.14E-01
EPHA2	0.39	2.03E-01
HLA-A;HLA-H	0.39	2.07E-02
SLC1A5	0.39	6.48E-02
RPL27A	0.39	3.56E-01
SLC7A5	0.38	2.55E-02
AGRN	0.38	4.85E-01
FLOT1	0.37	2.41E-01
RPL34	0.37	4.27E-01
RTN4	0.36	8.83E-02
CPNE8	0.36	1.01E-01
VAT1	0.35	3.73E-02

(A) Cont.

DSC1	2.61	3.74E-01
CKB	2.59	2.56E-01
COL5A1	2.58	5.07E-03
COL18A1	2.52	3.01E-02
EIF3D	2.49	1.45E-01
PSMC6	2.46	1.75E-01
TNC	2.45	6.93E-02
VCAN	2.44	1.39E-01
SERPINB3	2.44	6.36E-01
PNP	2.44	1.56E-01
COL6A3	2.43	2.23E-02
DYNC1H1	2.31	2.08E-01
PKP1	2.31	3.35E-01
MUC5AC	2.29	2.09E-01
CD109	2.27	1.37E-01
PGK1	2.25	3.50E-01
MAP1B	2.25	1.91E-01
LGALS7	2.24	5.58E-01
B4GAT1	2.24	3.19E-01
HUWE1	2.20	6.45E-02
APLP2	2.19	1.64E-01
CSTA	2.19	2.19E-01
EIF3F	2.15	2.19E-01
COL4A1	2.12	2.62E-01
PGM1	2.12	1.65E-01
HSPA1B;HSPA1A	2.05	1.35E-01
HPD	2.03	1.08E-01
COL12A1	2.03	4.58E-01
F13A1	2.03	3.12E-01
UBA1	2.00	3.47E-01

(B) Cont.

GNA11	0.35	3.01E-01
AGL	0.34	3.53E-01
RPL24	0.34	9.55E-02
HSPA4	0.33	1.59E-01
LAMP1	0.32	1.30E-02
GYG1	0.32	5.43E-02
RALY	0.31	2.78E-02
RPS27	0.31	4.12E-02
SLC16A3	0.30	2.95E-02
ANXA1	0.30	1.82E-02
RRAS2	0.29	2.04E-01
ITGAV	0.29	1.33E-03
ATP1B1	0.29	1.42E-01
BASP1	0.29	6.49E-02
ITGB4	0.28	9.02E-03
PSMA2	0.28	1.19E-01
EGFR	0.28	2.49E-02
PSMB6	0.27	1.89E-01
S100A11	0.27	1.73E-01
EIF3L	0.27	1.10E-03
NPM1	0.26	1.86E-01
SET;SETSIP	0.26	5.84E-02
ATP1B3	0.23	1.55E-02
ANXA4	0.23	1.45E-02
GNAI3	0.23	2.21E-01
FAM129B	0.22	2.81E-04
GNAS	0.22	2.60E-02
CPNE1	0.20	1.77E-02
ANXA11	0.19	3.41E-02
ANPEP	0.18	1.90E-01
SCARB2	0.18	8.54E-02
ANXA6	0.16	3.48E-03
ANXA5	0.16	5.36E-03
GNAI2	0.15	9.45E-02
AHNAK2	0.15	5.89E-04
GYS1	0.06	4.48E-02

Supplementary Figure 9. All proteins up-or down-regulated by 2-fold in DMSO-induced EVs

(A) *Gene names for all proteins identified with a fold change ≥ 2 and* ***(B)*** *with a fold change ≤ 0.5 (LFQ intensity DMSO – LFQ intensity untreated), with corresponding fold change and p-value.*
Proteins sorted by fold change value.

(A)

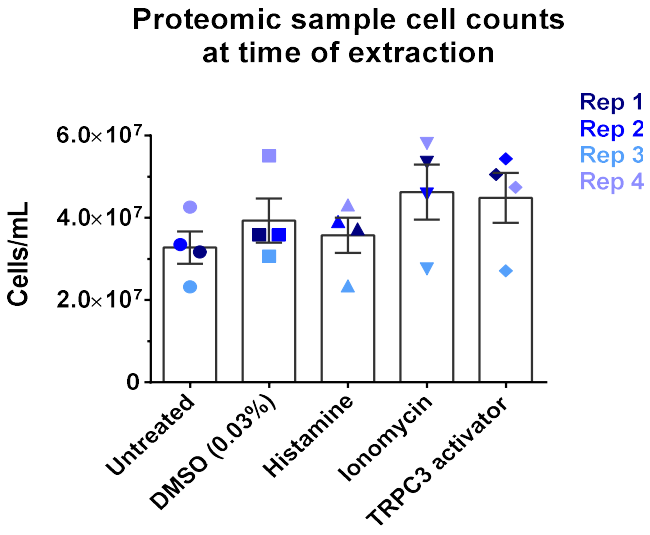

(B)

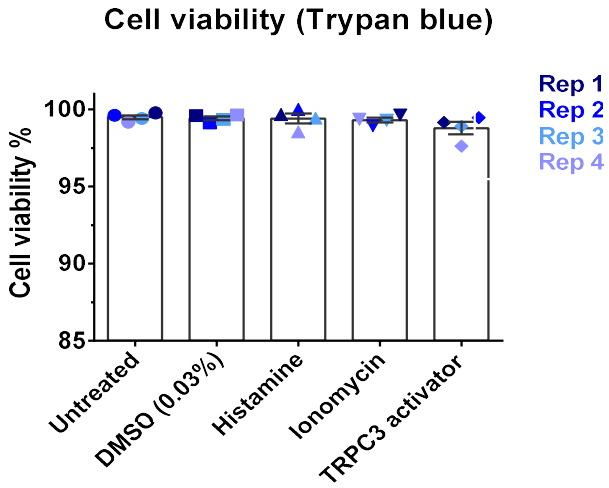

Supplementary Figure 10. Cell counts and viability of SKOV3 cells at time of EV extraction for proteomic analysis

SKOV3 cells were conditioned in plain serum-free media (untreated), or serum-free media supplemented with DMSO (0.03%), 100μM histamine, 1.25μM ionomycin or 0.3μM TRPC3 activator for 4hrs. At the time of EV extraction, cells were counted with trypan blue, with total cell counts shown in ***(A)*** *and percentage viability in* ***(B)****. Data represents mean ± SEM of four independent experiments.*

References

8. References

1. Wei, CJ, Xu, X, Lo, CW. Connexins and cell signaling in development and disease. Annu Rev Cell Dev Biol 2004;20:811-838.
2. Hanahan, D, Coussens, LM. Accessories to the crime: functions of cells recruited to the tumor microenvironment. Cancer Cell 2012;21(3):309-322.
3. Dominiak, A, Chełstowska, B, Olejarz, W, et al. Communication in the Cancer Microenvironment as a Target for Therapeutic Interventions. Cancers 2020;12(5):1232.
4. Chow, MT, Luster, AD. Chemokines in cancer. Cancer immunology research 2014;2(12):1125-1131.
5. Sethi, G, Shanmugam, MK, Ramachandran, L, et al. Multifaceted link between cancer and inflammation. Biosci Rep 2012;32(1):1-15.
6. Witsch, E, Sela, M, Yarden, Y. Roles for growth factors in cancer progression. Physiology (Bethesda, Md) 2010;25(2):85-101.
7. Wolf, P. The Nature and Significance of Platelet Products in Human Plasma. British Journal of Haematology 1967;13(3):269-288.
8. Aaronson, S, Behrens, U, Orner, R, et al. Ultrastructure of intracellular and extracellular vesicles, membranes, and myelin figures produced by Ochromonas danica. Journal of Ultrastructure Research 1971;35(5):418-430.
9. Dalton, AJ. Microvesicles and Vesicles of Multivesicular Bodies Versus "Virus-Like" Particles. JNCI: Journal of the National Cancer Institute 1975;54(5):1137-1148.
10. Trams, EG, Lauter, CJ, Norman Salem, Jr., et al. Exfoliation of membrane ecto-enzymes in the form of micro-vesicles. Biochimica et Biophysica Acta (BBA) - Biomembranes 1981;645(1):63-70.
11. Harding, C, Heuser, J, Stahl, P. Endocytosis and intracellular processing of transferrin and colloidal gold-transferrin in rat reticulocytes: demonstration of a pathway for receptor shedding. Eur J Cell Biol 1984;35(2):256-263.
12. Pan, BT, Johnstone, RM. Fate of the transferrin receptor during maturation of sheep reticulocytes in vitro: selective externalization of the receptor. Cell 1983;33(3):967-978.
13. Raposo, G, Nijman, HW, Stoorvogel, W, et al. B lymphocytes secrete antigen-presenting vesicles. The Journal of experimental medicine 1996;183(3):1161-1172.
14. Holm, MM, Kaiser, J, Schwab, ME. Extracellular Vesicles: Multimodal Envoys in Neural Maintenance and Repair. Trends Neurosci 2018;41(6):360-372.
15. Rak, J. Microparticles in Cancer. Semin Thromb Hemost 2010;36(08):888-906.
16. Raposo, G, Stoorvogel, W. Extracellular vesicles: Exosomes, microvesicles, and friends. Journal of Cell Biology 2013;200(4):373-383.
17. van Niel, G, D'Angelo, G, Raposo, G. Shedding light on the cell biology of extracellular vesicles. Nature Reviews Molecular Cell Biology 2018;19(4):213-228.
18. Poon, IKH, Lucas, CD, Rossi, AG, et al. Apoptotic cell clearance: basic biology and therapeutic potential. Nature Reviews Immunology 2014;14(3):166-180.
19. Di Vizio, D, Kim, J, Hager, MH, et al. Oncosome formation in prostate cancer: association with a region of frequent chromosomal deletion in metastatic disease. Cancer research 2009;69(13):5601-5609.
20. Minciacchi, VR, You, S, Spinelli, C, et al. Large oncosomes contain distinct protein cargo and represent a separate functional class of tumor-derived extracellular vesicles. Oncotarget 2015;6(13):11327-11341.
21. Zhang, H, Freitas, D, Kim, HS, et al. Identification of distinct nanoparticles and subsets of extracellular vesicles by asymmetric flow field-flow fractionation. Nat Cell Biol 2018;20(3):332-343.

22. Zhang, Q, Higginbotham, JN, Jeppesen, DK, et al. Transfer of functional cargo in exomeres. Cell reports 2019;27(3):940-954. e946.
23. Tavano, S, Heisenberg, C-P. Migrasomes take center stage. Nature Cell Biology 2019;21(8):918-920.
24. Jeppesen, DK, Fenix, AM, Franklin, JL, et al. Reassessment of Exosome Composition. Cell 2019;177(2):428-445.e418.
25. Zhao, H, Zhang, Y, Zhang, SB, et al. The structure of the nucleosome core particle of chromatin in chicken erythrocytes visualized by using atomic force microscopy. Cell Research 1999;9(4):255-260.
26. Turchinovich, A, Weiz, L, Langheinz, A, et al. Characterization of extracellular circulating microRNA. Nucleic Acids Res 2011;39(16):7223-7233.
27. Roseblade, A, Luk, F, Ung, A, et al. Targeting microparticle biogenesis: a novel approach to the circumvention of cancer multidrug resistance. Current Cancer Drug Targets 2015;15(3):205-214.
28. Sapet, C, Simoncini, S, Loriod, B, et al. Thrombin-induced endothelial microparticle generation: identification of a novel pathway involving ROCK-II activation by caspase-2. Blood 2006;108(6):1868-1876.
29. VanWijk, MJ, VanBavel, E, Sturk, A, et al. Microparticles in cardiovascular diseases. Cardiovascular research 2003;59(2):277-287.
30. Zwaal, R, Comfurius, P, Bevers, E. Surface exposure of phosphatidylserine in pathological cells. Cellular and Molecular Life Sciences CMLS 2005;62(9):971-988.
31. Freyssinet, JM, Toti, F. Formation of procoagulant microparticles and properties. Thromb Res 2010;125 Suppl 1:S46-48.
32. Daleke, DL. Regulation of transbilayer plasma membrane phospholipid asymmetry. J Lipid Res 2003;44(2):233-242.
33. Al-Nedawi, K, Meehan, B, Micallef, J, et al. Intercellular transfer of the oncogenic receptor EGFRvIII by microvesicles derived from tumour cells. Nat Cell Biol 2008;10(5):619-624.
34. Perrin, BJ, Amann, KJ, Huttenlocher, A. Proteolysis of cortactin by calpain regulates membrane protrusion during cell migration. Molecular biology of the cell 2006;17(1):239-250.
35. Storr, SJ, Carragher, NO, Frame, MC, et al. The calpain system and cancer. Nature Reviews Cancer 2011;11(5):364-374.
36. Del Conde, I, Shrimpton, CN, Thiagarajan, P, et al. Tissue-factor–bearing microvesicles arise from lipid rafts and fuse with activated platelets to initiate coagulation. Blood 2005;106(5):1604-1611.
37. Muralidharan-Chari, V, Clancy, J, Plou, C, et al. ARF6-regulated shedding of tumor cell-derived plasma membrane microvesicles. Curr Biol 2009;19(22):1875-1885.
38. Schlienger, S, Campbell, S, Claing, A. ARF1 regulates the Rho/MLC pathway to control EGF-dependent breast cancer cell invasion. Mol Biol Cell 2014;25(1):17-29.
39. Wang, T, Gilkes, DM, Takano, N, et al. Hypoxia-inducible factors and RAB22A mediate formation of microvesicles that stimulate breast cancer invasion and metastasis. Proc Natl Acad Sci U S A 2014;111(31):E3234-3242.
40. Sedgwick, AE, Clancy, JW, Olivia Balmert, M, et al. Extracellular microvesicles and invadopodia mediate non-overlapping modes of tumor cell invasion. Sci Rep 2015;5:14748.
41. Li, B, Antonyak, MA, Zhang, J, et al. RhoA triggers a specific signaling pathway that generates transforming microvesicles in cancer cells. Oncogene 2012;31(45):4740-4749.
42. Nabhan, JF, Hu, R, Oh, RS, et al. Formation and release of arrestin domain-containing protein 1-mediated microvesicles (ARMMs) at plasma membrane by recruitment of

TSG101 protein. Proceedings of the National Academy of Sciences of the United States of America 2012;109(11):4146-4151.
43. Shen, B, Fang, Y, Wu, N, et al. Biogenesis of the posterior pole is mediated by the exosome/microvesicle protein-sorting pathway. The Journal of biological chemistry 2011;286(51):44162-44176.
44. de Gassart, A, Geminard, C, Fevrier, B, et al. Lipid raft-associated protein sorting in exosomes. Blood 2003;102(13):4336-4344.
45. Escola, JM, Kleijmeer, MJ, Stoorvogel, W, et al. Selective enrichment of tetraspan proteins on the internal vesicles of multivesicular endosomes and on exosomes secreted by human B-lymphocytes. J Biol Chem 1998;273(32):20121-20127.
46. Zöller, M. Tetraspanins: push and pull in suppressing and promoting metastasis. Nat Rev Cancer 2009;9(1):40-55.
47. Caruso, S, Poon, IKH. Apoptotic Cell-Derived Extracellular Vesicles: More Than Just Debris. Frontiers in immunology 2018;9:1486-1486.
48. Wickman, G, Julian, L, Olson, MF. How apoptotic cells aid in the removal of their own cold dead bodies. Cell Death Differ 2012;19(5):735-742.
49. Sebbagh, M, Renvoizé, C, Hamelin, J, et al. Caspase-3-mediated cleavage of ROCK I induces MLC phosphorylation and apoptotic membrane blebbing. Nat Cell Biol 2001;3(4):346-352.
50. Coleman, ML, Sahai, EA, Yeo, M, et al. Membrane blebbing during apoptosis results from caspase-mediated activation of ROCK I. Nat Cell Biol 2001;3(4):339-345.
51. Doyle, LM, Wang, MZ. Overview of Extracellular Vesicles, Their Origin, Composition, Purpose, and Methods for Exosome Isolation and Analysis. Cells 2019;8(7):727.
52. Théry, C, Boussac, M, Véron, P, et al. Proteomic analysis of dendritic cell-derived exosomes: a secreted subcellular compartment distinct from apoptotic vesicles. J Immunol 2001;166(12):7309-7318.
53. Klumperman, J, Raposo, G. The complex ultrastructure of the endolysosomal system. Cold Spring Harbor perspectives in biology 2014;6(10):a016857-a016857.
54. Gould, GW, Lippincott-Schwartz, J. New roles for endosomes: from vesicular carriers to multi-purpose platforms. In: Nat Rev Mol Cell Biol. Vol 10. 2009.
55. Möbius, W, Ohno-Iwashita, Y, van Donselaar, EG, et al. Immunoelectron microscopic localization of cholesterol using biotinylated and non-cytolytic perfringolysin O. J Histochem Cytochem 2002;50(1):43-55.
56. Wubbolts, R, Leckie, RS, Veenhuizen, PT, et al. Proteomic and biochemical analyses of human B cell-derived exosomes. Potential implications for their function and multivesicular body formation. J Biol Chem 2003;278(13):10963-10972.
57. Borges, FT, Melo, SA, Özdemir, BC, et al. TGF-β1-containing exosomes from injured epithelial cells activate fibroblasts to initiate tissue regenerative responses and fibrosis. J Am Soc Nephrol 2013;24(3):385-392.
58. Kowal, J, Tkach, M, Théry, C. Biogenesis and secretion of exosomes. Current Opinion in Cell Biology 2014;29:116-125.
59. Trajkovic, K, Hsu, C, Chiantia, S, et al. Ceramide Triggers Budding of Exosome Vesicles into Multivesicular Endosomes. Science 2008;319(5867):1244.
60. Goñi, FM, Alonso, A. Effects of ceramide and other simple sphingolipids on membrane lateral structure. Biochim Biophys Acta 2009;1788(1):169-177.
61. Kajimoto, T, Okada, T, Miya, S, et al. Ongoing activation of sphingosine 1-phosphate receptors mediates maturation of exosomal multivesicular endosomes. Nat Commun 2013;4:2712.
62. Trajkovic, K, Hsu, C, Chiantia, S, et al. Ceramide Triggers Budding of Exosome Vesicles into Multivesicular Endosomes. Science 2008;319(5867):1244-1247.

63. Charrin, S, Jouannet, S, Boucheix, C, et al. Tetraspanins at a glance. J Cell Sci 2014;127(Pt 17):3641-3648.
64. van Niel, G, Charrin, S, Simoes, S, et al. The tetraspanin CD63 regulates ESCRT-independent and -dependent endosomal sorting during melanogenesis. Dev Cell 2011;21(4):708-721.
65. Buschow, SI, Nolte-'t Hoen, EN, van Niel, G, et al. MHC II in dendritic cells is targeted to lysosomes or T cell-induced exosomes via distinct multivesicular body pathways. Traffic 2009;10(10):1528-1542.
66. Odintsova, E, van Niel, G, Conjeaud, H, et al. Metastasis suppressor tetraspanin CD82/KAI1 regulates ubiquitylation of epidermal growth factor receptor. J Biol Chem 2013;288(36):26323-26334.
67. Henne, William M, Buchkovich, Nicholas J, Emr, Scott D. The ESCRT Pathway. Developmental Cell 2011;21(1):77-91.
68. Tamai, K, Tanaka, N, Nakano, T, et al. Exosome secretion of dendritic cells is regulated by Hrs, an ESCRT-0 protein. Biochemical and Biophysical Research Communications 2010;399(3):384-390.
69. Hurley, JH. The ESCRT complexes. Critical reviews in biochemistry and molecular biology 2010;45(6):463-487.
70. Raiborg, C, Stenmark, H. The ESCRT machinery in endosomal sorting of ubiquitylated membrane proteins. Nature 2009;458(7237):445-452.
71. Hurley, JH, Hanson, PI. Membrane budding and scission by the ESCRT machinery: it's all in the neck. Nature reviews Molecular cell biology 2010;11(8):556-566.
72. Wollert, T, Wunder, C, Lippincott-Schwartz, J, et al. Membrane scission by the ESCRT-III complex. Nature 2009;458(7235):172-177.
73. Baietti, MF, Zhang, Z, Mortier, E, et al. Syndecan–syntenin–ALIX regulates the biogenesis of exosomes. Nature Cell Biology 2012;14(7):677-685.
74. Schmidt, O, Teis, D. The ESCRT machinery. Curr Biol 2012;22(4):R116-120.
75. Sinha, S, Hoshino, D, Hong, NH, et al. Cortactin promotes exosome secretion by controlling branched actin dynamics. J Cell Biol 2016;214(2):197-213.
76. Blanc, L, Vidal, M. New insights into the function of Rab GTPases in the context of exosomal secretion. Small GTPases 2018;9(1-2):95-106.
77. Hsu, C, Morohashi, Y, Yoshimura, S-I, et al. Regulation of exosome secretion by Rab35 and its GTPase-activating proteins TBC1D10A-C. The Journal of cell biology 2010;189(2):223-232.
78. Ostrowski, M, Carmo, NB, Krumeich, S, et al. Rab27a and Rab27b control different steps of the exosome secretion pathway. Nature Cell Biology 2010;12(1):19-30.
79. Hyenne, V, Apaydin, A, Rodriguez, D, et al. RAL-1 controls multivesicular body biogenesis and exosome secretion. J Cell Biol 2015;211(1):27-37.
80. Pfeffer, SR. Unsolved mysteries in membrane traffic. Annu Rev Biochem 2007;76:629-645.
81. Bonifacino, JS, Glick, BS. The mechanisms of vesicle budding and fusion. Cell 2004;116(2):153-166.
82. Verweij, FJ, Bebelman, MP, Jimenez, CR, et al. Quantifying exosome secretion from single cells reveals a modulatory role for GPCR signaling. J Cell Biol 2018;217(3):1129-1142.
83. Fader, CM, Sánchez, DG, Mestre, MB, et al. TI-VAMP/VAMP7 and VAMP3/cellubrevin: two v-SNARE proteins involved in specific steps of the autophagy/multivesicular body pathways. Biochim Biophys Acta 2009;1793(12):1901-1916.
84. Gross, JC, Chaudhary, V, Bartscherer, K, et al. Active Wnt proteins are secreted on exosomes. Nature cell biology 2012;14(10):1036-1045.

85. Gámez-Valero, A, Monguió-Tortajada, M, Carreras-Planella, L, et al. Size-Exclusion Chromatography-based isolation minimally alters Extracellular Vesicles' characteristics compared to precipitating agents. Scientific Reports 2016;6(1):33641.
86. Hessvik, NP, Llorente, A. Current knowledge on exosome biogenesis and release. Cellular and molecular life sciences : CMLS 2018;75(2):193-208.
87. Llorente, A, Skotland, T, Sylvänne, T, et al. Molecular lipidomics of exosomes released by PC-3 prostate cancer cells. Biochimica et Biophysica Acta (BBA)-Molecular and Cell Biology of Lipids 2013;1831(7):1302-1309.
88. Record, M, Carayon, K, Poirot, M, et al. Exosomes as new vesicular lipid transporters involved in cell-cell communication and various pathophysiologies. Biochim Biophys Acta 2014;1841(1):108-120.
89. Laulagnier, K, Grand, D, Dujardin, A, et al. PLD2 is enriched on exosomes and its activity is correlated to the release of exosomes. FEBS Lett 2004;572(1-3):11-14.
90. Valadi, H, Ekström, K, Bossios, A, et al. Exosome-mediated transfer of mRNAs and microRNAs is a novel mechanism of genetic exchange between cells. Nature Cell Biology 2007;9(6):654-659.
91. Ratajczak, J, Miekus, K, Kucia, M, et al. Embryonic stem cell-derived microvesicles reprogram hematopoietic progenitors: evidence for horizontal transfer of mRNA and protein delivery. Leukemia 2006;20(5):847-856.
92. Bellingham, SA, Coleman, BM, Hill, AF. Small RNA deep sequencing reveals a distinct miRNA signature released in exosomes from prion-infected neuronal cells. Nucleic Acids Res 2012;40(21):10937-10949.
93. Nolte-'t Hoen, ENM, Buermans, HPJ, Waasdorp, M, et al. Deep sequencing of RNA from immune cell-derived vesicles uncovers the selective incorporation of small non-coding RNA biotypes with potential regulatory functions. Nucleic Acids Research 2012;40(18):9272-9285.
94. Eldh, M, Ekström, K, Valadi, H, et al. Exosomes communicate protective messages during oxidative stress; possible role of exosomal shuttle RNA. PLoS One 2010;5(12):e15353.
95. Shirazi, S, Huang, C-C, Kang, M, et al. The importance of cellular and exosomal miRNAs in mesenchymal stem cell osteoblastic differentiation. Scientific Reports 2021;11(1):5953.
96. Dilsiz, N. Role of exosomes and exosomal microRNAs in cancer. Future Science OA 2020;6(4):FSO465.
97. Fabbri, M, Paone, A, Calore, F, et al. MicroRNAs bind to Toll-like receptors to induce prometastatic inflammatory response. Proc Natl Acad Sci U S A 2012;109(31):E2110-2116.
98. Au Yeung, CL, Co, N-N, Tsuruga, T, et al. Exosomal transfer of stroma-derived miR21 confers paclitaxel resistance in ovarian cancer cells through targeting APAF1. Nature communications 2016;7:11150-11150.
99. Skog, J, Würdinger, T, van Rijn, S, et al. Glioblastoma microvesicles transport RNA and proteins that promote tumour growth and provide diagnostic biomarkers. Nat Cell Biol 2008;10(12):1470-1476.
100. Ratajczak, J, Wysoczynski, M, Hayek, F, et al. Membrane-derived microvesicles: important and underappreciated mediators of cell-to-cell communication. Leukemia 2006;20(9):1487-1495.
101. Batagov, AO, Kurochkin, IV. Exosomes secreted by human cells transport largely mRNA fragments that are enriched in the 3'-untranslated regions. Biol Direct 2013;8:12.
102. Batagov, AO, Kuznetsov, VA, Kurochkin, IV. Identification of nucleotide patterns enriched in secreted RNAs as putative cis-acting elements targeting them to exosome nano-vesicles. *BMC genomics.* 12. Springer; 2011:1-14.

103. Théry, C, Zitvogel, L, Amigorena, S. Exosomes: composition, biogenesis and function. Nature Reviews Immunology 2002;2(8):569-579.
104. Kowal, J, Arras, G, Colombo, M, et al. Proteomic comparison defines novel markers to characterize heterogeneous populations of extracellular vesicle subtypes. Proceedings of the National Academy of Sciences 2016;113(8):E968.
105. Mathieu, M, Névo, N, Jouve, M, et al. Specificities of exosome versus small ectosome secretion revealed by live intracellular tracking of CD63 and CD9. Nature communications 2021;12(1):4389-4389.
106. Gurung, S, Perocheau, D, Touramanidou, L, et al. The exosome journey: from biogenesis to uptake and intracellular signalling. Cell Communication and Signaling 2021;19(1):47.
107. Buschow, SI, Liefhebber, JM, Wubbolts, R, et al. Exosomes contain ubiquitinated proteins. Blood Cells Mol Dis 2005;35(3):398-403.
108. Luhtala, N, Aslanian, A, Yates, JR, 3rd, et al. Secreted Glioblastoma Nanovesicles Contain Intracellular Signaling Proteins and Active Ras Incorporated in a Farnesylation-dependent Manner. J Biol Chem 2017;292(2):611-628.
109. Dashwood, MR, Andrews, HE, Wei, ET. Binding of [125I]Tyr-corticotropin-releasing factor to rabbit aorta is reduced by removal of the endothelium. Eur J Pharmacol 1987;135(1):111-112.
110. Tkach, M, Kowal, J, Zucchetti, AE, et al. Qualitative differences in T-cell activation by dendritic cell-derived extracellular vesicle subtypes. Embo j 2017;36(20):3012-3028.
111. Rana, S, Yue, S, Stadel, D, et al. Toward tailored exosomes: the exosomal tetraspanin web contributes to target cell selection. Int J Biochem Cell Biol 2012;44(9):1574-1584.
112. Ma, X, Chen, Z, Hua, D, et al. Essential role for TrpC5-containing extracellular vesicles in breast cancer with chemotherapeutic resistance. Proceedings of the National Academy of Sciences of the United States of America 2014;111(17):6389-6394.
113. Hoshino, A, Costa-Silva, B, Shen, T-L, et al. Tumour exosome integrins determine organotropic metastasis. Nature 2015;527(7578):329-335.
114. Bhatnagar, S, Schorey, JS. Exosomes released from infected macrophages contain Mycobacterium avium glycopeptidolipids and are proinflammatory. J Biol Chem 2007;282(35):25779-25789.
115. Chen, G, Huang, AC, Zhang, W, et al. Exosomal PD-L1 contributes to immunosuppression and is associated with anti-PD-1 response. Nature 2018;560(7718):382-386.
116. Robbins, PD, Dorronsoro, A, Booker, CN. Regulation of chronic inflammatory and immune processes by extracellular vesicles. The Journal of clinical investigation 2016;126(4):1173-1180.
117. Rajendran, L, Honsho, M, Zahn, TR, et al. Alzheimer's disease β-amyloid peptides are released in association with exosomes. Proceedings of the National Academy of Sciences 2006;103(30):11172-11177.
118. Camussi, G, Deregibus, MC, Bruno, S, et al. Exosomes/microvesicles as a mechanism of cell-to-cell communication. Kidney Int 2010;78(9):838-848.
119. Mathieu, M, Martin-Jaular, L, Lavieu, G, et al. Specificities of secretion and uptake of exosomes and other extracellular vesicles for cell-to-cell communication. Nature Cell Biology 2019;21(1):9-17.
120. Montecalvo, A, Larregina, AT, Shufesky, WJ, et al. Mechanism of transfer of functional microRNAs between mouse dendritic cells via exosomes. Blood 2012;119(3):756-766.
121. Parolini, I, Federici, C, Raggi, C, et al. Microenvironmental pH Is a Key Factor for Exosome Traffic in Tumor Cells*. Journal of Biological Chemistry 2009;284(49):34211-34222.
122. Mittelbrunn, M, Gutiérrez-Vázquez, C, Villarroya-Beltri, C, et al. Unidirectional transfer of microRNA-loaded exosomes from T cells to antigen-presenting cells. Nat Commun 2011;2:282.

123. Haimovich, G, Ecker, CM, Dunagin, MC, et al. Intercellular mRNA trafficking via membrane nanotube-like extensions in mammalian cells. Proceedings of the National Academy of Sciences 2017;114(46):E9873.
124. Schneider, P, Tschopp, J. Apoptosis induced by death receptors. Pharm Acta Helv 2000;74(2-3):281-286.
125. Mulcahy, LA, Pink, RC, Carter, DR. Routes and mechanisms of extracellular vesicle uptake. J Extracell Vesicles 2014;3.
126. Tian, T, Wang, Y, Wang, H, et al. Visualizing of the cellular uptake and intracellular trafficking of exosomes by live-cell microscopy. J Cell Biochem 2010;111(2):488-496.
127. Zhao, H, Yang, L, Baddour, J, et al. Tumor microenvironment derived exosomes pleiotropically modulate cancer cell metabolism. Elife 2016;5:e10250.
128. Bissig, C, Gruenberg, J. ALIX and the multivesicular endosome: ALIX in Wonderland. Trends Cell Biol 2014;24(1):19-25.
129. Bonsergent, E, Grisard, E, Buchrieser, J, et al. Quantitative characterization of extracellular vesicle uptake and content delivery within mammalian cells. Nature Communications 2021;12(1):1864.
130. Joshi, BS, de Beer, MA, Giepmans, BNG, et al. Endocytosis of Extracellular Vesicles and Release of Their Cargo from Endosomes. ACS Nano 2020;14(4):4444-4455.
131. Kanada, M, Bachmann, MH, Hardy, JW, et al. Differential fates of biomolecules delivered to target cells via extracellular vesicles. Proc Natl Acad Sci U S A 2015;112(12):E1433-1442.
132. Heusermann, W, Hean, J, Trojer, D, et al. Exosomes surf on filopodia to enter cells at endocytic hot spots, traffic within endosomes, and are targeted to the ER. The Journal of Cell Biology 2016;213(2):173-184.
133. Santos, MF, Rappa, G, Karbanová, J, et al. VAMP-associated protein-A and oxysterol-binding protein-related protein 3 promote the entry of late endosomes into the nucleoplasmic reticulum. J Biol Chem 2018;293(36):13834-13848.
134. Murphy, DE, de Jong, OG, Brouwer, M, et al. Extracellular vesicle-based therapeutics: natural versus engineered targeting and trafficking. Exp Mol Med 2019;51(3):1-12.
135. Tian, T, Zhu, YL, Hu, FH, et al. Dynamics of exosome internalization and trafficking. J Cell Physiol 2013;228(7):1487-1495.
136. Grant, BD, Donaldson, JG. Pathways and mechanisms of endocytic recycling. Nat Rev Mol Cell Biol 2009;10(9):597-608.
137. Shelke, GV, Yin, Y, Jang, SC, et al. Endosomal signalling via exosome surface TGFβ-1. J Extracell Vesicles 2019;8(1):1650458.
138. Randriamampita, C, Trautmann, A. Ca2+ signals and T lymphocytes; "New mechanisms and functions in Ca2+ signalling". Biol Cell 2004;96(1):69-78.
139. Lindau, M, Gomperts, BD. Techniques and concepts in exocytosis: focus on mast cells. Biochim Biophys Acta 1991;1071(4):429-471.
140. Bean, AJ, Zhang, X, Hökfelt, T. Peptide secretion: what do we know? Faseb j 1994;8(9):630-638.
141. Sudhof, TC. The synaptic vesicle cycle. Annu Rev Neurosci 2004;27:509-547.
142. Pang, ZP, Südhof, TC. Cell biology of Ca2+-triggered exocytosis. Current opinion in cell biology 2010;22(4):496-505.
143. Savina, A, Furlán, M, Vidal, M, et al. Exosome Release Is Regulated by a Calcium-dependent Mechanism in K562 Cells. Journal of Biological Chemistry 2003;278(22):20083-20090.
144. Messenger, SW, Woo, SS, Sun, Z, et al. A Ca2+-stimulated exosome release pathway in cancer cells is regulated by Munc13-4. Journal of Cell Biology 2018;217(8):2877-2890.

145. Krämer-Albers, E-M, Bretz, N, Tenzer, S, et al. Oligodendrocytes secrete exosomes containing major myelin and stress-protective proteins: Trophic support for axons? PROTEOMICS – Clinical Applications 2007;1(11):1446-1461.
146. Chalmin, F, Ladoire, S, Mignot, G, et al. Membrane-associated Hsp72 from tumor-derived exosomes mediates STAT3-dependent immunosuppressive function of mouse and human myeloid-derived suppressor cells. The Journal of clinical investigation 2010;120(2):457-471.
147. Savina, A, Fader, CM, Damiani, MT, et al. Rab11 Promotes Docking and Fusion of Multivesicular Bodies in a Calcium-Dependent Manner. Traffic 2005;6(2):131-143.
148. Tucker, WC, Chapman, ER. Role of synaptotagmin in Ca2+-triggered exocytosis. The Biochemical journal 2002;366(Pt 1):1-13.
149. Hoshino, D, Kirkbride, KC, Costello, K, et al. Exosome secretion is enhanced by invadopodia and drives invasive behavior. Cell reports 2013;5(5):1159-1168.
150. Sun, S, Zhou, X, Corvera, J, et al. ALG-2 activates the MVB sorting function of ALIX through relieving its intramolecular interaction. Cell Discovery 2015;1(1):15018.
151. Scheffer, LL, Sreetama, SC, Sharma, N, et al. Mechanism of Ca^{2+}-triggered ESCRT assembly and regulation of cell membrane repair. Nature communications 2014;5:5646-5646.
152. Odorizzi, G. The multiple personalities of Alix. Journal of Cell Science 2006;119(15):3025-3032.
153. Ambattu, LA, Ramesan, S, Dekiwadia, C, et al. High frequency acoustic cell stimulation promotes exosome generation regulated by a calcium-dependent mechanism. Communications Biology 2020;3(1):553.
154. Li, GH, Arora, PD, Chen, Y, et al. Multifunctional roles of gelsolin in health and diseases. Medicinal research reviews 2012;32(5):999-1025.
155. Zhang, W, Zhao, P, Xu, X-L, et al. Annexin A2 promotes the migration and invasion of human hepatocellular carcinoma cells in vitro by regulating the shedding of CD147-harboring microvesicles from tumor cells. PloS one 2013;8(8):e67268.
156. Taylor, J, Azimi, I, Monteith, G, et al. Ca(2+) mediates extracellular vesicle biogenesis through alternate pathways in malignancy. Journal of extracellular vesicles 2020;9(1):1734326-1734326.
157. Crawford, S, Diamond, D, Brustolon, L, et al. Effect of increased extracellular ca on microvesicle production and tumor spheroid formation. Cancer microenvironment : official journal of the International Cancer Microenvironment Society 2010;4(1):93-103.
158. Bucki, R, Bachelot-Loza, C, Zachowski, A, et al. Calcium induces phospholipid redistribution and microvesicle release in human erythrocyte membranes by independent pathways. Biochemistry 1998;37(44):15383-15391.
159. Taylor, J, Jaiswal, R, Bebawy, M. Calcium-calpain Dependent Pathways Regulate Vesiculation in Malignant Breast Cells. Curr Cancer Drug Targets 2017;17(5):486-494.
160. Monteith, GR, McAndrew, D, Faddy, HM, et al. Calcium and cancer: targeting Ca2+ transport. Nature Reviews Cancer 2007;7(7):519-530.
161. Berridge, MJ, Bootman, MD, Roderick, HL. Calcium signalling: dynamics, homeostasis and remodelling. Nature Reviews Molecular Cell Biology 2003;4(7):517-529.
162. Shapovalov, G, Ritaine, A, Skryma, R, et al. Role of TRP ion channels in cancer and tumorigenesis. Seminars in Immunopathology 2016;38(3):357-369.
163. Taylor, DD, Gercel-Taylor, C. MicroRNA signatures of tumor-derived exosomes as diagnostic biomarkers of ovarian cancer. Gynecologic Oncology 2008;110(1):13-21.
164. Keustermans, GC, Hoeks, SB, Meerding, JM, et al. Cytokine assays: an assessment of the preparation and treatment of blood and tissue samples. Methods 2013;61(1):10-17.
165. Szczepanski, MJ, Szajnik, M, Welsh, A, et al. Blast-derived microvesicles in sera from patients with acute myeloid leukemia suppress natural killer cell function via

membrane-associated transforming growth factor-beta1. Haematologica 2011;96(9):1302-1309.
166. Sahai, E. Mechanisms of cancer cell invasion. Curr Opin Genet Dev 2005;15(1):87-96.
167. Lee, AH, Ghosh, D, Quach, N, et al. Ovarian Cancer Exosomes Trigger Differential Biophysical Response in Tumor-Derived Fibroblasts. Scientific Reports 2020;10(1):8686.
168. Hanahan, D, Weinberg, RA. The Hallmarks of Cancer. Cell 2000;100(1):57-70.
169. Hanahan, D, Weinberg, Robert A. Hallmarks of Cancer: The Next Generation. Cell 2011;144(5):646-674.
170. Steeg, PS. Tumor metastasis: mechanistic insights and clinical challenges. Nat Med 2006;12(8):895-904.
171. Brooks, SA, Lomax-Browne, HJ, Carter, TM, et al. Molecular interactions in cancer cell metastasis. Acta Histochem 2010;112(1):3-25.
172. Nicolson, GL. Cell membrane fluid-mosaic structure and cancer metastasis. Cancer Res 2015;75(7):1169-1176.
173. Nishida, N, Yano, H, Nishida, T, et al. Angiogenesis in cancer. Vasc Health Risk Manag 2006;2(3):213-219.
174. Bergers, G, Benjamin, LE. Tumorigenesis and the angiogenic switch. Nat Rev Cancer 2003;3(6):401-410.
175. Dvorak, HF, Nagy, JA, Dvorak, JT, et al. Identification and characterization of the blood vessels of solid tumors that are leaky to circulating macromolecules. The American journal of pathology 1988;133(1):95-109.
176. Steinberg, F, Konerding, MA, Streffer, C. The vascular architecture of human xenotransplanted tumors: histological, morphometrical, and ultrastructural studies. J Cancer Res Clin Oncol 1990;116(5):517-524.
177. Thiery, JP, Acloque, H, Huang, RY, et al. Epithelial-mesenchymal transitions in development and disease. Cell 2009;139(5):871-890.
178. Ribatti, D, Tamma, R, Annese, T. Epithelial-Mesenchymal Transition in Cancer: A Historical Overview. Transl Oncol 2020;13(6):100773.
179. Byers, SW, Sommers, CL, Hoxter, B, et al. Role of E-cadherin in the response of tumor cell aggregates to lymphatic, venous and arterial flow: measurement of cell-cell adhesion strength. Journal of cell science 1995;108(5):2053-2064.
180. Hay, ED. An overview of epithelio-mesenchymal transformation. Acta Anat (Basel) 1995;154(1):8-20.
181. Dongre, A, Weinberg, RA. New insights into the mechanisms of epithelial-mesenchymal transition and implications for cancer. Nat Rev Mol Cell Biol 2019;20(2):69-84.
182. Liotta, LA, Kohn, EC. The microenvironment of the tumour–host interface. Nature 2001;411(6835):375-379.
183. Friedl, P, Wolf, K. Plasticity of cell migration: a multiscale tuning model. Journal of Cell Biology 2009;188(1):11-19.
184. Savagner, P. Leaving the neighborhood: molecular mechanisms involved during epithelial-mesenchymal transition. Bioessays 2001;23(10):912-923.
185. Fares, J, Fares, MY, Khachfe, HH, et al. Molecular principles of metastasis: a hallmark of cancer revisited. Signal Transduction and Targeted Therapy 2020;5(1):28.
186. Mahmood, N, Mihalcioiu, C, Rabbani, SA. Multifaceted Role of the Urokinase-Type Plasminogen Activator (uPA) and Its Receptor (uPAR): Diagnostic, Prognostic, and Therapeutic Applications. Frontiers in Oncology 2018;8.
187. Tan, G-J, Peng, Z-K, Lu, J-P, et al. Cathepsins mediate tumor metastasis. World journal of biological chemistry 2013;4(4):91-101.
188. Gonzalez-Avila, G, Sommer, B, Mendoza-Posada, DA, et al. Matrix metalloproteinases participation in the metastatic process and their diagnostic and therapeutic applications in cancer. Crit Rev Oncol Hematol 2019;137:57-83.

189. Friedl, P, Wolf, K. Tumour-cell invasion and migration: diversity and escape mechanisms. Nature reviews cancer 2003;3(5):362-374.
190. Blood, CH, Zetter, BR. Tumor interactions with the vasculature: angiogenesis and tumor metastasis. Biochimica et Biophysica Acta (BBA)-Reviews on Cancer 1990;1032(1):89-118.
191. Alitalo, K, Tammela, T, Petrova, TV. Lymphangiogenesis in development and human disease. Nature 2005;438(7070):946-953.
192. Farnsworth, RH, Achen, MG, Stacker, SA. The evolving role of lymphatics in cancer metastasis. Curr Opin Immunol 2018;53:64-73.
193. Strell, C, Entschladen, F. Extravasation of leukocytes in comparison to tumor cells. Cell Communication and Signaling 2008;6(1):10.
194. Smith, CW. Possible Steps Involved in the Transition to Stationary Adhesion of Rolling Neutrophils: A Brief Review. Microcirculation 2000;7(6):385-394.
195. Muller, WA. Mechanisms of Transendothelial Migration of Leukocytes. Circulation Research 2009;105(3):223-230.
196. Tsuji, K, Yamauchi, K, Yang, M, et al. Dual-color imaging of nuclear-cytoplasmic dynamics, viability, and proliferation of cancer cells in the portal vein area. Cancer research 2006;66(1):303-306.
197. Cook-Mills, JM, Johnson, JD, Deem, TL, et al. Calcium mobilization and Rac1 activation are required for VCAM-1 (vascular cell adhesion molecule-1) stimulation of NADPH oxidase activity. Biochemical Journal 2004;378(2):539-547.
198. van Wetering, S, van Buul, JD, Quik, S, et al. Reactive oxygen species mediate Rac-induced loss of cell-cell adhesion in primary human endothelial cells. Journal of cell science 2002;115(9):1837-1846.
199. Turowski, P, Martinelli, R, Crawford, R, et al. Phosphorylation of vascular endothelial cadherin controls lymphocyte emigration. Journal of cell science 2008;121(1):29-37.
200. Chambers, AF, Groom, AC, MacDonald, IC. Dissemination and growth of cancer cells in metastatic sites. Nature Reviews Cancer 2002;2(8):563-572.
201. Chaffer, CL, Thompson, EW, Williams, ED. Mesenchymal to epithelial transition in development and disease. Cells Tissues Organs 2007;185(1-3):7-19.
202. Liao, W-T, Ye, Y-P, Deng, Y-J, et al. Metastatic cancer stem cells: from the concept to therapeutics. American journal of stem cells 2014;3(2):46-62.
203. Yao, D, Dai, C, Peng, S. Mechanism of the mesenchymal-epithelial transition and its relationship with metastatic tumor formation. Mol Cancer Res 2011;9(12):1608-1620.
204. Kahlert, C, Kalluri, R. Exosomes in tumor microenvironment influence cancer progression and metastasis. Journal of molecular medicine (Berlin, Germany) 2013;91(4):431-437.
205. Dai, J, Su, Y, Zhong, S, et al. Exosomes: key players in cancer and potential therapeutic strategy. Signal Transduction and Targeted Therapy 2020;5(1):145.
206. Gulei, D, Petrut, B, Tigu, AB, et al. Exosomes at a glance – common nominators for cancer hallmarks and novel diagnosis tools. Critical Reviews in Biochemistry and Molecular Biology 2018;53(5):564-577.
207. Kim, J, Morley, S, Le, M, et al. Enhanced shedding of extracellular vesicles from amoeboid prostate cancer cells: potential effects on the tumor microenvironment. Cancer biology & therapy 2014;15(4):409-418.
208. Yang, L, Wu, XH, Wang, D, et al. Bladder cancer cell-derived exosomes inhibit tumor cell apoptosis and induce cell proliferation in vitro. Mol Med Rep 2013;8(4):1272-1278.
209. Choi, DY, You, S, Jung, JH, et al. Extracellular vesicles shed from gefitinib-resistant nonsmall cell lung cancer regulate the tumor microenvironment. Proteomics 2014;14(16):1845-1856.

210. Qu, JL, Qu, XJ, Zhao, MF, et al. Gastric cancer exosomes promote tumour cell proliferation through PI3K/Akt and MAPK/ERK activation. Dig Liver Dis 2009;41(12):875-880.
211. Li, C, Liu, D-R, Li, G-G, et al. CD97 promotes gastric cancer cell proliferation and invasion through exosome-mediated MAPK signaling pathway. World Journal of Gastroenterology: WJG 2015;21(20):6215.
212. Peinado, H, Alečković, M, Lavotshkin, S, et al. Melanoma exosomes educate bone marrow progenitor cells toward a pro-metastatic phenotype through MET. Nat Med 2012;18(6):883-891.
213. Abd Elmageed, ZY, Yang, Y, Thomas, R, et al. Neoplastic reprogramming of patient-derived adipose stem cells by prostate cancer cell-associated exosomes. Stem Cells 2014;32(4):983-997.
214. Cappellesso, R, Tinazzi, A, Giurici, T, et al. Programmed cell death 4 and microRNA 21 inverse expression is maintained in cells and exosomes from ovarian serous carcinoma effusions. Cancer Cytopathol 2014;122(9):685-693.
215. Li, X, Xin, S, He, Z, et al. MicroRNA-21 (miR-21) Post-Transcriptionally Downregulates Tumor Suppressor PDCD4 and Promotes Cell Transformation, Proliferation, and Metastasis in Renal Cell Carcinoma. Cellular Physiology and Biochemistry 2014;33(6):1631-1642.
216. Khan, S, Jutzy, JM, Aspe, JR, et al. Survivin is released from cancer cells via exosomes. Apoptosis 2011;16(1):1-12.
217. Valenzuela, MM, Ferguson Bennit, HR, Gonda, A, et al. Exosomes Secreted from Human Cancer Cell Lines Contain Inhibitors of Apoptosis (IAP). Cancer Microenviron 2015;8(2):65-73.
218. Greening, DW, Gopal, SK, Mathias, RA, et al. Emerging roles of exosomes during epithelial–mesenchymal transition and cancer progression. Seminars in Cell & Developmental Biology 2015;40:60-71.
219. Tauro, BJ, Mathias, RA, Greening, DW, et al. Oncogenic H-ras reprograms Madin-Darby canine kidney (MDCK) cell-derived exosomal proteins following epithelial-mesenchymal transition. Molecular & cellular proteomics 2013;12(8):2148-2159.
220. Galindo-Hernandez, O, Serna-Marquez, N, Castillo-Sanchez, R, et al. Extracellular vesicles from MDA-MB-231 breast cancer cells stimulated with linoleic acid promote an EMT-like process in MCF10A cells. Prostaglandins Leukot Essent Fatty Acids 2014;91(6):299-310.
221. Garnier, D, Magnus, N, Lee, TH, et al. Cancer cells induced to express mesenchymal phenotype release exosome-like extracellular vesicles carrying tissue factor. Journal of Biological Chemistry 2012;287(52):43565-43572.
222. Zhou, W, Fong, MY, Min, Y, et al. Cancer-secreted miR-105 destroys vascular endothelial barriers to promote metastasis. Cancer cell 2014;25(4):501-515.
223. Le, MT, Hamar, P, Guo, C, et al. miR-200-containing extracellular vesicles promote breast cancer cell metastasis. J Clin Invest 2014;124(12):5109-5128.
224. Aga, M, Bentz, GL, Raffa, S, et al. Exosomal HIF1α supports invasive potential of nasopharyngeal carcinoma-associated LMP1-positive exosomes. Oncogene 2014;33(37):4613-4622.
225. Cho, JA, Park, H, Lim, EH, et al. Exosomes from ovarian cancer cells induce adipose tissue-derived mesenchymal stem cells to acquire the physical and functional characteristics of tumor-supporting myofibroblasts. Gynecol Oncol 2011;123(2):379-386.
226. Webber, J, Steadman, R, Mason, MD, et al. Cancer exosomes trigger fibroblast to myofibroblast differentiation. Cancer Res 2010;70(23):9621-9630.

227. Wei, M, Yang, T, Chen, X, et al. Malignant ascites-derived exosomes promote proliferation and induce carcinoma-associated fibroblasts transition in peritoneal mesothelial cells. Oncotarget 2017;8(26):42262-42271.
228. Nakamura, K, Sawada, K, Kinose, Y, et al. Exosomes Promote Ovarian Cancer Cell Invasion through Transfer of CD44 to Peritoneal Mesothelial Cells. Mol Cancer Res 2017;15(1):78-92.
229. Shimoda, M, Principe, S, Jackson, HW, et al. Loss of the Timp gene family is sufficient for the acquisition of the CAF-like cell state. Nat Cell Biol 2014;16(9):889-901.
230. Colangelo, NW, Azzam, EI. Extracellular vesicles originating from glioblastoma cells increase metalloproteinase release by astrocytes: the role of CD147 (EMMPRIN) and ionizing radiation. Cell Commun Signal 2020;18(1):21.
231. Menck, K, Scharf, C, Bleckmann, A, et al. Tumor-derived microvesicles mediate human breast cancer invasion through differentially glycosylated EMMPRIN. J Mol Cell Biol 2015;7(2):143-153.
232. Graves, LE, Ariztia, EV, Navari, JR, et al. Proinvasive properties of ovarian cancer ascites-derived membrane vesicles. Cancer research 2004;64(19):7045-7049.
233. Chen, X, Zhou, J, Li, X, et al. Exosomes derived from hypoxic epithelial ovarian cancer cells deliver microRNAs to macrophages and elicit a tumor-promoted phenotype. Cancer Letters 2018;435:80-91.
234. Luga, V, Zhang, L, Viloria-Petit, Alicia M, et al. Exosomes Mediate Stromal Mobilization of Autocrine Wnt-PCP Signaling in Breast Cancer Cell Migration. Cell 2012;151(7):1542-1556.
235. Sung, BH, Ketova, T, Hoshino, D, et al. Directional cell movement through tissues is controlled by exosome secretion. Nat Commun 2015;6:7164.
236. Sung, BH, von Lersner, A, Guerrero, J, et al. A live cell reporter of exosome secretion and uptake reveals pathfinding behavior of migrating cells. Nature Communications 2020;11(1):2092.
237. Zhou, W, Fong, MY, Min, Y, et al. Cancer-secreted miR-105 destroys vascular endothelial barriers to promote metastasis. Cancer Cell 2014;25(4):501-515.
238. Tominaga, N, Kosaka, N, Ono, M, et al. Brain metastatic cancer cells release microRNA-181c-containing extracellular vesicles capable of destructing blood-brain barrier. Nature communications 2015;6:6716-6716.
239. Whiteside, TL. Exosomes and tumor-mediated immune suppression. The Journal of clinical investigation 2016;126(4):1216-1223.
240. Abusamra, AJ, Zhong, Z, Zheng, X, et al. Tumor exosomes expressing Fas ligand mediate CD8+ T-cell apoptosis. Blood Cells Mol Dis 2005;35(2):169-173.
241. Clayton, A, Mitchell, JP, Court, J, et al. Human tumor-derived exosomes selectively impair lymphocyte responses to interleukin-2. Cancer Res 2007;67(15):7458-7466.
242. Huber, V, Fais, S, Iero, M, et al. Human colorectal cancer cells induce T-cell death through release of proapoptotic microvesicles: role in immune escape. Gastroenterology 2005;128(7):1796-1804.
243. Kim, JW, Wieckowski, E, Taylor, DD, et al. Fas ligand-positive membranous vesicles isolated from sera of patients with oral cancer induce apoptosis of activated T lymphocytes. Clin Cancer Res 2005;11(3):1010-1020.
244. Natoni, A, Macauley, MS, O'Dwyer, ME. Targeting Selectins and Their Ligands in Cancer. Front Oncol 2016;6:93.
245. Heijnen, HF, Schiel, AE, Fijnheer, R, et al. Activated platelets release two types of membrane vesicles: microvesicles by surface shedding and exosomes derived from exocytosis of multivesicular bodies and alpha-granules. Blood 1999;94(11):3791-3799.

246. Bray, F, Ferlay, J, Soerjomataram, I, et al. Global cancer statistics 2018: GLOBOCAN estimates of incidence and mortality worldwide for 36 cancers in 185 countries. CA Cancer J Clin 2018;68(6):394-424.
247. Torre, LA, Trabert, B, DeSantis, CE, et al. Ovarian cancer statistics, 2018. CA: a cancer journal for clinicians 2018;68(4):284-296.
248. Cancer Research UK, Cancer Statistics; https://www.cancerresearchuk.org/health-professional/cancer-statistics-for-the-uk. Accessed March 2022.
249. Yoneda, A, Lendorf, ME, Couchman, JR, et al. Breast and ovarian cancers: a survey and possible roles for the cell surface heparan sulfate proteoglycans. J Histochem Cytochem 2012;60(1):9-21.
250. Lengyel, E. Ovarian cancer development and metastasis. The American journal of pathology 2010;177(3):1053-1064.
251. Reid, BM, Permuth, JB, Sellers, TA. Epidemiology of ovarian cancer: a review. Cancer biology & medicine 2017;14(1):9-32.
252. Chen, VW, Ruiz, B, Killeen, JL, et al. Pathology and classification of ovarian tumors. Cancer 2003;97(S10):2631-2642.
253. Sankaranarayanan, R, Ferlay, J. Worldwide burden of gynaecological cancer: the size of the problem. Best Pract Res Clin Obstet Gynaecol 2006;20(2):207-225.
254. Prat, J. Ovarian carcinomas: five distinct diseases with different origins, genetic alterations, and clinicopathological features. Virchows Arch 2012;460(3):237-249.
255. Shih Ie, M, Kurman, RJ. Ovarian tumorigenesis: a proposed model based on morphological and molecular genetic analysis. Am J Pathol 2004;164(5):1511-1518.
256. Gershenson, DM, Sun, CC, Lu, KH, et al. Clinical behavior of stage II-IV low-grade serous carcinoma of the ovary. Obstet Gynecol 2006;108(2):361-368.
257. Cortez, AJ, Tudrej, P, Kujawa, KA, et al. Advances in ovarian cancer therapy. Cancer chemotherapy and pharmacology 2018;81(1):17-38.
258. Armstrong, DK, Bundy, B, Wenzel, L, et al. Intraperitoneal cisplatin and paclitaxel in ovarian cancer. N Engl J Med 2006;354(1):34-43.
259. Neijt, JP, Engelholm, SA, Tuxen, MK, et al. Exploratory phase III study of paclitaxel and cisplatin versus paclitaxel and carboplatin in advanced ovarian cancer. J Clin Oncol 2000;18(17):3084-3092.
260. Parmar, MK, Ledermann, JA, Colombo, N, et al. Paclitaxel plus platinum-based chemotherapy versus conventional platinum-based chemotherapy in women with relapsed ovarian cancer: the ICON4/AGO-OVAR-2.2 trial. Lancet 2003;361(9375):2099-2106.
261. Peng, DJ, Wang, J, Zhou, JY, et al. Role of the Akt/mTOR survival pathway in cisplatin resistance in ovarian cancer cells. Biochem Biophys Res Commun 2010;394(3):600-605.
262. Galluzzi, L, Senovilla, L, Vitale, I, et al. Molecular mechanisms of cisplatin resistance. Oncogene 2012;31(15):1869-1883.
263. Motohara, T, Masuda, K, Morotti, M, et al. An evolving story of the metastatic voyage of ovarian cancer cells: cellular and molecular orchestration of the adipose-rich metastatic microenvironment. Oncogene 2019;38(16):2885-2898.
264. Liu, Q, Zhang, H, Jiang, X, et al. Factors involved in cancer metastasis: a better understanding to “seed and soil” hypothesis. Molecular Cancer 2017;16(1):176.
265. Paget, S. The distribution of secondary growths in cancer of the breast. 1889. Cancer Metastasis Rev 1989;8(2):98-101.
266. Tarin, D, Price, JE, Kettlewell, MG, et al. Mechanisms of human tumor metastasis studied in patients with peritoneovenous shunts. Cancer Res 1984;44(8):3584-3592.
267. Kalluri, R, Weinberg, RA. The basics of epithelial-mesenchymal transition. The Journal of clinical investigation 2009;119(6):1420-1428.

268. Veatch, AL, Carson, LF, Ramakrishnan, S. Differential expression of the cell-cell adhesion molecule E-cadherin in ascites and solid human ovarian tumor cells. Int J Cancer 1994;58(3):393-399.
269. Daraï, E, Scoazec, JY, Walker-Combrouze, F, et al. Expression of cadherins in benign, borderline, and malignant ovarian epithelial tumors: a clinicopathologic study of 60 cases. Hum Pathol 1997;28(8):922-928.
270. Symowicz, J, Adley, BP, Gleason, KJ, et al. Engagement of collagen-binding integrins promotes matrix metalloproteinase-9-dependent E-cadherin ectodomain shedding in ovarian carcinoma cells. Cancer Res 2007;67(5):2030-2039.
271. Sawada, K, Radjabi, AR, Shinomiya, N, et al. c-Met overexpression is a prognostic factor in ovarian cancer and an effective target for inhibition of peritoneal dissemination and invasion. Cancer Res 2007;67(4):1670-1679.
272. Lössner, D, Abou-Ajram, C, Benge, A, et al. Integrin alphavbeta3 mediates upregulation of epidermal growth-factor receptor expression and activity in human ovarian cancer cells. Int J Biochem Cell Biol 2008;40(12):2746-2761.
273. Cannistra, SA, Kansas, GS, Niloff, J, et al. Binding of ovarian cancer cells to peritoneal mesothelium in vitro is partly mediated by CD44H. Cancer Res 1993;53(16):3830-3838.
274. Rump, A, Morikawa, Y, Tanaka, M, et al. Binding of ovarian cancer antigen CA125/MUC16 to mesothelin mediates cell adhesion. J Biol Chem 2004;279(10):9190-9198.
275. Kenny, HA, Kaur, S, Coussens, LM, et al. The initial steps of ovarian cancer cell metastasis are mediated by MMP-2 cleavage of vitronectin and fibronectin. J Clin Invest 2008;118(4):1367-1379.
276. Nishida, N, Yano, H, Komai, K, et al. Vascular endothelial growth factor C and vascular endothelial growth factor receptor 2 are related closely to the prognosis of patients with ovarian carcinoma. Cancer 2004;101(6):1364-1374.
277. Feki, A, Berardi, P, Bellingan, G, et al. Dissemination of intraperitoneal ovarian cancer: Discussion of mechanisms and demonstration of lymphatic spreading in ovarian cancer model. Crit Rev Oncol Hematol 2009;72(1):1-9.
278. Eisenkop, SM, Spirtos, NM. The clinical significance of occult macroscopically positive retroperitoneal nodes in patients with epithelial ovarian cancer. Gynecol Oncol 2001;82(1):143-149.
279. Thomakos, N, Diakosavvas, M, Machairiotis, N, et al. Rare Distant Metastatic Disease of Ovarian and Peritoneal Carcinomatosis: A Review of the Literature. Cancers 2019;11(8):1044.
280. Jayson, GC, Kohn, EC, Kitchener, HC, et al. Ovarian cancer. Lancet 2014;384(9951):1376-1388.
281. Pradeep, S, Kim, SW, Wu, SY, et al. Hematogenous metastasis of ovarian cancer: rethinking mode of spread. Cancer Cell 2014;26(1):77-91.
282. Venkatachalam, K, Montell, C. TRP channels. Annual review of biochemistry 2007;76:387-417.
283. Nilius, B, Owsianik, G. The transient receptor potential family of ion channels. Genome Biology 2011;12(3):218.
284. Owsianik, G, D'hoedt, D, Voets, T, et al. Structure–function relationship of the TRP channel superfamily. 2006.
285. Gaudet, R. TRP channels entering the structural era. The Journal of physiology 2008;586(15):3565-3575.
286. Wes, PD, Chevesich, J, Jeromin, A, et al. TRPC1, a human homolog of a Drosophila store-operated channel. Proceedings of the National Academy of Sciences of the United States of America 1995;92(21):9652-9656.

287. Kamouchi, M, Philipp, S, Flockerzi, V, et al. Properties of heterologously expressed hTRP3 channels in bovine pulmonary artery endothelial cells. J Physiol 1999;518 Pt 2(Pt 2):345-358.
288. Lièvremont, J-P, Bird, GSJ, Putney, JW. Canonical transient receptor potential TRPC7 can function as both a receptor- and store-operated channel in HEK-293 cells. American Journal of Physiology-Cell Physiology 2004;287(6):C1709-C1716.
289. Hofmann, T, Schaefer, M, Schultz, G, et al. Subunit composition of mammalian transient receptor potential channels in living cells. Proc Natl Acad Sci U S A 2002;99(11):7461-7466.
290. Lichtenegger, M, Stockner, T, Poteser, M, et al. A novel homology model of TRPC3 reveals allosteric coupling between gate and selectivity filter. Cell Calcium 2013;54(3):175-185.
291. Liu, X, Singh, BB, Ambudkar, IS. TRPC1 is required for functional store-operated Ca2+ channels. Role of acidic amino acid residues in the S5-S6 region. J Biol Chem 2003;278(13):11337-11343.
292. Owsianik, G, Talavera, K, Voets, T, et al. Permeation and selectivity of TRP channels. Annu Rev Physiol 2006;68:685-717.
293. Lussier, MP, Lepage, PK, Bousquet, SM, et al. RNF24, a new TRPC interacting protein, causes the intracellular retention of TRPC. Cell Calcium 2008;43(5):432-443.
294. Lussier, MP, Cayouette, S, Lepage, PK, et al. MxA, a member of the dynamin superfamily, interacts with the ankyrin-like repeat domain of TRPC. J Biol Chem 2005;280(19):19393-19400.
295. Tang, J, Lin, Y, Zhang, Z, et al. Identification of common binding sites for calmodulin and inositol 1,4,5-trisphosphate receptors on the carboxyl termini of trp channels. The Journal of biological chemistry 2001;276(24):21303-21310.
296. Berridge, MJ. Capacitative calcium entry. The Biochemical journal 1995;312 (Pt 1)(Pt 1):1-11.
297. Irvine, RF. 'Quantal' Ca2+ release and the control of Ca2+ entry by inositol phosphates--a possible mechanism. FEBS Lett 1990;263(1):5-9.
298. Montell, C. The TRP superfamily of cation channels. Sci STKE 2005;2005(272):re3.
299. Venkatachalam, K, van Rossum, DB, Patterson, RL, et al. The cellular and molecular basis of store-operated calcium entry. Nat Cell Biol 2002;4(11):E263-272.
300. Liu, X, Bandyopadhyay, BC, Singh, BB, et al. Molecular analysis of a store-operated and 2-acetyl-sn-glycerol-sensitive non-selective cation channel. Heteromeric assembly of TRPC1-TRPC3. J Biol Chem 2005;280(22):21600-21606.
301. Cheng, KT, Liu, X, Ong, HL, et al. Local Ca^{2}+ entry via Orai1 regulates plasma membrane recruitment of TRPC1 and controls cytosolic Ca^{2}+ signals required for specific cell functions. PLoS biology 2011;9(3):e1001025-e1001025.
302. Kiselyov, K, Patterson, RL. The integrative function of TRPC channels. Front Biosci 2009;14(14):45-58.
303. Minke, B, Cook, B. TRP Channel Proteins and Signal Transduction. Physiological Reviews 2002;82(2):429-472.
304. Birnbaumer, L. The TRPC class of ion channels: a critical review of their roles in slow, sustained increases in intracellular Ca(2+) concentrations. Annu Rev Pharmacol Toxicol 2009;49:395-426.
305. Hofmann, T, Obukhov, AG, Schaefer, M, et al. Direct activation of human TRPC6 and TRPC3 channels by diacylglycerol. Nature 1999;397(6716):259-263.
306. Nilius, B, Owsianik, G, Voets, T, et al. Transient receptor potential cation channels in disease. Physiol Rev 2007;87(1):165-217.
307. Berridge, MJ, Lipp, P, Bootman, MD. The versatility and universality of calcium signalling. Nature reviews Molecular cell biology 2000;1(1):11-21.

308. Chang, HH, Cheng, YC, Tsai, WC, et al. Pyr3 Induces Apoptosis and Inhibits Migration in Human Glioblastoma Cells. Cellular Physiology and Biochemistry 2018;48(4):1694-1702.
309. Lin, D-C, Zheng, S-Y, Zhang, Z-G, et al. TRPC3 promotes tumorigenesis of gastric cancer via the CNB2/GSK3β/NFATc2 signaling pathway. Cancer Letters 2021;519:211-225.
310. Yang, SL, Cao, Q, Zhou, KC, et al. Transient receptor potential channel C3 contributes to the progression of human ovarian cancer. Oncogene 2009;28(10):1320-1328.
311. Wang, Y, Qi, Y-X, Qi, Z, et al. TRPC3 Regulates the Proliferation and Apoptosis Resistance of Triple Negative Breast Cancer Cells through the TRPC3/RASA4/MAPK Pathway. Cancers 2019;11(4):558.
312. Li, S, Jiang, K, Li, J, et al. Estrogen enhances the proliferation and migration of ovarian cancer cells by activating transient receptor potential channel C3. Journal of Ovarian Research 2020;13(1):20.
313. Tao, X, Zhao, N, Jin, H, et al. FSH enhances the proliferation of ovarian cancer cells by activating transient receptor potential channel C3. Endocrine-related cancer 2013;20(3):415-429.
314. Schwab, A, Fabian, A, Hanley, PJ, et al. Role of ion channels and transporters in cell migration. Physiol Rev 2012;92(4):1865-1913.
315. Friedl, P, Mayor, R. Tuning Collective Cell Migration by Cell-Cell Junction Regulation. Cold Spring Harb Perspect Biol 2017;9(4).
316. Fife, CM, McCarroll, JA, Kavallaris, M. Movers and shakers: cell cytoskeleton in cancer metastasis. Br J Pharmacol 2014;171(24):5507-5523.
317. Fioro Pla, A, Gkika, D. Emerging role of TRP channels in cell migration: from tumor vascularization to metastasis. Frontiers in physiology 2013;4:311.
318. Oda, K, Umemura, M, Nakakaji, R, et al. Transient receptor potential cation 3 channel regulates melanoma proliferation and migration. The Journal of Physiological Sciences 2017;67(4):497-505.
319. Rundhaug, JE. Matrix metalloproteinases and angiogenesis. Journal of Cellular and Molecular Medicine 2005;9(2):267-285.
320. Ge, P, Wei, L, Zhang, M, et al. TRPC1/3/6 inhibition attenuates the TGF-β1-induced epithelial–mesenchymal transition in gastric cancer via the Ras/Raf1/ERK signaling pathway. Cell Biology International 2018;42(8):975-984.
321. Smedlund, K, Tano, JY, Vazquez, G. The constitutive function of native TRPC3 channels modulates vascular cell adhesion molecule-1 expression in coronary endothelial cells through nuclear factor kappaB signaling. Circ Res 2010;106(9):1479-1488.
322. Wang, T, Ning, K, Lu, T-X, et al. Increasing circulating exosomes-carrying TRPC5 predicts chemoresistance in metastatic breast cancer patients. Cancer science 2017;108(3):448-454.
323. Liang, B, Peng, P, Chen, S, et al. Characterization and proteomic analysis of ovarian cancer-derived exosomes. Journal of Proteomics 2013;80:171-182.
324. Skog, J, Würdinger, T, van Rijn, S, et al. Glioblastoma microvesicles transport RNA and proteins that promote tumour growth and provide diagnostic biomarkers. Nature cell biology 2008;10(12):1470-1476.
325. Isola, AL, Chen, S. Exosomes: The Link between GPCR Activation and Metastatic Potential? Frontiers in genetics 2016;7:56-56.
326. Dulneva, A, Lee, S, Oliver, PL, et al. The mutant Moonwalker TRPC3 channel links calcium signaling to lipid metabolism in the developing cerebellum. Human Molecular Genetics 2015;24(14):4114-4125.
327. Hanson, SM, Sansom, MSP, Becker, EBE. Modeling Suggests TRPC3 Hydrogen Bonding and Not Phosphorylation Contributes to the Ataxia Phenotype of the Moonwalker Mouse. Biochemistry 2015;54(26):4033-4041.

328. Fogel, BL, Hanson, SM, Becker, EBE. Do Mutations in the Murine Ataxia Gene TRPC3 Cause Cerebellar Ataxia in Humans? Movement disorders : official journal of the Movement Disorder Society 2015;30(2):284-286.
329. Haley, J, Tomar, S, Pulliam, N, et al. Functional characterization of a panel of high-grade serous ovarian cancer cell lines as representative experimental models of the disease. Oncotarget 2016;7(22):32810-32820.
330. Mitra, AK, Davis, DA, Tomar, S, et al. In vivo tumor growth of high-grade serous ovarian cancer cell lines. Gynecol Oncol 2015;138(2):372-377.
331. Domcke, S, Sinha, R, Levine, DA, et al. Evaluating cell lines as tumour models by comparison of genomic profiles. Nat Commun 2013;4:2126.
332. Beaufort, CM, Helmijr, JC, Piskorz, AM, et al. Ovarian cancer cell line panel (OCCP): clinical importance of in vitro morphological subtypes. PLoS One 2014;9(9):e103988.
333. Hallas-Potts, A, Dawson, JC, Herrington, CS. Ovarian cancer cell lines derived from non-serous carcinomas migrate and invade more aggressively than those derived from high-grade serous carcinomas. Scientific Reports 2019;9(1):5515.
334. Hamilton, TC, Young, RC, Ozols, RF. Experimental model systems of ovarian cancer: applications to the design and evaluation of new treatment approaches. Semin Oncol 1984;11(3):285-298.
335. Huang, HK, Lin, YH, Chang, HA, et al. Chemoresistant ovarian cancer enhances its migration abilities by increasing store-operated Ca(2+) entry-mediated turnover of focal adhesions. J Biomed Sci 2020;27(1):36.
336. Xu, X, Lozinskaya, I, Costell, M, et al. Characterization of small molecule TRPC3 and TRPC6 agonist and antagonists. Biophysical Journal 2013;104(2):454a.
337. Kiyonaka, S, Kato, K, Nishida, M, et al. Selective and direct inhibition of TRPC3 channels underlies biological activities of a pyrazole compound. Proceedings of the National Academy of Sciences of the United States of America 2009;106(13):5400-5405.
338. Schindelin, J, Arganda-Carreras, I, Frise, E, et al. Fiji: an open-source platform for biological-image analysis. Nat Methods 2012;9(7):676-682.
339. Kelley, JB, Paschal, BM. Fluorescence-based quantification of nucleocytoplasmic transport. Methods 2019;157:106-114.
340. Todaro, GJ, Lazar, GK, Green, H. The initiation of cell division in a contact-inhibited mammalian cell line. Journal of Cellular and Comparative Physiology 1965;66(3):325-333.
341. Bäcker, V. ImageJ Macro Tool Sets for Biological Image Analysis. 2012.
342. Boyden, S. The chemotactic effect of mixtures of antibody and antigen on polymorphonuclear leucocytes. The Journal of experimental medicine 1962;115(3):453-466.
343. Koliha, N, Wiencek, Y, Heider, U, et al. A novel multiplex bead-based platform highlights the diversity of extracellular vesicles. Journal of extracellular vesicles 2016;5:29975-29975.
344. Härkönen, K, Oikari, S, Kyykallio, H, et al. CD44s Assembles Hyaluronan Coat on Filopodia and Extracellular Vesicles and Induces Tumorigenicity of MKN74 Gastric Carcinoma Cells. Cells 2019;8(3):276.
345. Tonzani, S. TIRF: imaging at the cellular edge. Nature Cell Biology 2009;11(1):S16-S16.
346. Mattheyses, AL, Simon, SM, Rappoport, JZ. Imaging with total internal reflection fluorescence microscopy for the cell biologist. J Cell Sci 2010;123(Pt 21):3621-3628.
347. Rietdorf, J, Seitz, A. Kymograph (time space plot) Plugin for ImageJ; 2008. https://www.embl.de/eamnet/downloads/kymograph/kymograph_description.pdf. Accessed January 2019.
348. Balaji, J. Time Series Analyzer; 2014. https://imagej.nih.gov/ij/plugins/time-series.html. Accessed January 2019.

349. Huang da, W, Sherman, BT, Lempicki, RA. Bioinformatics enrichment tools: paths toward the comprehensive functional analysis of large gene lists. Nucleic Acids Res 2009;37(1):1-13.
350. Huang da, W, Sherman, BT, Lempicki, RA. Systematic and integrative analysis of large gene lists using DAVID bioinformatics resources. Nat Protoc 2009;4(1):44-57.
351. Fels, B, Bulk, E, Pethő, Z, et al. The Role of TRP Channels in the Metastatic Cascade. Pharmaceuticals (Basel, Switzerland) 2018;11(2):48.
352. Déliot, N, Constantin, B. Plasma membrane calcium channels in cancer: Alterations and consequences for cell proliferation and migration. Biochimica et Biophysica Acta (BBA) - Biomembranes 2015;1848(10, Part B):2512-2522.
353. Schwab, A, Stock, C. Ion channels and transporters in tumour cell migration and invasion. Philosophical transactions of the Royal Society of London Series B, Biological sciences 2014;369(1638):20130102-20130102.
354. Iamshanova, O, Fiorio Pla, A, Prevarskaya, N. Molecular mechanisms of tumour invasion: regulation by calcium signals. J Physiol 2017;595(10):3063-3075.
355. Trebak, M, Lemonnier, L, Smyth, JT, et al. Phospholipase C-coupled receptors and activation of TRPC channels. Handb Exp Pharmacol 2007;(179):593-614.
356. Azimi, I, Milevskiy, MJG, Kaemmerer, E, et al. TRPC1 is a differential regulator of hypoxia-mediated events and Akt signalling in PTEN-deficient breast cancer cells. Journal of Cell Science 2017;130(14):2292-2305.
357. Zhu, Y, Pan, Q, Meng, H, et al. Enhancement of vascular endothelial growth factor release in long-term drug-treated breast cancer via transient receptor potential channel 5-Ca2+-hypoxia-inducible factor 1α pathway. Pharmacological Research 2015;93:36-42.
358. Aydar, E, Yeo, S, Djamgoz, M, et al. Abnormal expression, localization and interaction of canonical transient receptor potential ion channels in human breast cancer cell lines and tissues: a potential target for breast cancer diagnosis and therapy. Cancer Cell International 2009;9(1):23.
359. El Boustany, C, Bidaux, G, Enfissi, A, et al. Capacitative calcium entry and transient receptor potential canonical 6 expression control human hepatoma cell proliferation. Hepatology 2008;47(6):2068-2077.
360. Thebault, S, Flourakis, M, Vanoverberghe, K, et al. Differential Role of Transient Receptor Potential Channels in Ca²⁺ Entry and Proliferation of Prostate Cancer Epithelial Cells. Cancer Research 2006;66(4):2038.
361. Cai, R, Ding, X, Zhou, K, et al. Blockade of TRPC6 channels induced G2/M phase arrest and suppressed growth in human gastric cancer cells. International journal of cancer 2009;125(10):2281-2287.
362. Jiang, H-N, Zeng, B, Zhang, Y, et al. Involvement of TRPC channels in lung cancer cell differentiation and the correlation analysis in human non-small cell lung cancer. PloS one 2013;8(6):e67637-e67637.
363. Kim, JM, Heo, K, Choi, J, et al. The histone variant MacroH2A regulates Ca(2+) influx through TRPC3 and TRPC6 channels. Oncogenesis 2013;2(10):e77-e77.
364. Kwan, HY, Wong, CO, Chen, ZY, et al. Stimulation of histamine H2 receptors activates TRPC3 channels through both phospholipase C and phospholipase D. Eur J Pharmacol 2009;602(2-3):181-187.
365. Batra, S, Fadeel, I. Release of intracellular calcium and stimulation of cell growth by ATP and histamine in human ovarian cancer cells (SKOV-3). Cancer Lett 1994;77(1):57-63.
366. Popper, L, Batra, S. Muscarinic acetylcholine and histamine-receptor mediated calcium mobilization and cell-growth in human ovarian-cancer cells. Int J Oncol 1994;4(2):453-459.

367. Bandyopadhyay, BC, Swaim, WD, Liu, X, et al. Apical localization of a functional TRPC3/TRPC6-Ca2+-signaling complex in polarized epithelial cells: role in apical Ca2+ influx. Journal of Biological Chemistry 2005;280(13):12908-12916.
368. Rizzuto, R, Pinton, P, Ferrari, D, et al. Calcium and apoptosis: facts and hypotheses. Oncogene 2003;22(53):8619-8627.
369. Hogan, PG, Chen, L, Nardone, J, et al. Transcriptional regulation by calcium, calcineurin, and NFAT. Genes Dev 2003;17(18):2205-2232.
370. Blayney, JK, Davison, T, McCabe, N, et al. Prior knowledge transfer across transcriptional data sets and technologies using compositional statistics yields new mislabelled ovarian cell line. Nucleic Acids Res 2016;44(17):e137.
371. Jung-Hye, C, Kyung-Chul, C, Nelly, A, et al. Gonadotropins upregulate the epidermal growth factor receptor through activation of mitogen-activated protein kinases and phosphatidyl-inositol-3-kinase in human ovarian surface epithelial cells. Endocrine-Related Cancer Endocr Relat Cancer 2005;12(2):407-421.
372. Kobayashi, M, Salomon, C, Tapia, J, et al. Ovarian cancer cell invasiveness is associated with discordant exosomal sequestration of Let-7 miRNA and miR-200. Journal of translational medicine 2014;12:4-4.
373. Pokhriyal, R, Hariprasad, R, Kumar, L, et al. Chemotherapy Resistance in Advanced Ovarian Cancer Patients. Biomarkers in cancer 2019;11:1179299X19860815-11179299X19860815.
374. Hartmann, J, Dragicevic, E, Adelsberger, H, et al. TRPC3 channels are required for synaptic transmission and motor coordination. Neuron 2008;59(3):392-398.
375. Peavey, MC, Wu, S-P, Li, R, et al. Progesterone receptor isoform B regulates the Oxtr-Plcl2-Trpc3 pathway to suppress uterine contractility. Proceedings of the National Academy of Sciences of the United States of America 2021;118(11):e2011643118.
376. Onohara, N, Nishida, M, Inoue, R, et al. TRPC3 and TRPC6 are essential for angiotensin II-induced cardiac hypertrophy. The EMBO Journal 2006;25(22):5305-5316.
377. Fernández-Nogueira, P, Noguera-Castells, A, Fuster, G, et al. Histamine receptor 1 inhibition enhances antitumor therapeutic responses through extracellular signal-regulated kinase (ERK) activation in breast cancer. Cancer Lett 2018;424:70-83.
378. Stoyanov, E, Uddin, M, Mankuta, D, et al. Mast cells and histamine enhance the proliferation of non-small cell lung cancer cells. Lung Cancer 2012;75(1):38-44.
379. Zhao, J, Hou, Y, Yin, C, et al. Upregulation of histamine receptor H1 promotes tumor progression and contributes to poor prognosis in hepatocellular carcinoma. Oncogene 2020;39(8):1724-1738.
380. Mochida, S, Hunt, T. Calcineurin is required to release Xenopus egg extracts from meiotic M phase. Nature 2007;449(7160):336-340.
381. Xiao, Z-J, Liu, J, Wang, S-Q, et al. NFATc2 enhances tumor-initiating phenotypes through the NFATc2/SOX2/ALDH axis in lung adenocarcinoma. Elife 2017;6:e26733.
382. Ma, X, Cai, Y, He, D, et al. Transient receptor potential channel TRPC5 is essential for P-glycoprotein induction in drug-resistant cancer cells. Proceedings of the National Academy of Sciences 2012;109(40):16282-16287.
383. Urso, K, Fernández, A, Velasco, P, et al. NFATc3 controls tumour growth by regulating proliferation and migration of human astroglioma cells. Scientific Reports 2019;9(1):9361.
384. Pigozzi, D, Ducret, T, Tajeddine, N, et al. Calcium store contents control the expression of TRPC1, TRPC3 and TRPV6 proteins in LNCaP prostate cancer cell line. Cell Calcium 2006;39(5):401-415.
385. Liao, Y, Plummer, NW, George, MD, et al. A role for Orai in TRPC-mediated Ca²⁺ entry suggests that a TRPC:Orai complex may mediate store and

receptor operated Ca²⁺ entry. Proceedings of the National Academy of Sciences 2009;106(9):3202.
386. Liu, E-L, Zhou, Y-X, Li, J, et al. Long-Chain Non-Coding RNA SNHG3 Promotes the Growth of Ovarian Cancer Cells by Targeting miR-339-5p/TRPC3 Axis. OncoTargets and therapy 2020;13:10959-10971.
387. Ishise, H, Larson, B, Hirata, Y, et al. Hypertrophic scar contracture is mediated by the TRPC3 mechanical force transducer via NFkB activation. Scientific reports 2015;5:11620-11620.
388. McLean, GW, Carragher, NO, Avizienyte, E, et al. The role of focal-adhesion kinase in cancer — a new therapeutic opportunity. Nature Reviews Cancer 2005;5(7):505-515.
389. Tan, I, Leung, T. Myosin light chain kinases: division of work in cell migration. Cell adhesion & migration 2009;3(3):256-258.
390. Sood, AK, Coffin, JE, Schneider, GB, et al. Biological significance of focal adhesion kinase in ovarian cancer: role in migration and invasion. The American journal of pathology 2004;165(4):1087-1095.
391. McKenzie, AJ, Hicks, SR, Svec, KV, et al. The mechanical microenvironment regulates ovarian cancer cell morphology, migration, and spheroid disaggregation. Scientific Reports 2018;8(1):7228.
392. Hu, X, Li, D, Zhang, W, et al. Matrix metalloproteinase-9 expression correlates with prognosis and involved in ovarian cancer cell invasion. Arch Gynecol Obstet 2012;286(6):1537-1543.
393. Tsai, F-C, Seki, A, Yang, HW, et al. A polarized Ca2+, diacylglycerol and STIM1 signalling system regulates directed cell migration. Nature cell biology 2014;16(2):133-144.
394. Wei, C, Wang, X, Chen, M, et al. Calcium flickers steer cell migration. Nature 2009;457(7231):901-905.
395. Varankar, SS, Bapat, SA. Migratory Metrics of Wound Healing: A Quantification Approach for in vitro Scratch Assays. Frontiers in Oncology 2018;8(633).
396. Kalluri, R, Neilson, EG. Epithelial-mesenchymal transition and its implications for fibrosis. J Clin Invest 2003;112(12):1776-1784.
397. Thiery, JP, Sleeman, JP. Complex networks orchestrate epithelial-mesenchymal transitions. Nat Rev Mol Cell Biol 2006;7(2):131-142.
398. Wang, D, Li, X, Liu, J, et al. Effects of TRPC6 on invasibility of low-differentiated prostate cancer cells. Asian Pac J Trop Med 2014;7(1):44-47.
399. Eccles, SA, Patterson, L. In vitro assays for endothelial cell functions required for angiogenesis: proliferation, motility, tubular differentiation, and matrix proteolysis. In: Angiogenesis Protocols. Springer, 2016.
400. Friedl, P, Zänker, KS, Bröcker, EB. Cell migration strategies in 3-D extracellular matrix: differences in morphology, cell matrix interactions, and integrin function. Microsc Res Tech 1998;43(5):369-378.
401. Gupta, GP, Massagué, J. Cancer metastasis: building a framework. Cell 2006;127(4):679-695.
402. Wilhelmsen, K, Farrar, K, Hellman, J. Quantitative in vitro assay to measure neutrophil adhesion to activated primary human microvascular endothelial cells under static conditions. J Vis Exp 2013;(78):e50677.
403. Shen, X, Wang, C, Zhu, H, et al. Exosome-mediated transfer of CD44 from high-metastatic ovarian cancer cells promotes migration and invasion of low-metastatic ovarian cancer cells. Journal of Ovarian Research 2021;14(1):38.
404. Li, X, Tang, M, Zhu, Q, et al. The exosomal integrin α5β1/AEP complex derived from epithelial ovarian cancer cells promotes peritoneal metastasis through regulating mesothelial cell proliferation and migration. Cellular Oncology 2020;43(2):263-277.

405. Tang, MKS, Yue, PYK, Ip, PP, et al. Soluble E-cadherin promotes tumor angiogenesis and localizes to exosome surface. Nature communications 2018;9(1):2270-2270.
406. Reiner, AT, Tan, S, Agreiter, C, et al. EV-Associated MMP9 in High-Grade Serous Ovarian Cancer Is Preferentially Localized to Annexin V-Binding EVs. Disease markers 2017;2017:9653194-9653194.
407. Isola, AL, Eddy, K, Zembrzuski, K, et al. Exosomes released by metabotropic glutamate receptor 1 (GRM1) expressing melanoma cells increase cell migration and invasiveness. Oncotarget 2017;9(1):1187-1199.
408. Brunner, D, Frank J Fau - Appl, H, Appl H Fau - Schöffl, H, et al. Serum-free cell culture: the serum-free media interactive online database. 2010;(1868-596X (Print)).
409. Lehrich, BM, Liang, Y, Khosravi, P, et al. Fetal Bovine Serum-Derived Extracellular Vesicles Persist within Vesicle-Depleted Culture Media. International journal of molecular sciences 2018;19(11):3538.
410. Kornilov, R, Puhka, M, Mannerström, B, et al. Efficient ultrafiltration-based protocol to deplete extracellular vesicles from fetal bovine serum. Journal of extracellular vesicles 2018;7(1):1422674-1422674.
411. Lehrich, BM, Liang, Y, Fiandaca, MS. Foetal bovine serum influence on in vitro extracellular vesicle analyses. Journal of extracellular vesicles 2021;10(3):e12061-e12061.
412. Théry, C, Witwer, KW, Aikawa, E, et al. Minimal information for studies of extracellular vesicles 2018 (MISEV2018): a position statement of the International Society for Extracellular Vesicles and update of the MISEV2014 guidelines. Journal of extracellular vesicles 2018;7(1):1535750-1535750.
413. Graves, LE, Ariztia, EV, Navari, JR, et al. Proinvasive Properties of Ovarian Cancer Ascites-Derived Membrane Vesicles. Cancer Research 2004;64(19):7045.
414. Yokoi, A, Yoshioka, Y, Yamamoto, Y, et al. Malignant extracellular vesicles carrying MMP1 mRNA facilitate peritoneal dissemination in ovarian cancer. Nat Commun 2017;8:14470.
415. Naito, R, Kassai, H, Sakai, Y, et al. New Features on the Expression and Trafficking of mGluR1 Splice Variants Exposed by Two Novel Mutant Mouse Lines. Frontiers in Molecular Neuroscience 2018;11.
416. Moreno-Gonzalo, O, Villarroya-Beltri, C, Sánchez-Madrid, F. Post-Translational Modifications of Exosomal Proteins. Frontiers in Immunology 2014;5.
417. Williams, C, Royo, F, Aizpurua-Olaizola, O, et al. Glycosylation of extracellular vesicles: current knowledge, tools and clinical perspectives. Journal of Extracellular Vesicles 2018;7(1):1442985.
418. Mol, EA, Goumans, MJ, Doevendans, PA, et al. Higher functionality of extracellular vesicles isolated using size-exclusion chromatography compared to ultracentrifugation. Nanomedicine 2017;13(6):2061-2065.
419. Shelke, GV, Lässer, C, Gho, YS, et al. Importance of exosome depletion protocols to eliminate functional and RNA-containing extracellular vesicles from fetal bovine serum. Journal of extracellular vesicles 2014;3:10.3402/jev.v3403.24783.
420. Li, J, Lee, Y, Johansson, HJ, et al. Serum-free culture alters the quantity and protein composition of neuroblastoma-derived extracellular vesicles. Journal of extracellular vesicles 2015;4:26883-26883.
421. Riches, A, Campbell, E, Borger, E, et al. Regulation of exosome release from mammary epithelial and breast cancer cells – A new regulatory pathway. European Journal of Cancer 2014;50(5):1025-1034.
422. Keerthikumar, S, Gangoda, L, Liem, M, et al. Proteogenomic analysis reveals exosomes are more oncogenic than ectosomes. Oncotarget 2015;6(17):15375-15396.

423. Théry, C, Regnault, A, Garin, J, et al. Molecular characterization of dendritic cell-derived exosomes. Selective accumulation of the heat shock protein hsc73. J Cell Biol 1999;147(3):599-610.
424. Théry, C, Ostrowski, M, Segura, E. Membrane vesicles as conveyors of immune responses. Nat Rev Immunol 2009;9(8):581-593.
425. Mathivanan, S, Lim, JW, Tauro, BJ, et al. Proteomics analysis of A33 immunoaffinity-purified exosomes released from the human colon tumor cell line LIM1215 reveals a tissue-specific protein signature. Mol Cell Proteomics 2010;9(2):197-208.
426. Crescitelli, R, Lässer, C, Szabó, TG, et al. Distinct RNA profiles in subpopulations of extracellular vesicles: apoptotic bodies, microvesicles and exosomes. Journal of Extracellular Vesicles 2013;2(1):20677.
427. Willms, E, Cabañas, C, Mäger, I, et al. Extracellular Vesicle Heterogeneity: Subpopulations, Isolation Techniques, and Diverse Functions in Cancer Progression. Frontiers in Immunology 2018;9:738.
428. Kugeratski, FG, Hodge, K, Lilla, S, et al. Quantitative proteomics identifies the core proteome of exosomes with syntenin-1 as the highest abundant protein and a putative universal biomarker. Nature Cell Biology 2021;23(6):631-641.
429. Cheng, L, Wu, S, Zhang, K, et al. A comprehensive overview of exosomes in ovarian cancer: emerging biomarkers and therapeutic strategies. Journal of ovarian research 2017;10(1):73-73.
430. Li, C, Guo, B, Wilson, PB, et al. Plasma levels of soluble CD105 correlate with metastasis in patients with breast cancer. International Journal of Cancer 2000;89(2):122-126.
431. Zhang, J, Yuan, B, Zhang, H, et al. Human epithelial ovarian cancer cells expressing CD105, CD44 and CD106 surface markers exhibit increased invasive capacity and drug resistance. Oncol Lett 2019;17(6):5351-5360.
432. Hu, J, Guan, W, Yan, L, et al. Cancer stem cell marker endoglin (CD105) induces epithelial mesenchymal transition (EMT) but not metastasis in clear cell renal cell carcinoma. Stem cells international 2019;2019.
433. Li, Y, Zhai, Z, Liu, D, et al. CD105 promotes hepatocarcinoma cell invasion and metastasis through VEGF. Tumor Biology 2015;36(2):737-745.
434. Douglas, SR, Yeung, KT, Yang, J, et al. Identification of CD105+ Extracellular Vesicles as a Candidate Biomarker for Metastatic Breast Cancer. Journal of Surgical Research 2021;268:168-173.
435. Rappa, G, Mercapide, J, Anzanello, F, et al. Wnt interaction and extracellular release of prominin-1/CD133 in human malignant melanoma cells. Experimental cell research 2013;319(6):810-819.
436. Rappa, G, Fodstad, O, Lorico, A. The stem cell-associated antigen CD133 (Prominin-1) is a molecular therapeutic target for metastatic melanoma. Stem Cells 2008;26(12):3008-3017.
437. Rappa, G, Mercapide, J, Anzanello, F, et al. Biochemical and biological characterization of exosomes containing prominin-1/CD133. Molecular Cancer 2013;12(1):62.
438. Filipe, V, Hawe, A, Jiskoot, W. Critical evaluation of Nanoparticle Tracking Analysis (NTA) by NanoSight for the measurement of nanoparticles and protein aggregates. Pharm Res 2010;27(5):796-810.
439. Bachurski, D, Schuldner, M, Nguyen, PH, et al. Extracellular vesicle measurements with nanoparticle tracking analysis - An accuracy and repeatability comparison between NanoSight NS300 and ZetaView. J Extracell Vesicles 2019;8(1):1596016.
440. Yi, H, Ye, J, Yang, X-M, et al. High-grade ovarian cancer secreting effective exosomes in tumor angiogenesis. International journal of clinical and experimental pathology 2015;8(5):5062-5070.

441. Gudbergsson, JM, Johnsen, KB, Skov, MN, et al. Systematic review of factors influencing extracellular vesicle yield from cell cultures. Cytotechnology 2016;68(4):579-592.
442. Giusti, I, Di Francesco, M, D'Ascenzo, S, et al. Ovarian cancer-derived extracellular vesicles affect normal human fibroblast behavior. Cancer biology & therapy 2018;19(8):722-734.
443. Chen, X, Ying, X, Wang, X, et al. Exosomes derived from hypoxic epithelial ovarian cancer deliver microRNA-940 to induce macrophage M2 polarization. Oncol Rep 2017;38(1):522-528.
444. Vera, N, Acuña-Gallardo, S, Grünenwald, F, et al. Small Extracellular Vesicles Released from Ovarian Cancer Spheroids in Response to Cisplatin Promote the Pro-Tumorigenic Activity of Mesenchymal Stem Cells. International Journal of Molecular Sciences 2019;20(20):4972.
445. Li, W, Zhang, X, Wang, J, et al. TGFβ1 in fibroblasts-derived exosomes promotes epithelial-mesenchymal transition of ovarian cancer cells. Oncotarget 2017;8(56):96035-96047.
446. Reza, AMMT, Choi, Y-J, Yasuda, H, et al. Human adipose mesenchymal stem cell-derived exosomal-miRNAs are critical factors for inducing anti-proliferation signalling to A2780 and SKOV-3 ovarian cancer cells. Scientific reports 2016;6:38498-38498.
447. Chen, Q, Li, Y, Gao, W, et al. Exosome-Mediated Crosstalk Between Tumor and Tumor-Associated Macrophages. Frontiers in Molecular Biosciences 2021;8.
448. Heredia-Soto, V, Redondo, A, Berjón, A, et al. High-throughput 3-dimensional culture of epithelial ovarian cancer cells as preclinical model of disease. Oncotarget; Vol 9, No 31 2018.
449. Tudrej, P, Olbryt, M, Zembala-Nożyńska, E, et al. Establishment and Characterization of the Novel High-Grade Serous Ovarian Cancer Cell Line OVPA8. International Journal of Molecular Sciences 2018;19(7).
450. Samuel, P, Mulcahy, LA, Furlong, F, et al. Cisplatin induces the release of extracellular vesicles from ovarian cancer cells that can induce invasiveness and drug resistance in bystander cells. Philos Trans R Soc Lond B Biol Sci 2018;373(1737).
451. de Jong, OG, Murphy, DE, Mäger, I, et al. A CRISPR-Cas9-based reporter system for single-cell detection of extracellular vesicle-mediated functional transfer of RNA. Nature Communications 2020;11(1):1113.
452. Mutschelknaus, L, Peters, C, Winkler, K, et al. Exosomes Derived from Squamous Head and Neck Cancer Promote Cell Survival after Ionizing Radiation. PLoS One 2016;11(3):e0152213.
453. Josson, S, Gururajan, M, Sung, SY, et al. Stromal fibroblast-derived miR-409 promotes epithelial-to-mesenchymal transition and prostate tumorigenesis. Oncogene 2015;34(21):2690-2699.
454. Zhang, M, Jin, K, Gao, L, et al. Methods and Technologies for Exosome Isolation and Characterization. Small Methods 2018;2(9):1800021.
455. Andreu, Z, Yáñez-Mó, M. Tetraspanins in Extracellular Vesicle Formation and Function. Frontiers in Immunology 2014;5:442.
456. Hurwitz Stephanie, N, Nkosi, D, Conlon Meghan, M, et al. CD63 Regulates Epstein-Barr Virus LMP1 Exosomal Packaging, Enhancement of Vesicle Production, and Noncanonical NF-κB Signaling. Journal of Virology 91(5):e02251-02216.
457. Corrigan, L, Redhai, S, Leiblich, A, et al. BMP-regulated exosomes from Drosophila male reproductive glands reprogram female behavior. J Cell Biol 2014;206(5):671-688.
458. Ventimiglia, LN, Fernández-Martín, L, Martínez-Alonso, E, et al. Cutting Edge: Regulation of Exosome Secretion by the Integral MAL Protein in T Cells. J Immunol 2015;195(3):810-814.

459. Lu, A, Wawro, P, Morgens, DW, et al. Genome-wide interrogation of extracellular vesicle biology using barcoded miRNAs. eLife 2018;7:e41460.
460. Bobrie, A, Colombo, M, Krumeich, S, et al. Diverse subpopulations of vesicles secreted by different intracellular mechanisms are present in exosome preparations obtained by differential ultracentrifugation. Journal of Extracellular Vesicles 2012;1(1):18397.
461. Bebelman, MP, Bun, P, Huveneers, S, et al. Real-time imaging of multivesicular body–plasma membrane fusion to quantify exosome release from single cells. Nature Protocols 2020;15(1):102-121.
462. Repka-Ramirez, MS. New concepts of histamine receptors and actions. Current allergy and asthma reports 2003;3(3):227-231.
463. Aydar, E, Yeo, S, Djamgoz, M, et al. Abnormal expression, localization and interaction of canonical transient receptor potential ion channels in human breast cancer cell lines and tissues: a potential target for breast cancer diagnosis and therapy. Cancer cell international 2009;9:23-23.
464. Lavender, V, Chong, S, Ralphs, K, et al. Increasing the expression of calcium-permeable TRPC3 and TRPC7 channels enhances constitutive secretion. The Biochemical journal 2008;413(3):437-446.
465. van Niel, G, Raposo, G, Candalh, C, et al. Intestinal epithelial cells secrete exosome-like vesicles. Gastroenterology 2001;121(2):337-349.
466. Contento, RL, Molon, B, Boularan, C, et al. CXCR4–CCR5: a couple modulating T cell functions. Proceedings of the National Academy of Sciences 2008;105(29):10101-10106.
467. Harding, C, Stahl, P. Transferrin recycling in reticulocytes: pH and iron are important determinants of ligand binding and processing. Biochem Biophys Res Commun 1983;113(2):650-658.
468. Choi, DS, Kim, DK, Kim, YK, et al. Proteomics, transcriptomics and lipidomics of exosomes and ectosomes. Proteomics 2013;13(10-11):1554-1571.
469. Abels, ER, Breakefield, XO. Introduction to Extracellular Vesicles: Biogenesis, RNA Cargo Selection, Content, Release, and Uptake. Cellular and molecular neurobiology 2016;36(3):301-312.
470. Hedlund, M, Nagaeva, O, Kargl, D, et al. Thermal- and oxidative stress causes enhanced release of NKG2D ligand-bearing immunosuppressive exosomes in leukemia/lymphoma T and B cells. PloS one 2011;6(2):e16899-e16899.
471. Salomon, C, Ryan, J, Sobrevia, L, et al. Exosomal signaling during hypoxia mediates microvascular endothelial cell migration and vasculogenesis. PloS one 2013;8(7):e68451-e68451.
472. Cheng, Q, Li, X, Wang, Y, et al. The ceramide pathway is involved in the survival, apoptosis and exosome functions of human multiple myeloma cells in vitro. Acta Pharmacol Sin 2018;39(4):561-568.
473. Abu-Taha, IH, Heijman, J, Feng, Y, et al. Regulation of heterotrimeric G-protein signaling by NDPK/NME proteins and caveolins: an update. Laboratory Investigation 2018;98(2):190-197.
474. Schöneberg, J, Pavlin Mark, R, Yan, S, et al. ATP-dependent force generation and membrane scission by ESCRT-III and Vps4. Science 2018;362(6421):1423-1428.
475. Choi, D, Montermini, L, Jeong, H, et al. Mapping Subpopulations of Cancer Cell-Derived Extracellular Vesicles and Particles by Nano-Flow Cytometry. ACS Nano 2019;13(9):10499-10511.
476. Heizmann, CW. Ca2+-Binding Proteins of the EF-Hand Superfamily: Diagnostic and Prognostic Biomarkers and Novel Therapeutic Targets. In: Heizmann, CW, ed. Calcium-Binding Proteins of the EF-Hand Superfamily: From Basics to Medical Applications. New York, NY: Springer New York, 2019.

477. Jones, T, Naslavsky, N, Caplan, S. Eps15 Homology Domain Protein 4 (EHD4) is required for Eps15 Homology Domain Protein 1 (EHD1)-mediated endosomal recruitment and fission. PLoS One 2020;15(9):e0239657.
478. Sharma, M, Naslavsky, N, Caplan, S. A role for EHD4 in the regulation of early endosomal transport. Traffic (Copenhagen, Denmark) 2008;9(6):995-1018.
479. Crescitelli, R, Lässer, C, Lötvall, J. Isolation and characterization of extracellular vesicle subpopulations from tissues. Nature Protocols 2021;16(3):1548-1580.
480. Tunçer, S, Gurbanov, R, Sheraj, I, et al. Low dose dimethyl sulfoxide driven gross molecular changes have the potential to interfere with various cellular processes. Scientific Reports 2018;8(1):14828.
481. Krasny, L, Huang, PH. Data-independent acquisition mass spectrometry (DIA-MS) for proteomic applications in oncology. Molecular Omics 2021;17(1):29-42.
482. Bruderer, R, Bernhardt, OM, Gandhi, T, et al. Extending the Limits of Quantitative Proteome Profiling with Data-Independent Acquisition and Application to Acetaminophen-Treated Three-Dimensional Liver Microtissues *^[S]. Molecular & Cellular Proteomics 2015;14(5):1400-1410.
483. Barkovits, K, Pacharra, S, Pfeiffer, K, et al. Reproducibility, Specificity and Accuracy of Relative Quantification Using Spectral Library-based Data-independent Acquisition *. Molecular & Cellular Proteomics 2020;19(1):181-197.
484. Erozenci, LA, Pham, TV, Piersma, SR, et al. Simple urine storage protocol for extracellular vesicle proteomics compatible with at-home self-sampling. Scientific Reports 2021;11(1):20760.
485. de Jong, OG, Verhaar, MC, Chen, Y, et al. Cellular stress conditions are reflected in the protein and RNA content of endothelial cell-derived exosomes. J Extracell Vesicles 2012;1.
486. Trubiani, O, Salvolini, E, Staffolani, R, et al. DMSO modifies structural and functional properties of RPMI-8402 cells by promoting programmed cell death. Int J Immunopathol Pharmacol 2003;16(3):253-259.
487. Da Violante, G, Zerrouk, N, Richard, I, et al. Evaluation of the cytotoxicity effect of dimethyl sulfoxide (DMSO) on Caco2/TC7 colon tumor cell cultures. Biol Pharm Bull 2002;25(12):1600-1603.
488. Rana, S, Zöller, M. The Functional Importance of Tetraspanins in Exosomes. In: Zhang, H-G, ed. Emerging Concepts of Tumor Exosome–Mediated Cell-Cell Communication. New York, NY: Springer New York, 2013.
489. Perez-Hernandez, D, Gutiérrez-Vázquez, C, Jorge, I, et al. The intracellular interactome of tetraspanin-enriched microdomains reveals their function as sorting machineries toward exosomes. J Biol Chem 2013;288(17):11649-11661.
490. Little, KD, Hemler, ME, Stipp, CS. Dynamic regulation of a GPCR-tetraspanin-G protein complex on intact cells: central role of CD81 in facilitating GPR56-Galpha q/11 association. Mol Biol Cell 2004;15(5):2375-2387.
491. Emmanuel, N, Ragunathan, S, Shan, Q, et al. Purine Nucleotide Availability Regulates mTORC1 Activity through the Rheb GTPase. Cell Rep 2017;19(13):2665-2680.
492. Zou, W, Lai, M, Zhang, Y, et al. Exosome Release Is Regulated by mTORC1. Advanced science (Weinheim, Baden-Wurttemberg, Germany) 2018;6(3):1801313-1801313.
493. Bebelman, MP, Crudden, C, Pegtel, DM, et al. The Convergence of Extracellular Vesicle and GPCR Biology. Trends in Pharmacological Sciences 2020;41(9):627-640.
494. Colombo, M, Moita, C, van Niel, G, et al. Analysis of ESCRT functions in exosome biogenesis, composition and secretion highlights the heterogeneity of extracellular vesicles. Journal of Cell Science 2013;126(24):5553-5565.
495. Blomme, A, Fahmy, K, Peulen, O, et al. Myoferlin is a novel exosomal protein and functional regulator of cancer-derived exosomes. Oncotarget 2016;7(50):83669-83683.

496. Fukuda, M, Kanno, E, Ishibashi, K, et al. Large scale screening for novel rab effectors reveals unexpected broad Rab binding specificity. Mol Cell Proteomics 2008;7(6):1031-1042.
497. Bhuin, T, Roy, JK. Rab proteins: the key regulators of intracellular vesicle transport. Exp Cell Res 2014;328(1):1-19.
498. Waters, MG, Serafini, T, Rothman, JE. 'Coatomer': a cytosolic protein complex containing subunits of non-clathrin-coated Golgi transport vesicles. Nature 1991;349(6306):248-251.
499. Tomsig, JL, Creutz, CE. Biochemical characterization of copine: a ubiquitous Ca2+-dependent, phospholipid-binding protein. Biochemistry 2000;39(51):16163-16175.
500. Okumura, M, Ichioka, F, Kobayashi, R, et al. Penta-EF-hand protein ALG-2 functions as a Ca2+-dependent adaptor that bridges Alix and TSG101. Biochemical and Biophysical Research Communications 2009;386(1):237-241.
501. Nguyen, DB, Thuy Ly, TB, Wesseling, MC, et al. Characterization of Microvesicles Released from Human Red Blood Cells. Cellular Physiology and Biochemistry 2016;38(3):1085-1099.
502. Zhao, X, Jiang, M, Wang, Z. TPM4 promotes cell migration by modulating F-actin formation in lung cancer. Onco Targets Ther 2019;12:4055-4063.
503. Tang, HY, Beer, LA, Tanyi, JL, et al. Protein isoform-specific validation defines multiple chloride intracellular channel and tropomyosin isoforms as serological biomarkers of ovarian cancer. J Proteomics 2013;89:165-178.
504. Dube, DK, Dube, S, Abbott, L, et al. Cloning, Sequencing, and the Expression of the Elusive Sarcomeric TPM4α Isoform in Humans. Mol Biol Int 2016;2016:3105478.
505. Hoshino, A, Kim, HS, Bojmar, L, et al. Extracellular Vesicle and Particle Biomarkers Define Multiple Human Cancers. Cell 2020;182(4):1044-1061.e1018.
506. Fei, F, Qu, J, Zhang, M, et al. S100A4 in cancer progression and metastasis: A systematic review. Oncotarget 2017;8(42):73219-73239.
507. Lv, Y, Niu, Z, Guo, X, et al. Serum S100 calcium binding protein A4 (S100A4, metatasin) as a diagnostic and prognostic biomarker in epithelial ovarian cancer. Br J Biomed Sci 2018;75(2):88-91.
508. Lyu, T, Wang, Y, Li, D, et al. Exosomes from BM-MSCs promote acute myeloid leukemia cell proliferation, invasion and chemoresistance via upregulation of S100A4. Experimental Hematology & Oncology 2021;10(1):24.
509. Sun, H, Wang, C, Hu, B, et al. Exosomal S100A4 derived from highly metastatic hepatocellular carcinoma cells promotes metastasis by activating STAT3. Signal transduction and targeted therapy 2021;6(1):187-187.
510. Kuk, C, Kulasingam, V, Gunawardana, CG, et al. Mining the ovarian cancer ascites proteome for potential ovarian cancer biomarkers. Molecular & cellular proteomics : MCP 2009;8(4):661-669.
511. Vignesh, R, Sjölander, A, Venkatraman, G, et al. Aberrant environment and PS-binding to calnuc C-terminal tail drives exosomal packaging and its metastatic ability. Biochemical Journal 2021;478(12):2265-2283.
512. Kimura, N, Inoue, M, Okabayashi, S, et al. Dynein dysfunction induces endocytic pathology accompanied by an increase in Rab GTPases: a potential mechanism underlying age-dependent endocytic dysfunction. The Journal of biological chemistry 2009;284(45):31291-31302.
513. Lin, Y-S, Huang, K-Y, Yu, H-C, et al. Identification of phostensin in association with Eps 15 homology domain-containing protein 1 (EHD1) and EHD4. Biochemical and Biophysical Research Communications 2020;531(2):236-241.

514. Perez, RE, Calhoun, S, Shim, D, et al. Prolyl endopeptidase inhibitor Y-29794 blocks the IRS1-AKT-mTORC1 pathway and inhibits survival and in vivo tumor growth of triple-negative breast cancer. Cancer Biol Ther 2020;21(11):1033-1040.
515. Gawenda, J, Traub, F, Lück, HJ, et al. Legumain expression as a prognostic factor in breast cancer patients. Breast Cancer Res Treat 2007;102(1):1-6.
516. Ohno, Y, Nakashima, J, Izumi, M, et al. Association of legumain expression pattern with prostate cancer invasiveness and aggressiveness. World J Urol 2013;31(2):359-364.
517. Haugen, MH, Johansen, HT, Pettersen, SJ, et al. Nuclear legumain activity in colorectal cancer. PLoS One 2013;8(1):e52980.
518. Larrinaga, G, Perez, I, Blanco, L, et al. Prolyl endopeptidase activity is correlated with colorectal cancer prognosis. International journal of medical sciences 2014;11(2):199-208.
519. Perez, I, Blanco, L, Sanz, B, et al. Altered Activity and Expression of Cytosolic Peptidases in Colorectal Cancer. International journal of medical sciences 2015;12(6):458-467.
520. Wyganowska-Świątkowska, M, Tarnowski, M, Murtagh, D, et al. Proteolysis is the most fundamental property of malignancy and its inhibition may be used therapeutically (Review). Int J Mol Med 2019;43(1):15-25.
521. Zeng, B, Yuan, C, Yang, X, et al. TRPC Channels and Their Splice Variants are Essential for Promoting Human Ovarian Cancer Cell Proliferation and Tumorigenesis. Current Cancer Drug Targets 2013;13(1):103-116.
522. Yildirim, E, Kawasaki Brian, T, Birnbaumer, L. Molecular cloning of TRPC3a, an N-terminally extended, store-operated variant of the human C3 transient receptor potential channel. Proceedings of the National Academy of Sciences 2005;102(9):3307-3311.
523. Wei, Z, Batagov, AO, Carter, DRF, et al. Fetal Bovine Serum RNA Interferes with the Cell Culture derived Extracellular RNA. Scientific reports 2016;6:31175-31175.
524. Rashid, M-u, Coombs, KM. Serum-reduced media impacts on cell viability and protein expression in human lung epithelial cells. Journal of Cellular Physiology 2019;234(6):7718-7724.
525. Menck, K, Sönmezer, C, Worst, TS, et al. Neutral sphingomyelinases control extracellular vesicles budding from the plasma membrane. J Extracell Vesicles 2017;6(1):1378056.
526. Lee, S-S, Won, J-H, Lim, GJ, et al. A novel population of extracellular vesicles smaller than exosomes promotes cell proliferation. Cell Communication and Signaling 2019;17(1):95.
527. Matsumoto, Y, Kano, M, Murakami, K, et al. Tumor-derived exosomes influence the cell cycle and cell migration of human esophageal cancer cell lines. Cancer science 2020;111(12):4348-4358.
528. Roskoski Jr, R. Src protein-tyrosine kinase structure, mechanism, and small molecule inhibitors. Pharmacological research 2015;94:9-25.
529. Bilal, E, Alexe, G, Yao, M, et al. Identification of the YES1 kinase as a therapeutic target in basal-like breast cancers. Genes & cancer 2010;1(10):1063-1073.
530. Yeung, C, Ngo, V, Grohar, P, et al. Loss-of-function screen in rhabdomyosarcoma identifies CRKL-YES as a critical signal for tumor growth. Oncogene 2013;32(47):5429-5438.
531. Sancier, F, Dumont, A, Sirvent, A, et al. Specific oncogenic activity of the Src-family tyrosine kinase c-Yes in colon carcinoma cells. PLoS One 2011;6(2):e17237.
532. Oneyama, C, Iino, T, Saito, K, et al. Transforming potential of Src family kinases is limited by the cholesterol-enriched membrane microdomain. Molecular and cellular biology 2009;29(24):6462-6472.
533. Hamanaka, N, Nakanishi, Y, Mizuno, T, et al. YES1 Is a Targetable Oncogene in Cancers Harboring YES1 Gene Amplification. Cancer Research 2019;79(22):5734-5745.

534. Demory Beckler, M, Higginbotham, JN, Franklin, JL, et al. Proteomic analysis of exosomes from mutant KRAS colon cancer cells identifies intercellular transfer of mutant KRAS. Mol Cell Proteomics 2013;12(2):343-355.
535. Chan, YK, Zhang, H, Liu, P, et al. Proteomic analysis of exosomes from nasopharyngeal carcinoma cell identifies intercellular transfer of angiogenic proteins. Int J Cancer 2015;137(8):1830-1841.
536. He, M, Qin, H, Poon, TC, et al. Hepatocellular carcinoma-derived exosomes promote motility of immortalized hepatocyte through transfer of oncogenic proteins and RNAs. Carcinogenesis 2015;36(9):1008-1018.